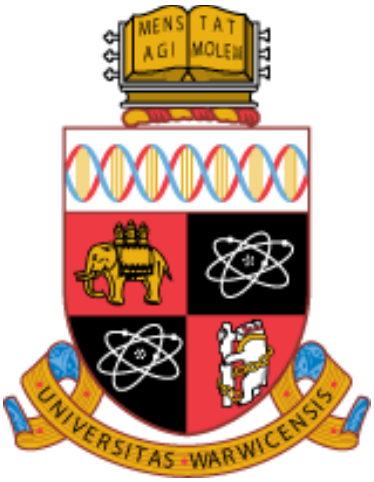

Performance Evaluation and Analysis of the Use of CO_2 Cooling for Conventional Drilling of Carbon Fibre Reinforced Plastics

by

Pipat Bhudwannachai

WMG

University of Warwick

A thesis submitted for admission to the degree of

Doctor of Philosophy

December 2014

Abstract

Machining defects induced by conventional drilling of carbon fibre reinforced plastics (CFRPs), of which the most concern is delamination damage both to the surface of the component and to the machined surface of the hole, usually occur due to the heterogeneity and anisotropic properties of the material. Among previous research work on conventional drilling of CFRPs, attempts to minimise delamination damage have focused on the optimisation of tool material, geometry and cutting parameters. Although the application of cryogenic cooling has been shown to improve performance in metal machining, there has been little research work reported on its application to conventional drilling of CFRPs. Therefore, the objectives of this research were to evaluate the application of cryogenic cooling, for which CO_2 was used as the main cutting fluid, in conventional drilling of CFRPs and present a detail explanation of the effect on machining performance and mechanism associated with cryogenic machining of these materials.

Drilling experiments with liquid nitrogen (LN_2) pre-cooled tools, with CO_2 cooling and when machining dry at room temperature were performed on CFRPs (carbon/epoxy) plaques using TiAlN and diamond coated solid tungsten carbide drills. The performance evaluation was based on measurement of thrust force, tool wear and delamination damage to the entry/exit of the hole and internal damage to machined surface of the hole. Cutting temperature and characteristics of machined surface (fracture behaviour of carbon fibres and epoxy matrix) produced when drilling with cryogenic cooling and dry at room temperature were also investigated.

In this research, it was found that application of cryogenic cooling (LN_2 pre-cooling and CO_2 cooling) to conventional drilling of CFRPs resulted in an improvement in machining performance with respect to quality of the hole. Less exit delamination damage and internal damage to machined surface of the hole were produced when machining with cryogenic cooling compared to room temperature dry drilling. However, the use of cryogenic cooling in conventional drilling of CFRPs did not improve machining performance with respect to cutting forces and tool wear. In fact, it resulted in higher thrust force and average flank wear compared to machining dry at room temperature. The reduction of delamination and internal damage and the increase of thrust force and rate of tool wear were found to be due to the higher abrasiveness, strength and stiffness of CFRP plaques that were retained during drilling with cryogenic cooling. The cutting temperature was shown to be lower than room temperature dry drilling due to the more effective removal of heat from the cutting zone. It was shown that the cutting temperature was reduced by 14-27% when drilling with cryogenic cooling, for which the use of a CO_2 cooling system provided the highest cooling ability, at a cutting speed and feed rate of 100 m/min and 0.06 mm/rev respectively. It was shown that drilling with cryogenic cooling resulted in a more brittle fracture behaviour and less thermal softening of the epoxy matrix in CFRP plaques compared to that produced by room temperature dry drilling. This indicates higher strength and stiffness of the epoxy matrix that were retained during drilling with cryogenic cooling hence resulting in higher abrasiveness, strength and stiffness of the plaque due to more rigid support of the matrix. Since the drilling-induced damage, which was shown in previous research work to degrade the mechanical properties and performance of CFRP components, was reduced, the application of cryogenic cooling can therefore be beneficial when implemented in conventional drilling of CFRPs to improve productivity. However, tool material has to be optimised to compensate with shorter tool life due to increased rate of tool wear. Although no significant difference in thrust force was produced when drilling with CO_2 cooling and when drilling with a LN_2 pre-cooled tool at the same cutting speed and feed rate, less damage to the machined surface was produced when drilling with CO_2 cooling. This was found to be due to higher capability in reducing the cutting temperature than LN_2 pre-cooling of the tool. Therefore, the application of cryogenic cooling by continual supply of CO_2 (or LN_2) is more preferable and more practical to be implemented in the production process in industry than cryogenic pre-cooling of the tool.

Declaration

This thesis is the original work of the author submitted to the University of Warwick in support of my application for the degree of Doctor of Philosophy. The research was performed at WMG of the University of Warwick. The practical machining work associated with the drilling trials with cryogenic pre-cooling of the tool described in Section 5.1 was performed under the author's supervision as part of the MSc project of Miss Aishah Najiah Dahnel (an MSc graduate in 2012). All of the data analysis was carried out exclusively by the author. Some of the practical machining work associated with the drilling trials with the use of CO_2 cooling described in Section 5.2 was carried out under the author's supervision as part of undergraduate students' final project. The rest of the practical machining work and all of the data analysis of the data were performed out exclusively by the author. The CT-scanning analysis of samples for the drilling trials described in Section 5.3 was performed in collaboration with Miss Nadia Kourra (an EngD candidate at WMG) and Professor Mark Williams (Product Evaluation Technologies Group Leader at WMG). The CT-scanning of the samples was performed by Miss Nadia Kourra and all of the data analysis was carried out exclusively by the author. The rest of the experimental work in this thesis and the analysis of associated data were performed by the author. This thesis has not been submitted in whole or in part as consideration for other degree qualification at this or any other university. Where other work has been used it has been acknowledged. In accordance with the Degree Committee of the Faculty of Sciences, the length of this thesis is less than 70,000 words.

Pipat Bhudwannachai
WMG
University of Warwick
April 2014

Acknowledgments

I would like to thank my supervisor Dr Stuart Barnes for his great support and guidance throughout the completion of this thesis. Also, I would like to thank him for his confidence in my ability and taking me as a student under his supervision.

Also, I would like to thank Mr Paul Grimley and Mr Darren Grant for their supervision on the practical machining work in this thesis, and other technicians in WMG workshop including Mr Paul Johnson, Mr John Pillier, Mr Zachary Parkinson and Mr Stefan Kousoulas for their support on the experimental and analysis work being performed in WMG workshop.

I also would like to extend my appreciation to Dr Mike Keeble (Technical Development Manager, Buehler UK, Ltd.) for the help and support on the optical microscopic analysis and mounting and polishing work using Buehler equipment.

I would like to thank DMG / MORI SEIKI for supplying the machining centres, SGS Carbide Tool (UK) Ltd. and Guhring Ltd. for supplying the drilling tools, and BAE Systems for supplying the workpiece materials.

Personally, I would like to thank my colleagues in room IMC 359 for cheering me up and making a great working atmosphere during the time of my study. I also would like to thank all of my friends for keeping me motivated and cheering me up during the hard time of my study.

Most importantly, I would like to thank my parents for their great support on everything since the start until the completion of my thesis.

Without all the support, this thesis would not have been completed.

Publications arising from this work

Barnes, S., Bhudwannachai, P. and Dahnel, A. N., Drilling Performance of Carbon Fiber Reinforced Epoxy Composite when Machined Dry, with Conventional Cutting Fluid and with a Cryogenically Cooled Tool, *Proc. of the ASME 2013 Int. Mechanical Engineering Congress & Exposition, IMECE 13,* San Diego, California, USA, Nov. 15-21 2013, 2013.

Dahnel, A. N., Barnes, S. and Bhudwannachai, P., Experimental Analysis of Tool Wear when Drilling Carbon Fibre Composite (CFC) without Cutting Fluid, with Cutting Fluid and with a Pre-Cryogenically Cooled Tool, *Applied Mechanics and Materials*, **372**, 2013, pp. 512-515.

Dahnel, A. N., Barnes, S. and Bhudwannachai, P., Drilling of Carbon Fibre Composites: A Review, *Advanced Materials Research*, **903**, 2014, pp. 3-8.

Barnes, S., Ascroft, H., Bhudwannachai, P., Dahnel, A. N. and Gupta, A., 2014, Advances in Cryogenic and Ultrasonic Assisted Machining, *The 16th International Conference on Machine Design and Production*, İzmir, Turkiye, June 30-July 3 2014.

Contents

Page

Page

Page

Page

List of Tables

Page

List of Figures

Page

Page

Page

Page

Page

Page

Page

Page

Page

Page

Page

Page

Page

List of Abbreviations and Symbols

2-D	Two Dimensional
3-D	Three Dimensional
θ	Relative Angle of Fibre Orientation
γ	Shear Strain
µm	Micrometer
°C	Degree Celcius
A_0	Area of Drilled Hole
A_d	Actual Area of Delamination
A_{del}	Total Area of Delamination
A_{max}	Area of Delamination Calculated from Maximum Diameter of Delamination
atm	Atmosphere
Carbon/Epoxy	Carbon Fibre Reinforced Epoxy
CFRP	Carbon Fibre Reinforced Plastic
CMCs	Ceramic Matrix Composites
Co	Cobalt
CO_2	Carbon Dioxide
CT	Computerised Tomography
CTE	Coefficient of Thermal Expansion
D_0	Diameter of Drilled Hole
D_{max}	Maximum Diameter of Delamination
DI-NAMITE	Pure Crystalline Diamond Coating
F_{ad}	Adjusted Delamination Factor
F_d	Delamination Factor
F_{da}	Area-Delamination Factor
HV	Vickers Hardness
HSS	High Speed Steel
kg	Kilogram
l	Litre

LN_2	Liquid Nitrogen
m	meter
min	minute
mm	Millimeter
mm^2	Square Millimeter
MMCs	Metal Matrix Composites
N	Newton
N_2	Nitrogen gas
PCD	Polycrystalline Diamond
PMCs	Polymer Matrix Composites
rev	Revolution
RPM	Revolution per Minute
RT	Room Temperature
s	second
TiAlN	Titanium Aluminium Nitride Coating
Ti-NAMITE	Titanium Coating
WC	Tungsten Carbide

1 Introduction

1.1 Research Background

Polymer matrix composites (PMCs) have been increasingly used and are replacing conventional unreinforced materials for lightweight structures and components in aerospace, automotive and marine industries [1-5]. The most widely used PMCs in high strength applications such as commercial and military aircraft components and structures are long continuous carbon fibre-reinforced plastics (CFRPs), especially carbon fibre reinforced epoxy (carbon/epoxy) composites, due to high specific strength and stiffness, improved fatigue property, negative coefficient of thermal expansion (CTE) and high specific thermal and electrical conductivity of reinforcing carbon fibres [5, 6]. Although CFRPs can be manufactured to near-net-shape parts, secondary machining processes are generally required in order to achieve the desired specification, tolerance and functionality of the final parts. Among the secondary machining processes, conventional drilling is commonly applied to CFRP parts to produce holes for mechanical joining, especially in the aerospace industry [3, 4, 7-9]. Although adhesive bonding can be used to join CFRP parts, mechanical joining such as bolting and riveting is still important and widely used for CFRP part joining in the aerospace industry due to resistance to environmental degradation and ease of disassembly for repairing and maintenance [4, 8, 9]. Unfortunately, machining defects induced by conventional drilling processes usually occur due to the heterogeneity, anisotropic properties and abrasiveness of CFRPs in addition to the low thermal tolerance of polymeric matrix [4, 7, 9-11]. Such defects include delamination damage to the entry and exit laminates, thermal damage to the matrix, matrix cracking and internal damage to the machined surface of the drilled hole in the form of material chip-out (fibre/matrix pull-out) and delamination [4, 7, 9-11]. This drilling-induced damage degrades the mechanical properties and performance of CFRP parts and components, which are critical to high performance applications, and hence limit the application of CFRPs [7, 9, 10, 12]. The drilling-induced defect of most concern is delamination damage, which accounts for 60% of final part rejection in the aircraft industry [7, 9]. In addition, it was also shown that delamination damage significantly reduced static and fatigue properties of the CFRP parts [12]. According to private communication with BAE Systems [13], the extent of material chip-out on the machined surface of the hole is another criterion, in addition to exit delamination damage, for the evaluation of drilling performance. For these reasons, there have been many attempts to minimise delamination damage induced from the conventional drilling of CFRPs.

Among the research work that has been performed on conventional drilling of CFRPs, the attempt to minimise delamination damage has focused on optimising material and

geometry of the drill, optimising cutting parameters and modification of the drilling process such as drilling a pilot hole and drilling with a back-up plate [14-27]. There has been little research work which reports the application of cutting fluids or cryogenic cooling to improve the performance of conventional drilling of CFRPs by reducing delamination damage. However, there have been attempts to minimise or eliminate the use of conventional water-based cutting fluids in the machining process in industry to reduce cost associated with the maintenance and treatment/disposal of the cutting fluid, environmental problems from chemicals and additives in the cutting fluid if they were disposed without proper treatment and health problems to machining operators of the exposure level is not controlled [28-31]. In industry, the drilling of CFRP parts is carried out either without a cutting fluid to avoid material degradation due to moisture absorption and reduce the cost of cleaning [10, 13, 32], or with the use of a cutting fluid for dust suppression purposes or for controlling cutting temperature in some cases [13]. Although cutting fluids are used in some machining processes, the goal is to improve performance while maintaining "dry machining" condition when drilling CFRPs in industry [13]. For these reasons, it is suggested that the application of cryogenic cooling using liquid nitrogen (LN_2) or liquid carbon dioxide (CO_2) as a cutting fluid would be preferable to the use of conventional cutting fluids for improving performance of conventional drilling of CFRPs in the machining aspect. It has been reported that changing from conventional cutting fluids to cryogenic cooling provides advantages by significantly reducing solid waste, water usage, global warming potential and aquatic toxicity, while eliminating the machining operators' health concerns due to exposure to the chemical in the conventional cutting fluids [29, 33]. The additional cost of after-process cleaning is also eliminated since the cryogen will be evaporated from the machined surface to the atmosphere after dissipating heat from the cutting zone [30, 31, 34-36]. With regard to machining, the application of cryogenic cooling has been shown to improve machining performance of metallic materials, especially difficult-to-machine aerospace alloys, by extending tool life and reducing cutting forces as a result of a reduction in cutting temperatures [35, 37-44]. Due to limited study on its application to conventional drilling of CFRPs, questions on whether cryogenic cooling results in an improvement in machining performance similar to the case of metal machining and how it affects machining behaviours associated with CFRPs was considered. As a consequence of this research question, the objective of this research was to investigate the performance of cryogenic cooling in conventional drilling of CFRPs and its effect on the machining mechanisms associated with these materials. Due to concern about the effect of extremely low temperature (-196°C) which is generated by a LN_2 cutting fluid on the workpiece material and cutting tools/holders as well as the potential harm to the machining operators, a CO_2 cutting fluid was used as the main cutting fluid for the cryogenic cooling in

this research. In addition, it has been proposed that the use of a CO_2 cutting fluid can reduce the cost associated with the production of cutting fluids because CO_2 can be obtained as a by-product from the chemical industry and power plants [29, 30, 35, 38, 45] compared to using LN_2, which requires energy for cryogenic distillation.

1.2 Objectives

The objectives of this research were as follows:

1. Evaluate the performance of the application of cryogenic cooling using a CO_2 cutting fluid in conventional drilling of CFRPs
    1.1. Determine the effect of cryogenic cooling on drilling thrust force as compared with when drilling dry at room temperature
    1.2. Determine the effect of cryogenic cooling on drilling-induced damage (entry/exit delamination and internal damage to the machined surface) as compared with when drilling dry at room temperature
2. Explain the effect of CO_2 cooling on conventional drilling of CFRPs in relation to machining theory and present a detailed explanation of the mechanisms associated with cryogenic machining of these materials
    2.1. Determine cutting temperature produced when drilling with cryogenic cooling and the effect of cryogenic cooling in reducing cutting temperature
    2.2. Determine the effect of cryogenic cooling on fracture behaviour and material properties of CFRPs during machining
3. Explain wear mechanism of carbide tools when drilling CFRPs with cryogenic cooling

2 Introduction to Polymer Matrix Composites

Prior to discussing the machining of CFRPs, it is important to consider an overview of composite materials in general. Consequently, this chapter will be presenting the general description of composite materials and their properties with emphasis on polymeric matrix composites (PMCs), which is a class of material used in this research.

2.1 Overview of composite materials

According to Schwartz [2], Davim [3], and Campbell [5], a composite is a material which is manufactured to combine two or more constituents or phases of distinctive physical and chemical properties, resulting in a material with properties that cannot be achieved by using each material separately. Composite materials consist of two principal phases; the reinforcement and the matrix. The reinforcement, which can be in various forms, including particles, whiskers (large single crystals), discontinuous short fibres, and continuous long fibres, Figure 2.1, provides strength and stiffness for the composites and, in the case of fibre-reinforced composites, mainly supports the loads applied in the longitudinal direction to the fibre axis of the composites [2, 5]. However, the reinforcing fibres are also used to increase toughness and strength of the matrix in ceramic matrix composites (CMCs) [1, 2, 4, 5, 46]. The matrix binds and keeps reinforcements in the desired order, helps equally distribute the loads to the reinforcements, supports the reinforcing fibres during compression loading. It also protects the reinforcements from any hostile environment, provides toughness and enhances material properties in transverse direction providing interlamina shear strength and through-the-thickness strength [2, 4, 5]. Properties of the matrix material, such as temperature resistance and weight, also determine the field of applications of the composite [3, 5]. For example, metal matrix composites (MMCs) can be used in higher temperature applications compared to polymer matrix composites (PMCs) because of their higher thermal stability and temperature resistance [4, 5, 46]. In contrast, PMCs are widely used in lightweight structural applications due to their low density [4-6, 46]. In addition to reinforcement and matrix, there can be other minor phases present in composites to enhance desired properties. For example, crosslinking agents such as diaminodiphenyl sulfone (DDS) can be added to an epoxy resin to promote crosslinkings and assisting in transforming the resin to a solid cured epoxy matrix [5]. Coupling agents, such as organotitanates and organozirconates, are used for coating carbon fibres to improve fibre-to-matrix bonding with thermosets such as epoxy, polyurethane, polyester, and vinyl ester resins [1].

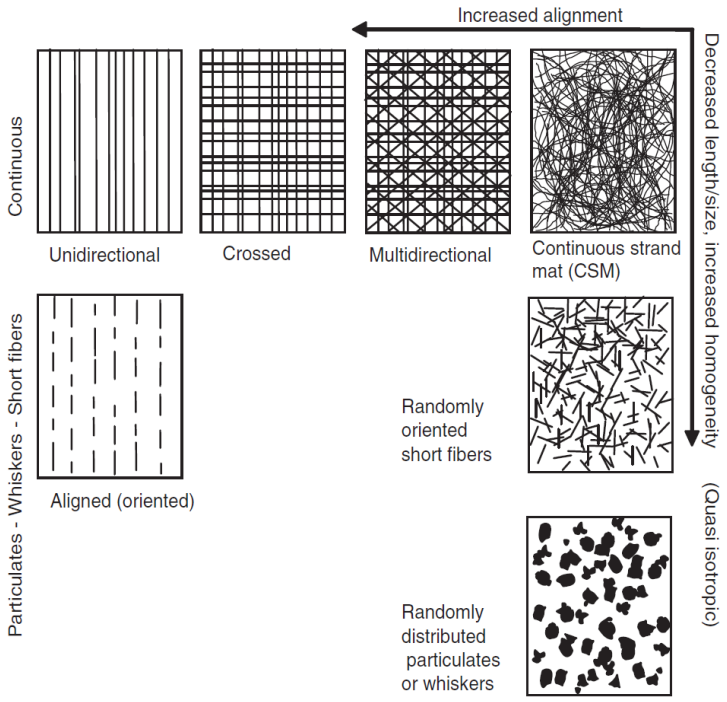

Figure 2.1: Different forms and arrangements of reinforcement in composites [4]

With the combination of material properties from the reinforcement and the matrix, composite materials provide performance advantages compared to their base material without reinforcements in the case of metals, polymers and ceramic materials. The reinforcing fibres in composites, especially high-strength continuous fibres, increase strength-to-weight and modulus-to-weight ratio of polymeric and metallic matrix composites, while they increase toughness of ceramic matrix composites compared to their unreinforced base materials [4, 5, 46]. Due to their anisotropic properties and heterogeneous structures, composite materials can be tailored (e.g., by appropriately choosing the reinforcement and matrix materials, proportions of each material, fibre-to-matrix bonding, morphologies and the degree of crystallinity of the composites) to optimize material properties that match the requirements of specific applications [4-6]. In addition, composite materials also offer other performance advantages, including improved fatigue resistance compared with conventional aerospace alloys, good corrosion resistance (e.g., with glass fibre reinforcement), and greater design flexibility due to a reduction in assembly parts and tooling [2, 4, 5]. For these reasons, composite materials are replacing conventional materials in both high-performance and commercial applications.

Despite the many performance advantages previously mentioned, there are some limitations when using composite materials. High processing costs, high cost of materials in continuous fibre form, and absence of large-volume production methods have limited the use of composites in the application where cost is the most important factor [2, 4-6]. The

anisotropic properties of composites and the abrasive nature of many reinforcements also result in problems during machining. In the case of PMCs, for example, machining problems such as interlamina delamination, matrix cracking, fibre pull-out, incomplete cut fibres, matrix burn-out, high rate of tool wear, and machine tool damage usually occur due to abrasive nature of the fibres, weakness in through-the-thickness direction and transverse direction to fibre orientation, brittleness and low thermal stability of the matrix [3, 4, 7, 10, 47].

Based on the type of matrix material, composite materials can be classified as; [2-5]

1) Metal Matrix Composites (MMCs),
2) Ceramic Matrix Composites (CMCs),
3) Polymer Matrix Composites (PMCs)

Within each class of composites, they can be further classified based on types of reinforcement; particulate, short fibre or whisker, and continuous fibre composites, with random or preferred orientation [4, 5].

2.1.1 Metal Matrix Composites (MMCs)

Compared to their base metals, MMCs have higher specific strength and modulus, higher elevated-temperature resistance, lower coefficient of thermal expansion (CTE), better fatigue resistance and better wear resistance [2, 5, 48]. With higher specific strength and modulus than unreinforced metals, the use of MMCs in structural applications for aerospace and military industries, such as the use of SiC particulate-reinforced aluminium MMCs skin for an aircraft fuselage, can provide major weight reduction [48]. MMCs also have great potential for use in electronic parts, such as heat sinks, due to their low CTE and high thermal conductivity [46]. In addition, thermal conductivity of MMCs can be further improved if carbon fibres with high degree of graphitic structure are used as reinforcement [46].

Reinforcements for MMCs can be in the form of particles, whiskers or short fibres and continuous fibres with aligned multifilaments or large monofilaments [5, 48, 49]. Whisker- or short fibre reinforced MMCs provide better mechanical properties than particulate MMCs but they are more expensive and it is more difficult to align the reinforcements in the matrix than particulate MMCs [5]. The greatest increase in mechanical and thermal properties of MMCs is can be achieved with the use of continuous long fibre reinforcements. However MMCs with continuous long fibre reinforcement are expensive, due to difficulties of processing [5, 48-50]. As a consequence, discontinuous reinforced (particulate, whisker and short fibre) MMCs are more widely used than continuous fibre-reinforced MMCs [5, 48, 50]. Continuous fibre-reinforced MMCs are used only for the applications where

performance outweighs cost consideration, e.g., the use of SiC monofilament-reinforced Ti MMCs as nozzle actuator controls for the F119 engine in F-16 [48].

The common reinforcement materials for MMCs are particulates of silicon carbide (SiC), alumina (Al_2O_3) and titanium diboride (TiB_2); whiskers and short fibres of SiC and Al_2O_3 and continuous fibres of SiC, Al_2O_3, boron (B) and graphite (C) [2, 5, 48]. The matrix materials for MMCs are pure metals or alloys of metals such as aluminium, magnesium, titanium, copper, and nickel [2, 5, 46, 48]. The most commonly used matrix materials for MMCs are aluminium alloys due to their low density, excellent strength and toughness and low cost of fabrication and processing [5, 48].

Compared to PMCs, MMCs have higher thermal stability and higher thermal resistance (e.g., maximum temperature usage of 815°C for Ti MMCs [5]) and they do not absorb moisture like PMCs resulting in higher resistance to environmental degradation [46, 48, 50]. In addition, due to the metallic matrix, MMCs have higher ductility, toughness and also transverse strength than PMCs [2, 5, 46]. Consequently, MMCs are suitable for use in applications which require higher temperature resistance and stability and higher damage tolerance (e.g., the use of SiC particulate-reinforced Al MMCs for fuselage skin and in the fan-exit guide vane of an aircraft engine [48]). However, MMCs are heavier than PMCs, so they are not as widely used as PMCs for lightweight structural applications with low to medium temperature usage [2, 4, 5, 46]. In addition, high cost of materials and high costs of processing have limited the applications of MMCs [5, 46].

2.1.2 Ceramic Matrix Composites (CMCs)

CMCs have potential in applications where high strength and stiffness are required at elevated temperature due to their higher thermal stability, higher oxidation resistance, lower thermal expansion and higher strength and modulus, compared to MMCs and PMCs [2, 5, 46, 50]. Applications of CMCs include aircraft engine exhaust and heat-exchanging tubes [50]. However, CMCs are not suitable for structural applications where high toughness and impact resistance are required because they are brittle and do not deform plastically, resulting in a high possibility for crack propagation [2, 5, 46, 50].

Reinforcements in CMCs are used to improve toughness and also increase strength of the composites [2, 5, 46]. When the crack is approaching the fibre-to-matrix interface, the fibres are debonded and partially pulled out from the matrix, dissipating the energy and preventing crack propagation [5, 46], Figure 2.2. Since crack propagation has to be retarded by energy dissipation mechanisms such as fibre-matrix debonding and fibre pull-out, weak bonding between the fibres and the matrix is required [2, 5, 46]. However, the bonding

should be strong enough to enable strengthening effect of the fibres [46]. This is in contrast to PMCs in which strong interfacial bonding between the fibres and the matrix is required.

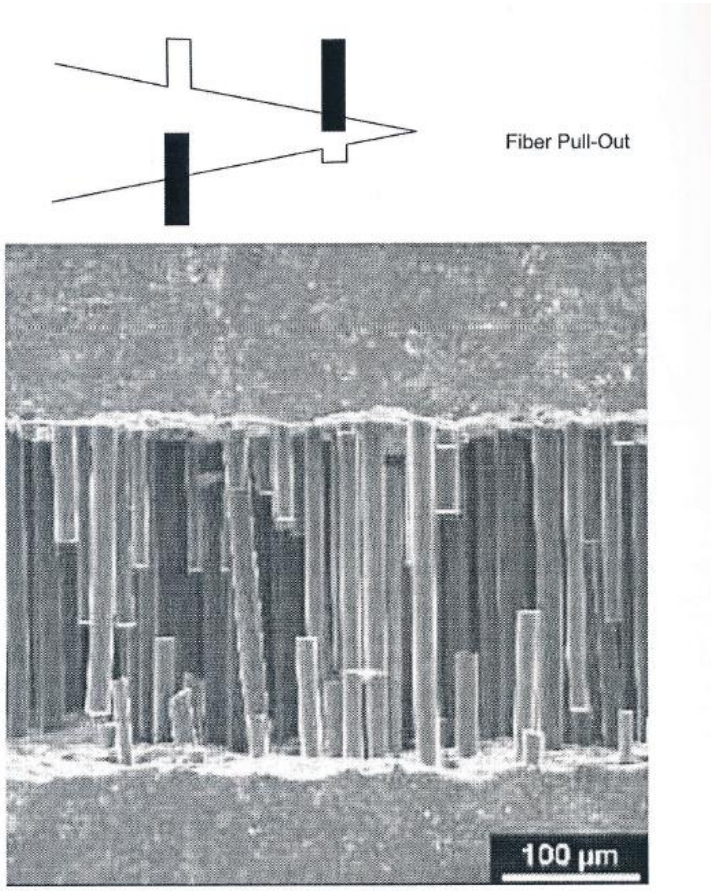

Figure 2.2: Crack dissipation mechanisms [5]

The common reinforcement materials for CMCs are particulates of SiC and Al_2O_3, whiskers of SiC, silicon nitride (Si_3N_4) and Al_2O_3 and oxide fibres (Al_2O_3) and nonoxide fibres (SiC and C) [2, 5, 50]. The typical matrix materials for CMCs are glass-ceramic, carbon, SiC, Si_3N_4 and Al_3O_3 [2, 5, 50].

Carbon fibres are reinforced in a carbon matrix, forming C-C composites, for use in structural applications where high temperature and thermal shock resistances are needed. Applications include rocket motor casings, heat shields, leading edges, thermal protection and brakes of an aircraft because of their high specific strength and modulus combined with thermal stability at temperature of up to 2205°C in nonoxidinzing atmosphere [2, 5, 50, 51]. However, oxidation-resistance coating systems such as SiC overcoated with glass and oxidation inhibitors such as boron are used to enable elevated-temperature usage of C-C composites in oxidizing atmosphere [5, 51].

Since higher temperatures and pressures are involved in CMCs processing compared to MMCs and PMCs, CMCs are more difficult and more expensive to produce than MMCs and PMCs and therefore their applications are limited [2, 5, 46, 52]. In addition, due to their

brittleness and low impact tolerance, CMCs are not as widely used as PMCs in lightweight structural application [2, 4, 5, 46].

2.1.3 Polymer Matrix Composites (PMCs)

PMCs are the most widely used composites in both commercial and high-performance applications in such sectors as aerospace, marine, automotive and sports equipment. This is because of their lightweight, high specific strength and stiffness compared to conventional aerospace alloys, resistance to corrosion and ease and low cost of processing compared to MMCs and CMCs [1, 2, 4, 5, 46]. In aerospace applications where lightweight and high dimensional stability are required, PMCs with continuous long carbon fibres are suitable due to their low density, high strength and modulus, and negative coefficient of thermal expansion (CTE) [2, 4]. As a consequence, carbon fibre reinforced plastics (CFRPs), especially carbon fibre reinforced epoxy composites, are the most widely used PMCs in high-performance applications, including in aerospace applications [5, 6]. Unfortunately, PMCs are limited to use at low to moderate temperature (125°-190°C for epoxy composites [5, 53]) because of lower temperature resistance than MMCs and CMCs [2, 4, 5]. In addition, polymer matrices are weaker than metal matrices, resulting in inferior properties of the composites in through-the- thickness direction compared to MMCs [4, 5]. The major reinforcement materials for PMCs are glass, aramid, and carbon fibres, while the matrix material can be either thermosetting plastics or thermoplastics [2-5]. More detail on PMCs including the reinforcement and matrix materials and general properties of PMCs will be presented in the later sections.

2.2 Polymer Matrix Composites (PMCs)

2.2.1 Introduction

PMCs, as mentioned in Section 2.1.3, are the most commonly used type of composites in both commercial and high-performance applications. Due to the lightweight and high specific strength and stiffness of reinforcing fibres, continuous carbon fibre PMCs, for example, are replacing conventional unreinforced materials for lightweight structural parts in high-performance applications such as commercial and military aircraft [4-6]. An example is shown in Figure 2.3 where 50% by weight of a Boeing 787 structure consists of composites including glass and carbon reinforced plastics [54]. In addition, negative coefficient of thermal expansion (CTE) of continuous carbon fibres enables the design of structural parts with CTE approaching zero [1, 4]. High specific thermal and electrical conductivity of carbon fibres with high degree of graphitic in the structures also improves thermal and electrical conductivity of reinforced polymers [1, 5]. In addition to carbon fibre-reinforced

PMCs, glass fibre reinforced PMCs are also widely used in applications where corrosion resistance and lightweight are needed e.g., marine applications such as in ship hulls and decks and submarine fairings [4, 52].

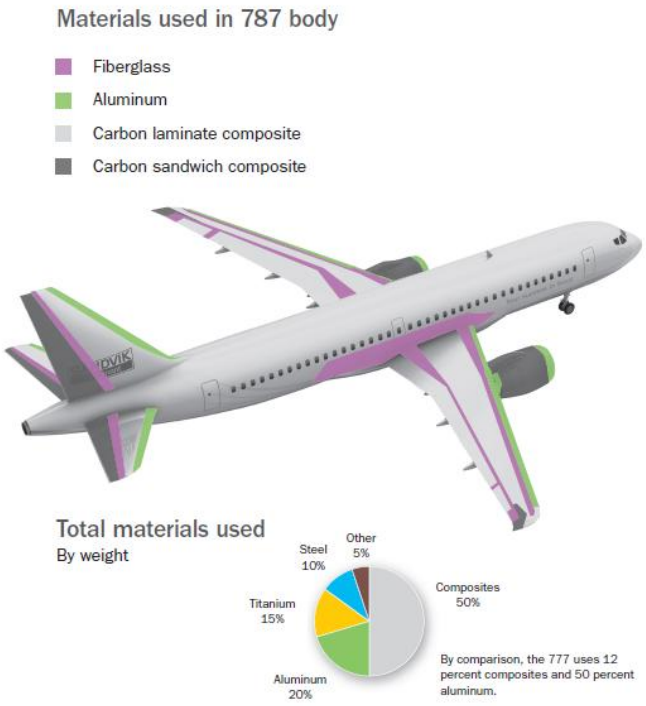

Figure 2.3: Proportions of materials used in the body of Boeing 787 shown in percentage by weight [54]

From the manufacturing point of view, PMCs are easier and cheaper to process compared to MMCs and CMCs due to lower processing temperatures and pressures involved [2, 5, 52]. For example, the processing temperatures for thermoplastic composites are in the range of 300-400°C [5, 46], while the processing temperatures of MMCs and CMCs are above 500°C [5, 52]. Despite the advantages from a manufacturing point of view, low melting point of polymers results in lower temperature resistance and thermal stability of PMCs than MMCs and CMCs [2, 4, 46]. In addition, PMCs tend to absorb moisture, which further reduces the maximum service temperature of PMCs (less than 120°C for high-temperature-cure epoxy composites when used in moist environment [6]). This prohibits the use of PMCs in applications where high strength and stiffness must be retained at elevated temperature such as in the combustor and exhaust of an aircraft engine [52]. Since polymers are weaker and more brittle than metals, PMCs have lower strength in through-the-thickness direction and lower resistance to impact damage, which are dominated by strength and toughness of the matrix, compared to MMCs [4, 5]. The low temperature resistance, low through-the-thickness strength, and anisotropy of material properties (different strength of reinforcing fibres and polymeric matrix) cause many problems during machining including

matrix burn-out, matrix cracking, delamination, fibre pull-out and poor surface finish, which will be discussed in Chapter 3 [3, 4, 10, 55, 56].

2.2.2 Polymeric Matrices

Polymer resins used as the matrix in PMCs provide toughness, impact and abrasive resistance, and mechanical properties in transverse direction such as 90° tensile and compressive stress and interlaminar shear strength. They also provide support and prevent the high-strength but brittle fibre reinforcements from microbuckling due to compression loads [4, 5]. The properties of polymer resins also determine the final usage temperature and field of applications of PMCs. According to Sheikh-Ahmad [4], all polymers exhibit a sudden change in properties such as stiffness when heated to a glass transition temperature, which is a temperature at which a polymer resin softens and changes from a glassy solid into a weaker and more flexible resin. At the glass transition temperature, a polymer resin will undergo a sudden reduction in stiffness and lose its ability to support the fibre reinforcements [4, 5]. As a consequence, PMCs are limited to be used in the temperature ranges below the glass transition temperature of their polymeric matrix.

Polymeric matrices for composite materials can be made from either a thermosetting resin or a thermoplastic resin.

2.2.2.1 Thermosetting Matrices

A thermosetting resin is a rigid polymer which forms crosslinks between the main polymer chains in the structure, Figure 2.4. These crosslinks, which are covalent bonds, impart stiffness, thermal stability, and ability to support the reinforcing fibres during compression loadings for thermosetting resins [5]. The crosslinking within the structure results from the polymerization reaction which is driven either by the heat generated from the exothermic reaction or externally supplied heat during the curing process [3-5]. The crosslinking reaction during the curing process changes a thermosetting resin from a low molecular weight, low viscosity resin to a more rigid, stronger, and higher molecular weight solid resin. The crosslinking of the structure continues as more heat is supplied until a thermosetting resin is fully cured. After being fully cured, additional heat does not cause any changes in the thermosetting resin's structure but, instead, degradation of the resin will occur if the temperature exceeds the cure temperature of the resin [4, 5]. This means a thermosetting resin cannot be remelted or reprocessed after being fully cured. A thermosetting matrix for PMCs, therefore, has to be cured during the manufacturing process [3]. In addition, a thermoset resin usually requires long processing time to allow the chemical reactions that cause crosslinkings in the structure to take place [3-5]. Nevertheless,

thermosetting resins are more widely used in composite applications than thermoplastics because of their superior mechanical properties and lower cost and ease of processing, which results from lower processing temperatures involved [2, 4, 5].

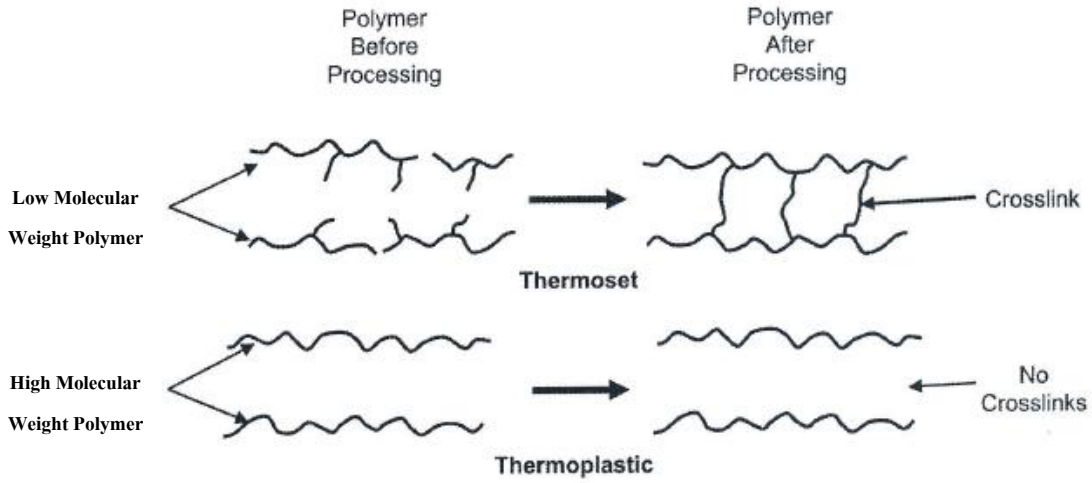

Figure 2.4: Schematic diagrams representing the structure of a thermosetting resin and a thermoplastic resin [5]

The most widely used thermosetting resins for PMCs in high performance application at low to moderate temperature usage are epoxy resins. Epoxy resins offer advantages of high strength and stiffness with lower processing temperatures compared to other high-performance thermosetting resins that are used in higher temperature applications than epoxies including bismaleimides, cyanate esters, polyimides, and phenolics [2, 5, 57]. The usage temperature of epoxy resins is in the range of 125-175°C [2, 53]. The high strength and stiffness of epoxy resins also come with brittleness, which is not suitable for structural applications requiring damage tolerance and impact resistance. As a consequence, toughening methods for epoxies and other high-stiffness thermosetting resins have been developed (which will be discussed later). The increase in toughness of epoxy resins results in a reduction in the glass transition temperature, thus, the maximum usage temperature of the resin [2, 5]. Polyesters and vinyl esters can also be used in the same temperature range of epoxy resins. However, because of their lower mechanical properties, higher volumetric shrinkage after processing, and lower cost of material compared to epoxies, polyesters and vinyl esters are used in commercial applications of PMCs instead of high-performance applications such as in military and aerospace sectors [2, 3, 5]. Other thermosetting matrices have been developed to be used in high-temperature composite applications. Examples include bismaleimides, cyanate esters, polyimides, and phenolics. Bismaleimides and cyanate esters can be used up to 200-230°C, while polyimides can be used up to 316°C [2, 53, 58, 59]. Due to good smoke and fire resistance, phenolics are primarily used in aircraft interior structures [5, 59].

2.2.2.2 Toughened Thermosetting Matrices

As previously mentioned, crosslinks between the main polymer chains in thermosetting resins' structure directly results in high stiffness and high thermal stability of the thermosetting polymers. In addition, the higher the crosslink density, the stiffer and more thermally stable a polymer becomes [5].

As discussed by Campbell [5], the slipping motions between the main polymer chains in the structure of a resin under loading will be restricted by the crosslinks between those chains thus resisting deformation as a result of the loading. If there are more crosslinks per unit length of the main polymer chains (higher crosslink density), Figure 2.5, the slipping motions of the main polymer chains under loading will be restricted further, resulting in higher stiffness of the thermosetting resin. A higher crosslink density also results in higher thermal resistance for thermosetting resin. Since the crosslinks are strong covalent bonds, which are more thermally resistant than weak secondary bonds such as van der Waals bonds, they can help retain strength and stiffness of the resin at elevated temperatures. With more crosslinks in the structure, the strength and stiffness of the resin can be maintained at higher temperatures or at temperatures closer to the glass transition temperature.

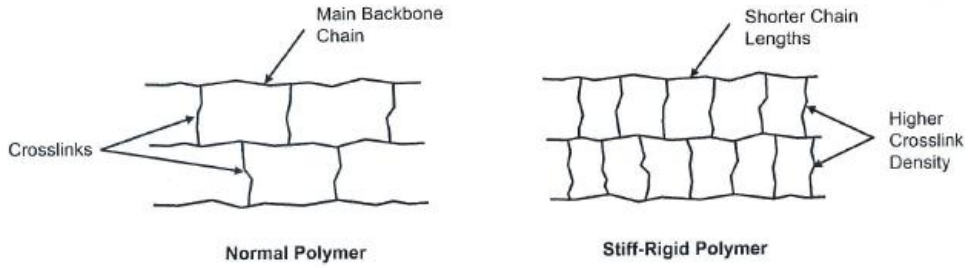

Figure 2.5: Effect of crosslink densities on rigidity of a polymer [5]

Despite high strength, stiffness and thermal stability, high crosslink density also results in brittleness and low damage tolerance of thermosetting matrices [2, 5]. Without or with a few crosslinks between backbone chains of the polymer, the slipping motions between the main polymer chains are not restricted, enabling the polymer to absorb impact energy and resist damage [5]. Consequently, with high crosslink density, the slipping motions between the main polymer chains are restricted, prohibiting impact energy absorption and resulting in low toughness and low damage tolerance. This disadvantage of high crosslink density is the major concern in the use of untoughened thermosetting matrices primary structures of an aircraft [2]. As a consequence, there have been several methods developed to produce toughened thermosetting matrix composites. According to Schwartz [2] and Campbell [5], there are four major toughening methods.

The first method is to lower the crosslink density by altering the structure of monomers in the main polymer backbone chains. The reduction of crosslink density can be done by

using longer and higher molecular weight monomers in the main backbone polymer chains to increase the length between each crosslink or using monomers with fewer numbers of functional groups to reduce the number of crosslinking sites. However, the increased toughness and damage tolerance from the reduction of crosslink density also results in a decrease in glass transition temperature and stiffness of the resin [5].

The other three toughening methods involve the introduction of a more ductile resin into the stiff thermosetting matrix composites instead of altering microstructure of a thermosetting resin. One method is to disperse a second-phase rubber elastomer at the interlamina interfaces of a thermosetting matrix composite to prevent interlamina crack growth by enhancing plastic deformation at the crack tip. Another method is to mix a thermosetting resin with a thermoplastic resin in a co-continuous form. The thermoplastic resin will increase toughness and damage tolerance of the composite, while the thermosetting resin will maintain strength and stiffness of the composite. Finally, toughness of a thermosetting matrix composite can be increased by mixing a continuous or discrete particle interlayering of a tough, ductile resin between lamina of the thermosetting composite to increase low-velocity impact resistance. Similar to the network alteration method, the introduction of a tougher, more ductile resin into thermosetting matrix composites also decreases modulus and thermal stability of the toughened thermosetting matrix composite [5].

2.2.2.3 Thermoplastic Matrices

Thermoplastic matrices are high molecular weight polymers without crosslinks or transverse covalent bonds between polymer chains in the structure, Figure 2.4. Instead, the main polymer chains in thermoplastic resins are held together by weak van der Waals bonds [4]. Since thermoplastic resins lack crosslinking, they are less stiff but tougher and more damage tolerant than the untoughened thermosetting resins [2, 4, 5]. Thermoplastic matrices are already fully cured or polymerized in a semi-finished product before being processed into composite materials. During the composite manufacturing process, a thermoplastic resin is heated until it melts and it is then formed into the composite material with desired shape and properties after consolidation without crosslinking reactions as in the case of thermosetting resins. As a consequence, thermoplastic matrices require shorter processing time than thermosetting matrices. In addition, since crosslinking does not occur in thermoplastic resins, the process of melting and consolidation can be reversed, providing advantages from recycling point of view. However, thermoplastics resins can be reprocessed for a limited number of cycles because the processing temperatures are close to the degradation temperature of the resin and the resin will eventually degrade if it is heated to

that temperature repeatedly [4, 5]. Although, shorter processing times are needed, much higher processing temperatures and pressures are required during the processing of thermoplastic resins than that of thermosetting resins because of the higher melting point and viscosity of thermoplastic resins [4, 5]. The processing temperature range of 120-175°C, for example, is required for processing epoxies, while higher a temperature range of 260-425°C is required for processing high performance thermoplastics [5].

The most important thermoplastics used in composite materials are polyetheretherketone (PEEK), polyetherketoneketone (PEKK), polyphenylene sulfide (PPS), polypropylene (PP) and polyetherimide (PEI) [2, 4, 5]. Due to the good strength and stiffness combined with higher tolerance to velocity impact when compared to epoxy resins, carbon fibre reinforced PEEK is competing with carbon fibre reinforced epoxies in aircraft industry applications [6]. In addition to the good mechanical properties, PEEK, as a thermoplastic, also requires shorter time to process and has unlimited shelf-life at room temperature. However, the major limitation of carbon fibre reinforced PEEK is the high processing cost [5, 6].

2.2.3 Fibre Materials for PMCs

The most common types of fibres used in PMCs are glass, aramid, and carbon fibres [2-4]

2.2.3.1 Glass Fibres

Glass fibres are extensively used in commercial PMC applications because of their good tensile strength, corrosion resistance, and good impact resistance incorporated with lower cost compared to aramid and carbon fibres [2, 4, 5, 52, 60]. In addition to commercial composite applications, glass fibres are also used primarily in the applications where good corrosion resistance is required such as piping in chemical industry and marine applications [2, 4]. However, glass fibres are not extensively used in high-performance applications where high strength and stiffness are required (such as the structural parts in aerospace sector) because of their inferior strength, modulus and fatigue resistance compared to carbon fibres [2, 4, 5].

The production of glass fibres [4, 52, 60, 61] starts by melting the mixture of silica (SiO_2) with other oxides such as Al_2O_3 and B_2O_3, which are added to the silica mixture in order to improve mechanical properties and workability. The melted mixture is then extruded through a platinum alloy bushing and then drawn into thin filaments. The thin filaments are quenched by air or water spray to achieve “rapid cooling rate”. The rapid cooling rate yields fibres with amorphous structure (glass) instead of semicrystalline

structure (quartz) from slow cooling rate [5]. The amorphous structure of glass fibres results in isotropic properties of the fibres [4, 52, 60]. Finally, protective coatings such as polyester and epoxy are applied to protect the fibres during handling and improve fibre-to-matrix bonding [5, 61].

The most commonly used types of glass fibres are E-glass and S-glass. E-glass fibres are low cost, general purpose glass fibres with excellent electrical properties, while S-glass fibres are more expensive, high-performance glass fibres with superior strength, stiffness, and thermal stability than E-glass fibres [2, 4, 5, 60, 61]. The tensile strength and Young's modulus for E-glass fibres are 3.5 GPa and 70 GPa respectively, and those for S2-glass fibres, which are the cheaper and lower performance version of S-glass fibres, are 4.5 GPa and 87 GPa respectively [5].

2.2.3.2 Aramid Fibres

Aramid fibres offer intermediate strength and modulus between glass and carbon fibres [4, 5]. With lowest density compared to other fibres (1.44 g/cm^3), the specific tensile strength of aramid fibres can approach or exceed that of carbon fibres [2, 60, 62]. However, the specific modulus of aramid fibres is lower than that of carbon fibres [4, 5, 60]. Aramid fibres also offer higher toughness and damage tolerance compared to glass and carbon fibres, with good thermal stability [4, 60, 62]. With higher specific strength and modulus than glass fibres combined with high toughness and damage tolerance, aramid fibres are replacing glass fibres in high performance applications such as in interior structures of an aircraft, protective military armour, and sport equipment [2, 4, 5, 60]. Nevertheless, low compressive strength of aramid fibres (20% of tensile strength [2]) limits the use of aramid fibres in the applications with high-strain compressive or flexural loadings [5]. Toughness and high strain-to-failure of aramid fibres also makes it difficult to completely cut the fibres during machining [2, 4, 63].

Aramid fibres are produced by wet-spinning of aromatic polyamides (aramids) dissolved in sulphuric acid solution [4, 5, 52, 60, 62]. The microstructure of dissolved aramids are already arranged in crystalline structure with weak hydrogen bonds holding molecules in the transverse direction, directly resulting in anisotropic properties of aramid fibres [52, 60]. The dissolved solution of aramids is then extruded through the spinnerets, washed, dried, and finally wound up. Shearing during extrusion yields a higher degree of molecular orientation of aramid fibres along the fibre axis, resulting in higher degree of anisotropic properties [4, 52, 60, 62]. Heat treatment under tension at 150-550°C is carried out to increase molecular orientation in the fibre axis direction, improving modulus of the fibres in longitudinal direction [4, 5, 62].

The most prevalent aramid fibres are Kevlar 29, Kevlar 49, and Kevlar 149 [2, 5, 60]. Kevlar 29, which has highest toughness but lowest stiffness due to lowest degree of crystalline structure compared to the other two grades of Kevlar, is widely used in conventional PMC applications [2, 5, 60]. Kevlar 49 is also widely used in PMC applications such as military body armour and helmet [2, 5, 52]. In addition, Kevlar reinforced PMCs are also used in aerospace industry in applications such as the radome and fairing skins of the Airbus A-320 [52].

2.2.3.3 Carbon Fibres

Carbon fibres are defined as fibres containing at least 93% carbon content by weight [5]. The microstructure of carbon fibres is arranged in graphitic structure, which consists of parallel hexagonal basal planes of carbon atoms with covalent bonds holding carbon atoms in the basal planes and van der Waals bonds holding the basal planes in the transverse direction [1, 2], Figure 2.6. Due to the difference in strength of bonding in longitudinal and transverse directions, carbon fibres have higher tensile strength, modulus, electrical and thermal conductivity in the fibre axis direction than in the transverse direction [1]. This results in highly anisotropic properties of carbon fibres. In addition, the degree of anisotropy of carbon fibres increases with increasing graphitic structure [1, 2, 5].

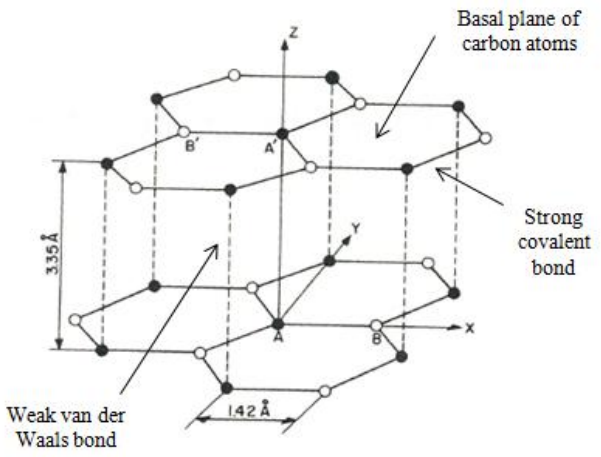

Figure 2.6: Schematic diagram of graphitic structure in carbon fibres showing hexagonal basal plane of carbon atoms with covalent bonds between carbon atoms and van der Waals bonds between basal planes [1]

Among the reinforcing fibres for PMCs, carbon fibres are the most prevalent fibres used in high-performance PMC applications [2, 4]. Because of the high strength, high modulus, and light weight of high-performance carbon fibres, they are used for structural applications for aerospace sector where weight reduction combined with high strength and stiffness are critical [1, 2, 5, 64], refer to Figure 2.3. High thermal conductivity (900-

1000 W/mK) of carbon fibres with high degree of graphitic structure is also an attractive property for using carbon fibres in heat dissipation parts [5]. In addition, carbon fibres possess negative CTE, which enable the design of PMC parts with high dimensional stability [2, 4]. However, brittleness and low impact resistance are the main limitations to the application of carbon fibres in structural parts [1, 2, 5]. Strong bonding between carbon fibres and the matrix is therefore required to enable the matrix to support the fibres during compressive loads and interlamina shear [1]. From the machining point of view, abrasiveness and high electrical conductivity of carbon fibres causes problems during machining, e.g., high rate of abrasive wear on the tool, wear on the machine tool surfaces, and short-circuit of electrical equipment in machine tool [2, 4, 47].

In Table 2.1, specific tensile strength, specific modulus, and maximum usage temperature of carbon fibres are compared with glass and aramid fibres. High-strength carbon fibres offer higher specific strength than both E-glass and S-glass fibres. Although the specific strength of carbon fibres is lower than that Kevlar fibres, the maximum usage temperature and specific modulus of both high-strength and high-modulus carbon fibres are higher than Kevlar fibres. Considering specific modulus, carbon fibres (both high-strength and high-modulus) have the highest specific modulus when compared to glass and Kevlar fibres. However, the cost of carbon fibres is higher than those of glass fibres and Kevlar fibres, so they are limited to use in high-performance applications [2, 5].

Table 2.1: **Comparison of specific tensile strength, specific modulus, and maximum usage temperature in an oxidizing atmosphere for glass, aramid (Kevlar), and carbon fibres, Note: [a]data from[65], [b]data from[5], [c]data from[66], [d]data from [67]**

Fibre material	Density[a] (g/cm^3)	Modulus of Elasticity[a] (GPa)	Tensile Strength[a] (GPa)	Specific Tensile Strength ($Pa/(kg/m^3)$)	Specific Modulus ($Pa/(kg/m^3)$)	Maximum Usage Temperature in an oxidizing atmosphere (°C)
E-glass	2.58	75	3.5	1.36	29.07	500[b,c]
S-glass	2.46	90	4.5	1.83	36.59	
Kevlar29	1.44	65	2.8	1.94	45.14	200[b,d]
Kevlar49	1.44	125	3.5	2.43	86.81	
T-300 carbon fibre (High-strength)	1.76	235	3.2	1.82	133.52	500[b]
Amoco P-100 carbon fibre (High-modulus)	2.15	725	2.2	1.02	337.21	

Carbon fibres for high-performance PMC applications are manufactured from either polyacrylonitrile (PAN) or mesophase pitch [1, 2, 4, 5].

PAN-based Carbon Fibres

The Polyacrylonitrile (PAN) precursor results from the polymerization of acrylonitrile monomer (CH_2=CH-CN) [1, 5]. Since PAN tends to decompose before it melts, PAN precursor fibres are produced by wet-spinning a solution produced by dissolving PAN in solvents such as sodium thiocyanate and dimethyl formamide [5, 64]. The PAN precursor solution is extruded through a spinnerette into a coagulation bath. In the coagulation bath, extruded PAN solution is precipitated into PAN fibres composed of a fibrillar, or ribbon like network structure with preferred orientation along the fibre axis direction due to the shearing force during extrusion [1, 5, 64]. Stretching is then applied to increase structural orientation along the fibre axis direction to yield carbon fibres with adequate strength and modulus in longitudinal direction after final heat treatment step [1, 5, 64]. After stretching, the as-spun PAN fibres have to be stabilized to be able to withstand high temperatures and maintain molecular and fibrillar orientation during carbonization step [5, 64]. Oxidative stabilization of PAN fibres is conducted in air at temperatures of 230-280°C under tension, which is applied to minimize the relaxation of PAN fibre structure [64]. This step will crosslink PAN fibres, forming ladder PAN polymers that can withstand high temperatures during the carbonization step [68]. The stabilized PAN fibres are then carbonized in an inert atmosphere, which prevents oxidization during the process [1], at temperatures of 980-1595°C to convert them into carbon fibres [5]. During the carbonization step, non-carbon elements are eliminated in the form of gases such as water vapour, carbon dioxide (CO_2), ammonia (NH_3), hydrogen cyanide (HCN), and methane (CH_4) [5, 68]. Due to the fibrillar or ribbon-like network structure of PAN fibres, PAN-based carbon fibres are composed of ribbons of hexagonal planes of carbon atoms in the form of turbostratic graphite layers in the structure [1, 5, 64, 68], Figure 2.7. If graphite fibres, which consist of 99% carbon content and have higher modulus than carbon fibres [5], are required, graphitization can be done in an inert atmosphere at the temperatures above 2700°C to increase degree of graphitic structures and, thus, modulus of the fibres [1, 5].

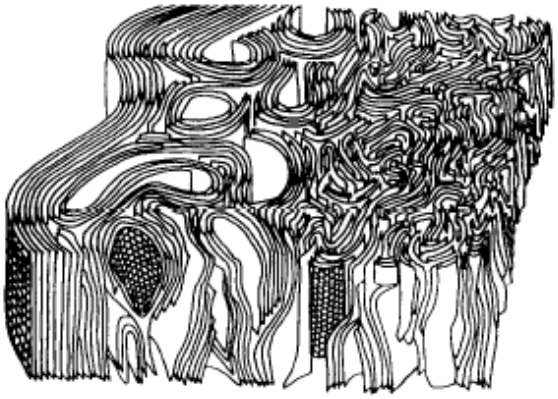

Figure 2.7: Schematic diagram representing microstrcuture of PAN-based carbon fibre by Johnson [69]

Due to this fibrillar nature and turbostratic structure, PAN-based carbon fibres are less sensitive to flaw-induced failure and, hence, have higher tensile strength than mesophase pitch-based carbon fibres [1, 5, 64, 69]. Johnson [69] was the first who explained this by using Reynolds and Sharp's brittle-failure mechanism, Figure 2.8. Although fibrils in the structure of PAN-based carbon fibres are aligned and oriented parallel to the fibre axis direction, there are still some misalignments such as interlinks between turbostractic layers in the structure, Figure 2.8a. As tension is applied parallel to the direction of the fibre axis, the turbostractic layers are stretched and increasingly aligned until the movement is limited by interlinks between these layers. Consequently, tensile stress is building up within these interlinks. When the tensile stress reaches a sufficient level, these interlinks are broken, causing a crack in the direction normal to the fibre axis, Figure 2.8b. This crack within the structure will not cause failure unless its size is greater than critical flaw size of the fibre, Figure 8c. For the crack to be greater than critical flaw size of the fibre, the crack must occur within the interlinks having crystallite size greater than critical flaw size, or there must be continuity in graphitic structure surrounding the crack so that it can propagate [69]. In PAN-based carbon fibre, there is low degree of graphitization and spaces between turbostratic layers are larger than those of graphitic crystallite [5, 64]. This limits the size and continuity of graphitic crystallite, enabling a PAN-based carbon fibre to withstand higher tensile stress. Consequently, PAN-based carbon fibres can be produced to possess higher tensile strength (up to 7 GPa) than mesophase pitch-based carbon fibres (up to 4 GPa), which have higher degree of graphitic structure and lager crystallite size [1, 5, 64]. PAN-based carbon fibres are therefore the main precursors for producing high-strength carbon fibres [1, 2, 4, 5].

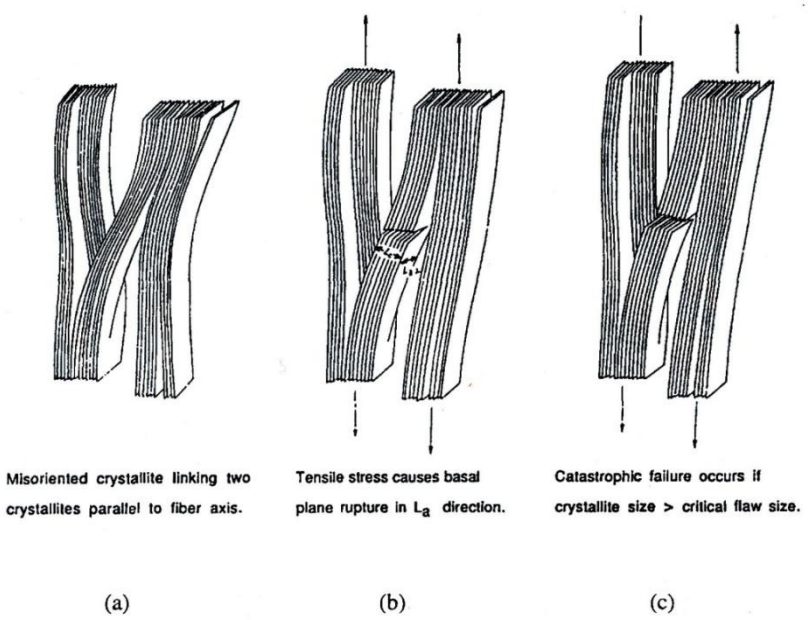

Figure 2.8: Diagrams representing Reynolds and Sharp mechanism of tensile failure in carbon fibres [69]

The less ordered, fibrillar structures with low degree of graphitization of PAN-based carbon fibres also results in lower elastic modulus of the carbon fibres that can be produced (up to 585 GPa) compared to mesophase pitch-based carbon fibres (up to 900 GPa) [1, 2, 4, 5, 64]. However, the elastic modulus of carbon fibres can be increased by increasing the final heat treatment temperature, which results in the increased molecular orientation of graphitic structure in the fibre axis direction [1, 2, 4, 5, 68]. The alignment of graphitic structure in carbon fibres increases with increasing heat treatment temperature, thus increasing elastic modulus of the carbon fibres [1, 2, 5, 64], Figure 2.9. In addition, tensile strength of carbon fibres also increases with increasing heat treatment temperature due to higher degree of molecular orientation along the fibre axis [1, 5, 64, 68]. Nevertheless, tensile strength of carbon fibres abruptly decreases when the heat treatment temperature exceeds 1600°C [70], beyond the red line in Figure 2.9. This is because the increased alignment of graphitic structure and the increase in crystallite size due to increasing heat treatment temperature provide greater continuity for the cracks during tensile loading to propagate, leading to flaw-induced failure as previously discussed [5, 70].

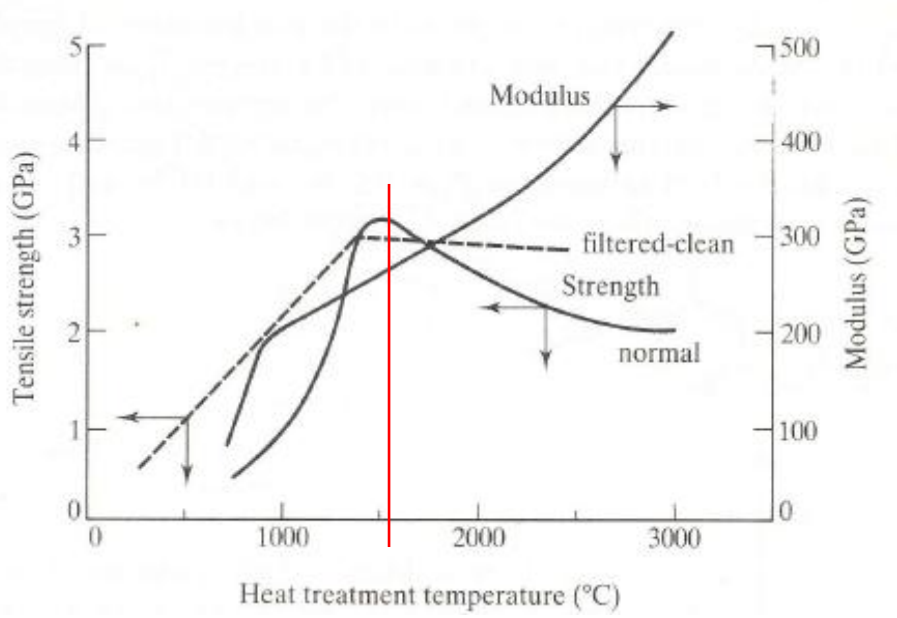

Figure 2.9: Effect of heat treatment temperature on tensile strength and modulus of carbon fibres [68]

Pitch-based Carbon Fibres

High performance pitch-based carbon fibres are manufactured from mesophase pitch, which is an anisotropic liquid crystalline with polyaromatic layers aligned parallel in longitudinal direction [1, 5, 64, 71]. Mesopahse pitch precursor can be produced by heating isotropic pitch, which is the precursor for low cost, low strength and low modulus pitch-based carbon fibres, to a temperature of 400-425ºC for up to 40 hours [1, 5]. Due to polyaromatics in the structure, mesophase pitch precursor has good thermal stability and it does not decompose before melting [5, 64]. As a consequence, mesophase pitch precursor fibres are manufactured by melt spinning process [1, 2, 4, 5, 64, 71].

The production process of mesophase pitch-based carbon fibres starts by melting the mesophase pitch precursor and extruding the melted precursor through a spinneret to form precursor fibres. The shearing force during extrusion enhances molecular orientation of mesophase pitch precursor fibres along the fibres direction, as in the case of PAN-based precursor fibres [5, 71]. The pitch precursor fibres are then stabilized in air at the temperatures of 230-280ºC in order to crosslink the thermoplastic pitch, converting into thermosetting pitch fibres that can withstand high temperatures and maintain molecular orientation during carbonization step [1, 64]. After being stabilized, mesopahse pitch fibres are carbonized in an inert atmosphere at the temperatures of 1000-2000ºC to convert the pitch fibres into carbon fibres [1, 5]. Similar to the production process of PAN-based carbon fibres, non-carbon elements are eliminated as gases such as water vapour, carbon dioxide (CO_2), methane (CH_4), and ammonia (NH_3) [1, 5, 64, 71]. Then graphitization in an inert atmosphere at 2760-3040ºC can be done if graphite fibres are needed [5].

As previously discussed, mesophase pitch-based carbon fibres have higher elastic modulus and lower tensile strength than PAN-based carbon fibres because of higher degree of graphitic crystallite and higher molecular orientation along the fibre axis direction [1, 2, 4, 5, 64, 71]. Similar to PAN-based carbon fibres, elastic modulus of the fibres continuously increases with increasing heat treatment temperature during carbonization process but tensile strength of the fibres increases until reaching a maximum at 1600ºC and abruptly decreases [2, 5, 64, 70], Figure 2.9. In addition, because of more alignment of graphitic structure along the fibre axis compared to PAN-based carbon fibres, mesophase pitch-based carbon fibres have higher thermal conductivity (900-1000 W/mK) in fibre axis direction than PAN-based carbon fibres (10-20 W/mK) [5, 71]. As a consequence, mesophase pitch-based carbon fibres are mainly used for the applications in which stiffness and good heat dissipation capability are more important than strength [5, 71].

2.3 Conclusion

In conclusion, among various types of composite materials, PMCs are suitable for the applications in which light weight, high specific strength and modulus are required. However, they are limited to lower temperature applications compared to MMCs and CMCs due to lower thermal stability of the polymeric matrix. The most commonly used PMCs in high-performance applications such as in aerospace applications are thermosetting plastics, especially epoxy resin for low to moderate temperature applications, reinforced with long continuous carbon fibres or CFRPs. The reason is because of higher mechanical properties with lower processing temperature of thermosetting plastics compared to thermoplastics and high strength, stiffness and light weight of long continuous carbon fibres. Unfortunately, the abrasive nature and anisotropy of CFRPs result in problems during machining which will be discussed in detail in Chapter 3.

3 Review of Conventional Drilling of Carbon Fibre Reinforced Plastics

3.1 Introduction

As discussed in Chapter 1, secondary machining processes are generally applied to produce final CFRP parts or components with desired specification, tolerance and functionality even though they can be produced in a near-net-shape. Among the secondary machining processes, drilling is commonly applied in order to produce holes for assembly of CFRP parts or components [3, 4, 7-9]. Several drilling processes are used for CFRP parts including conventional drilling processes and non-conventional processes such as laser drilling, ultrasonic drilling, and abrasive water jet drilling. Among the hole-making processes, conventional drilling processes using a drilling tool are essential and the most widely used for routine hole-making processes in the aerospace industry [3, 4, 7-9, 11, 47, 55]. However, there are still machining problems associated with conventional drilling processes of CFRPs such as delamination, fibre pull-out, poor quality of machined surface and high rate of tool wear due to heterogeneity, anisotropic properties and abrasive nature of the material [4, 7-10]. Since the use of CFRPs in high-performance applications in automotive and aerospace industry has been growing, much of the research work, which aims to understand the drilling process associated with CFRPs, develop drilling technologies to reduce drilling-induced problems and increase productivity of the production process has been performed. This chapter therefore presents a review of the literature and discuss the fundamentals of the conventional drilling processes, drilling-induced defects and the technological development of conventional drilling processes aiming to reduce the defects associated with drilling of CFRPs. In addition, a brief discussion about non-conventional drilling processes is presented in this chapter as a comparison to conventional drilling processes. Since carbon/epoxy composite is widely used in aerospace industries and is being used as the workpiece material in this research, the review of the literature focuses on the conventional drilling of carbon/epoxy composites. Finally, the motivation and research gap contributing to the objectives of this research regarding application of CO_2 gas as a cutting fluid in the conventional drilling of CFRPs is discussed.

3.2 Fundamentals of Conventional Drilling of Carbon Fibre Reinforced Plastics

3.2.1 Mechanics of Chip Formation

In metal machining, the major mechanism controlling chip formation is shearing with extensive plastic deformation of workpiece material in primary and secondary shear zones [3, 72, 73]. As a result of high cutting pressure, shearing of the workpiece material ahead of the edge of the cutting tool (primary shear zone) and at the interface where the tool and the workpiece are in contact (secondary shear zone) occurs, resulting in extensive plastic deformation in the shear zones. Chips are produced once the force of the cutting process is sufficient to overcome shearing strength of the workpiece material in primary shear zone and overcome seizure between the tool and the workpiece and friction at the boundary of the seizure zone in secondary shear zone. However, the mechanism controlling the chip formation in the machining of CFRPs differs from the metal machining due to the anisotropic properties, lower strength and ductility of the workpiece material [4, 8, 74, 75]. When machining CFRPs, chips are produced from a series of brittle fractures combined with shearing at the fibre/matrix interfaces with limited plastic deformation and without significant shear zones, which is observed in metal machining, [4, 8, 74-78]. Discontinuous chips are therefore produced as a result of this brittle fracture mode of chip formation with limited plastic deformation attributed to brittleness of epoxy matrix and carbon fibres [4, 8, 75, 79]. The angle of fibre orientation relative to the cutting direction, which will be referred as “relative fibre orientation”, has a dominant influence on the mechanism of cutting as the material will respond differently to the cutting force depending on the direction of the applied load [4, 8]. This dependence of the cutting mechanism on the relative fibre orientation also contributes to variations in cutting forces and characteristics of machined surface. Cutting mechanisms, associated cutting forces and characteristics of machined surfaces for different relative fibre orientations have been discussed in previous work by other researchers [4, 8, 17, 74-78, 80]. A schematic diagram showing a summary of the major types of cutting mechanism based on the varied relative fibre orientation when machining CFRPs is presented in Figure 3.1.

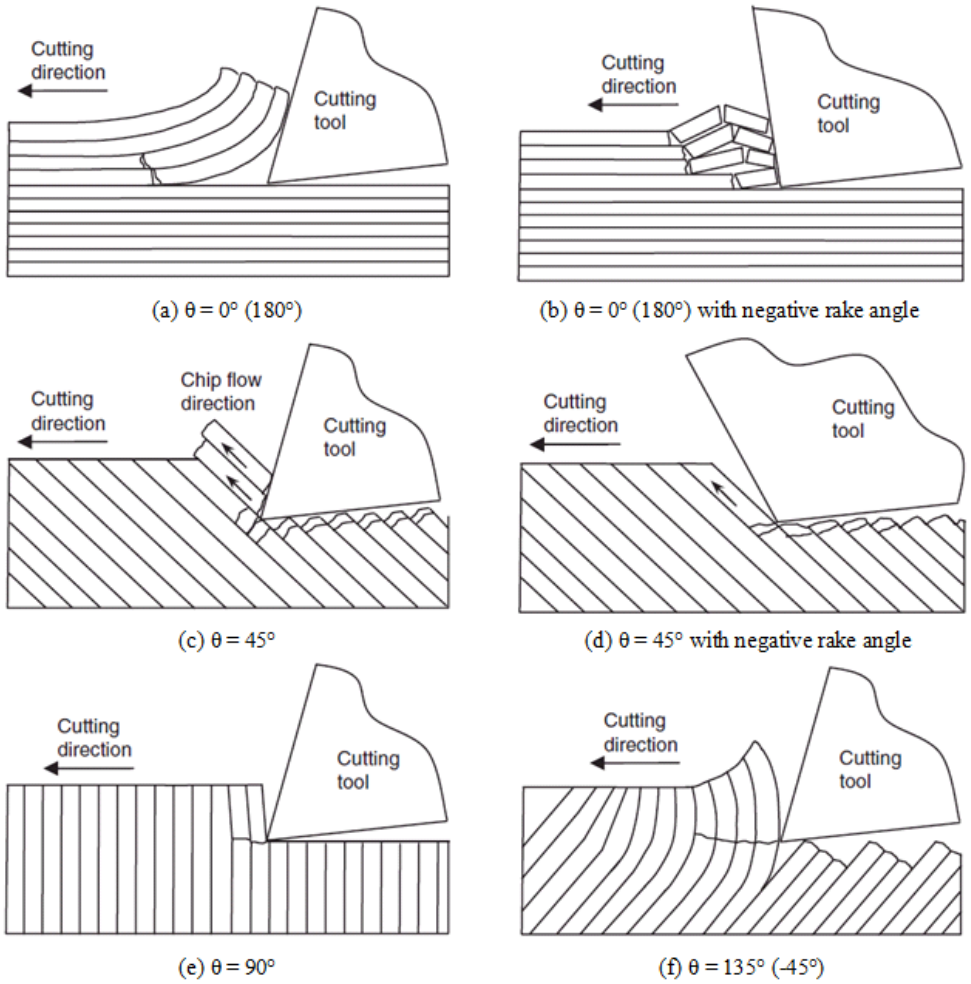

Figure 3.1: Schematic diagram showing the major types of cutting mechanism based on different angles of fibre orientation relative to the cutting direction (θ) when machining CFRPs. (a) θ = 0° (180°), (b) θ = 0° with negative rake angle of the tool, (c) θ = 45°, (d) θ = 45° with negative rake angle of the tool, (e) θ = 90° and (f) θ = 135° (-45°) (adapted from [4, 78])

Relative Fibre Orientation (θ) of 0°

When machining at θ = 0°, the mechanism of chip formation when machined with a tool with positive rake angle is dominated by delamination along the fibre/matrix interface as a result of mode I (peeling/opening) loading and bending-induced fracture of the laminates [75-78], Figure 3.1a. During the cutting process, cracks are initiated at the fibre/matrix interface ahead of the cutting edge of the tool as a result of the cutting load from the tool. As the tool moves in the cutting direction, the laminates are subjected to peel-up force by the cutting edge of the tool causing crack propagation in the cutting direction along fibre/matrix interface and, hence, delamination due to mode I (opening) loading. Delamination due to mode II (in-plane shearing) loading also occurs as laminates are subjected to pushing force from the advancement of the tool. However, it was proposed that delamination resulting from peeling up of laminates (mode I fracture) is more dominated when machining with a tool with positive rake angle [4, 75, 78]. The peeled up laminates

then move up the rake face of the tool during the advancement of the tool, causing bending of laminates similar to a cantilever beam. Finally, bending-induced fracture of laminates in the direction perpendicular to the fibre axis occurs ahead of the tool, producing a discontinuous chip. This cycle of delamination, bending and fracture of laminates producing discontinuous chips is repeated as the cutting process continues. In addition, this repeated cycle of chip formation contributes to high fluctuations of the cutting forces [4, 75, 78].

When machining with a tool with negative rake angle, the chip formation is more dominated by delamination as a result of mode II (in-plane shearing) loading and buckling-induced fracture of the laminates [4, 8, 78], Figure 3.1b. In this case, the laminates are subjected to compressive loading as a result of the advancement of the tool in the cutting direction, causing buckling of the laminates and crack initiation at the fibre/matrix interface. As the tool continues moving in the cutting direction, cracks are propagated in the direction parallel to the fibre orientation and delamination occurs as a result of mode II (in-plane shearing) loading. Finally, fracture resulting from the continuous buckling of the laminates occurs in the direction perpendicular to the fibre axis, producing a discontinuous chip, which is shorter compared to that being produced when machining with a positive rake-angle tool. This cycle of delamination, buckling and fracture is then repeated as the cutting process continues. This repeated cycle of chip formation also contributes to fluctuations of the cutting forces.

An example of the machined surface resulting from the orthogonal cutting of CFRPs at $\theta = 0°$ is shown in Figure 3.2. It can be observed in Figure 3.2 that fibres on the machined surface are partly embedded in the epoxy matrix due to elastic recovery of the fibres after being subjected to bending or buckling load from the tool [4, 77, 78]. In addition, as the tool moves along the machined surface, the cutting edge of the tool causes compressive load on the fibres, resulting in fracture perpendicular to the fibre direction [4, 77, 78].

Figure 3.2: SEM image of the machined surface resulting from the orthogonal cutting of CFRPs at θ = 0° showing fibres partly embedded in the epoxy matrix and cracks across the fibre axis [74]

Relative Fibre Orientation (θ) of 45°

When machining at θ = 45°, the mechanism of chip formation is dominated by fracture across the fibre axis as a result of compression-induced shearing and stretching of the fibres combined with shearing fracture along the fibre/matrix interface as the tool proceeds in the cutting direction [75, 77, 78], Figures 3.1c and 3.1d. During the cutting process, the fibres are compressed by the cutting edge of the tool as it moves in the cutting direction. This results in compressive-induced shearing and stretching (tension) of the fibres in the area where the fibres are subjected to compression by the cutting edge of the tool. Cracks are then initiated below and above the point of compression (cutting point), and fractures of the fibres occur in a direction perpendicular to the fibre axis. After fracture, fibres elastically return to their initial position before they were stretched [4, 75, 78]. It was proposed that this elastic recovery of the fibres causes abrasive wear on flank face of the tool as the fibres make contact with the flank face when the tool proceeds during the elastic recovery of the fibres [4, 75, 78]. It was also reported that highest flank wear and thrust force were produced when machining at θ = 45-60° due the elastic recovery of the fibres [78, 80-82]. Then, the fractured laminates above the cutting point move along the rake face during the advancement of the tool. Due to friction at the tool/workpiece interface on the rake face, fractured laminates are forced to flow in the direction parallel to the fibre orientation, resulting in shear stress at the fibre/matrix interface. Finally, a discontinuous chip is produced when shearing fracture at the fibre/matrix interface occurs. This mechanism of chip formation also applies to machining at 0° < θ < 90° [4, 8, 17, 78, 80]. However, the length of the discontinuous chips decreases as relative fibre orientation increases [4, 8, 78]. This is due to the increase of shearing stress at the fibre/matrix interface with the increase of relative angle of fibre orientation, resulting in more possibility for shearing fracture forming

the discontinuous chips [4, 8, 78, 80]. The length of the chips also decreases when machined with a tool with negative rake angle, Figure 3.1d, which is also due to the higher shear stress at the fibre/matrix interface as the laminates move up the rake face of the tool [4, 78].

Since the machined surface produced when machining at θ = 45° results from shearing and stretching-induced fractures of the fibres, the machined surface was observed to be more irregular compared to at θ = 0°, which results from peeling of the laminates, revealing short broken fibres being covered with smeared epoxy matrix [4, 8, 77, 78]. Due to the uncontrollable fracture point during cutting of the fibres, protrusion of fibres with varying lengths on the machined surface was observed [4, 8, 77, 78].

Relative Fibre Orientation (θ) of 90°

The mechanism of chip formation when machining at θ = 90° also involves fracture across the fibre axis and interlamina shear fracture along the fibre/matrix interface [75-78] , Figure 3.1e, similar to at θ = 45°. However, fracture across the fibre axis ahead of the cutting edge results from severe bending of the fibres due to compression by the cutting edge as the tool advances in the cutting direction [75-78]. In addition, the severe bending of the fibres also causes delamination as a result of the mode I (opening) load [75-78]. Combined with a compressive load from the tool tip during the advancement of the tool, cracks along the fibre/matrix interfaces into the machined surface (0.1-0.3 mm deep [76]) are produced [75-78]. After being fractured, the laminates above the fracture plane make contact with the rake face as the tool moves forward. Similar to machining of 45° relative fibre orientation, interlamina shear stress occurs along the fibre/matrix interfaces as a result of friction at the tool/workpiece interface on the rake face. Finally, interlamina shear fracture at the fibre/matrix interface occurs, producing a discontinuous chip. As previously discussed, the increase of relative angle of fibre orientation results in an increase of interlamina shear stress along the fibre/matrix interfaces due to the higher friction a the tool/workpiece interface [4, 8, 78, 80]. As consequence, it was proposed that the discontinuous chips produced when machining at θ = 90° are smaller and shorter than those produced when machining at θ = 45° [4, 8, 77, 78]. After fracture, the fibres elastically return to their position at which they were before being bended [4, 75, 78], similar to θ = 45°. This, again, contributes to abrasive wear on the flank face as the fibres make contact with the flank face of the tool during their elastic recovery [4, 75, 78]. However, thrust force, which was due to contact between the elastically recovered fibres and the cutting edge, when machining at θ = 90° was reported to be lower than that for machining θ = 45-60° [74, 75, 78, 80, 81]. The author suggests that this was because the fibres have weaker support from the laminates when they make contact with the tool during their elastic recovery when machining at θ = 90°, which was due to increased damage of the laminates on the machined surface. However, the cutting force was reported

to be higher than that for machining at θ = 0°, 45° and 135° as a result of the higher force required for severe bending of the fibres before cutting and higher interlamina shear stress along the fibre/matrix interfaces required for producing the chips [74, 75, 78, 80, 81].

Similar to θ = 45°, the machined surface resulting from machining at θ = 90° was observed to be irregular with fractured fibres protruding to various lengths from the machined surface [4, 76-78], Figure 3.3. The variations in the length of the protruding fibres was because of the uncontrollable bending-induced fracture point of fibres during cutting [4, 8, 76, 78]. A cover of smeared epoxy matrix was also observed [4, 76-78], Figure 3.3. As previously discussed, the bending-induced delamination in mode I fracture and compressive load from the tool tip results in cracks into the machined surface along the fibre/matrix interface being observed [4, 8, 76, 78].

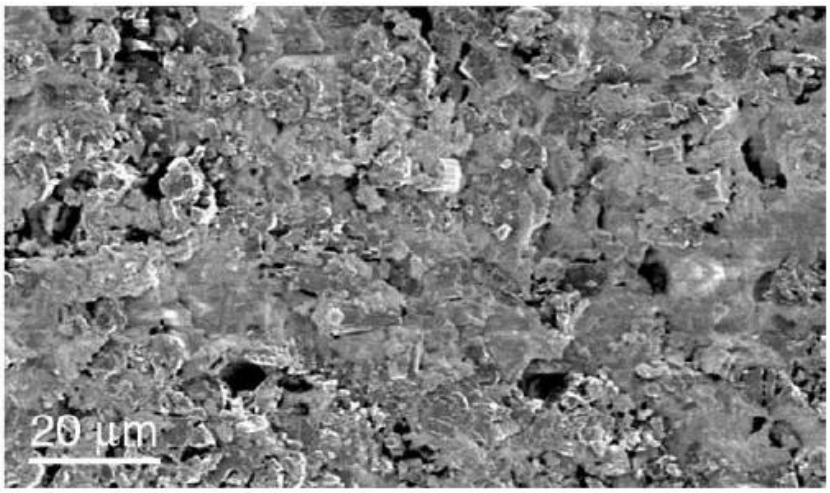

Figure 3.3: SEM image of the machined surface resulting from the orthogonal cutting of CFRPs at θ = 90° showing fractured fibres protruding from the machined surface with a cover of smeared epoxy matrix [74]

Relative Fibre Orientation (θ) of 135°

When machining at θ = 135° or 90° < θ < 180°, the mechanism of chip formation is dominated by macro fracture of the fibre bundles, combined with delamination and interlamina shear fracture along the fibre/matrix interface, as a result of severe bending and compression on the laminates by the tool [4, 8, 75, 77, 78], Figure 3.1f. As the tool moves in the cutting direction, the fibre bundles are subjected to severe bending and compression from the cutting edge resulting in macro fracture ahead of the cutting edge perpendicular to fibre orientation. In addition, delamination and interlamina shear fracture along the fibre/matrix interfaces below the fracture point (into the machined surface) also occur due to the extensive bending and compressive load on the laminates. As the tool advances, fractured laminates above the fracture plane are bent as they move along the rake face of the tool, causing shear stress along the fibre/matrix interfaces. Finally, large discontinuous chips

in bulk form are produced as these laminates are fractured and pulled-out. Similar to when machining at θ = 45° and 90°, the fractured fibre bundles below the fracture point elastically recover to their initial positions prior to fracture contributing to abrasive wear on the flank face as they make contact with the flank face during their elastic recovery [4, 75, 78]. Since fracture occurs on the plane significantly lower than the contact point between the cutting edge and laminate when machining at θ = 135°, Figure 3.1f, thrust force due to the contact by the elastically recovered fibres was observed to be lower than that for θ = 45° and 90° [4, 8, 74, 75]. However, cutting force was reported to be higher than that for when machining at θ = 0° and 45° due to severe bending and compression of the laminates [4, 8, 74, 75]. Nevertheless, the cutting force was reported to be lower than that for θ = 90° [4, 8, 74, 75]. This was because, when machining at θ = 90°, fibres are bent and cut rather than being bent and pull-out when machining at θ = 135°, thus requiring higher force for cutting [75]. Piquet *et al.,* [17] also suggested that the fibres undergo most elastic deformation when machining at θ = 90°, resulting in the expected highest cutting force being produced.

An example of the machined surface resulting from when machining at 90° < θ < 180° is shown in Figures 3.4 and 3.5. As a consequence of macro fracture of fibre bundles and severe bending and compression of the laminates, rough machined surface consisting of protruding fibre bundles with various lengths is produced from the machining of these fibre orientations, Figure 3.4. Damage on the machined surface in the form of delamination and interlamina fracture along the fibre/matrix interface into the machined surface could also be observed, Figure 3.5. In addition, the evidence of severe bending of the fibre bundles could also be observed in the cross-section of the machined surface in Figure 3.4.

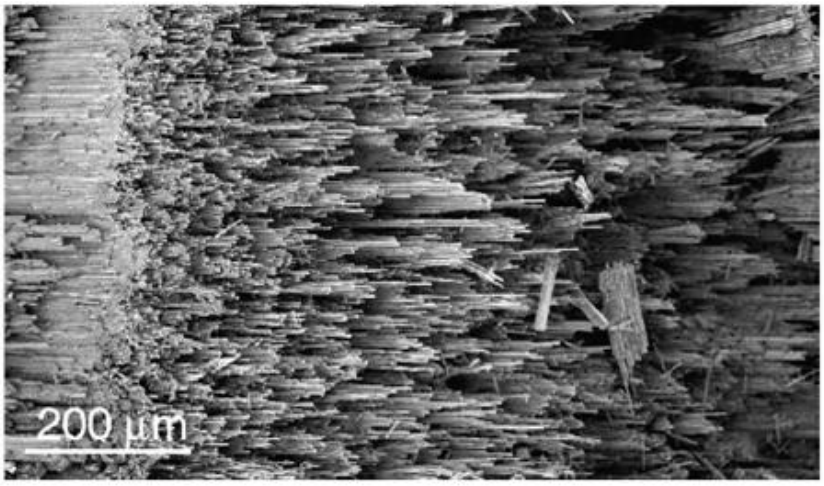

Figure 3.4: SEM images showing top view of machined surface resulting from the orthogonal cutting of CFRPs at θ = 150° showing protruding of fibre bundles with various lengths [74]

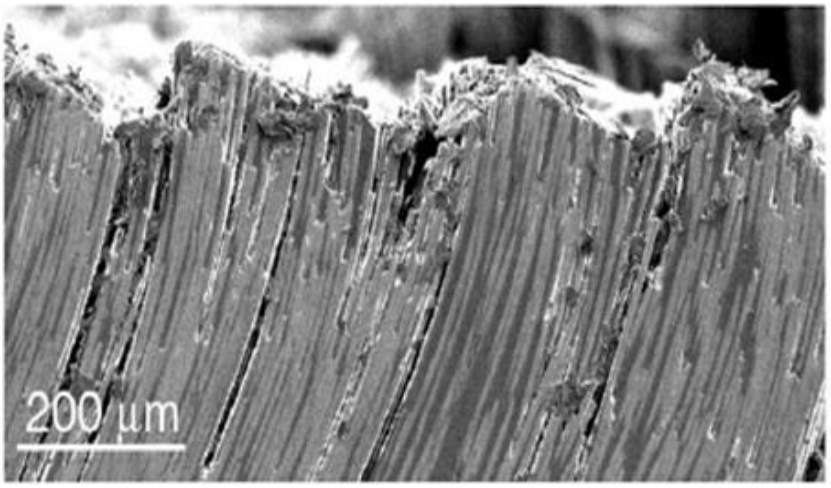

Figure 3.5: SEM image showing cross-section of the machined surface resulting from the orthogonal cutting of CFRPs at θ = 120° showing the evidence of severe bending of the fibre bundles and interlamina fracture along the fibre/matrix interface into the machined surface [74]

The influence of relative fibre orientation angle on cutting mechanism and resulting cutting forces and machined surface also occurs in drilling of CFRPs but the relative fibre orientation will vary in one revolution of the drill. When drilling uni-directional CFRPs, the cutting edges will undergo cutting at various relative fibre orientations as they rotate during the revolution of the drill [4, 8], Figure 3.6. As a consequence, cutting mechanism and resulting drilling forces and characteristics of the machined surface vary in cyclic during one revolution of the drill [4, 8]. When drilling multi-directional CFRPs, they vary both during one revolution of the drill as well as for different laminates in through-the-thickness direction as the fibre orientation also varies for different laminates [4, 77, 83]. The dynamic cutting mechanism during drilling would contribute to poor quality of surface finish and damage to the machined surface such as fibre pull-out, delamination, material chip-out and matrix cracking when drilling CFRPs [3, 4, 8-10]. However, the variations in drilling force based on different relative fibre orientations would not affect performance evaluation when drilling CFRPs as the average or maximum value during steady region of the force will be used [4].

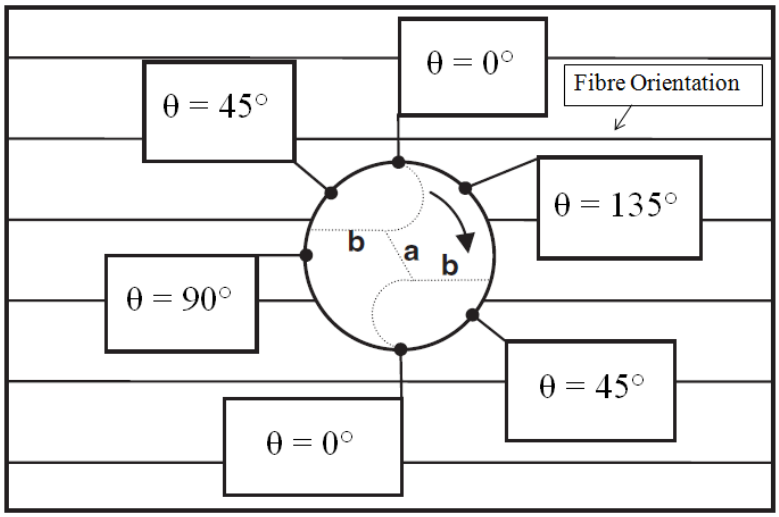

Figure 3.6: Schematic diagram showing variations in relative angle of fibre orientation (θ) during one revolution of the drill when drilling a uni-directional CFRP with 0° fibre orientation (adapted from [4])

3.2.2 Thrust Force and Torque

Thrust force during a drilling process is one of the important factors for performance evaluation because the amount of thrust force produced significantly affects tool life and quality of the drilled holes, particularly the amount of delamination damage in the drilling of carbon/epoxy composites [7, 9, 10, 47, 55]. Drilling torque is another factor that can be used for performance evaluation of drilling processes because it also indicates the cutting force required and, hence, affects tool life [7, 9, 10, 47, 55]. For this reason, it is useful to understand the characteristics of thrust force and torque being produced when drilling CFRPs as well as the factors affecting them. Before discussing the profile of thrust force and torque and their influencing factors, it will be useful to know typical geometry parameters of a drill such as chisel edge, major cutting edges or lips, drill point angle and minor cutting edge which have a dominant effect on the profile and variations of thrust force and torque. A schematic diagram showing geometry parameters of a conventional two flute twist drill is shown in Figure 3.7.

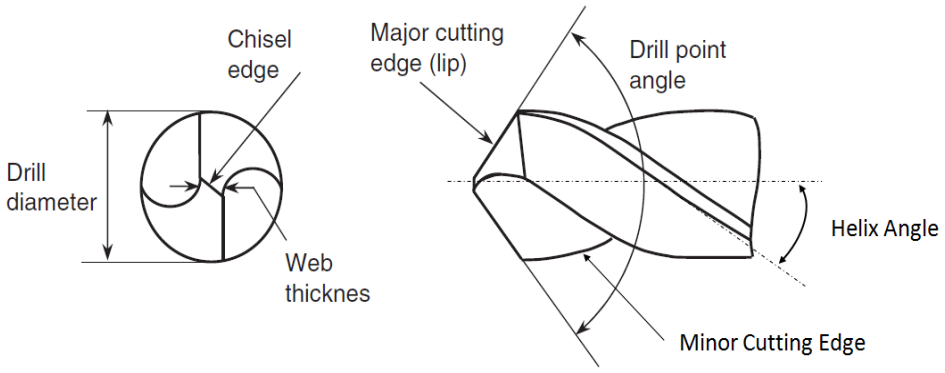

Figure 3.7: Geometry parameters for a conventional two flute twist drill (adapted from [4])

3.2.2.1 Profile of Thrust Force and Torque

A schematic diagram showing the typical profile of thrust force and torque with time when drilling a through-hole in CFRP laminates by a standard two-flute twist drill is shown in Figures 3.8. As the chisel edge of the tool engages the top laminates of the workpiece, (a) in Figures 3.8a and 3.8b, thrust force significantly increases but torque gradually increases at a relatively slow rate compared to thrust force [3, 14, 47, 84]. As the cutting lips begins to the engage in the cutting, (b) in Figures 3.8a and 3.8b, both thrust force and torque gradually increase [3, 14, 47, 84]. Then, thrust force continues increasing until reaching a maximum value when both the chisel edge and full length of the main cutting lips of the drill engage in the cutting [3, 14, 17, 47, 84], (c) in Figure 3.8a. However, torque significantly increases at a faster rate relative to thrust force when the full length of the main cutting lips of the drill engage in cutting, (c) in Figure 3.8b even though it has not reach a maximum value [3, 14, 47, 84]. During the period from full engagement of the chisel edge and the main cutting lips to the moment when the drill reaches the exit of the laminates, (c)-(d) in Figures 3.8a and 3.8b, thrust force remains constant [3, 17, 47, 84] but torque gradually increases until reaching a maximum value at the moment when the chisel edge of the drill reaches the exit of the laminates [3, 14, 47, 84], (d) in Figure 3.8b. However, it was demonstrated by Di Paolo *et al.*, [14] that thrust force slightly decreased during this period of the drilling process and suggest this to result from the softening of the epoxy matrix by the accumulated heat of the process. The author suggests the slight decrease of thrust force during this period of drilling process was also due to the decrease of uncut thickness of the laminates, which contributed to lower thrust force as a result of these being less resistance to the cutting. As the chisel edge of the drill penetrates through the exit of the laminates, (e) in Figure 3.8a, thrust force significantly decreases and drops to a negligible value, which could consider a "zero" value, when the chisel edge and the main cutting lips both emerge out of the laminates [3, 14, 17, 47, 84], (f) in Figure 3.8a. Abrate and Walton [47] and Davim *et al.*, [3] proposed that thrust force could decrease to a negative value, as a pulling force, when the chisel edge of the drill penetrate through the exit of the laminates. This could be due to the retraction of the drill. However, torque gradually decreases as the chisel edge of the drill penetrates through the exit of the laminates [3, 14, 47, 84], (e) in Figure 3.8b. It is then reduced to a "non-zero" value when the chisel edge and the main cutting lips penetrate the laminates as a result of force due to friction between minor cutting edges and the hole surface [3, 14, 47, 84], (f) in Figure 3.8b. Finally, thrust force and torque remain constant until the end of the drilling process, from (f) in Figures 3.8a and 3.8b. The thrust force and torque during the period from the moment when the chisel edge and main

cutting lips of the drill emerge out of the laminates until the end of the process, from (f) in Figures 3.8a and 3.8b, result from the force due to friction between the minor cutting edges of the drill and the hole surface [3, 14, 47].

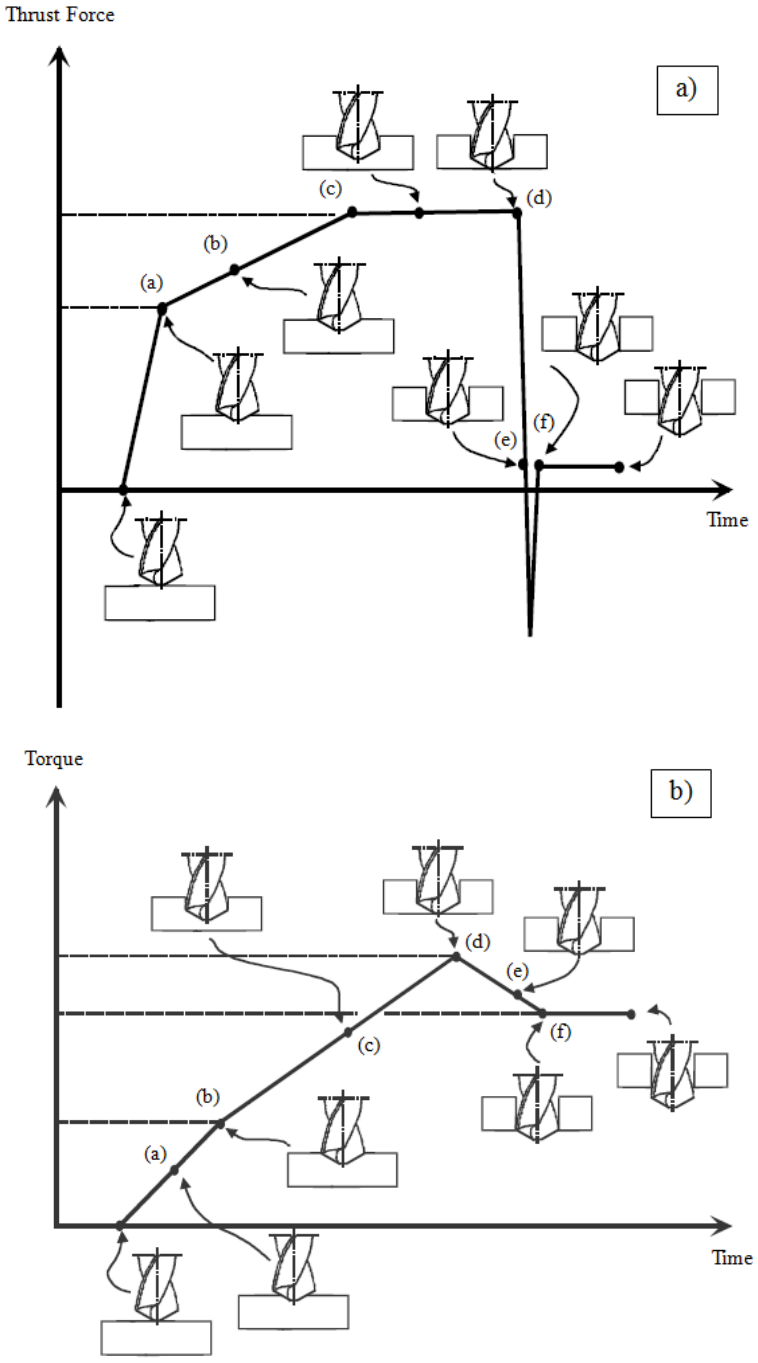

Figure 3.8: Diagram showing a typical progress of (a) thrust force and (b) torque with time when drilling a through-hole in CFRP laminates by a standard two-flute twist drill (adapted from [3])

From the progressive increase in thrust force in Figure 3.8a, it can be seen that the indentation force by the chisel edge and the cutting force by the main cutting lips of the drill

both contribute a significant proportion of total thrust force, while the force due to friction between secondary cutting edges of the drill and the hole surface contributes a negligible proportion. In addition, it is also shown that the indentation action by the chisel edge of the drill contributes a major proportion of total thrust force as indicated by the significant increase of thrust force when the chisel edge engages in the drilling process and the significant decrease of thrust force when the chisel edge penetrates through the exit of the laminates, (a) and (e) in Figure 3.8a. This dominant effect of the chisel edge of the drill on the amount total thrust force produced when drilling CFRPs has been reported by other researchers [24, 25, 85, 86]. It was reported by Jain and Yang [85] that the indentation action by the chisel edge of the drill contributed 40-60% of the total thrust force. However, the progress of torque in Figure 3.8 indicates that the chisel edge of the drill does not contribute a major proportion of total torque as reported by other researchers [3, 14, 17, 47]. This is because the indentation of the chisel edge of the drill more dominantly contributes to pushing force in the vertical or axial direction [3, 14, 17, 47]. It was demonstrated by Murphy *et al.,* [87] that the chisel edge of the drill also contributed a major proportion of total thrust force but not for total torque when drilling CFRPs with a four-flute drill. Finally, it can be seen in Figure 3.8b that the force due to friction between the minor cutting edge and the hole surface contribute a more significant proportion of torque compared to that for thrust force, resulting in a "non-zero" value of torque at the end of the drilling process. This is because this frictional force by the minor cutting edge contributes cutting forces in radial dial direction rather than in axial or vertical direction.

3.2.2.2 Effect of Machining Parameters on Thrust Force

The amount of thrust force and torque being produced in conventional drilling of CFRPs are affected by the drill geometry, refer to Figure 3.7. Since indentation action by the chisel edge of the drill has been shown to contribute a major proportion of the total thrust force as previously discussed in Section 3.2.2.1, using drill geometry that reduces the chisel edge action would result in a reduction of thrust force [16, 25, 88, 89]. It has been reported by Jain and Yang [88] and Tsao and Hocheng [25] that thrust force decreased as the length of chisel edge of a twist drill was reduced, given that diameter of the drill, cutting speed and feed rate were kept constant. This was because the effect of indentation action by the chisel edge decreased as the chisel edge length was redcued [88]. Jain and Yang [88] also showed that the thrust force decreased as the point angle of a twist drill was decreased even though its effect on the amount of drilling thrust force was not as significant as that by the chisel edge length. This corresponds to the work of Piquet *et al.,* [17], Chen [16] and Enemouh *et al.,* [89] for which they suggested that a drill with small point angle should be

used to reduce thrust force. Although it was not discussed in their work, the author suggested that this would be because the chisel edge length decreased as the point angle of the drill was decreased, which resulted in a reduction of indentation action by the chisel edge. In addition, it was shown in the work of Chen [16] that thrust force was decreased as the web thickness of the drill was reduced due to the decrease of chisel edge length. However, the author suggested that the strength and rigidity of the drill should also be considered as they would be reduced as the chisel length, web thickness and point angle decreased. Increasing the drill diameter was also shown to result in higher thrust force because of the increase of chisel edge action in the cutting as a result of the increasing chisel edge length [24, 63, 84]. It was shown by Chen [16] that the total thrust force could also be reduced by increasing the helix angle of a twist drill. This was because the orthogonal rake angles at each point on the main cutting lips were increased as the helix angle increased, hence reducing the cutting force from the main cutting lips [16]. However, the effect of a reduction of cutting force on the total amount of thrust force being produced was not as significant as that of a reduction of indenting force by the chisel edge [16]. In addition to changing the geometry of a twist drill, it has been reported that the thrust force was reduced by using the drill with specially designed geometry, which eliminated or reduced the chisel edge action and enhanced cutting action by the main cutting lips [17, 19, 21, 22, 90-92]. This will be discussed later in detail in Section 3.3.2. As previously discussed in Section 3.2.2.1, the total amount of torque was more dominantly affected by the cutting force from the main cutting edges rather than by the indenting force from the chisel edge. As a consequence, the total torque being produced would be decreased by using the drill geometry that reduces the cutting force from the action of the main cutting edges. It has been shown by Chen [16] that torque being produced in the drilling of CFRPs decreased as the point angle and helix angle of a twist drill increased due to the larger orthogonal rake angles along the main cutting lips, which reduced the cutting force from the main cutting lips.

In addition to the drill geometry, the amount of thrust force and torque produced when drilling CFRPs are also affected by feed rate and cutting speed. Similar findings for the effect of feed rate on thrust force and torque have been reported among other researchers. Regardless of the drill geometry and material, it has been shown that thrust force [16, 22, 24, 63, 79, 84, 89, 93-102] and torque [16, 63, 97, 102] increased as feed rate increased. This was due to the larger quantity of workpiece material to be indented by the chisel edge and cut by the main cutting lips as the feed rate increased [4, 24]. For cutting speed, different trends of its effect on thrust force and torque have been reported among other researchers. In the work of Chen [16], Won and Dharan [63] and Tsao and Hocheng [98] it has been reported that thrust force and torque did not vary with cutting speed. Other researchers [89, 94, 95, 101, 103, 104] have shown that thrust force decreased with increasing cutting speed.

It is suggested to be due to the more heat being generated as the cutting speed increased, which decreased the strength of epoxy matrix in the carbon/epoxy composite as a result of higher cutting temperature; hence resulting in lower thrust force as proposed by other researchers [105-108]. Marques *et al.,* [96] proposed that there was a critical value of cutting speed (53 m/min) above and below which the thrust force increased within the tested range of 30-102 m/min for a 6 mm diameter drill. The reason for this trend of the effect was not mentioned in their work and it was suggested that further validation of the results was required. However, it was shown that the effect of feed rate on thrust force was more dominant compared to that of cutting speed [16, 63, 95, 96, 98, 99, 102]. The author suggests that this is because the indenting force in the axial direction, which contributes a major proportion of the total thrust force, is more dominantly affected by the value of feed rate (mm/rev), which determines the quantity of workpiece material to be indented as the drill progresses in the axial direction, rather than by cutting speed. However, Lin and Chen [15] proposed that the effect of cutting speed on thrust force and torque was more dominant compared to the effect of feed rate when drilling CFRPs at high speed (210-850 m/min with 7 mm diameter of the drill). The less dominant effect of feed rate at high cutting speed range was also shown by Gaitonde *et al.,* [105], Karnik *et al.,* [106] and Rubio *et al.,* [107] (600 m/min for 5 mm diameter of the drill). It was reported in the work of Lin and Chen [15] that thrust force and torque increased with the increasing cutting speed. They proposed that the increase of cutting speed in high speed range significantly increased the rate of tool wear, which decreased orthogonal rake angle of the cutting edge as a result of drastic change of tool geometry; hence resulting in higher thrust force and torque [15]. This was contradictory to what has been reported by other researchers that drilling CFRPs at high speed (188-235 m/min [108, 109] and 600 m/min [105-107] for 5 mm diameter of the drill) has shown the benefit of thrust force and, hence, delamination damage reduction [105-108]. The reduction of thrust force with increasing cutting speed was suggested to be attributed to the higher cutting temperature being produced as the cutting speed was increased, which reduced the strength of epoxy matrix [105-108].

3.2.3 Drilling Temperature

The cutting temperature in drilling of CFRPs is relatively low compared to that in machining of most metallic materials, especially aerospace alloys [4, 32]. It was reported by Brinksmeier *et al.,* [110] that the temperature of 191.6°C (measured 0.2 mm off the cutting edge) was produced when drilling 10 mm thick carbon/epoxy laminates at the cutting speed of 120 m/min and feed rate of 0.08 mm/rev with a 16 mm diameter carbide drill. Rawta and Attia [108] showed that a steady state temperature of 210°C (measured 1 mm away from the

cutting edge) was achieved when drilling the 23.6 mm thick carbon/epoxy laminates at the cutting speed of 23.5 m/min and feed rate of 0.02 mm/rev with a 5 mm diameter carbide drill. Other researchers also reported that the cutting temperature in drilling carbon/epoxy composites could reach 200-400°C depending on the machining conditions and thickness of the workpiece material [16, 32, 109]. In comparison, a temperature of over 900°C was reported when machining titanium alloys (Ti-6Al-4V) at 19 m/min [72]. It was suggested by other researchers [4, 16] that the lower cutting temperature in drilling CFRPs is attributed to the absence of extensive plastic deformation in the mechanism of cutting, which would occur in metal machining. In addition, the author suggests that this is also because of the lower strength of CFRPs compared to high-performance alloys [2, 5]. Although cutting temperature being generated when drilling CFRPs is not as high as that when drilling metals, thermal-induced machining problems such as matrix burn-out on the machined surface and error in dimensional accuracy of the drilled hole could occur [32, 108]. It was suggested by Rawat and Attia [108] and Weinert and Kempmann [32] that this was because of low temperature tolerance of the CFRPs (130-180°C for the T_g of epoxy matrix [5, 108]) and low thermal conductivity of the CFRPs (30 W/mK for a carbon/epoxy composite compared to 120 W/mK for a WC tool [17]), which caused the generated heat to be concentrated on the machined surface, resulting in thermal damage to the surface, and contributed to a radial expansion of the drilling tool, resulting in an expansion of diameter of the drilled hole.

3.2.3.1 Measurement of Cutting Temperature when Drilling CFRPs

Due to complexity of the drilling process and anisotropy in the material properties of CFRPs, there has been limited research work on the approach for measuring the cutting temperature in drilling CFRPs. A common approach among other researchers is using a K-type thermocouple embedded on the flank face of the drill for measuring the cutting temperature of the drilling process, which was carried out by drilling a hole on a rotating CFRP workpiece, which was fixed by a special fixture on the spindle head, with a stationary drill [16, 32, 108, 110]. However, the technique for embedding the thermocouples varies among different researchers. In the work of Chen [16], a K-type thermocouple was embedded in a groove of 0.5 mm wide on the flank face of the drill, which was machined by an EDM process, and its tip was welded 0.5 mm away from the cutting edge. In the work of Brinksmeier *et al.*, [110], the thermocouple was embedded through a 0.35 mm diameter hole, which was machined on the flute of the drill at 5 mm above the cutting edge by an EDM process. The tip of the thermocouple was welded at the end of the hole, which was 0.2 mm away from the cutting edge, and the thermocouple wire was drawn along a 0.6 mm wide groove on the flute of the drill [110]. In the work of Rawat and Attia [108] and Weinert

and Kempmann [32], the thermocouple was embedded through a through-tool coolant hole and its tip was welded at the end of the hole on the flank face. Although the embedded thermocouple technique was commonly used by other researchers, the author suggests that this measurement technique still could not measure the temperature at the cutting point where highest temperature was generated. Brinksmeier *et al.,* [110] also used a pyrometer, which detects heat radiation of an object, to measure the temperature of the CFRP workpiece close the cutting point. In this approach, a 5.1 mm diameter though-hole was drill at the edge of the CFRP plaque to enable a pyrometer to measure the temperature of the plaque closet to the cutting point. However, since CFRPs have low thermal conductivity, the author suggests that the temperature of the workpiece detected by a pyrometer would not represent temperature at the cutting point.

3.2.3.2 Effect of Machining Parameters on Drilling Temperature

It has been reported by other researchers [15, 16, 32, 110] that the cutting temperature in drilling CFRPs is affected by cutting speed and feed rate. It was shown that increasing cutting speed resulted in a higher drilling temperature because more heat from friction between the minor cutting edges of the drill and the workpiece and from the deformation of workpiece material was generated [16, 32, 110]. An increase of drilling temperature would contribute to higher possibility of thermal damage on the machined surface [16, 32, 110] and a higher rate of tool wear [15]. Therefore, the author suggests that the issues of thermal damage and high rate of tool wear should also be considered when drilling CFRPs at high speed even though thrust force could be reduced. For the effect of feed rate, contradicting results were reported among other researchers. Chen [16] and Brinksmeier *et al.,* [110] showed that the drilling temperature decreased with increasing feed rate, which was suggested to be because of less heat from friction between the minor cutting edges and the workpiece being generated as the time of contact was reduced with the increasing feed rate. However, Weinert and Kempmann [32] showed that the drilling temperature increased with increasing feed rate. They argued that, as feed rate increased, the amount of material to be deformed per revolution of the drill increased, resulting in more heat being generated [32]. This heat being generated from deformation of the workpiece material would compensate the effect of a reduction of frictional heat with increasing feed rate, hence higher drilling temperature was generated [32]. Based on these findings, the author suggests that the effect of feed rate on the drilling temperature is less dominant compared to that of cutting speed since the variations of frictional heat would be compromised with the variations of heat being generated from the deformation of workpiece material as feed rate varied.

3.2.4 Tool Wear

3.2.4.1 Characteristics and Wear Mechanism

High rate of tool wear is one of the machining problems which limit productivity of the process when drilling CFRPs due to high abrasiveness of the material [4, 9, 109]. Due to fracture dominated mechanism of chip formation and low cutting temperature, the possibility of diffusion/dissolution wear is eliminated when drilling CFRPs [111, 112]. It was reported that abrasive wear was observed as the major wear mechanism of the tool when drilling CFRPs with carbide drills, which are commonly used for drilling applications of CFRPs in research work and in industry [9, 99, 109]. Rawat and Attia [109], Masuda *et al.* [111] and Wang *et al.* [112] proposed that abrasive wear for carbide tools when drilling CFRPs could not be explained by traditional abrasive wear mechanism in which the abrasive workpiece material cause wear on the tool by direct abrasion. This is because CFRPs are not hard enough to cause significant wear on tungsten carbide (WC) grains of carbide tools directly [109, 111, 112]. They reported that the abrasive wear was a result of removal of cobalt (Co) binder between WC grains on the surface of a carbide tool by highly abrasive carbon fibres which consequently caused tool wear by fracture and dislodging of WC grains [109, 111, 112] and direct abrasion by the fractured and dislodged grains [109, 112]. Although carbon fibres could not contribute to significant wear on WC grains directly, they could remove Co binder, which has lower hardness, between the grains on the surface of the tool. As Co binder was removed, more surface area of WC grains was exposed to dynamic cutting stress as a result of brittle fracture-dominated cutting mechanism when machining CFRPs. This resulted in generation of cracks in WC grains, brittle fracture of the grains and finally dislodging of the fractured grains. Then, the fractured and dislodged grains further caused abrasive wear by direct abrasion as they moved along the cutting edge under pressure during the drilling process. From SEM investigation, Masuda *et al.* [111] showed evidence indicating that Co binder between WC grains were removed and cracks in the grains occurred. Wang *et al.* [112] also evidence indicating removal of Co binder as well as dislodging of WC grains as voids on the worn surface of the tool were observed. However, clear evidence of cracks or fracture of WC grains in high magnification was not provided in their work. Wang *et al.* [112] also reported that diamond coated and TiAlN coated drills underwent the same mechanism of abrasive wear as uncoated drills when machining CFRPs.

The author considers the proposed mechanism of abrasive wear of carbide tool when drilling CFRPs to be plausible. This is because it has been reported that the hardness of WC at room temperature is approximately 2000 HV and is reduced to approximately 1700 HV at 300°C [73, 113], while the hardness of carbon fibres was reported to be 800-1100 HV [114]

depending on the type of carbon fibres. As a consequence, the fractured carbon fibres could not significantly wear WC grains directly. However, they could remove the Co binder of which the hardness was reported to be in the range of 410-1225 HV [115].

As a result of abrasive wear, a uniformly distributed wear band on flank face along the cutting edges, Figure 3.9a, and cutting edge rounding, Figure 3.9b, are common characteristics and dominant types of tool wear produced when drilling CFRPs [9, 99, 108, 109, 111, 112, 116]. Wang *et al.* [112] explained that this is because, when drilling CFRPs, cutting edges are not covered by stagnation zone of workpiece material in which the workpiece material seizes to the cutting edges and protects them from mechanical wear such as abrasion. The stagnation zone is stable in metal machining due to chip formation mechanism with extensive plastic deformation in the shear zones [112]. Since chip formation mechanism in machining with CFRPs is dominated by a series of brittle fractures without seizure between workpiece and cutting edges, the workpiece flows around the cutting edges without protection from stagnation zone, causing rounding of the cutting edges and abrasive wear on the flank face [112]. In addition to abrasive wear on flank face and cutting edge rounding, chipping of the cutting edge, which was resulted from the fluctuating load acting on sharp cutting edges when drilling anisotropic materials, and adhesion of the CFRP chips on the flank face, which was due to the frictional heat as the drill rubs against the machined surface, could also be observed [9, 109, 112].

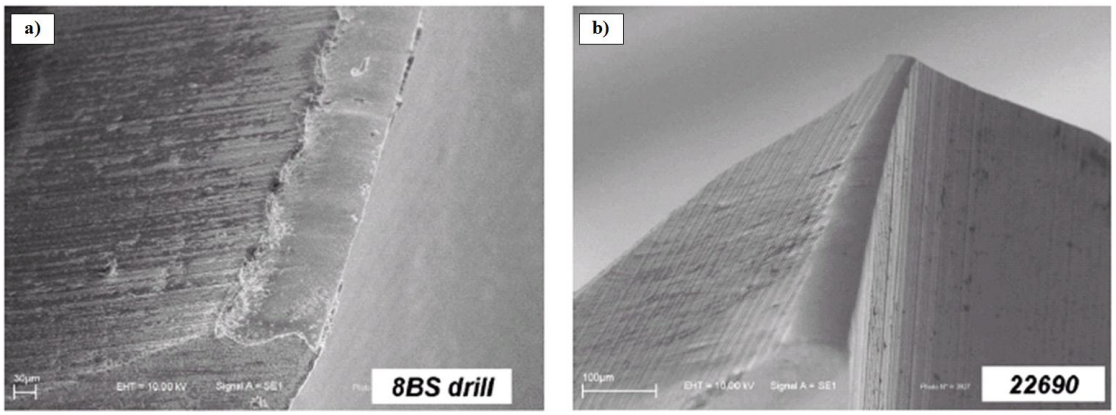

Figure 3.9: (a) A uniformly distributed wear along the cutting edge on the flank face of a diamond coated solid carbide drill and (b) rounding of the cutting edge of an uncoated solid carbide drill result from drilling CFRPs [99]

Width of a uniformly distributed flank wear was commonly used as an evaluating criterion for measuring tool wear and determining its effect on the drilling performance of CFRPs [87, 97, 99, 108, 109, 117]. However, Faraz *et al.* [116] proposed use of cutting edge rounding value, which was determined from radius of the major cutting edge using an optical fringe microscope for 3-D profilography of the cutting edge, as a new evaluating

criterion for measurement of tool wear. It was shown by Faraz *et al.* [116] that the value of cutting edge rounding could be effectively used to show the effect of tool wear on thrust force and delamination damage while providing an advantage over the conventional flank wear measurement in term of ease of tool wear assessment. They suggested that the disadvantage of the conventional flank wear measurement was because of difficulty in accessing the flank face and less visibility of the flank wear band being distributed along the longer and increased number of cutting edges of specially designed drills such as multifaceted or multiple-cutting edge drills, which were increasingly used to improve drilling performance [116]. Wang *et al.* [112] also used cutting edge rounding, which was determined from 2-D profile of the cutting edge, as an evaluating criterion for measurement of tool wear when drilling CFRPs. In their work, it was shown that drilling thrust and torque increased as cutting edges of the drill were more rounded [112].

For progress of tool wear, Rawat and Attia [109] showed that progress of tool wear with number of drilled holes when drilling CFRPs was not uniform and could be divided into three stages:

1) Initial stage of wear

During the initial stage of wear, rapid rate of tool wear occurred and chipping of the cutting edge and chisel edge could be observed. Since the cutting edges of the drill were still sharp at the beginning of the drilling process, the cutting edges of the drill subjected to high cutting stress as they carried cutting force over a small tool/workpiece contact area. As a consequence, tool wear increased in rapid rate and chipping or cracking of the cutting edges could be observed as the cutting edges could not withstand the high cutting stress. Chipping of the cutting edges during the initial stage of wear was also observed in the work of Lin and Chen [15].

2) Secondary/steady stage of wear

As the drilling process continued, the sharpness of the cutting edges was reduced as a result of cutting edge rounding. Due to lower sharpness, which resulted in larger tool/workpiece contact area, the cutting edges were subjected to lower cutting stress compared to that during the initial stage of wear. As a consequence, in the secondary/steady stage of wear, tool wear gradually increased in nearly constant rate. The steady increase of tool wear continued until reaching the final/catastrophic stage of wear, in which tool wear increased with high rate and reached the end of tool life.

3) Final/catastrophic stage of wear

In the final stage of wear, in which the tool was severely worn, high rates of tool wear occurred again because of high cutting stress on the cutting edge combined with the effect of thermal degradation of the tool strength, which were attributed to the extensively increased cutting force and cutting temperature.

This non-linear progress of tool when drilling CFRPs (showing initial stage and steady stage of wear) was also shown by Murphy *et al.* [87], Faraz *et al.* [116] and Shyla *et al.* [117].

3.2.4.2 Effect of Tool Wear on Machining Output

It has been reported that an increase of tool wear resulted in an increase in thrust force and hence larger delamination damage being produced [15, 16, 87, 97, 99, 104, 109, 116]. This is because the cutting mechanism was suggested to change from clean cutting to rubbing and punching as the drill had been worn due to the change of cutting edge geometry (rounding of the cutting edge and reduction of radial and axial rake angle) with increased tool wear [15, 16, 116]. Rawat and Attia [109] has reported that thrust force and the size of delamination damage increased in a similar pattern of the progress of tool wear, for which they increased with a high rate during the initial and final stage of tool wear and with a steady rate during the steady stage of tool wear. They also reported that hole circularity error, hole diameter error and surface roughness increased as tool wear increased, for which they increased with a high rate once tool wear reached the final stage.

In order to minimise tool wear, low cutting speed and feed rates should be used since it was reported that tool wear increased with increasing cutting speed and feed rate [9, 10, 15, 16, 104]. It was suggested by Chen [16] and Lin and Chen [15] that the increase of cutting temperature, which would result in a reduction of tool strength, would be the major factor contributing to higher tool wear being produced as cutting speed was increased. Although it was not discussed in other researchers' work, the author proposes that the increase of tool wear with increasing feed rate was due to the increase of amount of material to be deformed as feed rate was increased. However, the concern of higher frictional heat being generated at low feed rate as previously discussed in Section 3.2.3, which could result in thermal degradation of tool strength, should also be considered. In addition to minimising cutting speed and feed rate, rate of tool wear could be reduced by using a carbide drill with diamond coating. It was reported that a lower rate of tool wear was produced when drilling with a diamond coated carbide drill compared to uncoated and TiAlN coated carbide drills [87, 99, 112]. This was because of higher resistance to abrasive wear of diamond coating which better protects Co binder from being removed and protects the tool from abrasion by

fractured and dislodged WC grains [87, 112]. It was also shown that using a carbide drill with TiAlN coating did not reduce rate of tool wear compared to an uncoated drill [87, 112]. Wang *et al.* [112] suggested that this might be due to formation of TiO_2 and Al_2O_3, which have lower resistance to abrasive wear than TiAlN coating, as a result of oxidation of TiAlN coating. Due to wear mechanism by removal of Co binder, Masuda *et al.* [111] showed that tool wear decreased as Co content in a carbide tool decreased, which reduced rate of Co binder removal. Faraz *et al.* [116] showed that using a drill with longer and increased number of cutting edges could resulted in a lower rate of tool wear compared to a conventional twist drill as wear was distributed over longer length as well as higher number of cutting edges. It was also shown in the work of Shyha *et al.* [117] that using a step drill resulted in a decrease of tool wear compared to the conventional twist drill since the load on the cutting edges was reduced as a result of two stages of drilling (pilot drilling and reaming).

3.2.5 Damage Induced by Conventional Drilling Process

In addition to high rate of tool wear, damage induced by conventional drilling of CFRPs usually occurs due to factors including heterogeneity, anisotropy in material properties, low temperature tolerance and thermal conductivity of polymeric matrix, resulting in degradation of mechanical properties and performance of CFRP components, poor quality of surface finish and dimensional accuracy error of the hole [4, 7, 9-11]. This damage includes delamination at the entry and exit of the hole, fibre pull-out, thermal damage to the matrix, matrix cracking, and damage to the machined surface in the form of material chip-out and delamination [4, 7, 9-11]. Examples of drilling-induced damage are shown in Figures 3.10 and 3.11.

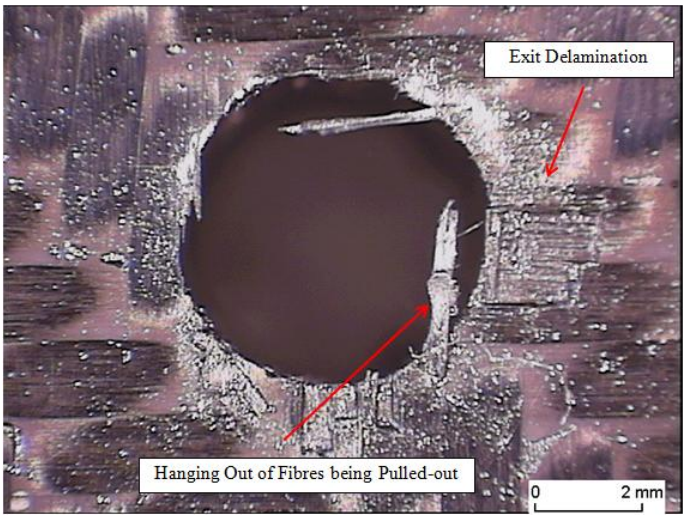

Figure 3.10: Optical microscope image showing exit delamination and hanging out of fibres which have been pulled out when drilling CFRPs

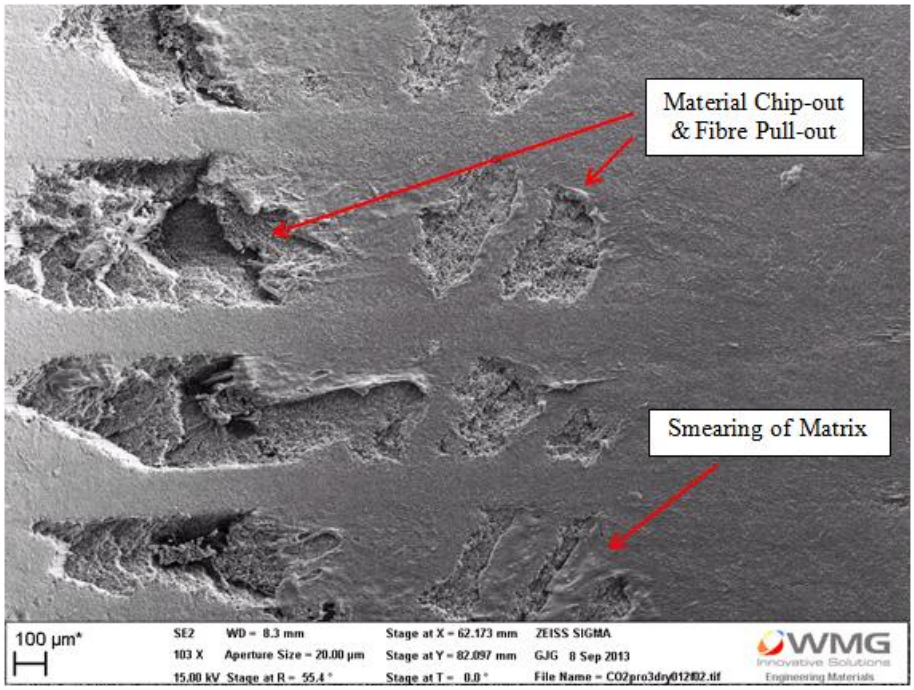

Figure 3.11: SEM image showing material chip-out, fibre pull-out and smearing of the matrix on the machined surface when drilling CFRPs

As discussed in Section 3.2.1, the cutting mechanism varies in one revolution of the drill when drilling uni-directional CFRPs and also varies through the thickness of the plaque when drilling multi-directional CFRPs due to change of angle of fibre orientation relative to the cutting edges [3, 4, 8]. This contributes to a fluctuation in cutting forces and variation in characteristics of the machined surface along the circumference and through the thickness of the hole [3, 4, 8]. As a consequence, a machined surface with high variation in surface roughness is produced. Piquet *et al.* [17] proposed that varied characteristics of the

machined surface due to changing cutting mechanism along circumference of the hole also resulted in error in circularity of the hole.

When machining at the fibre orientation angle where CFRP laminates are subjected to severe bending and compression, i.e. $90° \leq \theta < 180°$, damage to the machined surface including fibre pull-out, matrix cracking, delamination (debonding of laminates) and material chip-out is susceptible to occur [4, 8, 77, 78]. Cracking in the matrix and fibre pull-out occur due to differences in strength of polymeric matrix and carbon fibres [4, 8, 109]. Due to lower strength of polymer compared to carbon fibres, lower cutting forces are required when machining the polymeric matrix compared to when machining carbon fibres. As a consequence, cracks and fracture in the matrix usually occur before the fibres are completely cut when CFRP laminates are subjected to fluctuating cutting forces during drilling [4, 8, 109]. As the matrix is already fractured, the fibres are pulled out instead of being cut completely due to lacking of a support from the matrix [4, 8, 109]. In some cases, the fibres and surrounding matrix are both pulled out resulting in damage to the machined surface in the form of material chip-out [4].

Thermal damage to the matrix can also occur when drilling CFRPs due to low temperature tolerance of polymeric matrix [11, 32, 47, 109]. As discussed in Section 3.2.3, it was reported that cutting temperatures when drilling CFRPs could reach 200-400°C [16, 32, 109]. At this range of temperature, strength and stiffness of the matrix would be reduced as the glass transition temperature of polymeric matrix, particularly epoxy matrix of which glass transition temperature was reported to be 150-200°C [5], is exceeded. This results in smearing of the matrix instead of complete cutting and eventually results in matrix burning [11, 32, 47, 109]. A reduction in strength and stiffness of the matrix also accelerates fibre pull-out because interfacial bonding strength between the fibres and matrix decreases and the fibres are supported by a weaker matrix during cutting [109]. This thermal damage to the matrix and mechanical damage on the machined surface discussed previously result in reduced structural integrity, assembly tolerance and poor quality of surface finish of CFRP components [4, 7, 9-11].

Delamination or debonding of laminates occurs due to low interlamina strength of CFRPs as they are manufactured in laminate form [3, 5, 9]. It was reported that interlamina strength of CFRPs, which is strength between laminates in through-the-thickness direction is lower than strength in the direction of fibre orientation and within the laminate [4, 5]. It was shown by Campbell [5] that strength in through-the-thickness direction of a quasi-isotropic carbon/epoxy composite is 15% of the strength within the laminate. This is because interlamina strength of CFRPs is dominated by strength of the polymeric matrix which is lower than that of reinforcing carbon fibres [4, 5]. Tensile strength of a high-strength fibre

was reported to be in the range 3.2-3.5 GPa [5, 65] while tensile strength of polymeric matrix was in the range 35-70 MPa [5]. As a consequence of low interlamina strength, delamination at the entry, exit and through the thickness of CFRP laminates is susceptible to occur during drilling. Discussion on drilling-induced delamination in more detail will be presented in Sections 3.3 and 3.4.

3.3 Drilling-induced Delamination

Delamination induced by conventional drilling of CFRPs is interlamina failure which occurs when cracks and brittle fracture resulting from cutting forces propagate between laminates towards direction of interlamina bonding causing separation or debonding of the laminates [4, 9]. Delamination is considered the drilling-induced damage of most concern as it severely reduces structural integrity, assembly tolerance, mechanical properties and performance of CFRP components such as bearing strength and strength under fatigue load [3, 4, 7, 9]. It has been reported that drilling-induced delamination accounts for 60% of final CFRP component rejection in aerospace industry [7, 9]. It was shown by Persson *et al.* [12] that delamination damage induced by drilling reduced static and fatigue bearing strength of a pin-loaded CFRP component by 1.7-11.2% and 9.2-26.8% respectively depending on type of the tool being used. It was also reported by Marques *et al.* [96] and Durao *et al.* [118] that bearing strength of a CFRP component was reduced as larger delamination was produced. Durao *et al.* [118] showed that a 59% increase in quantity of delamination resulted in a 12% decrease in bearing strength of a component. As a consequence, much of the research work in conventional drilling of CFRPs has been focused on approaches to minimise delamination damage.

3.3.1.1 Mechanism of Delamination

Mechanism of peel-up delamination at the entry and push-down delamination at the exit of the plaque, which are considered as the two major types of delamination observed when drilling CFRPs [3, 4, 9], is presented in schematic diagram in Figure 3.12. Mechanism of these types of delamination has been explained by other researchers [3, 17, 47, 84, 92, 119] among which Hocheng and Dharan [120] were the first to propose this mechanism with associated model of delamination.

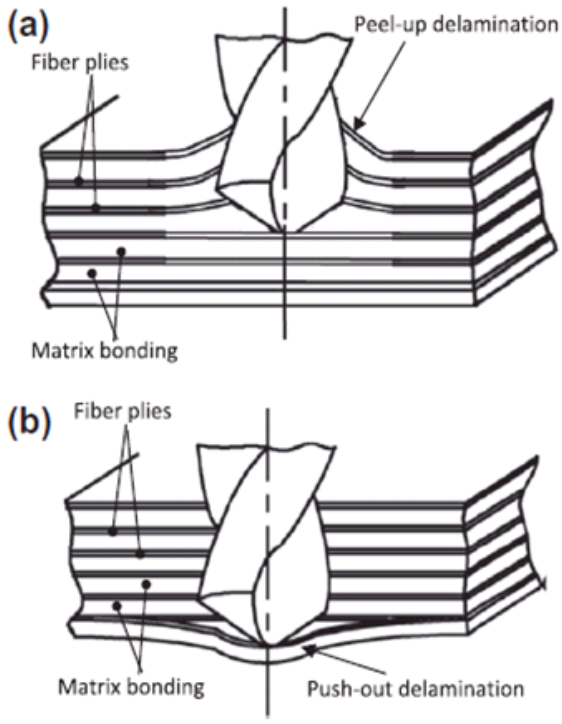

Figure 3.12: Schematic diagram showing mechanism of (a) peel-up delamination at the entry and (b) push-down delamination at the exit of CFRP plaque [9]

Delamination observed at the entry of the plaque, Figure 3.12a, is resulting from debonding of the upper laminates from uncut laminates under the drill by upward peeling force due to action of the major cutting edges of the drill [3, 17, 47, 92, 119, 120]. When major cutting edges engage in cutting the laminates at entry of the plaque, it tends to lift and pull these laminates up the flute before they are machined completely as the drill proceeds through the thickness of the plaque. This action results in upward peeling force which causes bending of laminates and delamination in mode I fracture once it exceeds the interlamina bonding strength of upper laminates. This upward peeling force is mainly dominated by cutting forces in the radial direction due to action of the major cutting edges [120]. As the drill proceeds further through the thickness of the plaque, possibility of delamination resulting from peel-up mechanism is reduced due to higher resistance to bending of peeled up laminates as thickness of the laminates above the point of peeling action increases [84, 120].

Delamination observed at the exit of the plaque, Figure 3.12b, is resulting from debonding of laminates under the drill by push-down thrust force action of the chisel edge and major cutting edges of the drill [3, 47, 84, 92, 119, 120]. As the drill approaches the exit of the plaque, thickness of uncut laminates under the drill reduces resulting in lower resistance to bending of the laminates by downward thrust force. When the downward thrust force exceeds interlamina bonding strength of the uncut laminates, delamination occurs in mode I (opening) fracture as a result of bending of laminates before the drill completely

penetrates through the exit laminates. Di Paolo *et al.* [14] proposed that delamination at the exit also occurs in mode III (shearing) fracture as a result of twisting and tearing of the laminates in addition to mode I fracture, which is due to bending of the laminates. Evidence from real-time imaging showing delamination onset at the exit of the plaque as a result of fracture in mode I and III was provided in their work. They explained that delamination initially occurred in mode I fracture due to bending of the laminates by pushing down action of the chisel edge. As the chisel edge penetrated through the plaque, the debonded laminates were subjected to twisting and tearing due to axial thrust force and radial cutting force by action of major cutting edges resulting in further delamination in mode III fracture. It has been reported by other researchers that push-down delamination observed at the exit was more severe and more critical to quality of the drilled hole when drilling CFRPs [3, 4, 7, 9, 117]. However, the reason for more severe delamination observed at the exit was not discussed in their work.

3.3.1.2 Assessment of Delamination

3.3.1.2.1 Assessment Technique

Visual inspection using an optical microscope with analysis software was commonly used by other researchers for examining delamination at the entry and exit of the hole when drilling CFRPs [19, 20, 89, 105-109]. Although this assessment technique is considered a simple and quick method for analysis of entry/exit delamination of large number of samples, the author suggests that there would be variations in the measurement of delamination and it is difficult to determine the actual diameter or area of damage when using this assessment technique. This is because this technique of delamination assessment depends on visibility of the contrast of defects within the optical microscope images. Hocheng and Tsao [23, 93] also proposed that it is difficult to evaluate delamination damage when drilling CFRPs by visual inspection using an optical microscope because of color and contrast of CFRPs within the microscope image. In addition, internal damage and delamination through the thickness of the hole cannot be examined.

Zhang *et al.* [100] used a destructive analysis technique for assessment of delamination through the thickness of the hole when drilling CFRPs. In their assessment technique, a CFRP sample was cut in half through the diameter to enable visual inspection of delamination through the thickness using metallographic microscope. However, methods of sample preparation for investigation under the microscope were not described in their work. This assessment technique was used by Zhang *et al.* [100] to determine the number of laminate in CFRP plaque at which delamination occurred rather than to determine the actual

depth of internal delamination. The author suggests that this destructive assessment technique would not be suitable for evaluation of delamination through the thickness in terms of actual depth of damage. This is because cutting the sample in half could cause additional damage to the damage induced by the drilling process, resulting error in the measurement of actual depth of drilling-induced damage.

To enhance visibility of damage and contrast between damaged and undamaged area around the hole, X-ray radiography inspection of CFRP samples which had been immersed in contrasting fluid, e.g., di-iodomethane [92, 96, 118, 121], or coated with tetrabromethane [16] was used. In the assessment technique used by Durao *et al.* [92, 121] and Marques *et al.* [96], a CFRP sample was immersed in di-iodomethane, which is a radiography opaque fluid, for 1.5 hr before it was examined using X-ray radiography inspection. In the technique used by Durao *et al.* [118], the sample was immersed in di-iodomethane for 15-20 min before examined in X-ray radiography. Then, the images acquired from X-ray radiography were used for measurement of diameter or area of delamination around the hole [92, 96, 118, 121]. Chen [16] also used enhanced X-ray radiography to determine diameter of delamination but, in his technique, the sample was coated with tetrabromethane. Although this assessment technique could enhance visibility of damage and contrast within the acquired image, mechanism property of CFRP components would be degraded due to moisture absorption and contamination of fluid. Hence, it is suggested that it would not be practical for industrial application.

Another non-destructive technique which has been widely used for analysis of delamination when drilling CFRPs is an ultrasonic C-scanning analysis method. It was used by other researchers to determine the maximum diameter of delamination and maximum extent of delamination (difference between diameter of delamination and diameter of drilled hole) induced by drilling of CFRPs [22, 90, 101, 104, 122, 123]. In this technique, an image showing delamination around the hole was constructed from data of attenuation of ultrasonic wave at different areas of CFRP sample [22, 90, 123]. During the scanning, the ultrasonic wave was sent through the sample, which was submerged in a water bath, from a transducer to a receiver. Then, values of attenuation of ultrasonic wave at different areas of the sample were recorded and the image of the hole was acquired from those values. The area consisting of drilling-induced damage would contribute to a higher value of ultrasonic wave attenuation compared to the area without damage due to lower density [22, 90, 123]. This results in contrast between damaged and undamaged area in the image. Then, diameter and area of delamination were measured from the acquired image using analysis software.

The ultrasonic C-scanning analysis technique is capable of evaluating entry/exit delamination without dependence of contrast on illumination and visibility of damage in the image, which is a concern in visual inspection of microscope image, and it is capable of

assessing internal damage of the hole without causing additional damage to the sample [22, 90, 123]. However, the author suggests that this analysis technique would not be suitable if the sample is required for further investigation and evaluation of mechanical properties. This is because the properties of the sample would be affected by moisture absorption as the sample is submerged in water during scanning. In addition, it was proposed by Hocheng and Tsao [23, 93] that there would be difficulty and possible error in interpretation of data of ultrasonic wave attenuation due the high level of heterogeneity of CFRPs. This is because the ultrasonic wave would be scattered and attenuated by the area containing voids due to the heterogeneity of the material rather than due to drilling-induced damage.

Hocheng and Tsao [23, 93] showed that an X-ray computerised tomography (CT) scanning analysis method was as effective as ultrasonic C-scanning analysis method for evaluation of delamination at the surface and through the thickness when drilling CFRPs. In their analysis method, a CFRP sample was exposed to X-ray radiography to obtain 2-D cross-sectional images of the hole at each slice through the thickness of the sample. The contrast in these 2-D cross-sectional images was resulting from variations in the absorption of X-rays within the sample [23, 93]. Variations in the absorption of X-rays within the sample were a result of variations in density and content within the area of the sample being inspected [5, 23, 93]. Since density of an area containing internal voids as a result of drilling induced damage was lower compared to an area without defects, higher intensity of X-ray would be allowed to transmit through the area with drilling-induced defects [5]. This created contrast between damaged and undamaged area in 2-D image of the hole from which maximum diameter of delamination and extent of delamination compared to diameter of the drilled hole were determined [23, 93]. The 2-D cross-sectional images of the holes were also reconstructed to obtain a 3-D image of the sample and determine the location of delamination through the thickness of the sample [23, 93]. The author suggests that the X-ray CT-scanning analysis method would be a more preferable option than the ultrasonic C-scanning analysis method for evaluation of damage in drilling of CFRPs in industry which further investigation of mechanical property and performance of the sample would be required. This is because the mechanical properties of the sample are not affected by contamination of fluid during investigation process.

Although the X-ray CT scanning and ultrasonic C-scanning analysis techniques would be more accurate for assessing entry/exit delamination and internal damage than the visual inspection using an optical microscope and the destructive analysis technique used by Zhang *et al.* [100], it is suggested that these analysis techniques are not suitable for delamination assessment of large size of sample because of the longer processing time for the assessment. The visual inspection using an optical microscope would still be commonly used for delamination assessment in industrial applications where large size of samples is

required. However, the processing time for the X-ray CT scanning and the ultrasonic C-scanning analysis techniques was not quoted in the work of Hocheng and Tsao [23, 93].

3.3.1.2.2 Quantification of Delamination

Delamination has been quantified using dimensional and non-dimensional parameters depending on different researchers. The dimensional parameter which was most commonly used for quantification of delamination was delamination extent [23, 93, 101, 123, 124]. Delamination extent was determined from the difference between diameter of damaged area and diameter of the hole [23, 93, 101, 123, 124].

Another group of researchers has used non-dimensional parameters for quantification of delamination to enable comparison of the results to those reported by other researchers [7]. A non-dimensional parameter which was most commonly used by other researchers for quantification of delamination [16, 19, 20, 90, 96, 105-109] is delamination factor, which was first proposed by Chen [16]. Delamination factor (F_d) is the ratio of maximum diameter of delamination damage (D_{max}) to diameter of the hole (D_o) [16], Figure 3.13.

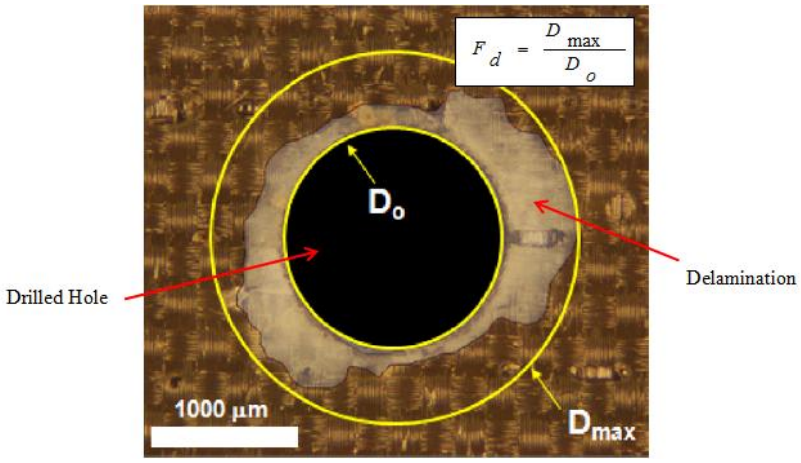

Figure 3.13: Schematic diagram showing quantification of delamination in term of delamination factor (F_d) (adapted from [97])

However, Davim *et al.* [125] and Faraz *et al.* [116] argued that quantification of delamination in terms of F_d would not be suitable for evaluation of delamination produced when drilling CFRPs because it does not represent the actual area of damage resulting from drilling at a particular machining condition. Due to the high level of anisotropy in CFRPs, it has been observed that delamination produced when drilling CFRPs was irregular in shape, in some cases, consisting of sharp cracks from fibres being peeled up at the entry and pushed down at the exit [116, 125]. When quantified in terms of F_d, delamination damage with sharp cracks will result in a high value even though the actual area of damage around is minimal because only maximum diameter of delamination is considered rather than actual

area of damage. This could contribute to deceptive results for investigation of the effect of a machining condition on damage to the drilled hole.

Davim *et al.* [125] proposed quantification of delamination in terms of adjusted delamination factor (F_{ad}) which calculates delamination factor by considering significance of the size of crack and actual area of damage, Figure 3.14. It was shown by Davim *et al.* [125] and Shyla *et al.* [97] that quantification of delamination in terms of F_{ad} was more suitable to represent the variation of delamination damage resulting drilling at different machining condition compared to quantifying in terms of F_d.

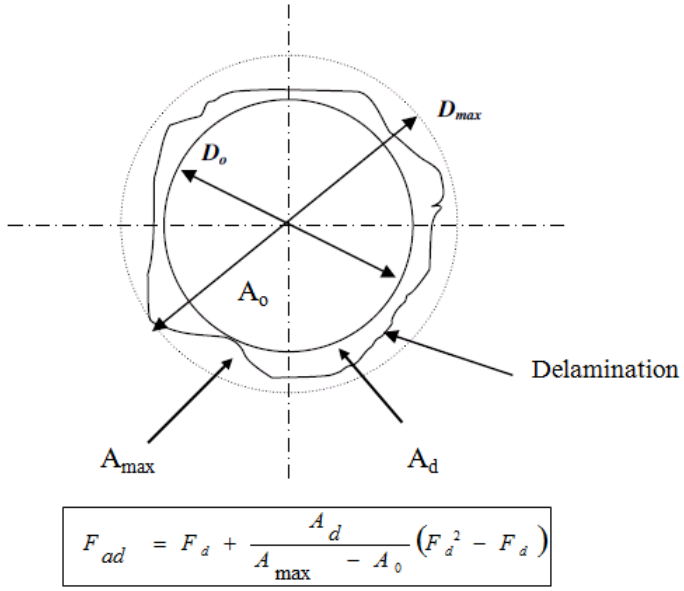

Figure 3.14: Schematic diagram showing quantification of delamination in terms of adjusted delamination factor (F_{ad}), where F_d = Delamination factor (D_{max}/D_o), A_{max} = Area of delamination calculated from maximum diameter of delamination, A_d = Actual area of delamination and A_o = Area of drilled hole (adapted from [106])

Quantification of delamination by considering the actual damage area was also used by Faraz et al. [116]. In their work, delamination was evaluated in terms of damage percentage (DF) which is the ratio of the difference between actual area of delamination and area of the hole ($A_d - A_o$) to area of the hole (A_o) [116].

3.3.1.3 Correlation between Thrust Force and Delamination

It was reported that there is a positive correlation between thrust force and drilling-induced delamination when drilling CFRPs showing that diameter or area of delamination increases as higher thrust force is produced regardless of the type of drill [16, 22, 23, 85, 120, 126]. This positive correlation between thrust force and diameter or area of delamination has been shown in experimental work by Chen [16], Hocheng and Tsao [22, 23, 93, 101]. Hocheng and Tsao [22, 23, 93] proposed that an increase in size of delamination with increased thrust force is because the increase of thrust force contributes to

greater quantity of work done for initiation and propagation of cracks resulting in increased size of delamination.

Based on a positive correlation between thrust force and size of delamination, it has been proposed that there is a critical thrust force at which delamination occurs [55, 120]. It was first shown in experimental work by Konig *et al.* [55] that no delamination induced by drilling of CFRPs was produced when thrust force was below a critical value (25 N when drilling 5 mm thick CFRP plaque at cutting speeds of 50-500 m/min and feed rates of 0.01-0.05 mm/rev). Hocheng and Dharan [120] proposed an analytical model for determining a critical thrust force at which delamination as result of push-down mechanism occurs when drilling with a standard twist drill. Their model was developed using elastic fracture mechanics and plate bending theory based on assumptions stating that;

1. CFRP laminates were subjected to pure bending during drilling, i.e. delamination occurred only in mode I fracture.
2. CFRP laminates were considered an isotropic material during drilling, resulting in circular shape of delamination.
3. The laminates were subjected to a point load concentrated at the centre of laminates by indentation action of the drill, i.e. cutting load distributed along the major cutting edges did not contribute to delamination.

It was indicated from Hocheng and Dharan's delamination model [120] that a critical thrust force is dominated by uncut thickness of laminates and elastic bending modulus of laminates under the drill. This indicates that critical thrust force for push-down delamination decreases as the drill proceeds towards the exit of the plaque because of less uncut thickness, which contributes to lower elastic modulus, i.e., lower resistance to bending load, of the laminates under the drill. This results in high possibility of delamination onset at the exit of the plaque. A value of critical thrust force calculated from Hocheng and Dharan's model [120] corresponded to the value obtained from drilling experiments by Konig *et al.* [55] when drilling CFRP with the same thickness.

Jain and Yang [85, 88] argued that the assumptions used by Hocheng and Dharan [120] stating that delamination was produce in circular shape as isotropic property of CFRP was assumed did not represent the actual drilling process. They showed in their experimental work that delamination did not occur in circular shape and it was observed that more propagation of crack occurred in direction of fibre orientation [85, 88]. As a consequence, Jain and Yang [85, 88] proposed a delamination model using an assumption stating that delamination occurred in elliptical shape with more crack propagation in direction of fibre orientation when drilling uni-directional CFRPs. Other assumptions were the same as that used by Hocheng and Dharan [120]. A critical thrust force calculated by Jain and Yang's

model [85, 88] was validated by the results of drilling experiments in their work with an error less than 1%. However, an accuracy of their model in calculating a critical thrust force was not compared to that of Hocheng and Dharan's model.

Tsao and Hocheng [127] and Zhang *et al.* [100] also proposed a delamination model based on similar assumptions used by Jain and Yang [85, 88] for prediction a location through the thickness at which delamination occurred. The results of critical thrust force and location of delamination calculated using a delamination model by Tsao and Hocheng [127] and by Zhang *et al.* [100] were validated by the results of drilling experiments in their work. Since it has been reported that thrust force increases with increased feed rate, they suggested that this delamination model should be used to determine a critical feed rate above which thrust force would exceed a critical value for drilling at different location through the thickness of the plaque [100, 127].

In addition to a delamination model for drilling with a twist drill, Hocheng and Tsao [21, 22] proposed delamination models for determining a critical thrust force at which delamination occurs when drilling with a saw drill, candle-stick drill, core drill and step drill. These delamination models were developed based on similar assumptions used by Hocheng and Dharan [120] for developing a delamination model for drilling with a twist drill.

3.3.1.4 Effect of Tool Wear and Machining Parameters on Delamination

It was reported by Tsao and Hocheng [104] that an increase in tool wear resulted in larger delamination when drilling CFRPs due to higher thrust force being produced. They developed a delamination model for calculating a critical thrust force at which delamination occurs when drilling with an unworn twist drill, which was similar to that developed by Hocheng and Dharan [120], and with a worn twist drill [104]. Since it was assumed that CFRP laminates were subjected to pure bending load by indentation of chisel edge, only wear on the chisel edge was considered [104]. It was assumed that laminates were subjected to distributed load along the worn chisel edge when drilling with a worn tool in contrast to drilling with an unworn tool for which pointed load exerted at the centre of laminates was assumed [104]. Although it was shown that an increase in tool wear resulted in a higher critical thrust force during drilling, the results of drilling experiments showed that it contributed to a more dominant increase in drilling thrust force, hence resulting in larger delamination [104]. An increase in size of delamination due to increased tool wear was also shown by Chen [16].

Similar effect of feed rate on delamination has been reported among other researchers. It was reported that larger delamination was produced as feed rate increased when drilling

CFRPs regardless of drill material and geometry due to increased thrust force [19, 89, 92, 96, 101, 107, 117, 124, 128]. An increase in thrust force with increased feed rate was previously discussed in Section 3.2.2.2. However, different results of effect of cutting speed on delamination have been reported. Some researchers showed that increases in cutting speed resulted in larger delamination being produced [19, 20, 128]. The reason for an increase in delamination with increased cutting speed was not discussed in their work. It is suggested that this was because an increase in tool wear, which resulted in higher thrust force, and higher cutting temperature produced, which would result in lower strength of material and resistance to delamination, with increased cutting speed. In contrast, it was reported by other researchers that less delamination was produced as cutting speed increased [89, 101, 105-108, 124]. It is suggested that this was attributed to a decrease in thrust force with increased cutting speed [105-108]. A reduction in drilling thrust force with increased cutting speed was due to a decrease in strength of workpiece material as a result of higher cutting temperature [105-108]. However, Tsao and Hocheng [90] and Marques *et al.* [96] reported that the effect of cutting speed on delamination was less dominant compared to the effect of feed rate.

3.4 Review on the Attempts to Reduce Delamination Damage

As mentioned in Section 3.3, there has been much research work reported on the attempts to minimise or eliminate drilling-induced delamination in conventional drilling of CFRPs. This is because of criticality and significant effect of delamination on quality, assemble tolerance and mechanical properties of a component [3, 4, 7, 9, 12, 96, 118]. Due to a positive correlation between thrust force and delamination discussed in Section 3.3.3, the attempts to reduce delamination have been focused on reducing drilling thrust force or increasing critical thrust force at which delamination occurs. These attempts will be reviewed in the following aspects.

3.4.1 Optimisation of Machining Parameters

It was proposed by other researchers that low feed rate should be used to minimise thrust force and hence delamination when drilling CFRPs [19, 89, 92, 96, 101, 107, 117, 124, 128]. However, it is suggested that an objective of improving productivity of the process should also be considered when selecting a value of feed rate.

In order to achieve delamination-free drilling while improving productivity of the process, Stone and Krishnamurthy [119] and Piquet *et al.* [17] proposed drilling process using a varied feed rate through the thickness of CFRP plaque. It was shown in their work that drilling with a varied feed rate through the thickness of the plaque produced less

delamination, which was examined by visual inspection, compared to drilling with a constant feed rate [17, 119]. However, the amount of delamination reduction was not quoted in their work. In the drilling process used by Stone and Krishnamurthy [119], feed rate was varied according to critical thrust force values at different locations through the thickness of the plaque, which was calculated from Hocheng and Dharan's delamination model [120]. In contrast, feed rate was varied according to critical thrust force values calculated from a delamination model proposed by Jain and Yang [88].

As discussed in Section 3.3.4, different trends of the effect of cutting speed on delamination were reported among other researchers. As a consequence, it is proposed by a group of researchers that low cutting speed should be used to minimise drilling-induced delamination [19, 20, 128]. In contrast, other researchers proposed that a high cutting speed should be used to reduce delamination due to thrust force reduction in drilling CFRPs [105-108]. The reason for a reduction of thrust force with cutting speed was discussed previously in Section 3.3.4. It was shown by Rubio *et al.* [107] delamination in terms of F_d was reduced by 24-32% as cutting speed increased from 125 m/min (8,000 RPM) to 628 m/min (40,000 RPM) when drilling CFRPs with a 5 mm diameter carbide twist drill. A benefit of delamination reduction by high-speed drilling of CFRPs was also reported by Gaitonde *et al.* [105] and Karnik *et al.* [106] when drilling at a cutting speed of 600-630 m/min (38,197-40,000 RPM) with a 5 mm diameter carbide twist drill and by Rawat and Attia [108] when drilling at a cutting speed of 235.5 m/min (15,000 RPM) with a 5 mm diameter carbide twist drill. However, the author suggests that a high rate of tool wear, which results in shorter tool life, should also be considered when drilling at a high cutting speed as it was reported that tool wear increases with increasing cutting speed [15, 16].

3.4.2 Optimisation of Tool Material and Geometry

Since an increase in tool wear resulted in higher thrust force and, hence, larger delamination [16, 104], it is proposed that tool material or tool coating with high resistance to abrasion wear, which was observed the major wear mechanism when drilling CFRPs, should be used to reduce delamination. It was proposed that a diamond coated tungsten carbide drill and a polycrystalline diamond (PCD) drill were suitable for drilling CFRPs as tool life was improved due to higher resistance to abrasion wear compared a high speed steel (HSS) drill and uncoated tungsten carbide drill [10, 99, 129].

Since the indentation action by the chisel edge contributes to a major proportion of total thrust force as discussed in Section 3.2.2.1, quantity of delamination would be decreased by reducing or eliminating the action by chisel edge. It was reported by other researchers that using a drill with improved geometry to reduce or eliminate chisel edge action resulted in

less delamination compared to drilling with a standard twist drill [17, 20-23, 90, 92, 93, 121, 126].

Piquet *et al.* [17] proposed a carbide drill with specially designed geometry which had a small rake angle for preventing delamination at the hole entrance as a result of peeling action, three main cutting edges for improved heat dissipation due to increased tool/workpiece contact length and reduced chisel edge length to decrease indentation action by the chisel edge, Figure 3.15.

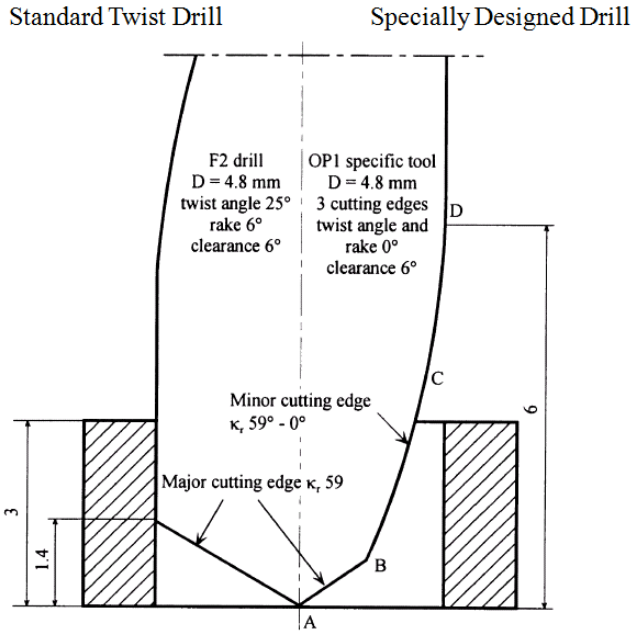

Figure 3.15: Schematic diagram of a drill with specially designed geometry proposed by Piquet *et al.* [17] compared to a standard twist drill

It was shown that drilling with a specially designed tool resulted in lower thrust force and less delamination compared to drilling with a standard carbide twist drill [17]. Piquet *et al.* [17] proposed that a benefit of thrust force reduction by a drill with specially designed geometry was due to the fact that the major cutting edges of a specially designed drill engaged in the cutting after the chisel edge had already penetrated through the plaque because of increased length and number of cutting edges, preventing simultaneous contribution from major cutting edges and chisel edge to the total thrust for during drilling the plaque. This was contradictory to drilling with a standard twist drill in which major cutting edges and chisel edge engaged in the cutting simultaneously during cutting. In addition, cutting load would be distributed on longer and more cutting edges of a drill with special geometry resulting in less flank wear along the cutting edges hence lower thrust force compared to a standard twist drill [17]. However, due to longer cutting edges, it is suggested that sufficient space below the exit of the plaque would be required, similar to

drilling with a Dagger drill [92, 96]. It is suggested that at least additional space of 6 mm high is required for this specially designed drill with 6 mm diameter, Figure 3.15.

Durao *et al.* [92] and Davim and Reis [20] reported that drilling with a Brad & Spur drill and with a Dagger drill resulted in less delamination compared to drilling with a twist drill due to lower thrust force produced. A benefit of thrust force and delamination reduction by a Brad & Spur drill is attributed to distribution of cutting load to cutting edges on the drill periphery, hence reducing indentation action by the chisel edge [20]. For a Dagger drill, having a small point angle reduces chisel edge length and, hence indentation action by the chisel [92]. In addition, having long cutting edges allows the chisel edge penetrates through the exit of the plaque before the major cutting edges engage in cutting, thus reducing thrust force by the chisel edge action [92].

It was shown by other researchers that using a saw drill, candle stick drill, core drill and step drill, Figures 3.16-3.19, resulted in less delamination compared to drilling with a standard twist drill [21-23, 90, 93].

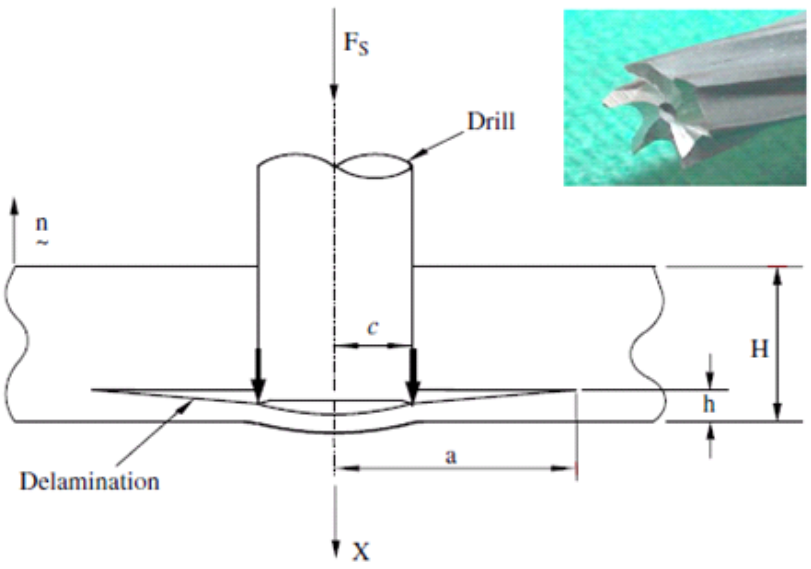

Figure 3.16: Image of a saw drill and associated delamination model when drilling CFRPs [22]

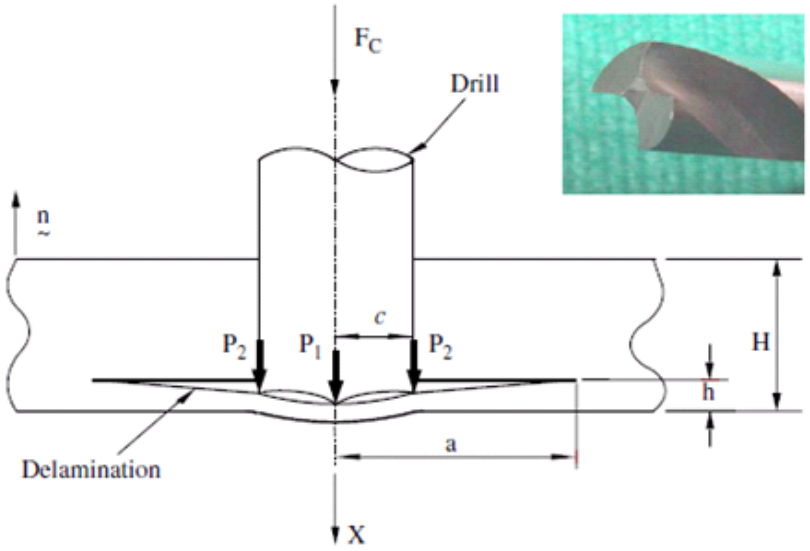

Figure 3.17: Image of a candle stick drill and associated delamination model when drilling CFRPs [22]

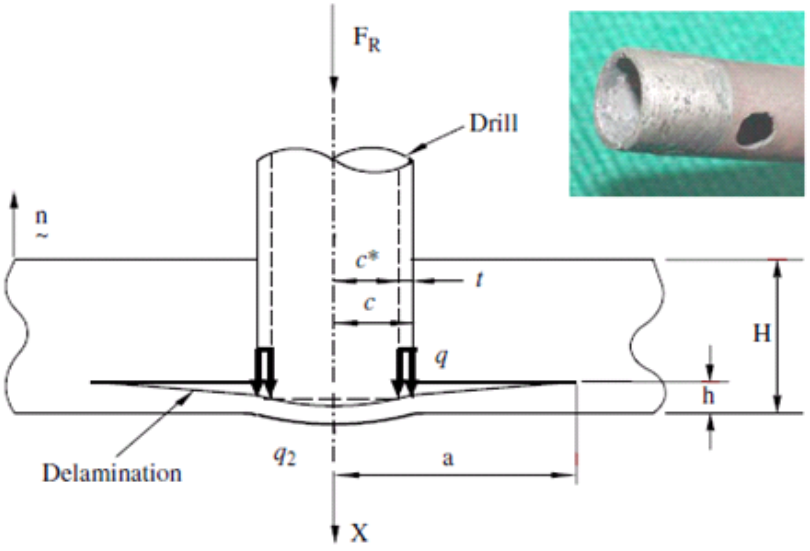

Figure 3.18: Image of a core drill and associated delamination model when drilling CFRPs [22]

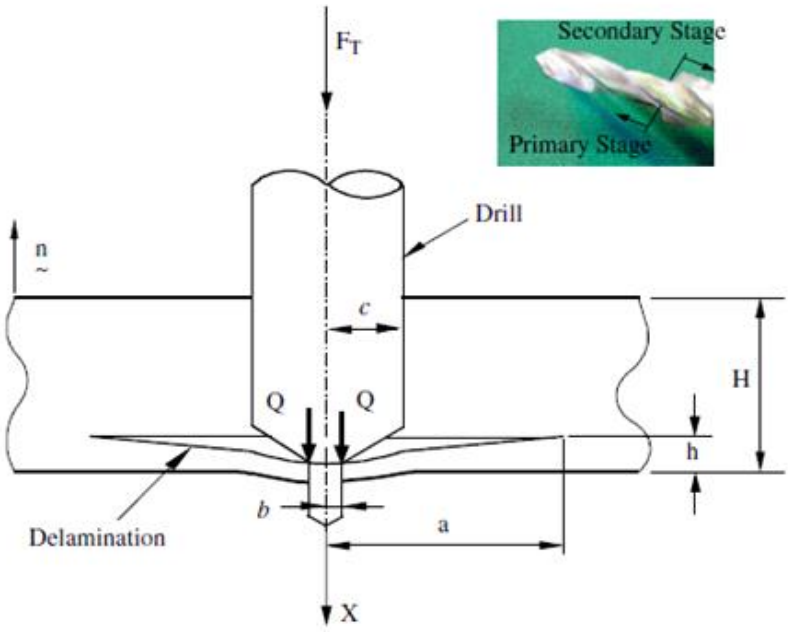

Figure 3.19: Image of a step drill and associated delamination model when drilling CFRPs [22]

Hocheng and Tsao [21, 22] developed a delamination model for a saw drill, a candle stick drill, a core drill and a step drill based on elastic fracture mechanic and plate bending theory using similar assumptions used by Hocheng and Dharan [120], Figures 3.16-3.19. It was calculated from their proposed delamination model that drilling with an improved tool geometry provided a benefit of higher critical thrust force compared to drilling with a conventional twist drill [21, 22], for which a critical thrust force was calculated from Hocheng and Dharan's delamination model [120]. It was also shown by the results of drilling experiments that lower thrust force was produced when drilling with an improved tool geometry compared to drilling with a conventioanl twist drill [22]. Due to higher critical thrust force plus lower drilling thrust force, less delamination extent was observed when drilling with an improved tool geometry [22]. Hocheng and Tsao [21, 22] explained that a benefit of thrust force and delamination reduction by a saw drill, a candle stick drill and a core drill was resulting from distribution of thrust force towards the drill periphery, hence reducing or eliminating concentrated load at the centre of laminates by the chisel edge as opposed to the case with a conventional twist drill. For a step drill, thrust force that contributed to delamination, which was critical to quality of the hole, i.e., delamination of size larger than hole diameter, was only resulting from cutting action by the major cutting edges in the secondary section rather than by the chisel edge in the pilot section [21, 22]. Consequently, exit laminates was subjected to less bending compared to drilling with a twist drill for which thrust force was resulting from the action by the chisel edge and the major cutting edges simultaneously. In addition, delamination caused by chisel edge in the pilot

section would be removed during cutting by the major cutting edges in the secondary section [21, 22]. A mechanism contributing to a reduction in thrust force and delamination by a step drill is similar to that by drilling with a pre-drilled pilot-hole [24, 25], which will be discussed in Section 3.4.3.

Marques *et al.* [96] and Durao *et al.* [121] also reported a benefit of thrust force and delamination reduction by drilling with a step drill, Figure 3.19. It was shown in their work that lower thrust force and less delamination were produced when drilling with a step drill compared to drilling with a twist drill, a Brad & Spur drill and a Dagger drill. However, Durao *et al.* [121] proposed that a diameter of the pilot section less than 3.4 mm is recommended for a step drill with 6 mm diameter in order to achieve thrust force and delamination reduction. They showed that drilling with a diameter of the pilot section larger than 3.4 mm resulted in larger delamination compared to drilling with a twist drill even though thrust force was reduced [121]. This was because of a reduction in resistance to delamination of the laminates during the cutting by cutting edges in the secondary section [121].

A benefit of thrust force and delamination reduction by drilling with a core drill compared to a twist drill was also reported by Jain and Yang [85]. The reason for an improved drilling performance by a core drill was similar to that proposed by Hocheng and Tsao [21, 22]. However, other researchers proposed that drilling with a core drill has disadvantages of low material removal rate and difficulty in removing chips from the interior part of a core drill even though it contributed to improved drilling performance [12, 24, 95, 101, 130, 131]. For this reason, Tsao [95, 123] and Tsao and Hocheng [101] proposed using a core-saw drill and core-twist drill, Figure 3.20, to improve drilling performance while reducing disadvantages associated with using a conventional core drill. It was shown in their work that a core-saw drill and a core-twist drill produced lower thrust force and less delamination compared to a standard twist drill and a conventional core drill [95, 101, 123]. An improvement in drilling performance by a core-saw drill and a core-twist drill was attributed to distribution of cutting load towards the drill periphery with improved chip removal from the interior part of the drill by the inner saw and twist drill [95, 101, 123].

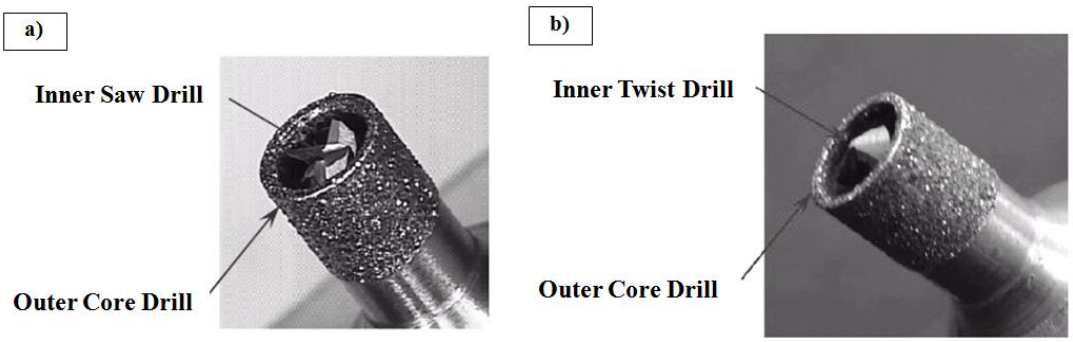

Figure 3.20: (a) Core-saw drill [123] and (b) Core-twist drill [95]

3.4.3 Conventional Drilling with Modified Process

In addition to drilling with improved tool geometry, the effect of indentation action by the chisel edge can also be reduced by drilling with a pre-drilled pilot hole [24, 25, 121], Figure 3.21. Since a pilot hole of which a diameter equal to the length of chisel edge has been drilled, CFRP laminates is not subjected to indention action by the chisel edge, which contributes to a major proportion of total thrust force, during drilling with a tool of actual size of hole diameter [24, 25, 121]. In addition, as diameter of a pilot hole is less than a diameter of the tool, delamination induced by drilling of a pilot hole would be removed by drilling with a tool of actual hole diameter and it would not be critical to quality of the hole [24, 25, 121].

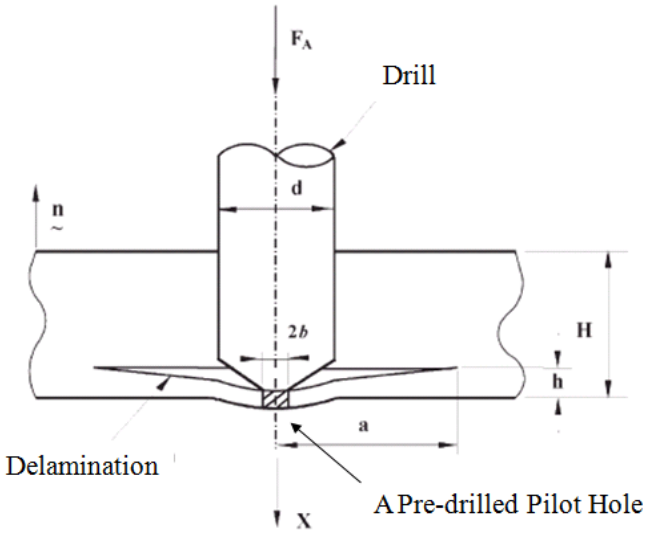

Figure 3.21: Schematic diagram showing drilling process with a pre-drilled pilot hole [25]

Won and Dharan [24] and Tsao and Hocheng [25] proposed a delamination model for calculating a critical thrust force at which delamination occurs when drilling using a twist drill with a pre-drilled pilot hole. It was shown that drilling with a pre-drilled pilot-hole resulted in lower critical thrust force compared to drilling without a pilot-hole [24, 25],

which was calculated by Hocheng and Dharan's delamination model [120]. They proposed that this was because bending strength and stiffness of uncut laminates, i.e., resistance to delamination, was decreased due to less amount of material under the drill [24, 25]. However, it was shown that lower thrust force was produced when drilling with a pre-drilled pilot hole [24, 25]. Tsao and Hocheng [25] reported that drilling with a pre-drilled pilot hole produced 25-50% lower thrust force compared to drilling without a pre-drilled pilot hole, resulting in a higher allowable feed rate at which no delamination would be produced. Won and Dharan [24] also reported that drilling with a pre-drilled pilot hole provided a wider range of allowable feed rates (0.1-0.7 mm/rev) at which delamination-free drilling was achieved compared to drilling without a pilot hole (0.1 mm/rev). However, Durao *et al.* [121] proposed that diameter of a pre-drilled pilot hole should be selected appropriately as resistance to delamination of the laminates would be reduced with increased diameter of a pilot hole, hence increasing possibility of delamination damage.

As mentioned previously, delamination can also be reduced by increasing critical thrust force at which delamination occurs, i.e., increasing resistance to delamination of the laminates. It was reported that this attempt to reduce delamination was achieved by drilling with a back-up plate [27] or a support structure at the exit of the plaque [26]. Tsao and Hocheng [27] reported that no delamination was observed throughout the whole range of feed rates used in their work (0.08-0.16 mm/rev) when drilling using a saw drill and a core drill with an exit back-up plate because thrust force produced was lower than a critical thrust force. Although it was shown that using an exit back-up plate resulted in higher drilling thrust force, it contributed to higher critical thrust force during drilling due to higher resistance to bending load as deflection of laminates at the exit was restricted [27]. An increase in critical thrust force while producing higher thrust force due to restriction of bending deflection of the laminates was also reported by Capello [26] when drilling by a twist drill with support structure at the exit.

3.5 Non-Conventional Drilling Process

In order to reduce delamination induced by conventional drilling of CFRPs, non-conventional drilling processes, e.g. vibration assisted drilling, laser machining, water jet or abrasive water jet machining and ultrasonic drilling, have been applied to CFRP components [4, 9, 11, 126]. In vibration-assisted drilling, workpiece material is removed by pulsed and intermittent cutting process due to vibration of the drill in axial direction as opposed to continuous cutting in conventional drilling process, resulting in lower thrust force and lower possibility of delamination damage [4, 9, 11, 126]. In ultrasonic drilling, ultrasonic vibration of the tool in axial direction causes localised impact between workpiece material and

abrasive slurry [4, 126]. This localised impact contributes to material removal by micro-chipping, resulting in good surface finish of drilled hole. In laser machining, a focused spot of high-energy beam (10^8 W/cm^2) with 0.1-1.0 mm diameter is used to remove material by melting, vaporization or chemical degradation through the thickness of workpiece material [4, 11, 126]. Laser machining offers a benefit of delamination elimination since there is no mechanical contact between the drilling tool and the workpiece [4, 55, 126]. However, thermal damage on the machined surface of the hole is a problem associated with laser machining due to difference in thermal conductivity of carbon fibres and polymeric matrix [4, 11, 55, 126]. Water jet or abrasive water jet machining also removes material by localised impact, hence resulting in improved quality of the machined surface [4, 126]. Although these non-conventional drilling processes have shown potentials for improving drilling performance associated with CFRPs, conventional drilling processes are still the most widely used routing hole-making process for CFRP components in industry [3, 4, 7-9, 11, 47, 55].

3.6 Conclusion

Among the hole-making processes in industry, conventional drilling processes using a drilling tool is still important and commonly applied for routine hole-making processes for CFRP components. However, damage induced by conventional drilling usually occurs due to high level of anisotropy in CFRPs. Delamination is considered the damage of most concern due its severe effect to the structural integrity and mechanical properties of CFRP components. For this reason, there has been much research work reported on approaches for reducing or eliminating delamination induced by conventional drilling of CFRPs. From the literature, there have been many attempts to reduce delamination by optimising machining parameters, using improved material and geometry of the tool and using conventional drilling with modified process. However, there has been little published work on the application of cutting fluids and cryogenic cooling to reduce delamination induced by conventional drilling of CFRPs. This indicates a research gap for the application of cutting fluids and cryogenic cooling to improve drilling performance of CFRPs. Due to an improvement in metal machining by cryogenic cooling, which has been reported in other published work, plus a trend for moving towards an eco-friendly machining process, application of cryogenic cooling has shown potential to be a preferable option for improving performance of drilling process of CFRPs.

4 An Overview of the Application of Cryogenic Cooling in Machining Processes

4.1 Introduction

As discussed in Chapter 3, there has been little published research on the application of cutting fluids to improve performance when drilling CFRPs. The conventional water-based emulsion cutting fluids are generally avoided when drilling CFRPs in industry to prevent material degradation due to moisture absorption and to reduce the cost of cleaning although they have been used for the purpose of dust suppression and for controlling cutting temperature in some cases [10, 13, 32]. In addition, there has been pressure on industries to minimise or eliminate the use of water-based emulsion cutting fluids in machining processes due to the cost implications plus health and environmental problems caused by the use of such conventional cutting fluids [28-31]. The cryogenic cooling by using cryogen medium in liquid or gaseous form has been claimed to be more environmental friendly cooling and lubricating method for machining processes and has shown improvement in the performance of metal machining processes [28-31, 36]. Therefore, cryogenic machining has the potential to be applied in the conventional drilling process for CFRPs to improve drilling performance without causing material degradation problems due to moisture absorption and additional cost of cleaning the parts since the cryogen medium such as liquid nitrogen (LN_2) or solid or gaseous carbon dioxide (CO_2) will evaporate to the atmosphere after absorbing the cutting heat [31, 34, 36]. Although there has been little published research work on the use of cryogenic cooling in the drilling of CFRPs, it is important to understand the application of this technique and its effect on the machining processes. For this reason, an overview of the application of cryogenic cooling will be presented in this chapter. Although various cryogen mediums exist such as nitrogen, carbon dioxide, helium and oxygen, the overview of the cryogenic cooling presented in this chapter will focus the cryogenic cooling by the use of nitrogen and carbon dioxide, which are the common medium used in the cryogenic cooling for machining work [31, 34, 36].

4.2 Reasons for the Application of Cryogenic Cooling in Machining Processes

Before considering the application techniques for cryogenic cooling and their effect on the performance of machining processes, the reasons why cryogenic cooling is used for improving machinability are worth considering. In the machining process of metallic materials, the cutting mechanism involves extensive amount of plastic deformation of the workpiece material in the primary shear zone, area (a) in Figure 4.1, with a typical shear

strain of γ = 2-5 and in the secondary shear zone, area (b) in Figure 4.1, with a typical shear strain of γ = 10-50 [72]. According to Trent and Wright [72] and Knight and Boothroyd [132], 99% of the energy which is used to cause this deformation is converted into heat because of the large amount of plastic deformation. In addition to the heat being generated in the primary and secondary shear zones, heat is also generated as a result of plastic deformation in the tertiary shear zone, area (c) in Figure 4.1, where the flank face of the tool makes contact with the newly formed surface of the workpiece. Most of the heat generated in the primary shear zone will be carried away with the chips, while some will be transmitted into the workpiece through conduction. Combined with the conduction of the heat generated in the tertiary shear zone, the heat in the primary shear zone which is conducted in to the workpiece increases the temperature of the workpiece, which needs to be controlled to prevent dimensional accuracy error due to thermal expansion of the workpiece. The heat generated in the secondary shear zone on the underside of the chip is of most concern and most difficult to remove. Since seizure between the chip and rake face of the tool usually occurs in the secondary shear zone, workpiece material in the secondary shear zone is subjected to a continuous and larger shear strain relatively to that in the primary shear zone, which was previously mentioned. Due to a continuous and larger shear strain, higher temperature is generated in the secondary shear zone. Consequently, this is where the maximum temperature of the cutting process is generated. The temperature in the secondary shear zone as high as 1150°C have been measured during the machining of AISA/SAE 4140 at 925 m/min [133]. Although some of the heat in the secondary shear zone can be carried away through conduction into the chip, most of the heat is accumulated at the interface between the rake face of the tool and the underside of the chip because of the continuous plastic deformation of the workpiece material in the secondary shear zone where seizure between the chip and rake face of the tool occurs. Since the underside of the chip is seized to rake face of the tool, the heat generated in the secondary shear zone in conducted into the cutting tool very efficiently resulting in an increase in the cutting tool temperature for which the maximum temperature of the rake face of the tool is the same as that in the secondary shear zone where seizure occurs. This results in lower hardness and strength of the tool which can significantly affect tool life, quality of the machined surface and hence limit productivity of the machining process since cutting temperature increases with the increased cutting speed [28, 31, 72].

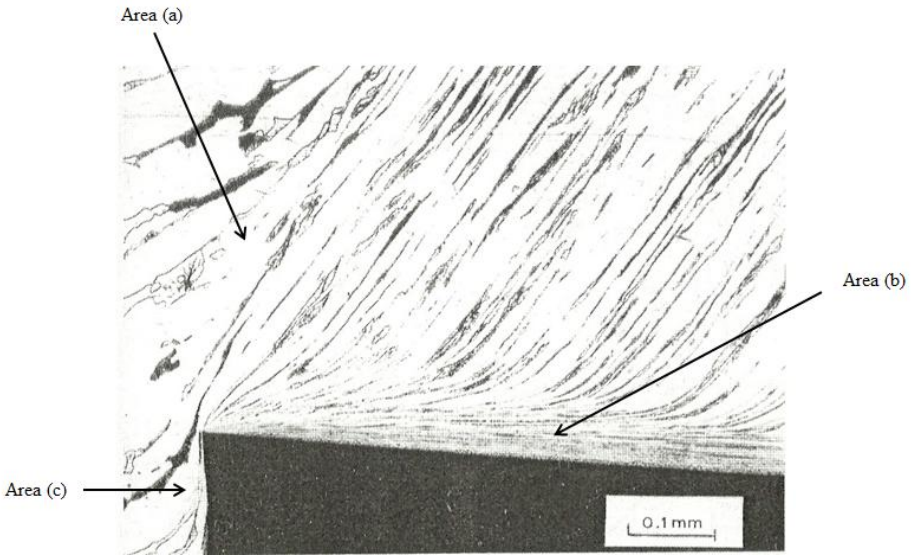

Figure 4.1: Quick-stop section showing deformation in the primary shear zone (area (a)), secondary shear zone (area (b)) and tertiary shear zone (area (c)) when machining 60/40 brass at 120 m/min (adapted from [72])

In addition to the effort to develop tool materials with higher elevated temperature strength and hardness, cutting fluids are used in machining process to remove heat generated in the cutting zone, which will reduce the cutting temperature, as well as reduce the friction at the tool/chip interface [28, 31, 72]. However, as previously mentioned, there has been a trend to minimise or eliminate the use of conventional water-based emulsion cutting fluids in machining processes in industry due to their economical, health and environmental problems [28-31]. The cost associated with the use of conventional cutting fluids, especially the maintenance and treatment/disposal cost, can be high and it is reported to be approximately 16% of the total manufacturing cost [134]. The additives and chemicals, which are added to conventional cutting fluids to obtain stability in the performance of the cutting fluids, as well as the heavy metals being carried with the cutting fluids during machining process, can cause environmental problems such as toxicity and contamination in ecological areas if the cutting fluids are not treated properly before disposed [29-31]. In addition, toxicity of the chemicals in conventional cutting fluids can cause health problems to machine operators such as skin cancer and respiratory system problems when they are in contact with the cutting fluids and inhale the mist of cutting fluids in the machining area [29-31]. As a consequence, there has been a trend to moving towards a more environmental-friendly machining process by minimising or eliminating the use of conventional cutting fluids.

Due to a low temperature of liquid cryogen mediums, cryogenic cooling using liquid nitrogen (-196°C) and liquid carbon dioxide (-80°C when expands to room temperature and air pressure [30]) have potential to replace conventional cutting fluids in removing the heat

generated in the cutting zone and reducing friction at the tool-chip interface by the application of a high-pressure jet in the cutting zone, while being environmental friendly and sustainable [30, 31, 34, 36]. It is reported that changing from using conventional cutting fluids to cryogenic cooling significantly reduces solid waste, water usage, global warming potential and aquatic toxicity, while eliminating the machine operators' health concerns due to exposure to the chemicals in conventional cutting fluids [29, 33]. Although the use of cryogenic cooling by LN_2 would increase the energy used for production of LN_2 cutting fluid, a higher productivity of the machining process obtained when using cryogenic cooling can compensate with this increase of energy usage [33]. Since a major proportion of air is nitrogen gas (78%), which is an inert gas, it is harmless when it evaporates in the machining area or when it is released to the atmosphere as long as the level of the gas is below the critical level which can kill machine operators by suffocation [33, 34, 36]. Although carbon dioxide (CO_2) is a greenhouse gas, the use of CO_2 in cryogenic machining is not considered a generator of greenhouse gases into the atmosphere because CO_2 can be obtained as a by-product from the chemical industry and power plants [30]. Since CO_2 can be obtained as a by-product from the chemical industry, power plants and a natural CO_2 gas well [3, 29, 30, 35, 44], it is suggested that the use of cryogenic cooling by CO_2 would reduce the energy and waste associated with the production of cutting fluids, including the cryogenic distillation of LN_2.

Although there has been a trend to avoid using conventional cutting fluids and move towards cryogenic machining, which is claimed to be cheaper and more environmental friendly, it is suggested that conventional cutting fluids will still be applied in a majority of industrial machining processes such as in high speed machining processes for many years in the future. Changing from using a conventional cutting fluid to cryogenic cooling will require additional cost and time for installing new cutting fluid systems. In addition, most of the machinists in industry are experienced in machining with a conventional cutting fluid, so they will require training for using a new machining system with cryogenic cooling. If a modern cutting fluid, which is developed to reduce harmful chemical and to increase service life, is maintained, treated and disposed properly, problems to environment and machine operators' health will not be an issue. Unfortunately, cost associated with the use of an effective maintenance, treatment and disposal systems will still be concerned when applying conventional cutting fluids. However, this increased cost might be compensated if a significant improvement in tool life and productivity of machining processes could be achieved.

4.3 The Cryogenic Machining Using Liquid Nitrogen (LN_2)

According to Yaildiz and Nalbant [34], the approaches of cryogenic machining using LN_2, which generates temperature of -196°C, can be classified into four groups:

1) Cryogenic pre-cooling of the workpiece
2) Indirect cryogenic cooling of the cutting tool
3) Cryogenic cooling of the cutting zone by the injection of cryogen
4) Cryogenic cooling of the tool before performing the cutting process, which Shokrani *et al.* [36] regarded as cryogenic processing (treatment) of the cutting tool.

4.3.1 Cryogenic Pre-Cooling of the Workpiece

The main objective of cryogenic cooling of the workpiece before or during machining is to change the properties of the workpiece material and improve chip breakability as a result of decreased temperature [34, 36]. Bhattacharryya *et al.* [135] achieved an improvement in surface finish when machining Kevlar composites, which generally produced a poor quality machined surface due to toughness of the Kevlar fibres, by two cooling approaches: 1) Dipping the workpiece in LN_2 bath before being machined and 2) Pouring LN_2 onto the workpiece during machining process. In the work of Hong *et al.* [136, 137], it was shown that the chip breakability of AISI 1008 low carbon steel, which possessed high welding tendency at the tool/chip interface and high susceptibility for built-up edge formation, was improved, hence reduced the cutting forces, by directing a LN_2 jet to the chips being produced to increase the brittleness of the chips. Although the improvement in chip breakability has been shown, it is suggested that this cooling approach is not practical for production process in industry due to high consumption of LN_2 [34, 37]. In addition, the cooling of the workpiece also resulted in negative effect by increasing cutting force and abrasion-induced wear due to the increase strength and hardness of the workpiece [34, 37]. The author also suggests that the cooling approach by dipping the workpiece in LN_2 bath or pouring LN_2 onto the workpiece is not practical to be applied in industrial machining processes and would cause problems in dimensional accuracy due to thermal contraction and expansion of the workpiece.

4.3.2 Indirect Cryogenic Cooling of the Cutting Tool

The main objective of indirect cryogenic cooling of the tool is to remove the heat being generated in the cutting zone by conduction through the cutting tool without direct contact of the cryogen with the tool/workpiece interface [34, 36]. In this cooling approach, LN_2 is applied to chamber over the rake face or underneath the back of the cutting tool where it absorbs heat from the cutting zone through conduction and evaporates to the atmosphere

through a releasing chamber. A schematic diagram showing an example of indirect LN_2 cooling on the back of the cutting tool is presented in Figure 4.2.

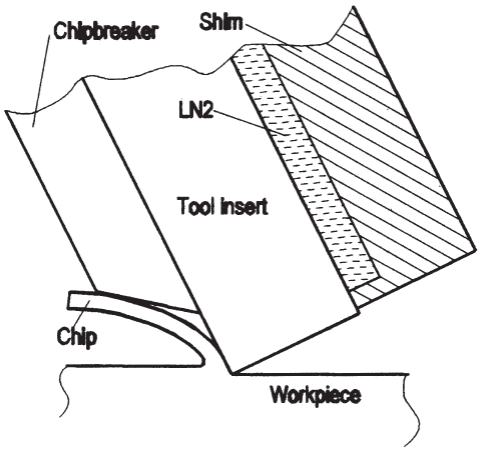

Figure 4.2: Schematic diagram showing the application of indirect LN_2 cooling to the back of the cutting tool [37]

Wang *et al.* [138] performed indirect cryogenic cooling to reduce the temperature and improve wear resistance of a polycrystalline boron nitride (PCBN) tool in a turning reaction bonded silicon nitride (RBSN) ceramic, which can maintain high strength at 1400°C. In their work [138], a cryogenic cooling circulation system, in which LN_2 was applied to the chamber in the cap over the rake face of the tool where it removed the generated heat from the cutting process by conduction through the tool and evaporated it through an outlet channel, was used, thus reducing the temperature of the cutting tool. It was shown that the use of a LN_2 cooled tool resulted in longer tool life, as tool wear was significantly reduced and better surface roughness was achieved compared to that when no cooling was applied [138]. This was because of the reduction of temperature of the tool (-160°C to -170°C measured 2 mm away and 1 mm above the cutting edge), which consequently result in higher wear resistance due to the retention of strength and hardness of the cutting tool and reduction of tool/chip contact length [138].

With the same cooling approach that was used by Wang *et al.* [138], Wang and Rajurkar [139] showed, from the finite element (FEM) analysis, that the temperature of the tool was decreased from 1153°C (without LN_2 cooling) to 829°C when LN_2 cooling of a PCBN tool was applied, contributing to improved tool life. In the later work of Wang and Rajurkar [140], it was shown that, with the same cooling approach, tool wear and surface roughness were significantly reduced compared to room temperature dry turning of RBSN with a PCBN tool and turning of Inconel 718 and tantalum with a carbide tool, and compared to machining with conventional cutting fluids when turning of Ti-6Al-4V with a carbide tool. This was because of the reduction of tool temperature which resulted in higher

wear resistance due to the retention of hardness and strength of the tool and reduction of chemical reactivity between the tool and the workpiece [140]. However, strength of the workpiece material hence cutting forces were not affected by the cooling because cryogen was applied only to the chamber in the cap above the tool without any contact on the workpiece [140].

Ahmed *et al.* [141] proposed an indirect cryogenic cooling approach by applying LN_2 to the back of the tool through a modified tool holder. The modified tool holder consisted of a chamber where LN_2 was stored and absorbed heat from the cutting zone by conduction through the tool. An inlet channel supplied LN_2 from the storage tank and an outlet channel removed and vaporised N_2 to be released [141]. The inlet and outlet channels were machined by electrical discharge machining process [141]. Although the amount of LN_2 being used in this cooling approach was not quoted in their work, Ahmed *et al.* [141] claimed that the use of LN_2 cooling of the tool by the modified tool holder could reduce the amount of LN_2 consumption while resulting in longer tool life (lower rate of tool wear) and better surface finish compared to the room temperature dry turning of AISI 4340 steel with carbide inserts, due to higher wear resistance of the tool as a result of reduction of tool temperature. It was also suggested by Ahmed *et al.* [141] that the outlet channel should be directed away from the cutting edge to prevent the increase of strength and hardness of the workpiece, which resulted in higher rate of tool wear and surface roughness, due to exposure to the cryogen. However, in the work of Ahmed *et al.* [141] performance of the cryogenic machining was only compared to the room temperature dry machining as they were aiming to avoid using conventional cutting fluids due to cost, environmental and health issues. The author suggests that a comparison between the applications of cryogenic cooling and conventional cutting fluids would be useful as it was shown by Avila and Abrao [142] longer tool life and better surface finish compared to room temperature dry machining were achieved by using a proper cutting fluid in turning AISI 4340 steel.

Although it has been shown that the indirect cryogenic cooling of the tool resulted in improved tool life and better quality surface finish compared to the conventional machining without affecting properties of the workpiece material, the effectiveness of the cooling approach is dependent on thermal conductivity of the cutting tool [37]. It is also suggested that the indirect cooling approach that was used in the work of Wang *et al.* [138-140] and Ahmed *et al.* [141] would add cost to the operation due to the manufacture of the modified tool holder if it will be used in the practical production process in industries.

4.3.3 Cryogenic Cooling of the Cutting Zone by Injection of Cryogen

The main objective of this cryogenic cooling approach is to remove the heat generated in the cutting zone, thus reducing the cutting temperature, while minimising the effect on properties of the workpiece material resulting from injection or spray of LN_2 directly to the cutting zone [34, 36]. Heat is removed from the cutting zone as well as reducing the coefficient of friction at the tool/chip interface, which will affect cutting forces, tool wear and surface roughness being produced [34, 36].

Zurecki *et al.* [143] developed a cryogenic cooling system in which a stream of LN_2 was sprayed into the cutting zone over the rake face of the tool through the cooling nozzle which was connected to the tool holder. It was found that machining with LN_2 cooling resulted in extended tool life and improved surface finish, which was shown by reduced plastic flow and smearing of workpiece material, compared to machining with conventional cutting fluid when finish-turning FN 0208 powder metallurgy steel [143]. This was attributed to lower temperature in the cutting zone [143]. Despite concerns regarding the effect of LN_2 temperature on the workpiece, the use of LN_2 cooling resulted in improved properties of the machined surface by retaining the surface hardness during machining [143]

In the work of Dhar *et al.* [144], a cryogenic cooling system, which delivered a jet of LN_2 to the principle and auxiliary cutting edges along grooves of the carbide insert, was developed. It was found that machining with a jet of LN_2 cooling produced lower cutting forces compared to room temperature dry machining when turning AISI 1040 and AISI 4320 steel [144]. This was attributed to lubrication effect of cryogenic cooling at the tool/chip interface, which consequently reduce the coefficient of friction at the tool/chip interface and hence tool/chip contact length [144]. It was also shown that cutting temperature, which was determined from FEM analysis, was reduced by 11-34% when machining with cryogenic cooling [144]. Although a reduction of cutting temperature would increase cutting forces due to increased strength of the workpiece, it was shown to result in improved tool/chip interaction by reducing plasticisation of the workpiece at the interface and retention of tool sharpness [144]. The improved tool/chip interaction, which resulted in a reduction of coefficient of friction and tool/chip contact length, is suggested to compensate the effect of increased strength of the workpiece due to lower cutting temperature, hence resulting in a reduction of cutting forces. Dhar *et al.* [144] also suggested that the effectiveness of the cryogenic cooling would be increased if applied along the groove design that enhance penetration to the cutting zone [144].

A reduction of cutting forces due to the lubrication effect of LN_2 jet cooling was also demonstrated in the work of Kumar and Choudhurry [145]. Kumar and Choudhurry [145] showed that machining with a jet of LN_2 jet (pressure of 490 kPa) directed to the cutting

edge over the rake face of the tool produced lower cutting forces compared to room temperature dry machining when turning SS202 stainless steel with carbide inserts. They proposed that the lubrication effect of LN_2 jet cooling was due to the presence of a cushion layer of N_2, which was formed by the evaporation of LN_2 after dissipating heat at the tool/chip interface. This reduced the coefficient of friction at the tool/chip interface and hence the tool/chip contact length. It was also shown that less flank wear was produced when machining with LN_2 jet cooling compared to room temperature dry machining due to lower cutting forces and lower cutting temperature, which resulted in the retention of hardness and strength of the tool [145].

In the work of Dhar *et al.* [144] and Kumar and Choudhurry [145], performance of cryogenic machining was not compared to when machining with a conventional cutting fluid. However, the author suggests that an application of LN_2 jet cooling to the cutting zone would provide better lubrication effect in the cutting zone compared to when machining with flooding of a conventional cutting fluid. This is because a jet of LN_2 would be able to access tool/chip interface, which seizure usually occurs, more effectively compared to machining with flooding of a cutting fluid.

With an application of two LN_2 jets simultaneously to the rake face and flank face using through-tool cooling nozzles, Venugopal *et al.* [40, 146] showed that tool wear on the rake face (crater) and flank face was reduced when compared to room temperature dry machining and machining with a conventional cutting fluid in the turning of Ti-6Al-4V with uncoated carbide inserts. Combined with a reduction in cutting temperature, the reduction of friction and chemical reactivity at the tool/chip interface due to the presence of a cushion layer of evaporating N_2 at the tool/chip interface contributed to the decrease of adhesion-dissolution-diffusion induced tool wear, which is temperature-dependent wear mechanism [40, 146].

Birmingham *et al.* [147] also developed a cryogenic cooling system directing two streams of LN_2 at a pressure of 827 kPa (8 atm) simultaneously to the rake face (through a nozzle in the tool holder) and flank face (though an auxiliary nozzle). It was shown by Birmingham *et al.* [147] that an increase in tool life and reduction of cutting force were achieved by machining with this cryogenic cooling approach compared to the room temperature dry turning of Ti-6Al-4V with uncoated carbide inserts. Based on a detailed study of chip morphology, Birmingham *et al.* [147] proposed that this improvement was attributed to; a reduction of the amount of plastic deformation associated with chip formation, which resulted in less heat being generated, combined with effective removal of heat from the cutting zone. Consequently, this resulted in a decrease in chemical reactivity at the tool/chip interface and higher wear resistance of the tool. Adhesion and diffusion-induced wear on the rake face and abrasion wear on the flank face were also decreased. It was also suggested by Birmingham *et al.* [147] that the reduction of cutting force was

attributed to lubrication effect of LN_2 directed onto the flank face rather than the effect of coefficient of friction at the tool/chip interface on the rake face. The author suggests that this was because a jet of LN_2 directed onto the flank face would be more effective in removing heat from the cutting zone as it is suggested to penetrate closer to the cutting zone compared to when directed to the rake face at which underside of the chip was seized to the rake face. Nevertheless, the cooling effect of LN_2 resulted in higher thrust force compared to the room temperature dry machining due to the increase of strength of the workpiece material [147].

However, it was shown in the later work of Birmingham *et al.* [43] that machining with LN_2 cooling (827 kPa) resulted in "slightly" shorter tool life when compared to the machining with high-pressure emulsion cutting fluid (10 MPa). Birmingham *et al.* [43] suggested that this was attributed to the better capability to decrease the amount of deformation, hence reducing heat generated in the chip formation process by the application of high-pressure emulsion cutting fluid.

In order to apply the cryogen as close to the cutting zone as possible, Khan and Ahmed [41] developed a cryogenic cooling system which applied a LN_2 cutting fluid to the cutting zone through a modified cutting tool, Figure 4.3. A LN_2 cutting fluid was supplied from a storage tank to an expanding chamber (7) through holes (3) and (4) in Figure 4.3. In the expanding chamber, LN_2 expanded to air pressure forming a low-temperature gaseous N_2 cutting fluid, which was directly applied to the cutting zone though the nozzle (6) underneath the cutting insert to provide cooling and lubrication effect at the cutting zone. Khan and Ahmed [41] showed that a four to five times increase of tool life was achieved by the machining with this cryogenic cooling system compared to the room temperature dry machining when turning AISI 304 stainless steel with titanium carbonitride (TiCN) coated carbide tools. However, the flow rate of LN_2 being used was not quoted in their work.

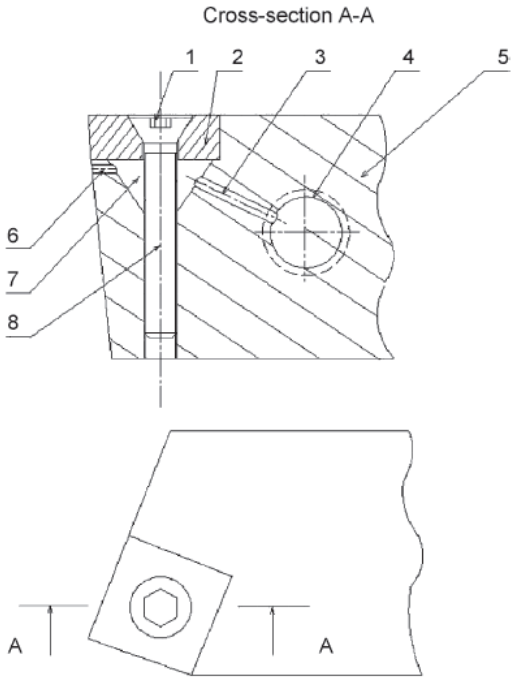

Figure 4.3: Schematic diagram showing a modified cutting tool for the cryogenic cooling system used by Kahn and Ahmed [41]. (1) Hexagonal slot of screw head, (2) Cutting insert, (3) A hole connecting LN_2 supply hole to the expanding chamber, (4) LN_2 supply hole (from storage tank), (5) Tool body, (6) A hole for releasing the expanded LN_2 in the chamber to the cutting zone, (7) Expanding chamber and (8) A threaded screw [41]

Dhananchezian and Kumar [42] also used a modified cutting insert to apply a LN_2 cutting fluid simultaneously at the rake and flank faces of the cutting edges. The LN_2 cutting fluid was applied onto the rake face and directed towards the flank face of the major and minor cutting edges through the electrical discharge machined hole. With this cooling approach, a reduction of cutting force, feed force, tool wear and surface roughness compared to room temperature dry machining was achieved when turning Ti-6Al-4V alloy with TiAlN coated carbide inserts [42]. Again, the flow rate of the LN_2 cutting fluid was not mentioned.

In order to reduce the amount of LN_2 usage, hence reducing the cost of the process, Hong *et al.* [37, 148, 149] developed a cooling system which locally applied a smaller quantity of LN_2 to the rake and flank faces of the cutting insert through two micro-nozzles, which were electrical discharge machined holes in a modified chip breaker, Figure 4.4. Directing LN_2 cutting fluid through these micro-nozzles inside the chip breaker enabled a precise supply of LN_2 along the rake face at the point where the chip had been lifted up by the chip breaker as well as along the flank face towards the cutting edge. With this cooling approach, the flow rate of LN_2 was reduced to 0.65 kg/min (compared to 3.36 kg/min for the conventional LN_2 jet cooling) while achieving a five times increase in tool life compared to the conventional machining when turning Ti-6Al-4V [149]. Machining with this LN_2 cooling approach also resulted in lower feed force, which is dominated by friction at the

tool/chip interface, due to the cooling and lubricating effect of LN_2 [148]. However, higher main cutting force was produced due to the increase of strength of the workpiece material as a result of lower cutting temperature, which was contrary to the findings of other researchers [42, 144, 145, 147].

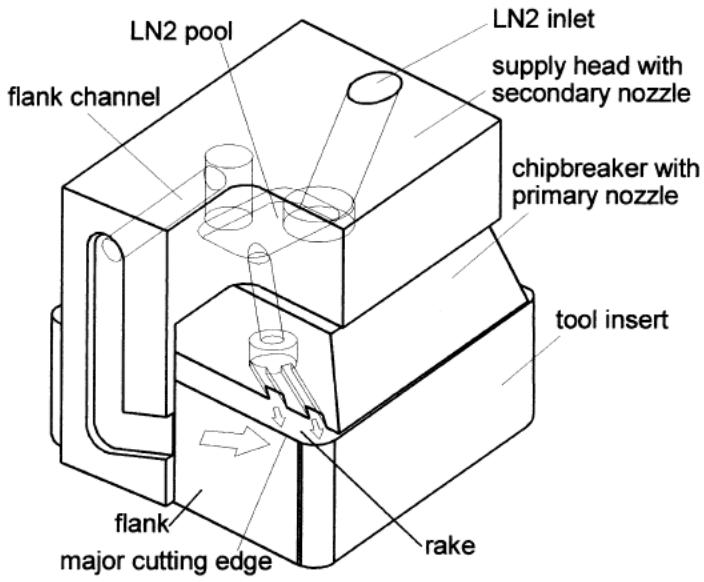

Figure 4.4: Schematic diagram of a modified chip breaker with two micro-nozzles for directing a small quantity of LN_2 precisely along the rake face and flank faces towards the cutting edge [37, 148, 149]

Since cryogenic cooling of the cutting zone by the injection of LN_2 has been shown to provide both cooling and lubrication effect at the cutting zone with the ability to minimise the quantity of LN_2 consumption, the author suggest that this cryogenic cooling approach is preferable as a practical production process in industry. Air Products Inc. and MAG Industrial Automation Systems are among the industries which implement cryogenic cooling in the commercial machine tools [31]. ICEFLY® cryogenic machining technology which is a cooling system implemented into a machine tool to deliver a jet of LN_2 to the cutting zone was developed by Air Products Inc. [150]. It has been reported that the machining with ICEFLY® cryogenic technology (0.72 kg/min, 698 kPa LN_2 jet) resulted in superior machining performance by improving properties of machined surface such as by reducing thickness of white layer, which reduces fatigue strength and wear resistance of the workpiece, and by retaining surface hardness of the workpiece when turning automotive powder metallurgy components [143, 151]. Better quality surface finish was also achieved due to a reduction of plastic flow and smearing of the workpiece material [143, 151]. Since superior properties of machined surface were achieved, production cost could be reduced by eliminating some steps such as pre-sinter, cleaning and draining, sinter, which was done in one step as sinter-harden and quench and temper process in the manufacturing process [143, 151, 152]. In the cooling system developed by MAG [153], minimum quantity of LN_2 is

delivered through the spindle, tool holder and tool and evaporates into gaseous form with rapid expansion (x700) near the cutting edge [154, 155]. This rapid expansion of LN_2 helps removing the chips from the cutting zone, which enable the cryogen to access closer to the cutting zone, and provides a cooling effect of the cutting zone by effectively turning the cutting tools into a heat sink [154, 155]. Due to the cooling effect, it was reported that a ten times increase in tool life and twice higher material removal rate were achieved when milling titanium while using 0.04 and 0.24 l/min LN_2 [155]. It was also reported that this cryogenic machining technology from MAG has been implemented in aircraft industry, oil and gas industry and medical industry and shown improvement in production process [154].

4.3.4 Cryogenic Processing of the Cutting Tool

The main objective of cryogenic processing of a cutting tool is to improve wear resistance of the tool, hence increase tool life, due to decreased temperature prior to the machining process [34, 36]. Da Silva *et al.* [156] found that using a cryogenically treated HSS tool improved tool life by 147-347% compared to an untreated tool when drilling AISI 8640 steel dry at room temperature. Firouzdor *et al.* [157] also reported that cryogenic treatment of a HSS tool resulted in 77-127% longer tool life when dry drilling CK40 carbon steel. The mechanism for an improvement in wear resistance of a cryogenically treated HSS tool was found to be the transformation of retained austenite in the structure of the tool material into martensite structure, which is harder thus contributes higher wear resistance [36, 156]. It was reported by Da Silva *et al.* [156] that cryogenic treatment reduced volume fraction of the retained austenite in the structure of a HSS tool from 25% to nearly 0%. In addition to the transformation of retained austenite into martensite, Firouzdor *et al.* [157] and Das *et al.* [158] found that an improvement in wear resistance of a cryogenically treated HSS tool was also attributed to the precipitation hardening carbides and more uniform distribution of these carbides in the structure as a result of cryogenic treatment. In the case of carbide tools, which are commonly used for industrial machining processes, Seah *et al.* [159] and Yong *et al.* [160] have reported that cryogenic treatment resulted in extended tool life due to higher wear resistance compared to the untreated tools when dry turning ASSAB 760 carbon steel. Yong *et al.* [161] found that using a cryogenically treated carbide tool resulted in an increase in tool life compared to using untreated tool when milling medium carbon steel. They also found that the performance of cryogenically treated tool was enhanced when machined with a conventional cutting fluid due to a reduction of cutting temperature [161]. It was found by Seah *et al.* [159] an improvement in performance of a cryogenic-processed carbide tool was attributed to an increase in η-phase, which is a mixed carbide of tungsten and other alloying metals e.g., titanium and tantalum, in the tool

microstructure after cryogenic treatment. This mixed carbide phase is harder and has higher elevated temperature strength thus increases wear resistance of the tool [159]. In addition to limited research, it is suggested that cryogenic processing of the tool is not stable for all machining applications and conditions and not applicable for modern cutting tool materials [34, 36].

4.4 The Cryogenic Machining Using Carbon Dioxide (CO_2)

In addition to LN_2, carbon dioxide (CO_2) has also been used by researchers as a cutting fluid and a cryogen to achieve cryogenic cooling in the machining process [35, 38, 44, 45, 162-165]. When liquid CO_2 or supercritical fluid CO_2 (T_c = 31.1°C, P_c = 72.8 atm [30]) expands to room temperature and air pressure, a mixture of solid and gaseous CO_2 with a temperature as low as -80°C is formed [30, 35], indicating the capability to remove heat generated in the cutting zone. Supercritical fluid CO_2 exists at temperatures and pressures above its critical point, which is 31.1°C and 7.14 MPa (72.8 atm) and has high diffusivity, low viscosity and high compressibility of a gas phase and high solubility of a liquid phase [30]. Although the use of a CO_2 cutting fluid does not generate a temperature lower than -153°C, which is defined as the "cryogenic" temperature [36], the machining processes using a CO_2 cutting fluid are referred by other researchers as the cryogenic machining processes [35, 38, 44, 45, 162-165]. Since the temperature generated by the use of a CO_2 cutting fluid was reported to be in the order of -70°C [166] to -80°C [30, 35], the potential harm to the machining operators, tools and equipment by CO_2 machining would be less than LN_2 cryogenic machining [35, 45] at -196°C. Cryogenic machining using a CO_2 cutting fluid is considered by some researchers to be more sustainable with respect to economic, environmental and health considerations than machining using a conventional cutting fluid, which was previously discussed in Section 4.2 [3, 29, 30, 35, 45].

De Chiffre *et al.* [39] performed an investigation involving parting/grooving and threading of AISI 304L and AISI 316L stainless steel using a mixture of CO_2 (0.36 l/min) and cutting oil compared to machining with a water-based cutting fluid. It was shown that the use of a CO_2/chlorinated oil cutting fluid resulted in improved tool life in a parting/grooving process, while the use of a CO_2/vegetable oil resulted in improved tool life in a threading process compared to the machining with a water-based cutting fluid. De Chiffre *et al.* [39] suggested that the improved tool life was due to the more effective removal of heat from the cutting zone by the use of a CO_2/oil cutting fluid which resulted in lower cutting temperature. As a consequence of lower cutting temperature, higher strength of the tool was retained resulting in higher wear resistance even though higher cutting force would be produced as strength of the workpiece material was increased. Although CO_2 can

be used alone as a cutting fluid for threading process, it was shown that a CO_2 cutting fluid was less effective in improving tool life compared to the use of a CO_2/vegetable oil cutting fluid, resulting in similar level of tool life compared to the machining with a water-based cutting fluid. The author suggests that this was because the benefit from lubrication effect by the cutting oil which reduced coefficient of friction at tool/chip interface.

It was reported by other researchers that using CO_2 alone as a cutting fluid could also improve the machining performance in turning process [35, 44, 45, 167]. Çakir *et al.* [167] showed that the cryogenic machining using a CO_2 cutting fluid by applying a high-pressure jet of CO_2 (481 kPa or 4.9 atm) to the cutting zone produced lower cutting force, thrust force and better surface finish compared to room temperature dry machining and machining with a water-based cutting fluid when turning AISI 1040 steel with carbide inserts. They proposed that this was because of the better cooling ability and lubrication effect at the tool/chip interface by the use of the CO_2 cutting fluid [167]. The temperature of the workpiece was found to be reduced to 13°C by the application of high-pressure jet of CO_2 before the turning process was carried out, indicating higher capability in removing heat from the cutting zone [167]. Although a reduction of workpiece temperature would result in an increase in cutting forces, it is proposed that this would also result in better conditions on the rake face, i.e., lower friction and shorter tool/chip contact length, due to less plasticisation of the workpiece at the interface. For lubrication effect, it was shown that machining with a CO_2 cutting fluid resulted in lower mean coefficient of friction at the tool/chip interface, which was calculated from the measured cutting force and thrust force by Merchant's theory [113], compared to dry machining and machining with a water-based cutting fluid [167]. The lower coefficient of friction contributed larger shear plane angle, which was calculated from the measurement of chip thickness, hence resulting in lower cutting force [167]. The author suggests that the benefit of lubrication effect by a CO_2 cutting fluid was similar to what has been proposed by Kumar and Choudhurry [145] and Venugopal *et al.* [40, 146] stating that friction and the tool/chip contact length were reduced due to the presence of cushion layer of evaporating cryogen at the interface as previously discussed in Section 4.2.3. Compared to the N_2 and O_2 cutting fluids, it was shown that the use of a CO_2 cutting fluid provided better cooling ability (lower temperature of the workpiece before the machining process was carried out) and lower coefficient of friction at the tool/chip interface hence resulting lower cutting force [167].

Machai and Biermann [35] also showed an improvement in machining performance using CO_2 when turning Ti-10V-2Fe-3Al titanium alloy with carbide inserts. In their work [35], liquid CO_2 (2.72 l/min) was applied to the cutting edge of the tool through the tool holder, which operated as a cooling nozzle. When expanded to room temperature and air pressure, the measured temperature of the CO_2 cutting fluid, which existed as a mixture

of solid and gaseous CO_2, was -80°C [35]. It was shown that the use of a CO_2 cutting fluid resulted in a 22-100% increase in tool life compared to the use of conventional cutting fluid as the rate of flank wear was reduced and the tool-life-limiting notch wear was eliminated when using cutting speeds of 50-150 m/min. Machai and Biermann [35] proposed that this was due to better cooling ability of a CO_2 cutting fluid as cutting heat was dissipated by low-temperature CO_2 cutting fluid, resulting in lower cutting temperature. As cutting temperature was reduced, strength and hardness of the tool was retained at higher level, contributing to higher wear resistance [35]. A reduction of cutting temperature also resulted in lower friction and shorter contact length between flank face of the tool and the workpiece due to less plasticisation of the workpiece [35]. Combined with higher wear resistance of the tool, this resulted in lower flank wear and absence of notch wear. Although a reduction of cutting temperature would result in an increase in cutting forces due to higher strength of the workpiece, it is proposed by Machai and Biermann [35] this was compensated by a reduction of friction at the tool/workpiece interfaces which reduced the cutting forces. Therefore, similar level of cutting forces between CO_2 machining and machining with conventional cutting fluid was produced in their work [35].

However, Jerold and Kumar [45] showed that CO_2 machining produced lower cutting forces compared to room temperature dry machining and machining with a conventional cutting fluid when turning medium carbon AISI 1045 steel. In their work, a jet of CO_2 with the measured temperature of -78°C when expended from liquid state to room temperature and air pressure was applied to the cutting zone through a cooling nozzle with a flow rate of 0.18 l/min. The reduction of the cutting forces when machining with a CO_2 cutting fluid was attributed to better effectiveness in reducing cutting temperature and lower friction at the tool/chip interface as a result of improved penetration of the CO_2 cutting fluid to the cutting zone compared to the room temperature dry and wet machining [45]. The lower cutting temperature and lower friction at the tool/chip interface consequently resulted in larger shear plane angle, which resulted in lower cutting forces [45]. In their work, it was shown that CO_2 cryogenic machining produced 5-22% lower cutting temperature and 6-21% larger shear plane angle compared to conventional machining [45]. Due to lower cutting temperature and lower friction at the tool/chip interface, which consequently shorten the tool/chip contact length and improved the chip breakability, 5-25% better surface finish was also produced when machined with a CO_2 cutting fluid compared to the conventional machining [45].

In the later work of Jerold and Kumar [44], which was also an investigation of the turning process with AISI 1045 steel, it was shown that CO_2 machining produced 2-12% lower cutting forces and 2-14% better surface finish compared to LN_2 machining even though 3-17% lower cutting temperature was produced by LN_2 machining. Jerold and

Kumar [44] proposed that since lower temperature was generated by a LN_2 cutting fluid compared to a CO_2 cutting fluid, lower cutting temperature would be produced when machining with a LN_2 cutting fluid due to the expected higher cooling ability. However, the lower cutting temperature resulting from the use of a LN_2 cutting fluid increased the strength and hardness of the workpiece material, resulting in higher cutting forces compared to CO_2 machining [44]. It was also shown that lower rate of flank wear was produced when machining with a CO_2 cutting fluid compared to that when machining with a LN_2 cutting fluid [44]. Although it was not suggested in the work of Jerold and Kumar [44], the author suggests that the higher tool wear when machining with a LN_2 cutting fluid was because of the higher cutting forces and the increased hardness and strength of the workpiece, which would contribute to more abrasive wear on the tool, as a result of lower cutting temperature when machining with a LN_2 cutting fluid. Due to the lower cutting forces and lower rate of tool wear, the CO_2 cryogenic machining was shown to produce 2-14% better surface finish compared to LN_2 machining [44]. From the results in the work of Çark *et al.* [167] and Jerold and Kumar [44], it is suggested that machining with a CO_2 cutting fluid is more favourable than machining with a LN_2 cutting fluid with respect to machining performance as lower cutting forces, lower rate of tool wear and better surface finish were produced, while reducing the concern on the effect of extreme temperature of LN_2 on the workpiece, tool and machine operators.

It should be noted that the flow rate of CO_2 cutting fluid in the cooling system used in the work of Machai and Biermann [35] (2.27 l/min) was more than that in the work of Jerold and Kumar [44, 45] (0.18 l/min). The author suggest that this was because a larger volume of CO_2 cutting fluid would be required to achieve sufficient cooling ability to reduce the cutting temperature in machining of titanium alloys in the work of Machai and Biermann [35], for which higher cutting temperature was produced compared to that for carbon steel [44, 72].

Similar to through-tool LN_2 cooling system discussed in Section 4.3.3, through-tool CO_2 cooling system has also been implemented in the commercial machine tools. In the machining centre developed by Starrag Group with collaboration from Walter AG Tooling [168], liquid CO_2 is delivered through the centre of the cutting tool and expands through a cooling channel at which it is directed towards the cutting edges of the tool insert to remove heat from the cutting zone. In addition to CO_2 cooling channel, a secondary channel through the cutting tool is also provided for additional application of MQL for improvement of machining performance. It was reported that an increase in productivity by 70% and a two-fold increase in tool life were achieve by this through-tool CO_2 cooling system when machining high-performance alloy turbine blade [168]. However, the quantity of liquid CO_2 used in the cooling system was not reported.

In addition to liquid CO_2, supercritical fluid of CO_2 ($scCO_2$) (T_c = 31.1°C, P_c = 7.14 MPa or 72.8 atm) has been used as a cutting fluid in a minimum quantity lubrication (MQL) system, in which an aerosol spray consisting of $scCO_2$ and cutting oil droplets was applied to the cutting zone to achieve cooling and lubrication [30, 38, 163-165]. Due to the low temperature generated when $scCO_2$ expands to room temperature and pressure (-60°C to -80°C) and better solubility of vegetable cutting oil in $scCO_2$, it is suggested that the use of $scCO_2$ in the MQL system would provide better cooling and lubricating ability with less quantity of cutting oil compared to other cutting fluid systems [30, 38, 163]. Clarens *et al.* [163] reported that $scCO_2$ MQL cooling systems significantly reduce the quantity of cutting oil, 0.001 g/s compared to 0.01-0.05 g/s for conventional MQL cooling system, while providing the highest effectiveness in removing heat compared to other cutting fluid systems. It was shown that machining with a $scCO_2$/oil cutting fluid resulted in improved tool life compared to machining with conventional cutting fluids by reducing the rate of tool wear when turning compacted graphite iron and Ti-6Al-4V titanium alloy [163] and when rough turning Inconel 750 [165]. This was attributed to the improved penetration of the cutting fluid to the cutting zone by the use of a high-pressure $scCO_2$/oil cutting fluid spray, resulting in better effectiveness of heat removal and reduction of friction at the tool/chip interface due to the lubrication effect [163, 165]. Machining with a $scCO_2$/oil cutting fluid spray also resulted in higher tapping torque efficiency compared the conventional machining, which was also attributed to the reduction of cutting temperature and friction at the tool/chip interface [38].

Although the use of $scCO_2$/oil cutting fluid improved the performance of machining process, the author suggests that the use of CO_2 alone as a cutting fluid is more favourable when machining CFRPs to avoid the contamination of the workpiece by the cutting oil and the associated cost of cleaning. It is suggested that the use of a $scCO_2$/oil cutting fluid would be suitable for high speed machining of difficult-to-cut material such as titanium and nickel alloys for which much heat is generated and contamination of the cutting oil would not be an issue.

4.5 Conclusion

Due to disadvantages with respect to the economic and environmental concerns associated with the use of conventional cutting fluids, cryogenic machining using LN_2 and CO_2 has been considered by some researchers as a more favourable process for sustainable machining. The use of LN_2 or CO_2 as a cutting fluid provides the benefits of reducing pollution, energy usage and cost associated with the production and maintenance of conventional cutting fluids. However, it is suggested that conventional cutting fluids will

still be applied in a majority of industrial machining processes for many years to come as long as significant improvement in machining performance is achieved while the cutting fluids are maintained and disposed properly. Although, there is few published research on the application of cryogenic cooling in conventional drilling of CFRPs, it has shown the improvement in machining process of metallic materials. As a consequence of an improvement in metal machining and the advantages in economic and environmental aspects over conventional cutting fluids, this indicates potential of cryogenic cooling for improving the performance of the conventional drilling of CFRPs in the aspect of the application of cutting fluids. In addition, using cryogenic cooling when machining CFRPs can achieve "dry machining" condition, which is the goal for machining CFRPs in industry to avoid the material degradation concern due to contamination of cutting oil and absorption of water and reduce cost of cleaning.

5 Research Methodology and Methods

In this chapter, the approaches with associated methodologies that were adopted to achieve the objectives of this research are presented.

5.1 Evaluation of Drilling Performance of Carbon Fibre Reinforced Plastics with a Tool Pre-cooled in LN_2

Prior to the investigation with a CO_2 cooling system, a set of drilling experiments on CFRPs with a tool pre-cooled in LN_2 were carried out to investigate the effect of cryogenic cooling on the performance of conventional drilling of CFRPs. Since the CO_2 cooling system was not available at the time when the drilling trials were carried out, LN_2 was used instead of CO_2 gas to cool the drilling process. However, the drilling trial with LN_2 cooling would still be useful for developing the basic understandings of conventional drilling process of CFRPs when machined with cryogenic cooling. The practical machining work for this drilling trial was performed under the author's supervision as part of the MSc project of Miss Aishah Najiah Dahnel (an MSc graduate in 2012). Further analysis of the results was performed exclusively by the author. The results are presented in Chapter 6.

5.1.1 Experimental Set-up and Procedure

To evaluate the drilling performance of CFRPs when drilling with cryogenic cooling compared to when machined dry at room temperature, two tests were carried out.

- Test 1: Room temperature dry drilling on a CFRP plaque
- Test 2: Drilling on a CFRP plaque with a tool pre-cooled in LN_2

Both drilling tests were carried out on a single CFRP plaque which was reported to be manufactured from woven carbon/epoxy prepeg from Cytec Industries Inc. [169] with the dimensions of 320 mm long x 300 mm wide x 18 mm thick, Figure 5.1. This woven carbon/epoxy plaque was previously manufactured in-house by WMG using vacuum-bagging curing. From the same plaque, two strips with the dimensions of 320 mm long x 20 mm wide x 18 mm thick were cut and clamped on the dynamometer for measurement of cutting forces, these strips were also used for damage analysis, Figure 5.2. These woven carbon/epoxy strips were referred as "dynamometer strips".

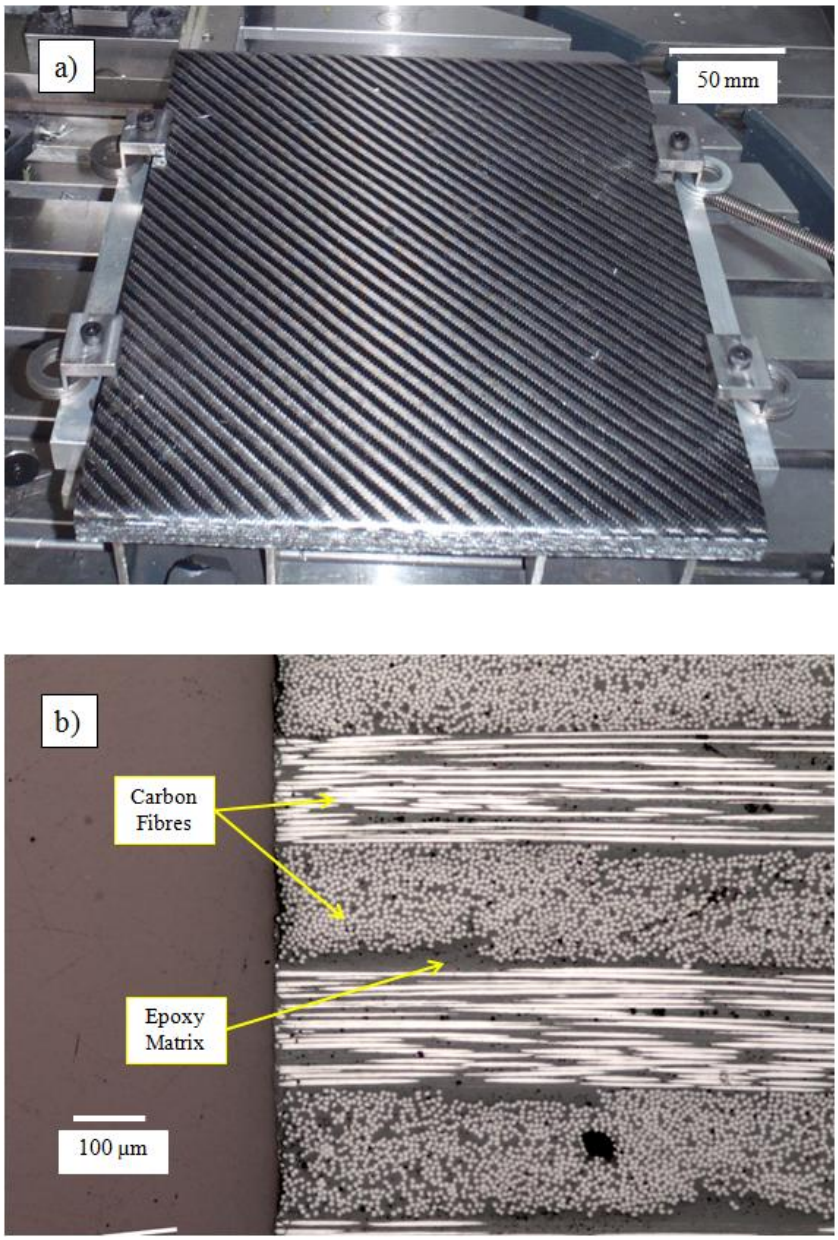

Figure 5.1: (a) Woven carbon/epoxy plaque used for drilling test 1 and 2 in the evaluation of the drilling performance of CFRPs with a tool pre-cooled in LN_2. (b) An optical microscope image showing the cross-section of the woven carbon/epoxy plaque

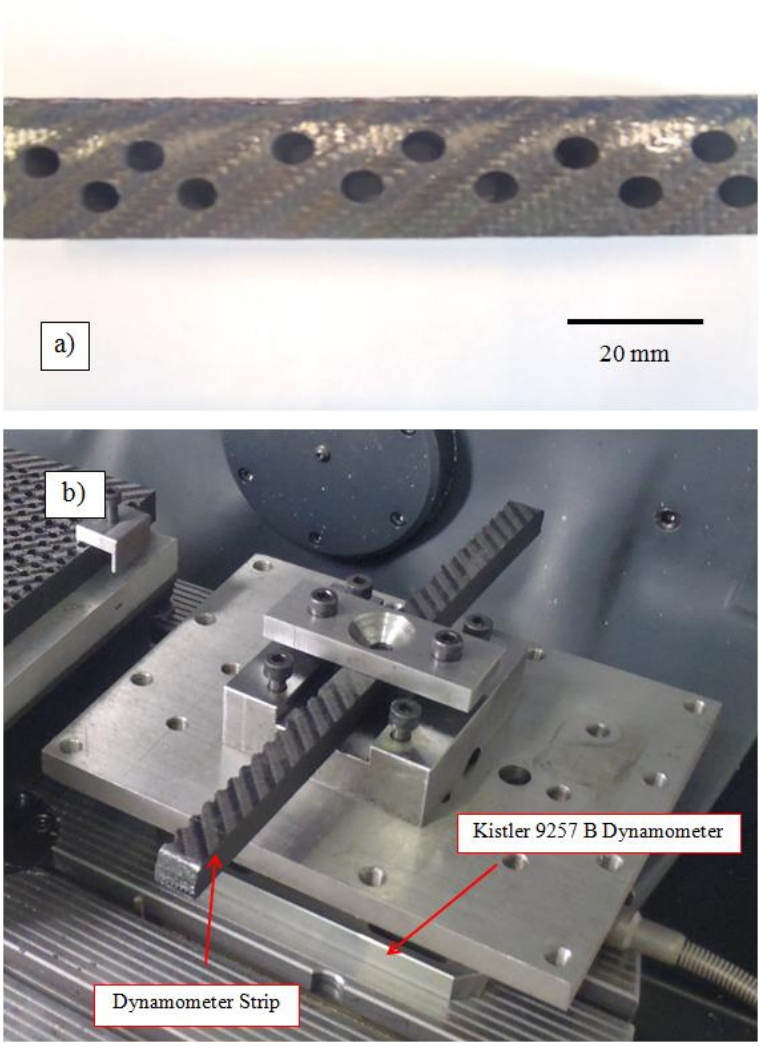

Figure 5.2: (a) Dynamometer strips used for measurement of cutting forces and damage analysis. (b) A dynamometer strip clamped on the Kistler 9257 B dynamometer

For both drilling tests, a Guhring DIN 6537 K, TiALN coated, solid tungsten carbide twist drill, Figure 5.3, was used to produce 6 mm diameter through-holes in the main CFRP plaque and in the dynamometer strips with constant cutting speed and feed rate of 94 m/min and 0.065 mm/rev respectively. This set of cutting speed and feed rate was suggested by Guhring Ltd. UK as the optimum machining parameters for this type of drill for CFRPs. A new tool was used for each set test.

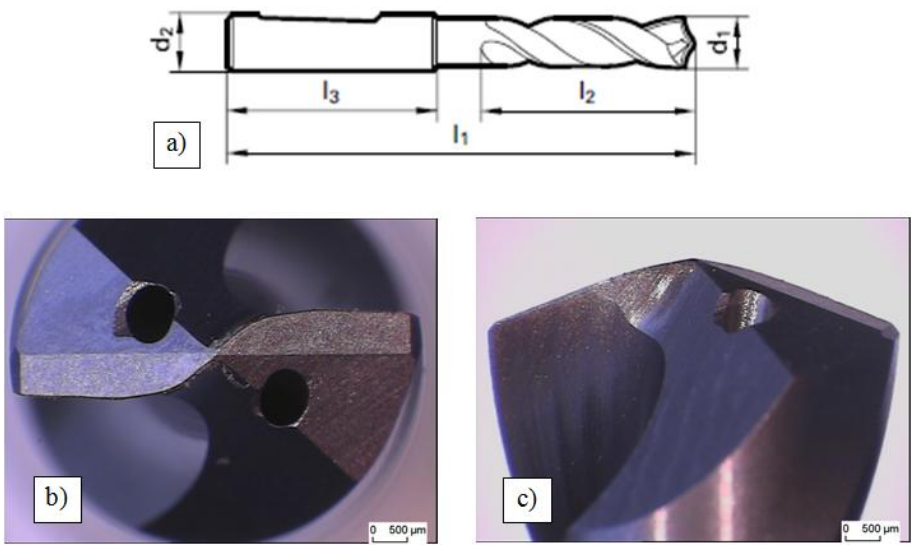

Figure 5.3: 6 mm diameter Guhring DIN 6537 K, TiAlN coated, straight shank solid tungsten carbide twist drill. (a) Side view, (b) Top view and (c) Tool tip

A DMG / MORI SEIKI DMU 65 monoBlock machining centre (a 5-axis milling centre with a maximum spindle speed of 10,000 RPM and working area in x-, y- and z-axis of 735 mm x 650 mm x 560 mm) was used to perform Test 1. The machining centre for performing Test 2 was changed to a DMG / MORI SEIKI DMU 50 machining centre (a 5-axis milling centre with a maximum spindle speed of 10,000 RPM and working area in x-, y- and z-axis of 500 mm x 450 mm x 400 mm) due to the availability of the machining centre at the time. This change of machining centre would not contribute to variations in the drilling process for the two tests because the range of cutting speed and feed rate that was used for the drilling trials did not exceed the machining capability of either of the machining centre. In addition, both machining centres were new machines. The experimental set-ups for Test 1 and Test 2 are shown in Figure 5.4. For Test 1, the main plaque for the drilling process was clamped on the drilling fixture on the machining table, Figure 5.4a. The strip for the measurement of cutting forces and damage analysis was clamped on the Kistler 9257 B dynamometer, Figure 5.4a. The set-up for Test 2 was similar to that of Test 1 except having polystyrene (PS) cups filled with LN_2 placed on the machining table for cooling the tool before drilling the through-holes on the dynamometer strip and the main plaque, Figure 5.4b.

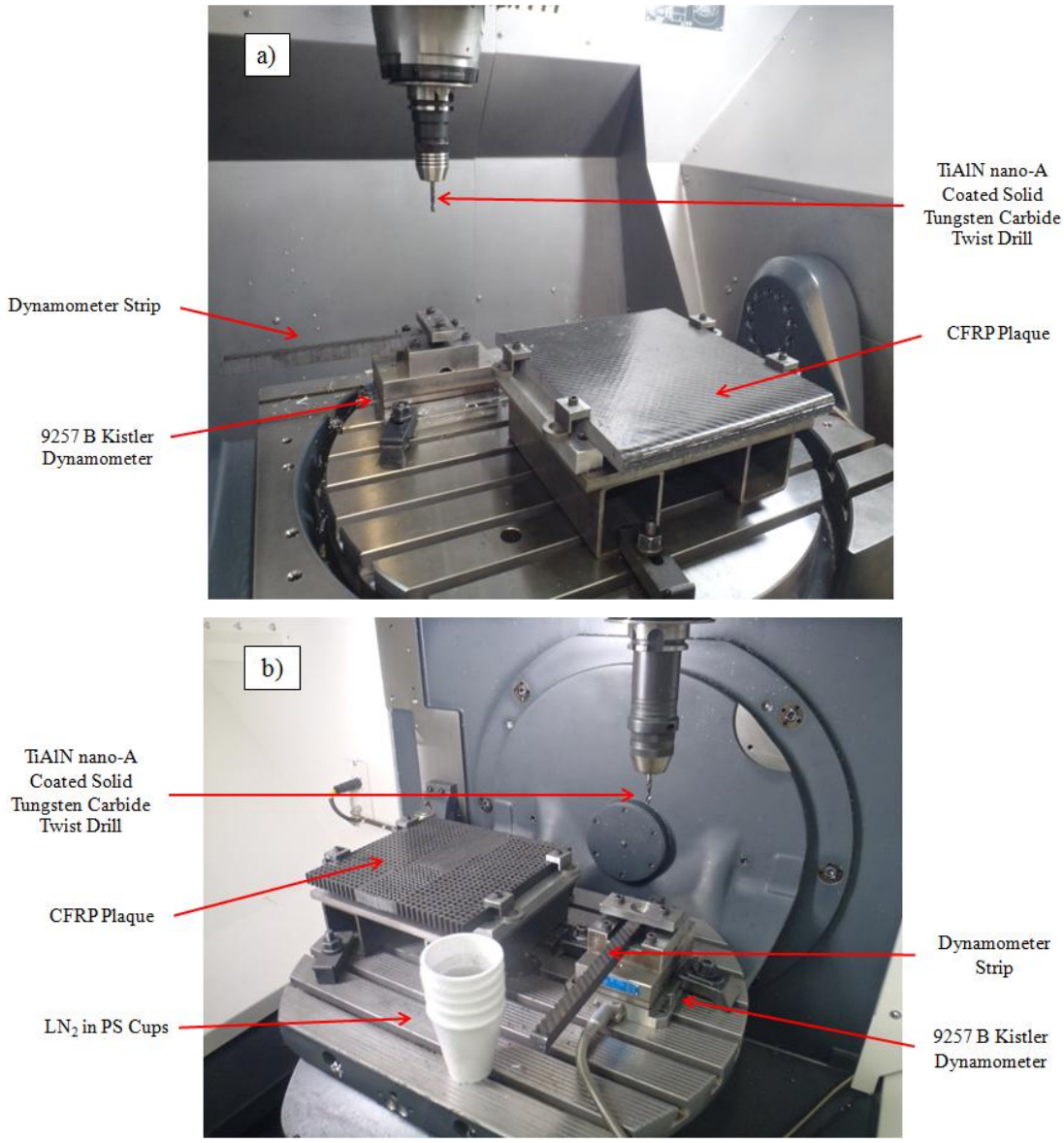

Figure 5.4: Set-up of (a) the drilling experiment on CFRPs when machined dry at room temperature (Test 1) and (b) the drilling experiment on CFRPs when machined with a tool pre-cooled in LN_2 (Test 2)

The drilling process for Test 1 started by drilling the first through-hole in the dynamometer strip to measure the cutting forces before performing the first drilling cycle. The tool was taken out from the spindle to examine the tool wear produced from the first hole. Then, the first drilling cycle started by drilling 24 through-holes consecutively in the main plaque and completed by drilling the 25^{th} hole of the drilling experiment in the dynamometer strip to measure cutting forces. The tool was then taken out from the spindle to measure flank wear produced after completing the first drilling cycle (25 holes plus one hole before drilling the first cycle). The second drilling cycle was then started by drilling another consecutive 24 through-holes in the main plaque. The drilling cycle was again completed by drilling the 50^{th} hole of the drilling experiment in the dynamometer strip for

measurement of cutting forces. The tool was again taken out from the spindle to examine flank wear. This drilling cycle was repeated until 13 drilling cycles had been completed.

The drilling process for Test 2 was similar to the process which was carried out for Test 1. However, the tool was pre-cooled in LN_2 held in PS cups before drilling every hole in the dynamometer strip and before drilling every five consecutive holes in the main plaque. The time for pre-cooling the tool in LN_2 was 10 s from the 1st to 10th drilling cycles. It was observed that there was still much bubbling in LN_2 cups for 10 s cooling. As a consequence, the pre-cooling time was changed to 30 s for the 11th to 13th drilling cycles to better cool the tool. Only 13 drilling cycles were performed for each drilling test because of insufficient quantity of the workpiece material to perform further drilling process.

The machining conditions for both drilling tests are summarised in Table 5.1.

Table 5.1: Summary of machining conditions for the drilling tests in the evaluation of the drilling performance of carbon/epoxy composites when machined room temperature dry and with a tool pre-cooled in LN_2

Machining Conditions	Test 1	Test 2
Cooling Technique	Dry drilling at room temperature	Drilling with a tool pre-cooled in LN_2
Machining Centre	A DMG / MORI SEIKI DMU 65 monoBlock	A DMG / MORI SEIKI DMU 50
Workpiece Material	320 mm (length) x 300 mm (width) x 18 mm (thickness) woven CFRP plaque	
	320 mm (length) x 20 mm (width) x 18 mm (thickness) dynamometer strips cut off from the main plaque	
Drilling Tool	DIN 6537 K TiAlN nano-A coated solid tungsten carbide twist drill with through-tool cutting fluid hole from Guhring Ltd. (6 mm diameter and 66 mm length)	
Cutting Speed	94 m/min (5,000 RPM)	
Feed Rate	0.065 mm/rev	
Hole Diameter	6 mm	
Number of Drilling Cycles	13 cycles of 25-hole drilling with 1st hole on dynamometer strip	
Total Number of Drilled Holes	325 holes	

5.1.2 Measurement

5.1.2.1 Thrust Force

It has been reported by other researchers that the thrust force produced during drilling was directly related to the level of damage associated with the drilled hole, especially exit

delamination, during conventional drilling of CFRPs [7, 9, 16, 88, 120]. For this reason, thrust force is one of the major criteria for the performance evaluation of the conventional drilling process on CFRPs, and was therefore used as one of the characteristic used for the performance evaluation of drilling trials in this section.

The measurement of thrust forces was obtained using a Kistler 9257 B piezo-elctreic dynamometer, which measured cutting forces in x-, y- and z-axis and torque. The results were shown in LaBView analysis software in which the average and maximum values of thrust force for the drilling process were determined.

5.1.2.2 Tool Wear

Tool wear is another important indicator for performance evaluation of a drilling processs. This is because it affects process time and cost by determining the tool life and how many tools are required for a drilling process [7, 8, 10, 55], and it also affects the amount of thrust force produced and the quality of the hole [4, 15, 16, 55, 109]. In drilling with CFRPs, it has been shown that a uniform wear band on the flank face of the tool due to an abrasive wear mechanism could be observed [9, 99, 108, 109]. Due to this uniformity of flank wear and the convenience of measurement, the tool flank wear has commonly been used as a criterion for the performance evaluation of conventional drilling processes on CFRPs [15, 16, 97, 102, 108, 109].

The measurement of tool flank wear was obtained using Olympus optical microscope connected to a PC with a4i analysis software. Since it was difficult to find a fixed reference point on the cutting edge, the width of flank wear was obtained by determining the difference between the width of unworn area of the used tool and that of the new tool. The average flank wear of a cutting edge was determined by taking the average value of flank wear band width at three points along the cutting edge, Figure 5.5. Finally, the average flank wear of the tool for each drilling cycle was determined by taking the average value of the average flank wear of each cutting edge.

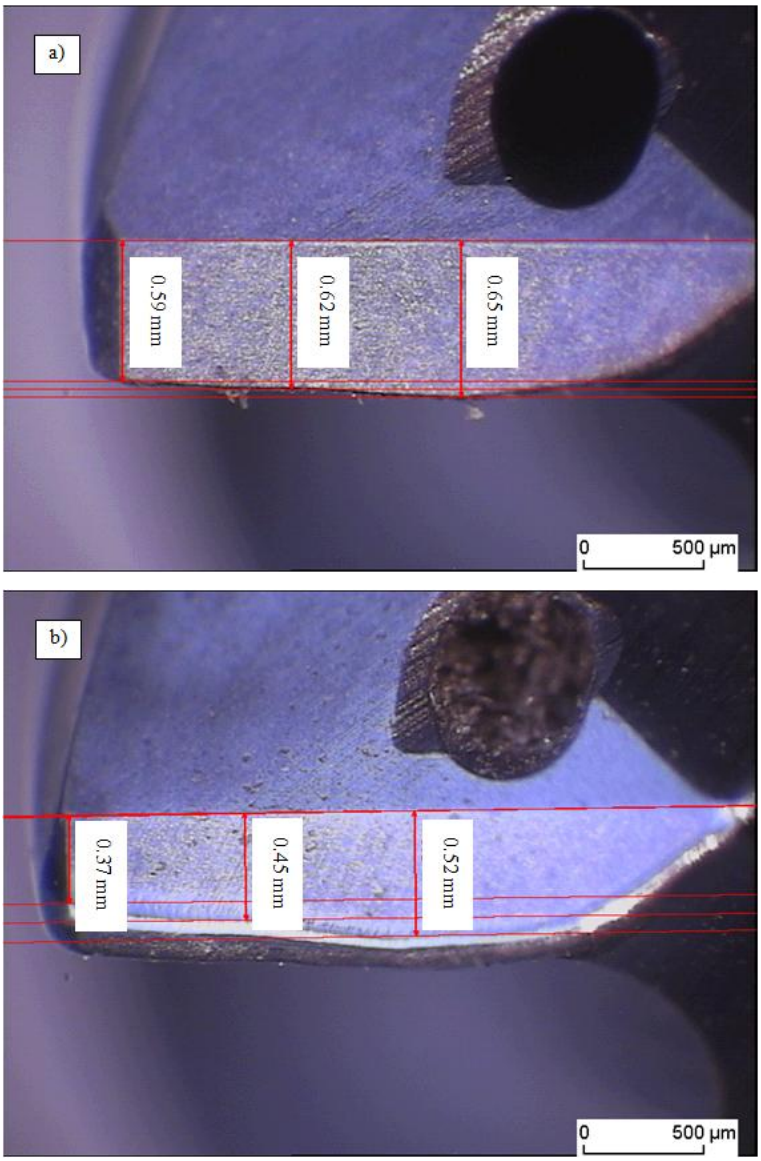

Figure 5.5: Optical microscope images demonstrating the measurement of the width of unworn area of (a) the unworn tool and (b) the tool after drilling 325 holes

After drilling 325 holes (end of the drilling test), the tool was examined using Carl Zeiss SIGMA HD scanning electron microscope (SEM) with a resolution of 1 nm to characterise the mechanism of tool wear for each drilling test, i.e., room temperature dry and pre-cooled drilling.

5.1.2.3 Entry and Exit Delamination

Surface delamination damage, especially exit delamination damage, directly determines the quality of the drilled hole as well as the performance of CFRP parts [4, 7, 9, 10, 12]. As a consequence, it is also an important criterion for the evaluation of drilling performance of CFRPs.

The entry and exit delamination damage was assessed using Olympus optical microscope connected to a PC with a4i analysis software. To quantify the entry and exit delamination damage, the delamination factor (F_d), which is the ratio of the maximum diameter of damaged area to the diameter of the drilled hole [16], was determined, Figure 5.6. The image of the hole at the entry/exit side was taken by the optical microscope, and the maximum diameter of the delaminated area was measured using the a4i analysis software. The quantification of entry and exit delamination damage in term of delamination factor (F_d) is often used by other researchers for assessing delamination damage when drilling CFRPs because the delamination damage can be determined using a non-dimensional value, which can be used to compare the drilling performance of different machining conditions [16, 19, 20].

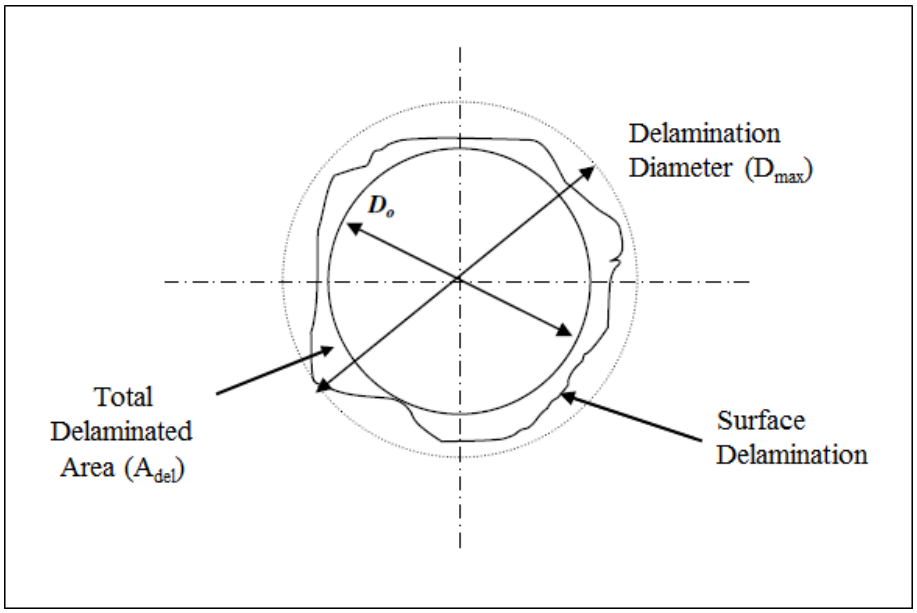

Figure 5.6: Schematic diagram showing the surface delamination to the drilled holes and the quantification of delamination damage in term of delamination factor (F_d) and total delaminated area (A_{del}) (adapted from [106])

Due to the high level of anisotropy in CFRPs, it has been observed that the shape of delamination damage when drilling is irregular, consisting of sharp cracks from fibres which have peeled up at the entrance and pushed down at the exit side around the edge of the drilled hole [116, 125]. For this reason, the assessment of surface delamination damage in terms of delamination factor (F_d), which considers only the maximum diameter of the delaminated area, might not be suitable to represent the effect of a machining condition on the actual delaminated area [116, 125]. An example of possible variations in the evaluation of surface delamination damage in term of F_d is demonstrated in Figure 5.7. In Figure 5.7, it is shown that the maximum diameter of delamination damage of hole 1 is larger than that of hole 2 ($D_{max1} > D_{max2}$), although the actual damaged area of hole 1 is smaller than that of

hole 2 ($A_{del1} < A_{del2}$). As a consequence, hole 1 will yield higher value of damage in terms of F_d than hole 2 even though its actual damaged area is smaller. Therefore, the surface delamination damage was also quantified in terms of total delaminated area around the edge of the hole, Figure 5.6. This method for quantifying surface delamination damage, which considers the significance of the damaged area rather than only the maximum diameter of the damage area, has been used as an alternative quantification of surface delamination in the drilling of CFRPs [116, 125, 170].

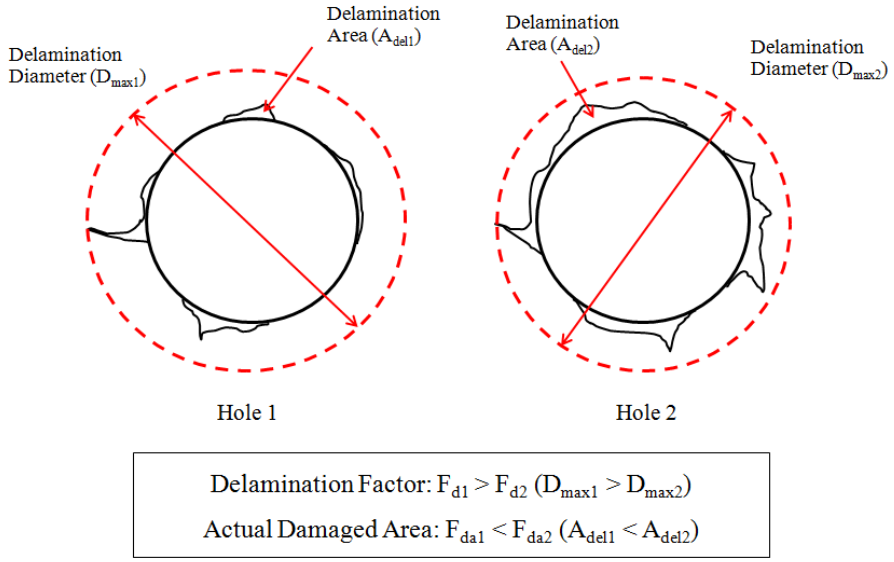

Figure 5.7: Schematic diagram showing an example of possible variations in the evaluation of surface delamination damage in term of F_d

5.1.2.4 Internal Damage

Internal damage in the form of material chip-out, fibre pull-out and matrix cracking also indicates the performance of a drilling process with CFRPs in respect to the quality of the drilled holes [4, 7-9]. According to the private communication with BAE Systems [13], the extent of material chip-out or delamination along the internal surface of the hole is considered as an important criteria for performance evaluation in addition to the entry/exit delamination damage.

Internal damage on the drilled surface was examined using Leica DM4000 M optical microscope connected to a PC with Buehler Ominet 9.5 analysis software and in Carl Zeiss SIGMA HD scanning electron microscope (SEM). The drilled samples for the 1st and 325th hole from the room temperature dry and cryogenic drilling experiments were sectioned through the diameter. One half of the sample was mounted in epoxy resin and polished for the optical microscope analysis, while the other half was investigated in the SEM, Figure 5.8. Total internal damage, which was determined by adding all values of material chip-out or delamination extent, D_i, along the edge of the hole, was determined using a4i

analysis software, Figure 5.9. Values of the total internal damage for each drilling experiment were compared for a quantitative evaluation of drilling performance. For SEM analysis, the samples were cleaned in an ultrasonic bath prior to being mounted on stubs and gold coated. The result of investigation in the SEM was used to determine the characteristics of the machined surface produced from each drilling experiment.

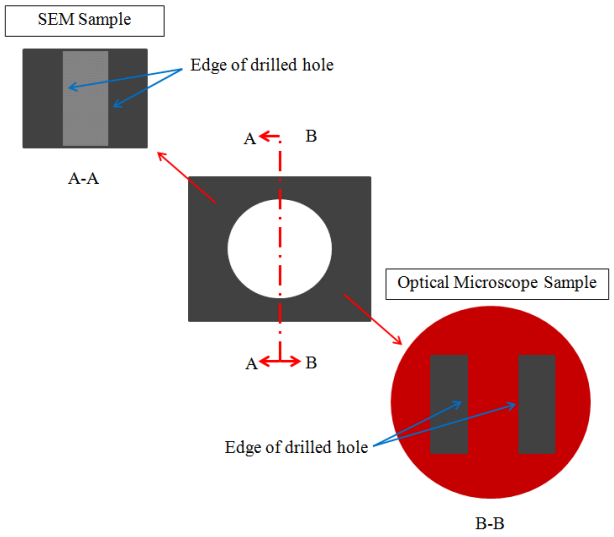

Figure 5.8: Schematic diagram showing sample preparation for examination under an optical microscope and in the SEM

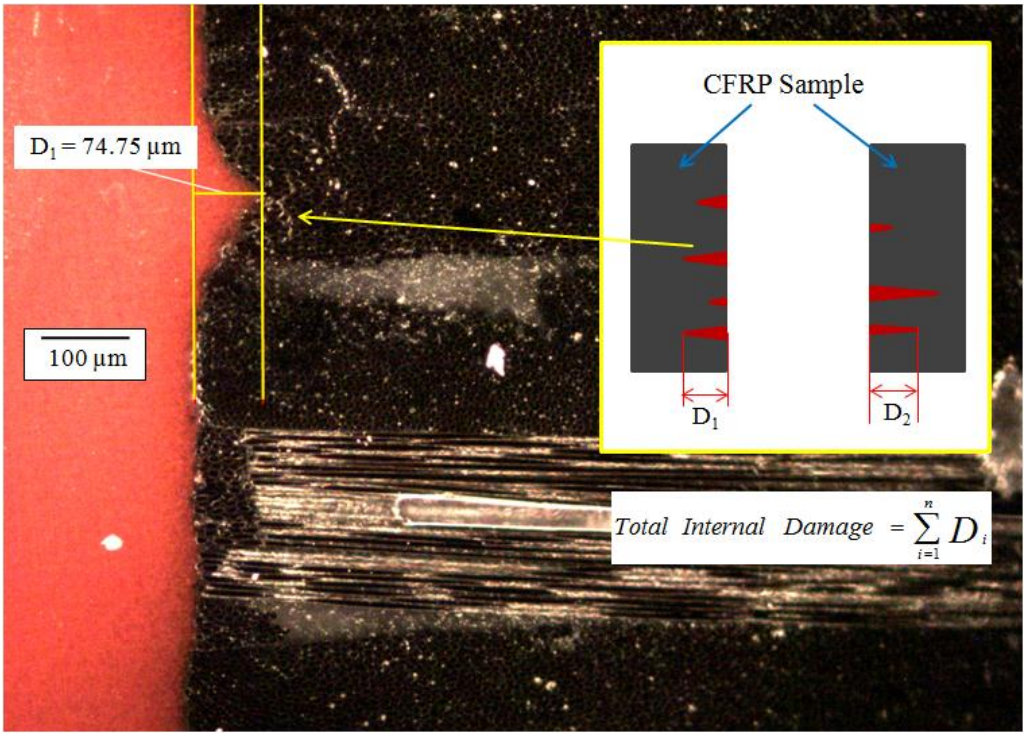

Figure 5.9: Optical microscope image showing internal damage at the edge of the hole induced from drilling of CFRP with schematic diagram showing measurement of the sum of internal damage at the edge of the hole

5.2 Evaluation of the Drilling Performance of Carbon Fibre Reinforced Plastics with a CO_2 Cooling System

After gaining basic understandings regarding the conventional drilling of CFRPs with cryogenic cooling, drilling experiments with a CO_2 cooling system were performed to investigate the effect of CO_2 gas cooling on the performance of conventional drilling. CO_2 machining technique has shown to improve the performance of the machining process for metallic materials compared to other cooling and lubricating methods and has the potential for reducing environmental problems [29, 30, 38, 171-175]. However, its application to CFRPs has not been systematically investigated. For this reason, the effect of CO_2 cooling on drilling performance with CFRPs was examined and compared to room temperature dry machining. The effect of machining parameters (cutting speed and feed rate) on the drilling performance with CO_2 cooling was also examined. Some of the practical machining work was carried out under the author's supervision of part of the final year projects for undergraduate students. The rest of the practical machining work and all of the analysis were performed exclusively by the author. The results are presented in Chapter 6.

5.2.1. Experimental Set-up and Procedure

Two sets of drilling tests: 1) room temperature dry drilling and 2) drilling with CO_2 cooling, which will be referred as "CO_2 drilling", were performed on two CFRP plaques, which were autoclave-cured CFRP manufactured from uni-directional IM7 and woven AS4 carbon fibres reinforced in Hexply 8552 toughened epoxy matrix with copper mesh layer on the entry side of the plaque, Figure 5.10. These CFRP plaques were aerospace-grade CFRPs supplied by BAE Systems. The dimension of each plaque was 450 mm long x 120 mm wide x 4 mm thick. A series of strips of material, 18 mm wide, was cut from the plaques and clamped on the dynamometer for the measurement of cutting forces and analysis of damage produced from the drilling process.

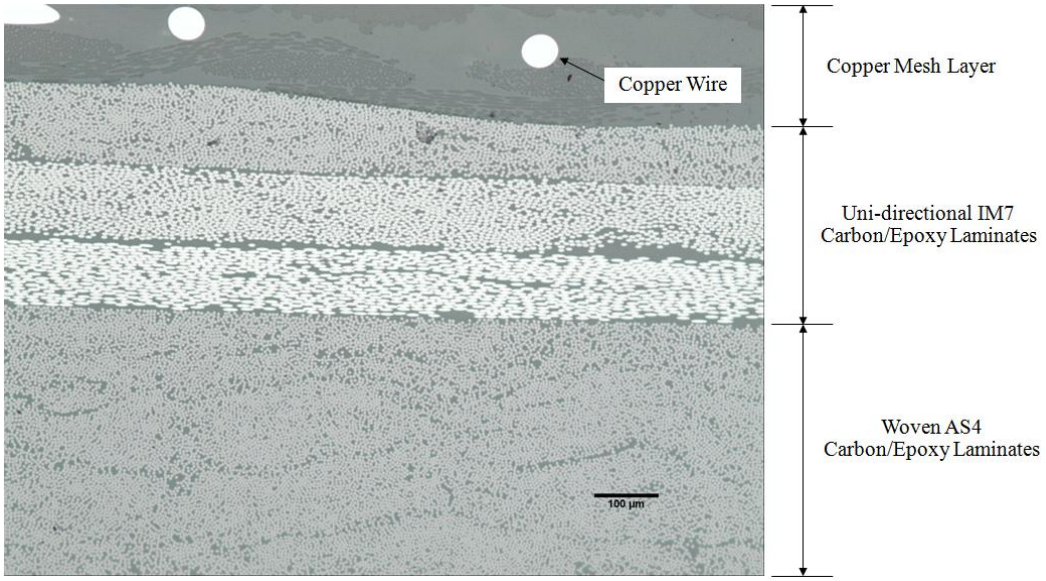

Figure 5.10: An optical microscope image showing the cross-section of the carbon/epoxy plaque manufactured from uni-directional IM7 and woven AS4 carbon fibres reinforced in Hexply 8552 toughened epoxy, which was used for the evaluation of drilling performance of CFRPs with a CO_2 cooling system

For room temperature dry drilling and CO_2 drilling tests, a SGS series 120 50017 DI-NAMITE (pure crystalline diamond) coated, solid carbide eight facet double angle drill, Figure 5.11, was used to produce 6 mm diameter through-holes in the CFRP strips. This type of drill is specially designed by SGS Tools, Ltd. for drilling CFRPs by having double point angles, creating four cutting edges along the drill point. The multiple cutting edges are designed to provide a reduction in entry/exit delamination by distributing the cutting load across the four cutting edges which are created by the double point angles [176], rather than being concentrated on a point of the cutting edge as in the case with a single point twist drill. The advantage of using a drill consisting of multiple cutting edges in reducing entry/exit delamination damage in drilling of CFRPs has been discussed in the work of Piquet *et al*. [17]. The drill was also coated with DI-NAMITE, which is a pure crystalline diamond coating, to extend tool life and improve surface finish [176]. The recommended cutting speed and feed rate for this type of drill for CFRPs are 100 m/min and 0.03 mm/rev respectively. Due to limited numbers of drills available, one drill was used to carry out the drilling experiments with various machining parameters for both dry and CO_2 machining.

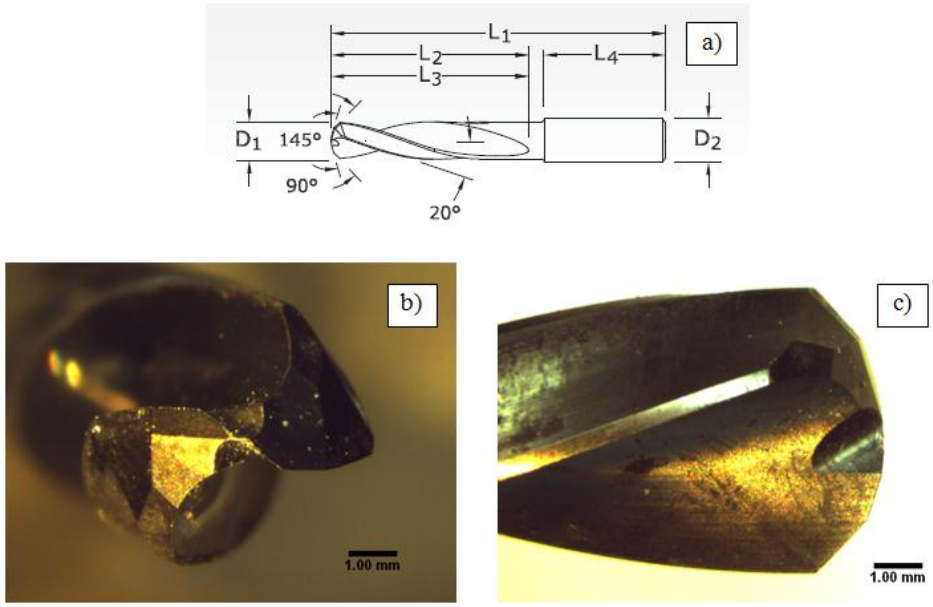

Figure 5.11: 6 mm diameter SGS series 120 50017 DI-NAMITE (pure crystalline diamond) coated, solid carbide eight facet double angle drill designed for CFRPs. (a) A schematic diagram [176], (b) Top view and (c) Side view

A DMG / MORI SEIKI Ultrasonic 65 monoBlock machining centre (a 5-axis ultrasonic milling centre with a maximum speed of 18,000 RPM and working area in x-, y- and z-axis of 650 mm x 650 mm x 560 mm) was use to perform the machining process for room temperature dry and CO_2 drilling tests. The experiment set-up is shown in Figure 5.12. All drilling was carried out on the dynamometer. The CFRP strip was clamped on a Kistler 9257 B dynamometer, which was fixed to the machining table, for measuring cutting forces during drilling process. This Kistler dynamometer was the same one that was used in the drilling tests previously described in Section 5.1. The drilling point for every machining condition was fixed at the centre of the dynamometer, but the strip was moved to allow through-holes to be produced along the length of strip. The nozzle of the CO_2 cooling system was adjusted to be pointing to the drilling point on the strip in order to deliver CO_2 gas as close to the cutting zone as possible.

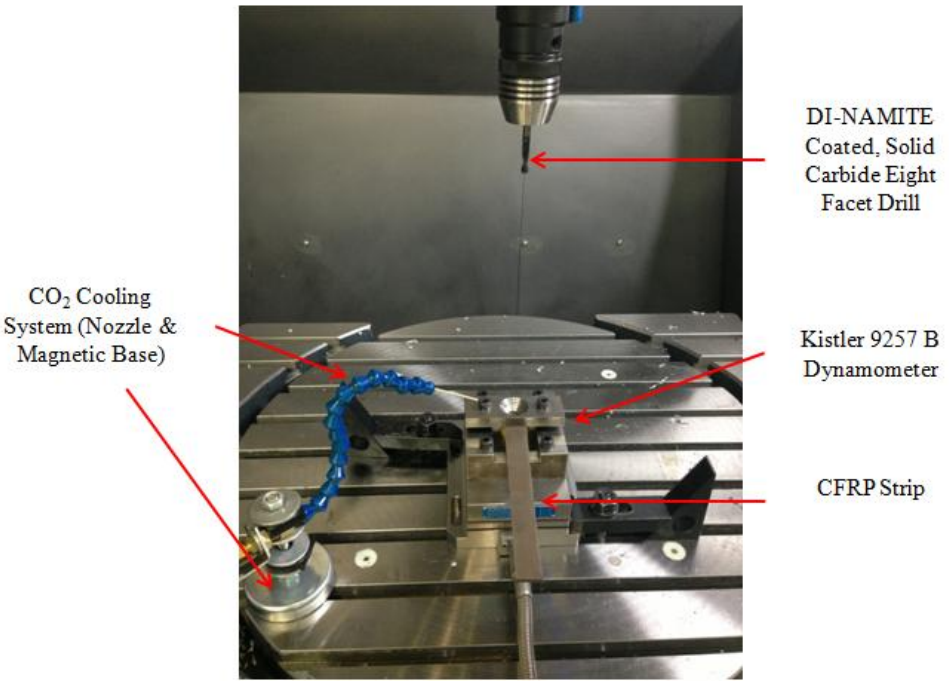

Figure 5.12: Set-up of the room temperature dry and CO_2 drilling experiments for the evaluation of drilling performance on CFRPs with a CO_2 cooling system

The CO_2 cooling system that was used in this research was provided by SGS Tools UK, Ltd. The cooling unit was used to control the delivery of compressed CO_2 gas from a storage tank to the cooling nozzle, which fed CO_2 gas externally to the cutting zone. The cryogenic system was capable of cooling the cutting zone down to -70°C. A calibration to determine the actual flow rate of CO_2 gas of the cooling unit was carried out. An Amprobe anemometer was used to measure the velocity of the CO_2 gas exiting the nozzle of the CO_2 cooling system. Since the cross-sectional area of the cooling nozzle was known, the flow rate of CO_2 gas of the cooling system could, therefore, be determined. The velocity of the CO_2 gas exiting the cooling nozzle was measured after 5, 30 and 60 s. of operating time to also investigate the effect of system stability to the flow rate. The average value of five measurements of the velocity was determined to obtain the velocity of the CO_2 gas at each measured time. Results showing a calibration to determine the flow rate of CO_2 gas of the cooling system are presented in Table 5.2. From Table 5.2, the flow rate of CO_2 was measured to be 3.37 l/min.

Table 5.2: Results showing a calibration to determine the flow rate of CO_2 gas of the CO_2 cooling system

Measured Time	Velocity (V) m/s	Area (A) ¶ x r^2 (10^{-6} m^2)	Flow Rate (Q) V x A (L/min)
5 s.	16.43	3.46	3.41
30 s.	16.24	3.46	3.37
60 s.	16.02	3.46	3.33
Average			3.37

For the room temperature dry and CO_2 drilling tests, through-holes were produced using a cutting speed in the range of 75-150 m/min and feed rates of 0.03-0.15 mm/rev. The CO_2 drilling tests were carried out at constant volume flow rate of 3.37 l/min, for all machining conditions. The drilling trial for each machining condition was repeated three times (total of 150 holes) to minimise the variation of performance due to the anisotropy of CFRPs.

As previously mentioned, one drill was used to perform both room temperature dry and CO_2 drilling tests regardless of changing machining conditions because of limited number of drills available. This was considered acceptable since the diamond coated tool did not exhibit any indication of wear because of the small number of holes drilled (which was limited by the available workpiece material). Therefore, the average tool flank wear being produced was not used for the evaluation of the drilling performance of CFRPs with a CO_2 cooling system in this case.

The machining conditions of the drilling tests for the evaluation of drilling performance of CFRPs with a CO_2 cooling system are summarised in Table 5.3.

Table 5.3: Summary of machining conditions for the drilling tests in the evaluation of the drilling performance of CFRPs with a CO_2 cooling system

Machining Conditions	Test 1	Test 2
Machining Centre	A DMG / MORI SEIKI Sauer Ultrasonic 65 monoBlock	
Workpiece Material	CFRP plaques manufactured from uni-directional IM7and woven AS4 carbon fibres reinforced in Hexply 8552 toughened epoxy with the dimension for each plaque of 450 mm long x 120 mm wide x 4 mm thick cut in to a series of strip of 18 mm wide	
Drilling Tool	Series 120 50017 DI-NAMITE (pure crystalline diamond) coated, solid carbide eight facet double angle drill from SGS Tools UK, Ltd. (6 mm diameter and 66 mm length). The recommended speed and feed rate for drilling CFRPs is 100 m/min and 0.03 mm/rev respectively.	
Cooling Method	Room Temperature Dry	CO_2 Cooling (flow rate of 3.37 l/min)
Cutting Speed	75, 100, 115, 130 and 150 m/min (using five values of feed rate for each cutting speed)	
Feed Rate	0.03, 0.06, 0.09, 0.12 and 0.15 mm/rev (using five values of cutting speed for each feed rate)	
Hole Diameter	6 mm	
Number of Drilled Holes	3 holes for each machining condition = Total of 150 holes	

5.2.2. Measurement

5.2.2.1. Thrust Force

Thrust forces generated during the drilling process were measured using the same Kistler 9257 B piezo-electric dynamometer discussed in Section 5.1 and the average and maximum values of thrust force were determined. The average value of thrust force produced from the three repetitions at each machining condition was determined and was quoted as the thrust forces for that machining condition.

5.2.2.2. Entry and Exit Delamination

From the drilling tests with LN_2 cooling (Section 5.1), it was found that there were large and random variations in the results of entry and exit delamination damage in term of delamination factor (F_d), as can be seen in Section 6.1.3. In addition, the initial assessment of exit delamination damage in terms of F_d for this set of drilling tests also showed large variations in the results, hence the trend of the drilling performance could not be determined. As discussed previously, the large level of anisotropy of CFRPs, which contributed to the irregular shape of entry/exit delamination damage, consisting of sharp cracks around the edge of the hole, could cause large variations in the results of delamination damage in terms

of F_d, which considered only the maximum diameter rather than the actual damaged area [116, 125]. As a consequence, the entry and exit delamination damage was quantified in terms of total area of delamination damage (A_{del}) around the hole in this case, refer to Figure 5.6.

The entry and exit delamination damage was assessed using Nikon SMZ745 optical microscope (magnification of 3.35-300x) connected to a PC with Buehler Ominet 9.5 analysis software in which the total area of delamination damage (A_{del}) to the hole was determined. Similar to the case of thrust force, the average of value of A_{del} produced from the three repetitions at each machining condition was determined and was quoted as the value of A_{del} for that machining condition.

5.2.2.3. Characteristics of Machined Surface

Characteristics of the machined surfaces resulting from different machining conditions were examined qualitatively in Carl Zeiss SIGMA HD SEM. The samples for being examined in the SEM were cross-sectioned and cleaned in an ultrasonic bath before being mounted on stubs and gold coated similar to the methodology previously described in Section 5.1.2.4, refer to Figure 5.8. The holes produced from the room temperature dry and CO_2 drilling tests at the cutting speed of 100 and 150 m/min and a feed rate of 0.03, 0.09 and 0.15 mm/rev (three values of feed rate for each cutting speed) were examined to determine the difference in characteristics of the machined surfaces as a result of CO_2 cooling as compared to room temperature dry machining at the optimum cutting speed (100 m/min) for the DI-NAMITE coated carbide drill and the highest cutting speed in this drilling trial (150 m/min). Two cutting speeds and three feed rates were chosen to investigate the effect of cutting speed and feed rate on the characteristics of machined surface for the room temperature dry and CO_2 drilling. The results of the examination of the characteristics of machined surface in this section are presented in Chapter 7.

5.3 Computerised Tomography (CT)-Scanning X-ray Analysis of Damage in Drilling of Carbon Fibre Reinforced Plastics with Cryogenically Pre-Cooled Tools, with CO_2 Cooling and when Machined Dry at Room Temperature

Although the entry/exit delamination damage around the edge of the hole in the drilling trials with LN_2 pre-cooling of the tool and CO_2 cooling was examined by visual inspection using an optical microscope and evaluated in terms of F_d and F_{da}, the author found that there were still variations in the measurement process due to the dependence of the contrast on illumination and visibility of the defects within the optical microscope images. Hocheng and Tsao [23, 93] have proposed that the visual inspection of delamination damage of CFRPs is

difficult due to the contrast and visibility of the defects during microscopic examination. In addition, the destructive analysis of internal damage on the drilled surface used in the drilling trials with LN_2 cooling by cross-sectioning, Figure 5.8, might create more damage during preparation and would not reveal the true internal damage around the edge of the hole caused by drilling. For these reasons, the computerised tomography (CT)-scanning analysis method was used in this drilling trial to examine the damage to the CFRP. The CT-scanning technique has been used by some researchers [12, 23, 93] as a non-destructive method for examining delamination damage to the hole through the thickness the laminates in drilling of CFRPs despite limited research on its applications when drilling CFRPs. The analysis of damage by the CT-scanning technique can eliminate the problems from the variations in the measurement process due to the dependence of the contrast on illumination and visibility of the defects in the visual analysis of damage using the optical microscope, which was used in the drilling trials described in Sections 5.1 and 5.2. The damage of the material as well as the thrust forces produced in drilling of CFRPs when machined room temperature dry, with CO_2 cooling and with a tool pre-cooled in LN_2 were examined and compared. The practical machining work and the analysis of the results were performed exclusively by the author, while the CT-scanning of the samples and the extraction of data from the scanning were carried out by Miss Nadia Kourra (an EngD candidate at WMG researching the CT scanning technology). The results are presented in Chapter 6.

5.3.1. Experimental Set-up and Procedure

The following machining conditions were used to produce through-holes in the CFRP plaques for the CT-scanning analysis of the damage:

1. Room temperature dry drilling
2. Drilling with CO_2 cooling
3. Drilling with a tool pre-cooled in LN_2 for 30 s
4. Drilling with a tool pre-cooled in LN_2 for 120 s

The CFRP plaques were the same batch of plaques as used in the drilling trial described in Section 5.2. Four strips with the dimension of 125 mm long x 18 mm wide were cut from the main plaque. Two of the strips were used for CT-scanning analysis of damage and the other two were used for measurement of thrust forces. From discussion with Miss Nadia Kourra [177], four reference lines were machined prior to drilling the hole which would enable the CT-scanning analysis to determine the "ideal" centre of the drilled hole, Figure 5.11a. The "ideal" centre of the hole was determined by calculating the point where the four reference lines intersect [177]. A flat surface at the base of the reference marks was essential to set a base line by which to align the sections relative to the drilling axis

(perpendicular to the drilling axis) [177]. Therefore, a 2-mm diameter, two-flute Q-coated tungsten carbide slot drill with flat end was used to produce four reference lines at the (-x, 0), (+x, 0), (-y, 0) and (+y, 0) coordinates around the hole on the entry side before drilling a though-hole in the strips that were used for the analysis of damage, Figure 5.13b. The grooves were 6 mm long and 0.7 mm deep and were 2 mm away from the edge of the hole to ensure that the engraving process would not produce additional delamination to the hole.

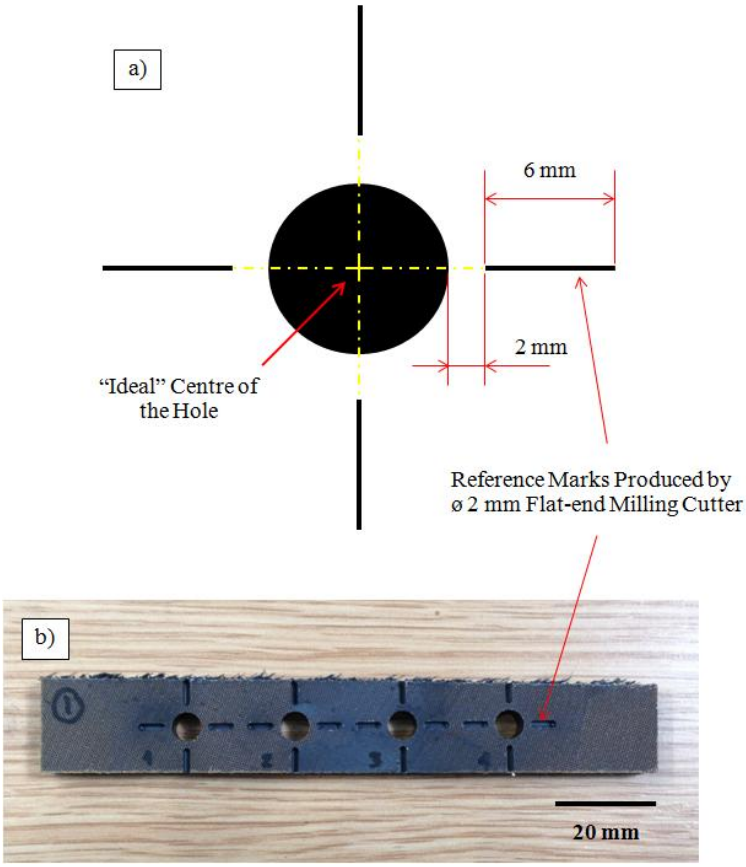

Figure 5.13: (a) Schematic diagram showing the engraving marks around the hole used as reference lines for determining the theoretical centre of the hole in the CT-scanning analysis of damage. (b) Actual sample with reference marks

For all machining conditions, an SGS series 135 M Ti-NAMITE "A" (TiAlN) coated, solid carbide Hi-Percarb twist drill, Figure 5.14, was used to produce 6 mm diameter through-holes in the CFRP strip with a constant cutting speed of 100 m/min and feed rates of 0.06 and 0.12 mm/rev. Although this type of drill was designed for the machining of metallic materials [178], it was recommended by SGS Tools UK, Ltd. for drilling CFRPs in this drilling trial. This was because the main objective of this drilling trial was to examine and compare the effect of different machining processes on thrust force and damage in the hole in drilling CFRPs rather than the effect of the type of drill. In addition, the same drill was used for all machining trials (for room temperature dry and cryogenic drilling) to

eliminate the variations of the results due to the drill material and geometry. The cutting speed and feed rate of 100 m/min and 0.06 mm/rev were chosen because they were commonly used in the research work on the conventional drilling of CFRPs [7, 9]. The feed rate of 0.12 mm/rev was also used to investigate the effect of an increase in feed rate on the induced damage in the hole for all machining conditions. Due to the limited quantity of the material available, only one hole was produced for each machining condition. More repetitions for each machining condition and further drilling test with other values of cutting speed and feed rare are suggested for further work.

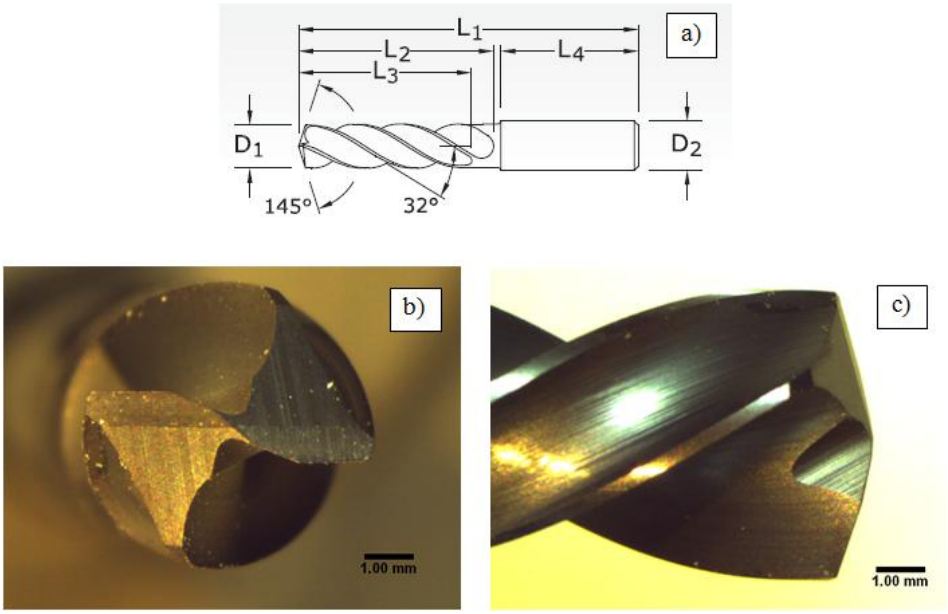

Figure 5.14: 6 mm diameter SGS series 135 M TiAlN coated solid carbide Hi-Percarb twist drill. (a) A schematic diagram [178], (b) Top view and (c) Side view

A DMG / MORI SEIKI Ultrasonic 65 monoBlock machining centre, which was the same machining centre used for the drilling trials in Section 5.2, was used to perform the drilling for all machining conditions. Set-up of the drilling experiments for producing holes in the strips for CT-scanning analysis of damage is shown in Figure 5.13. The strip was clamped on the drilling fixture on the machining table and was fixed at the same position throughout the drilling process. The experimental set-up was the same for drilling at all four machining conditions (room temperature dry, CO_2 cooling and 30 s and 120 s LN_2 cooling of the tool), except having the CO_2 cooling system in the machining area for drilling a with CO_2 cooling (similar to drilling process described in Section 5.2) and having the PS cups filled with LN_2 for the cooling the tool before drilling (similar to the drilling process described in Section 5.1). The CO_2 cooling system was the same system that was used in the drilling trial described in Section 5.2. The process for the first strip began by engraving the reference lines around the centre where the first hole would be produced. As mentioned

previously, a 2-mm diameter flat end milling cutter was used to produce the reference lines. Then, the first through-hole (6 mm diameter) was drilled dry at room temperature at a cutting speed and feed rate of 100 m/min and 0.06 mm/rev respectively. After drilling the first hole, the reference lines were produced around the new centre where the second hole would be produced without moving the strip. Then, the second hole was drilled at the new centre with CO_2 cooling (volume flow rate of 3.37 l/min) at the same cutting speed and feed rate as the first hole. This drilling process was repeated for the third and the forth holes. However, the tool was submerged in PS cups filled with LN_2 for 30 s and 120 s before drilling the third and the fourth holes respectively. Then, the drilling process for the first strip was completed, having one through-hole for each machining condition (room temperature dry drilling, CO_2 drilling and drilling with a cryogenically pre-cooled tool for 30 s and 120 s) in the strip, refer to Figure 5.13b. The drilling process for the second strip was the same as that for the first strip, except changing the feed rate from 0.06 to 0.12 mm/rev. Although it was observed that the slot drill with a flat end had been worn after completing the drilling process for two strips, flatness of the surface at the base of the reference marks was still sufficient to set a base line by which to align the sections relative to the drilling axis in the CT-scanning analysis [177]. However, a new slot drill would be required for producing the reference marks for further drilling tests to avoid error in setting up a base line to align the sections in the CT-scanning analysis.

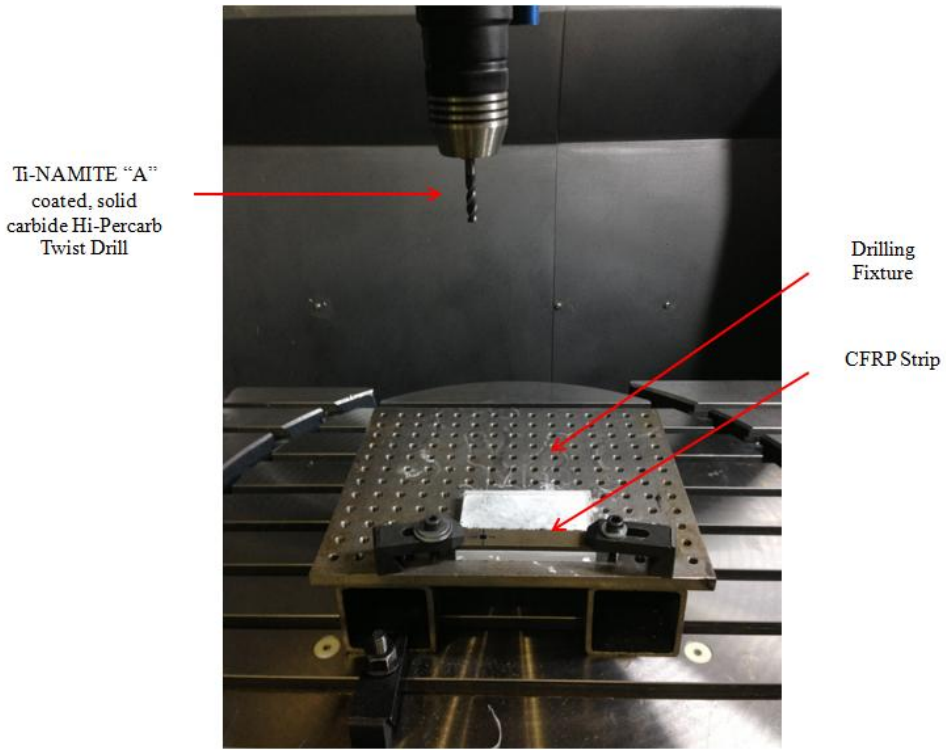

Figure 5.15: Set-up of the drilling test on a CFRP plaque for the CT-scanning analysis of damage when machined dry at room temperature

Although more repetitions for each machining condition would be desirable, only one hole was produced for each machining condition. This was because time for CT-scanning and analysis was limited as this analysis method was still in the initial development stage and hence scanning and analysis of each hole took a considerable amount of time (three to six hours for each hole [179]).

The set-up of the drilling test used for the measurement of thrust force is shown in Figure 5.16. The carbon/epoxy strip was clamped on the same Kistler dynamometer, which was fixed to the machining table. The drilling point for every machining condition was fixed at the centre of the dynamometer, but the strip was moved instead to produce holes along the strip. The drilling process was the same as that used for the CT-scanning analysis of damage but it was carried out on the dynamometer.

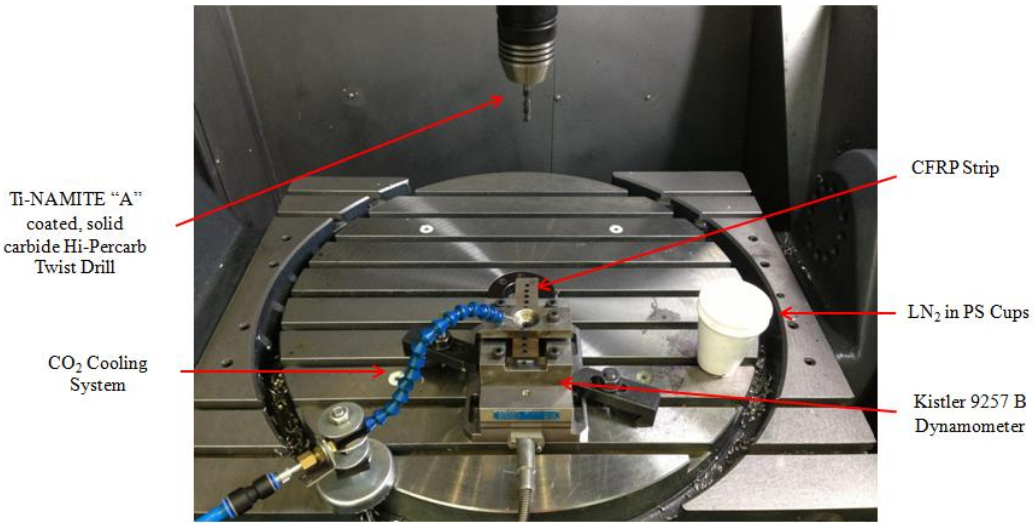

Figure 5.16: Set of the drilling test on a CFRP strip for the measurement of thrust force when machined dry at room temperature, with CO_2 cooling and with a cryogenically pre-cooled tool

The summary of machining conditions for the drilling tests in this section is presented in Table 5.4.

Table 5.4: Summary of the machining conditions for drilling tests for CT-scanning analysis of damage and measurement of thrust force in drilling of CFRPs when machined dry at room temperature, with CO_2 cooling and with a cryogenically pre-cooled tool

Machining Conditions	Test 1	Test 2	Test 3	Test 4
Machining Centre	A DMG / MORI SEIKI Sauer Ultrasonic 65 monoBlock			
Workpiece Material	CFRP plaques manufactured from uni-directional IM7and woven AS4 carbon fibres reinforced in Hexply 8552 toughened epoxy with the dimension for each plaque of 450 mm long x 120 mm wide x 4 mm thick cut in to four strips of 18 mm wide			
Drilling Tool	Series 135 M Ti-NAMITE "A" (TiAlN) coated solid carbide Hi-Percarb twist drill from SGS Tools UK, Ltd. (6 mm diameter and 66 mm length)			
Cooling Method	Room Temperature Dry	CO_2 cooling (flow rate of 3.37 l/min)	LN_2 pre-cooling (submerging time of 30 s)	LN_2 pre-cooling (submerging time of 120 s)
Cutting Speed	100 m/min			
Feed Rate	0.06 and 0.12 mm/rev			
Hole Size	6 mm			
Number of Drilled Holes	1 hole for each machining condition for CT-scanning = Total of 8 holes			
	3 holes for each machining condition for thrust force investigation = Total of 24 holes			

5.3.2. Measurement

5.3.2.1. Thrust Force

Similar to the drilling trials in Sections 5.1 and 5.2, the thrust force generated by each machining condition was measured using a Kistler 9257 B piezo-electric dynamometer with the results presented in LabView software where average and maximum values of thrust force were determined. The average value of the three repetitions at each machining condition was quoted as the thrust force for that machining condition.

5.3.2.2. Evaluation of Damage by X-ray CT-Scanning Technique

As previously mentioned, CT-scanning analysis has been used by other researchers [12, 23, 93] for non-destructive examination of delamination damage to the hole through the thickness of the laminates in drilling of CFRPs. The CT-scanning analysis method produces a 3-D image of a sample from the reconstruction of 2-D cross-sectional images of the sample using X-rays radiography (X-ray CT-scanning) [23, 93, 177, 180]. Variations in the density and content within the material being inspected cause variations in the absorption of X-rays within that material [5, 93, 125, 177, 180]. When exposed to X-rays, an area

containing internal voids or a gap as a result of delamination damage allows higher intensity of X-rays to pass through compared to an area without defects [5]. This variation in the intensity of X-rays transmitting through the sample therefore creates contrast on the image showing the cross-sectional profile of the material, which will then be reconstructed to produce a 3-D image. This enables the evaluation of the position and extent of delamination and internal damage in the hole through the thickness of the laminates.

The CFRP strips were scanned in the X-ray CT-scanning machine in WMG by Miss Nadia Kourra to obtain 2-D and 3-D images of the sample, Figure 5.17. The CT image showing the cross-sectional image of each slice of the hole, for which the thickness of each slice was 15 µm, were obtained [177]. The 3-D image of the hole is obtained by reconstructing the 2-D images of each slice of the hole. The slice images were imported to Matlab software to obtain the data relevant to the damage to the hole. Since this collaboration work was in the development stage at the time when this thesis was completed, only the data representing the maximum radius of the profile of the hole at each slice was used to determine the maximum depth of damage at various positions through the thickness of the plaque. Further development of the method (Matlab code) to obtain data for determining the area of damage at each slice in the through-the-thickness direction is suggested for further work. In the Matlab software, the radii of the hole profile of each slice image was calculated based on the "ideal" centre, which was determined from the reference lines around the hole. Then, the maximum value of those radii was selected by Matlab because it represented the radius covering the maximum depth of damage into the surface of the hole. The maximum depth of damage to the hole at each slice of the plaque in through-the-thickness direction was determined by subtracting the maximum radius of each slice of the hole by the "ideal" radius of the hole (3 mm) produced from a 6-mm diameter drill. The "ideal" radius of 3 mm of the hole was used to subtract from the maximum radius because the damage that is outside the nominal diameter of the hole is critical with respect to the quality of the hole [14]. A schematic diagram showing determination of the maximum depth of damage at each slice of the plaque is presented in Figure 5.18. The Matlab code for extracting the data from the CT-scanned images was written by Miss Nadia Kourra, but further analysis of the obtained data was done exclusively by the author.

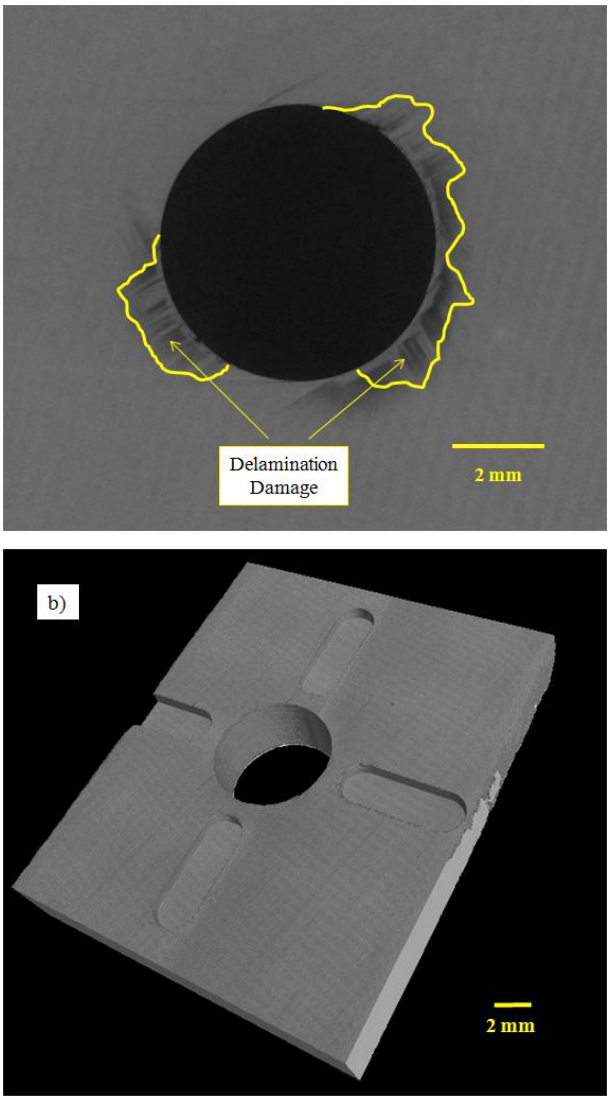

Figure 5.17: 2-D cross-sectional image (a) and a reconstructed 3-D image (b) of the drilled CFRP sample obtained by CT-scanning

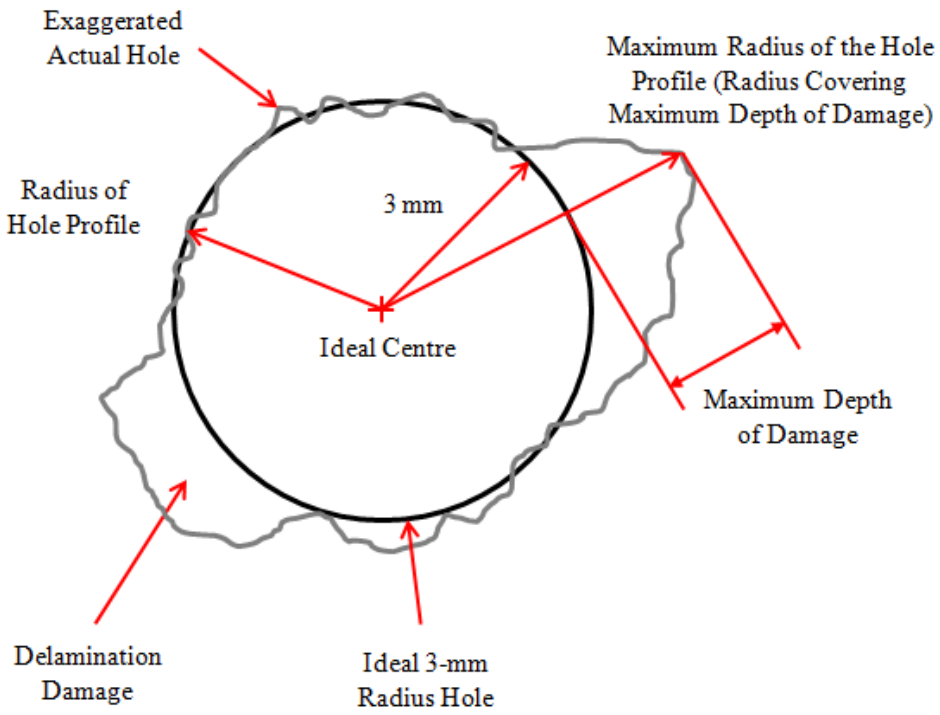

Figure 5.18: Schematic diagram showing delamination damage around the edge of the hole and determination of the maximum depth of damage at each slice through the thickness of the CFRP plaque

The concept of CT-scanning used to obtain 2-D and 3-D images of the sample in this research was similar to that used by other researchers [12, 23, 93]. However, in the work of Persson *et al.* [12] and Taso and Hocheng [23, 93], depth of delamination damage at each slice was determined by measuring the extent of damage from the hole edge based on the contrast in the image, which was processed by an image processing software. Six measurements of the extent of damage around the hole was carried and the average value was determined to quote as the depth of delamination damage for that sample [23, 93]. In their work [12, 23, 93], four reference lines, refer to Figure 5.13, were not produced prior to drilling process as it was done in this research. As previously discussed, these four reference lines with a flat surface at the bottom of the lines were used to determine an ideal centre of the hole and to set a base line for aligning the sections relative to the drilling axis. As the ideal centre is determined and the sections are aligned properly based on a flat surface relative to the drill axis, this will be useful for obtaining other types of data, e.g., circularity and cylindricity of the hole and deviation of actual drill axis from the ideal axis when the drill progress through the thickness of the plaque, in addition to maximum depth of damage at each slice.

From the initial CT-scanning, it was found that the copper-mesh layer on the entry side of the CFRP plaques caused difficulty in determining the ideal centre and obtaining the "correct" data from the images of each slice of the hole. This was due to the different

refraction of the X-rays by this much more dense copper-mesh layer compared to other part of the sample, creating a shadow in the image from the refracted X-rays [179]. As a consequence, the top laminates of both strips was machined (0.7 mm depth of cut) to remove the copper-mesh layer on the entry side. Then, the four reference lines were produced around the hole that had been drilled already in the same strips by using the 2-mm diameter flat end milling cutter to be used for determining the "ideal" centre of the hole as previously described. Although it is not ideal to produce reference lines after the holes were drilled, this method was the only option due to limited availability of the workpiece material and holes were accurately aligned when re-machining of the reference slots took place. The strips were then scanned in the X-rays CT-scanning machine again to obtain the sliced images of the hole and the data relevant to the damage to the hole. Since the top laminates of the strips were machined, the maximum depth of internal damage at the entry to the thickness of the plaque of 0.7 mm was not included. The scale of damage which is detectable within CT-scanning in this research is 15 µm.

For comparing advantages and disadvantages of the analysis of damage by CT-scanning technique and by visual inspection of cross-sectioned samples (described in Section 5.1.2.4), the CT-scanned samples were cross-sectioned and were investigated by visual inspection using Leica DM4000 M optical microscope connected to a PC with Buehler Ominet 9.5 analysis software.

5.1.2.5 Characteristics of Machined Surface

Similar to the methodology previously described in Section 5.1.2.4, the sample of the drilled hole produced from each machining condition was cross-sectioned the diameter, referred to Figure 5.8, and the characteristics of the machined surface was examined qualitatively in the SEM. The machined surface produced from different machining conditions was investigated in order to determine the effect of CO_2 and LN_2 cooling on the material behavior during the drilling process and compared to when machined dry at room temperature at the same cutting speed and feed rate. The results of the investigation of the characteristics of machined surface in this section are presented in Chapter 7.

5.4 Measurement of Cutting Temperature when Drilling Carbon Fibre Reinforced Plastics

In order to confirm a reduction in the cutting temperature by using LN_2 cooling of the tool or CO_2 cooling to reduce the cutting temperature when drilling CFRPs, it is important to determine the actual cutting temperature during the process. For the initial trials, temperature measurement using thermocouples embedded in the workpiece material and using a thermal

imaging camera was carried out. Thermocouples were embedded in CFRP strip through the holes which were drilled on both sides in the centre of the strip. However, these measurement techniques did not work. Therefore, cement-on K-type thermocouples from Omega, Figure 5.19, were used to measure the temperature of the last laminate of the plaque, at which it was expected to be a maximum temperature, as close the cutting edge as possible when the drill approaches the exit of plaque.

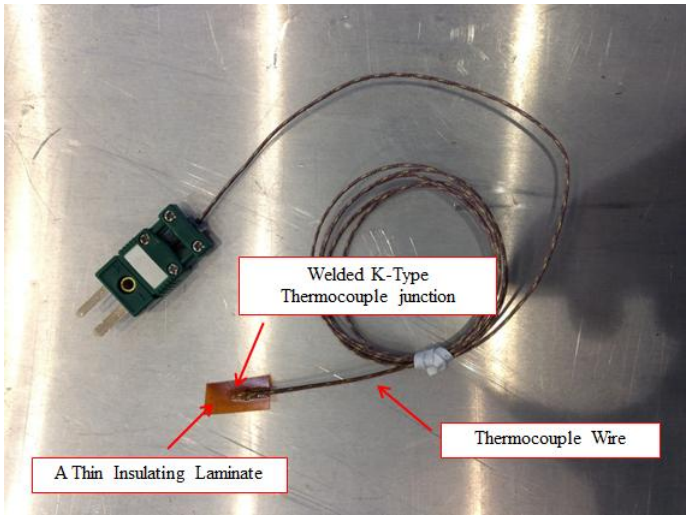

Figure 5.19: Cement-on K-type thermocouple from Omega manufactured from a welded K-type thermocouple embedded in a thin glass fibre reinforced polymer insulating laminate

The cement-on thermocouple was manufactured from a welded K-type thermocouples embedded in a thin laminate which was reported to be made of glass fibre reinforced polymer for supporting and insulating the welded thermocouple junction [181]. It was reported that this thermocouple can be used to measure temperature in the range of -190 to 370°C [181]. The thermocouples were attached to the exit side of the CFRP plaque, which was from the same batch as the plaque used for the drilling trial with CO_2 cooling in Section 5.2, using cyanoacrylate, Figure 5.20. The thermocouples were attached on the exit side of the plaque in order to measure the drilling temperature as the drill approaches the last laminate, at which the maximum cutting temperature is expected to be generated.

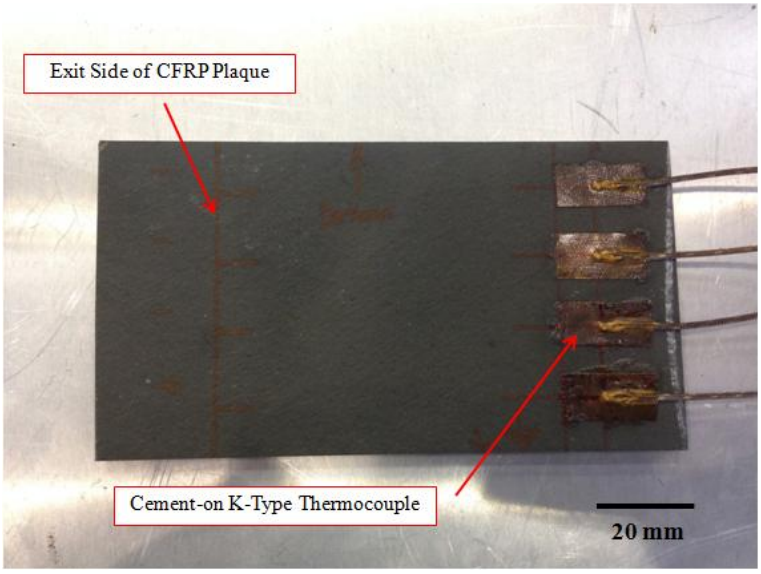

Figure 5.20: CFRP plaque with attached cement-on K-type thermocouple at the exit side used for the measurement of cutting temperature

Drilling process for producing 6 mm diameter through-holes in the CFRP plaque was carried out by the same type of drill and same machining centre used for the drilling trial in Section 5.3. The plaque, with the attached thermocouple was clamped on another CFRP plaque of the same type before clamping into the fixture, Figure 5.21. Another CFRP plaque of the same type was used to support during the drilling process to prevent the effect of surrounding environment such as heat convection from the air on the measurement of cutting temperature and mimic the thermal conductivity of the plaque being examined. The CO_2 cooling system and PS cups filled with LN_2 were placed in the machining area for drilling with cryogenic and CO_2 cooling, Figure 5.21. Four holes were produced in the plaque by drilling with a cutting speed of 100 m/min and the feed rate of 0.06 mm/rev with four machining conditions: 1) room temperature dry machining, 2) drilling with CO_2 cooling, 3) drilling with a tool pre-cooled in LN_2 for 30 seconds and 4) drilling with a tool pre-cooled in LN_2 for 120 seconds. One hole was produced using each machining condition. Holes were drilled at the position that the edge of the hole was 1 mm away from the tip of the cement-on thermocouple. Although a distance of 1 mm between the edge of the hole and the tip of the thermocouple would not represent actual temperatures at the cutting zone, this distance was chosen to avoid the risk of destroying the tip of the thermocouple. The results of measured temperatures during the drilling process were presented in PicoLog Recoder software. The results of the temperature measurement are presented and discussed in Chapter 7. Since the measured temperatures for this drilling trial would not represent actual temperatures at the cutting zone, the results of temperature measurement in this research (presented in Chapter 7) only represent an indication of a reduction of the cutting

temperature by using cryogenic cooling rather than representing actual drilling temperatures for each machining condition.

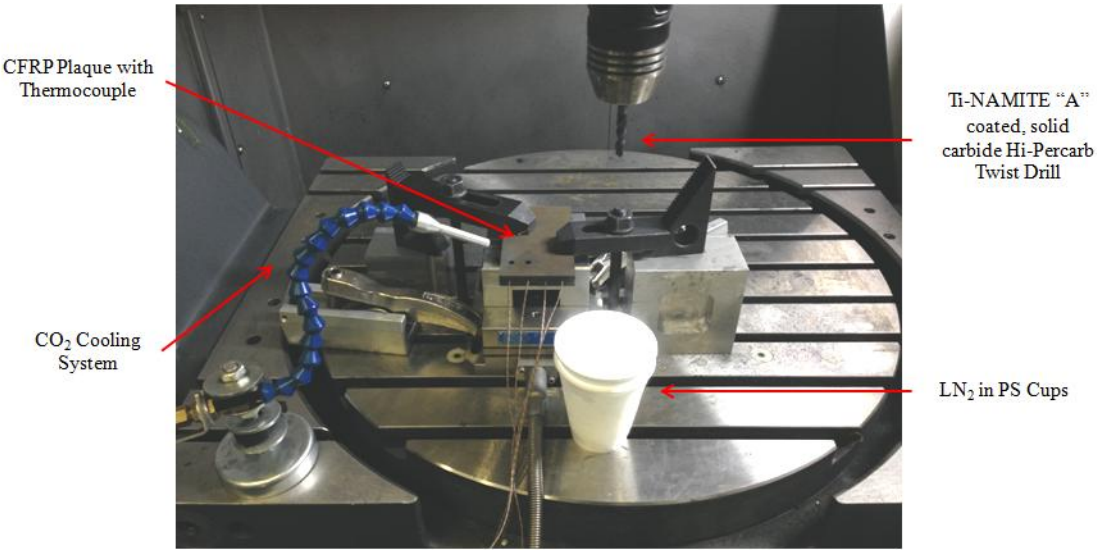

Figure 5.21: Experimental set-up of the drilling trials for measurement of cutting temperature

5.5 Investigation of Variations in Material Strength with Temperature

From discussion in Section 6.4, variations in strength and stiffness of CFRPs with temperature were proposed to be the main factors contributing to different amounts of tool wear, thrust force and damage to the hole when drilling with cryogenic cooling compared to when machined room temperature dry. In order to provide evidence to support this suggestion, micro-hardness testing of the CFRP plaque at various temperatures was carried out.

Micro-hardness testing was performed on a CFRP plaque from the same batch as the plaques used in the drilling trials in Section 5.2. The plaque was cut into a sample with the dimension of 20 mm long x 5 mm wide and mounted in EpoHeat epoxy resin, which was cured in an oven at a constant temperature of 55°C for 90 min, such that the through-the-thickness side was facing upwards, Figure 5.22a. A 1 mm diameter hole was drilled through the mounting epoxy into the plaque for inserting a K-type thermocouple to measure the temperature of the plaque at which the micro-hardness testing was performed, Figure 5.22b.

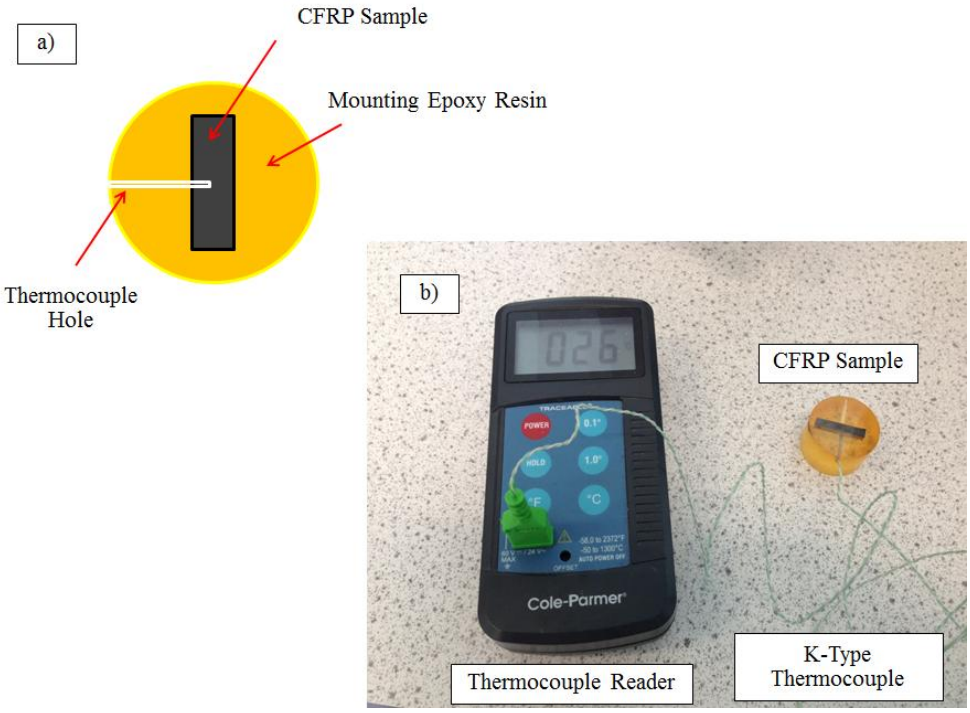

Figure 5.22: (a) Schematic diagram showing CFRP plaque mounted in epoxy resin with a 1-mm diameter hole for inserting a thermocouple. (b) A photo showing the CFRP sample with a K-type thermocouple and a thermocouple reader

The hardness of the plaque was measured at temperatures of -60°C, -40°C, -20°C, 0°C, +27°C (room temperature) and 100°C. The temperature of -60°C was the approximate temperature of CO_2 gas exiting the nozzle in the CO_2 cooling system [166] and the temperature of the tool after submerging in LN_2 for 30 s. Since CFRPs are highly anisotropic, variation in the results of hardness of the plaque were expected to occur depending on the point on which the plaque was indented. For this reason, the hardness was measured at various points on the plaque. The point that yielded the lowest hardness value at each temperature was selected to determine the variations of hardness of the epoxy matrix in the plaque with changing temperature because it was expected to yield the hardness value of epoxy matrix without any contribution from the carbon fibres. The results and discussion are presented in Chapter 7.

5.6 Investigation of the Wear Mechanism of Carbide Tools when Drilling Carbon Fibre Reinforced Plastics

From the drilling trials with LN_2 pre-cooling of the tool, abrasive wear was observed as the main mechanism of tool wear with light grooves indicating lines of abrasion at 90° to the cutting edge on flank face of the tool for room temperature dry and cryogenic drilling, Section 6.1.1.1. As previously discussed in Section 3.2.4.1, abrasive wear for carbide tools when drilling CFRPs was a result of removal of Co binder between WC grains by the carbon

fibres, which consequently resulted fracture and dislodging of WC grains, combined with direct abrasion by the fractured and dislodged grains [109, 111, 112]. Although this wear mechanism was proposed by other researchers, clear evidence with good quality and higher magnification of the image indicating cobalt removal with cracks and fracture of WC grains was not provided in their work. In the work of Masuda *et al*. [111], the evidence showing the removal of Co binders on the worn surface of the tool was demonstrated but clear evidence showing cracks and fracture of WC grains next to the area where the Co binders had been removed with high magnification was not shown. In the work of Wang *et al.* [112], the SEM images showing voids on the worn surface of the drill for which it was suggested by Wang *et al.* [112] to be the evidence of Co binder removal was provided. However, there was no clear visibility of WC grains and fracture of the grains in their work [112]. For this reason, a detailed investigation of wear mechanism of carbide tools when drilling CFRPs was performed.

The drilling experiment was carried out on the CFRP plaque that was used for the drilling experiments in Section 5.1. A Guhring SL-VHM SPIRALB K 0013915411 solid carbide twist drill, Figure 5.23, was used to produce 100 through-holes in the plaque. This type of drill is produced from straight tungsten-cobalt carbides with DK 460 UF universal grade for drilling [182]. The DK 460 UF grade of carbides, which is equivalent to ISO K30/K40 grade of carbide, is composed of 90% tungsten carbide (WC), for which the grain size is 0.55 µm, and 10% cobalt binders (Co) [183]. The hole size of 3 mm diameter was chosen to enable the drilling in the space between the holes that were produced by the drilling experiments in Section 5.1 and, hence, maximise the usage of the plaque. The drilling process was carried out room temperature dry at the cutting speed of 75.4 m/min (8,000 RPM) and the feed rate of 0.12 mm/rev. Since it is shown in Section 6.1.1.1 that similar characteristics of wear were observed for room temperature dry and cryogenic drilling, the drilling process for this investigation was carried out dry at room temperature to minimise the process time (eliminate the time for pre-cooing by LN_2). A high feed rate was chosen in order to generate sufficient tool wear from the limited quantity of workpiece material. Although a low feed rate could be used to generate a large amount of tool wear due to longer tool/workpiece contact time, a high feed rate was used instead to minimise the heat causing adhesion of epoxy matrix onto the cutting edge of the tool. The adhesion of epoxy onto the cutting edge caused problems with the examination of tool wear in the SEM.

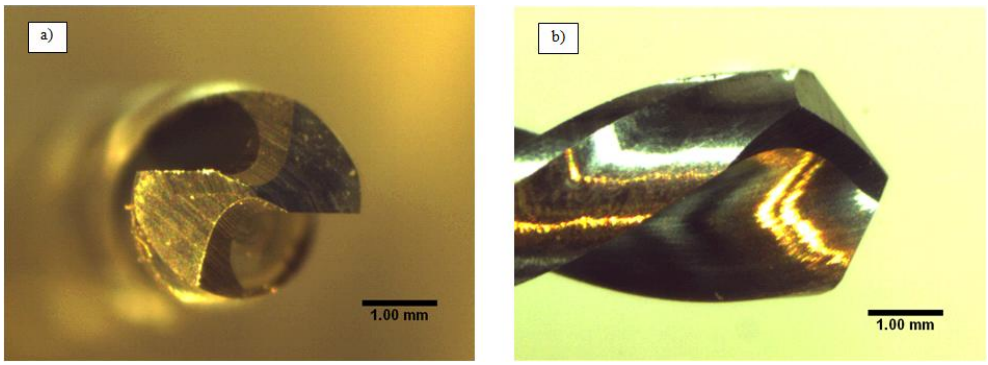

Figure 5.23: A 3 mm diameter Guhring SL-VHM SPIRALB K 0013915411 solid carbide twist drill. (a) Top view and (b) Side view

A DMG / MORI SEIKI DMC 635 V ECO machining centre (a 3-axis vertical milling centre with a maximum speed of 10,000 RPM) was used to perform the drilling process. The CFRP plaque was clamped in a fixture and the drilling process was carried out by continuously drilling 100 holes at room temperature. The tool was then examined in the SEM to determine the wear mechanism.

In order to overcome the problem of adhering epoxy on the flank face of the tool covering the worn surface, a 10 mm deep hole was drilled in an aluminium block after completing the drilling process on the CFRP plaque. The tool was then immersed in a sodium hydroxide (NaOH) solution to remove any aluminium that was adhering to the tool. From the investigation in the SEM, it was shown that this technique was effective at removing the adhering epoxy on the cutting edge of the tool enabling visibility of the WC grains on the worn surface. The results of the examination in the SEM are presented in Chapter 7.

6 Performance Evaluation of the Application of Cryogenic Cooling to Conventional Drilling of Carbon Fibre Reinforced Plastics

This chapter will present an evaluation of drilling performance of CFRPs when machined with cryogenic cooling. In Section 6.1, drilling performance of CFRPs when machined with a tool which had been cooled in LN_2 will be discussed as compared to that when machined dry at room temperature in order to develop the basic understanding of the effect of cooling the tool to cryogenic temperature during conventional drilling of CFRPs. In Section 6.2, drilling performance of CFRPs when machined with a CO_2 cooling system will be discussed as compared to when machined dry at room temperature. In this Section, the effect of machining parameters (cutting speed and feed rate) on drilling performance will also be considered. In addition, the effect of CO_2 cooling on drilling process will be discussed in comparison to LN_2 pre-cooling of the tool. In Section 6.3, the damage caused to the material, which was examined using a CT-scanning analysis method, by the conventional drilling when machined dry at room temperature, with CO_2 cooling and with a tool pre-cooled in LN_2 under the same machining conditions will be compared and discussed. Finally, discussion on the effect of cryogenic pre-cooling and CO_2 cooling on drilling performance of CFRPs based on the results in Sections 6.1-6.3 will be presented in Section 6.4.

6.1 Evaluation of Drilling Performance of Carbon Fibre Reinforced Plastics with a Tool Pre-cooled in LN_2

This section will evaluate the drilling performance of a CFRP plaque provided by WMG (reported to be a woven carbon/epoxy) [184] when machined with a tool pre-cooled in LN_2, referred as "cryogenic drilling" in this research, as compared with room temperature dry drilling. The evaluation of drilling performance is based on results for tool wear, thrust force, entry and exit delamination and internal damage. The methodology of the drilling trials and evaluation of the drilling performance in this section were previously described in Section 5.1. Raw data of the results of drilling trials discussed in Section 6.1 is presented Appendix A.

6.1.1 Tool Wear

6.1.1.1 Wear Mechanism

For both cryogenic and room temperature dry drilling, it is shown in the SEM images; Figures 6.1a and 6.1b, that flank face of the tool was uniformly worn along the cutting edge. The uniform wear band observed from the outer corner of the cutting edge to the chisel edge of the tool was similar to that previously reported by other researchers as typical characteristic of the wear produced when machining CFRPs [9, 99, 108, 109, 112, 116].

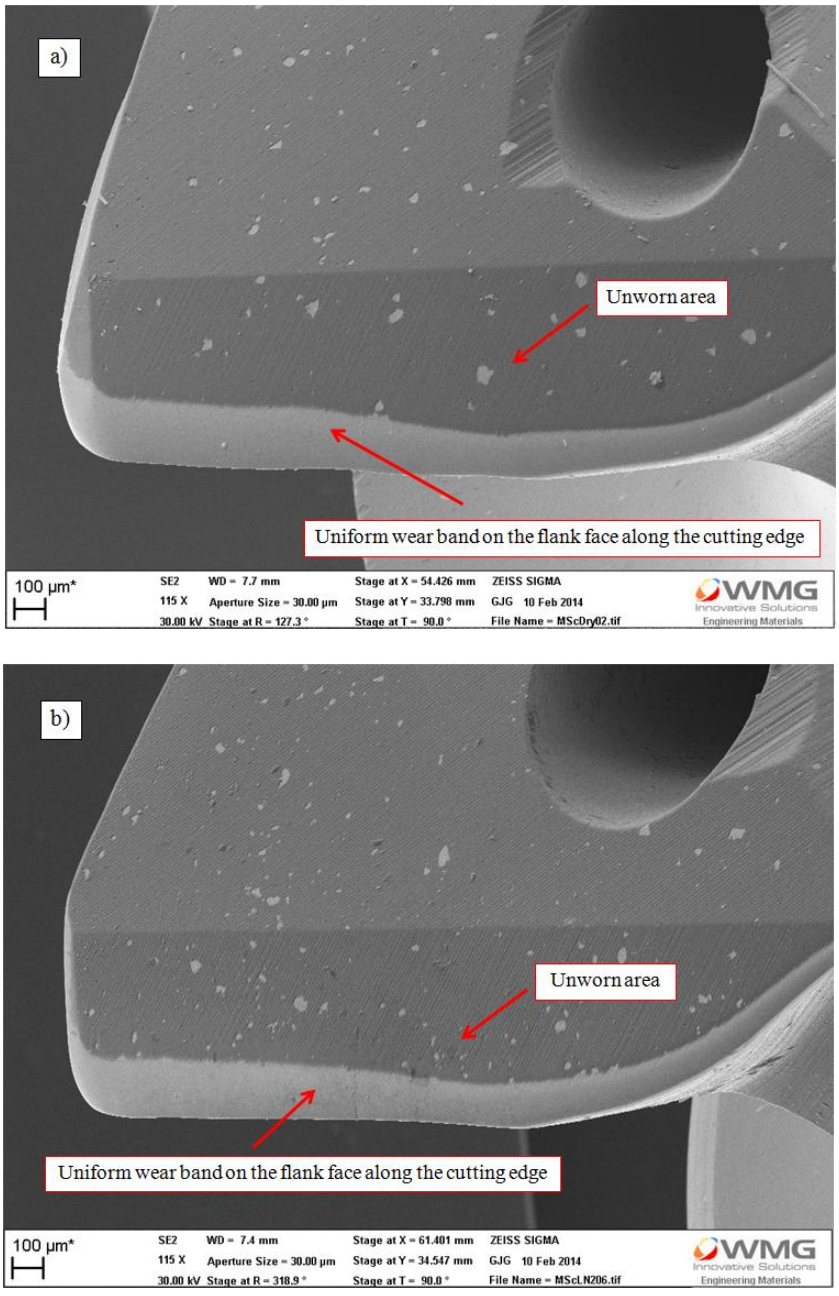

Figure 6.1: SEM images showing the uniform wear band along the cutting edge on flank face of the tool after drilling 325 through-holes in CFRP plaque (a) when machined dry at room temperature and (b) with a LN_2 pre-cooled tool

In the higher magnification image of the cutting edge and flank face of the tool, Figures 6.2, three distinct regions could be observed for cryogenic drilling. For room temperature dry drilling, three distinct regions on the flank face were also observed and SEM image at this magnification was identical to cryogenic drilling.

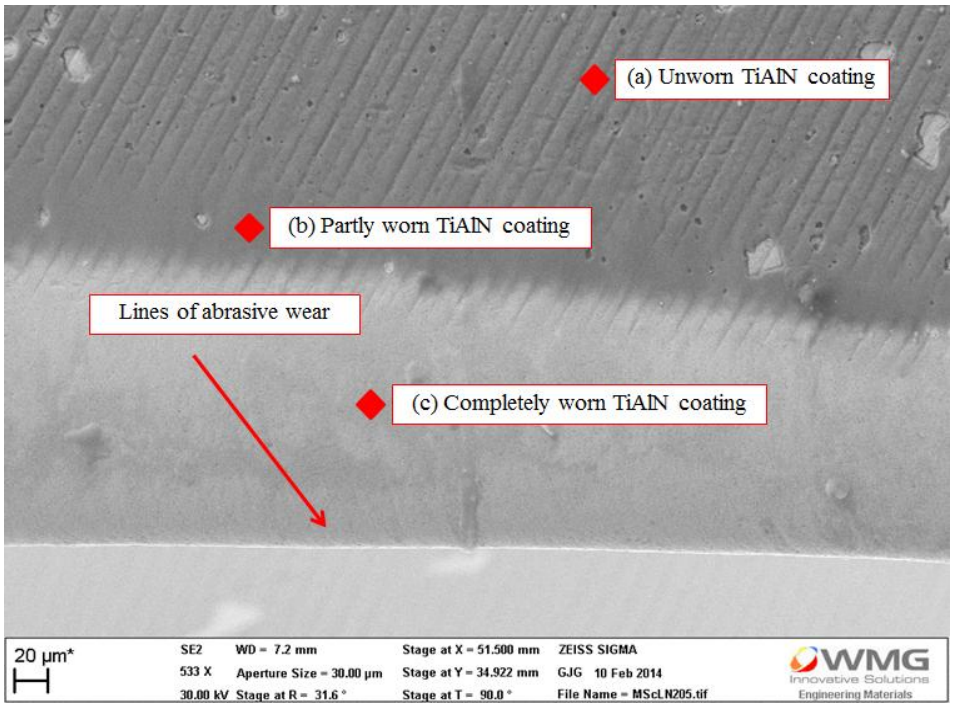

Figure 6.2: SEM image showing the area of (a) completely worn through of TiAlN coating, (b) partly worn through of TiAlN coating and (c) unworn TiAlN coating on the flank face of the tool after drilling 325 through-holes in CFRP plaque with LN_2 pre-cooling

The first region was an unworn area of the flank face. This area was observed as a darker area on the flank face with grinding lines from tungsten carbide substrate of the tool, area (a) in Figure 6.2. The result of energy dispersive spectroscopy (EDS) X-ray analysis for this unworn area is presented in Figure 6.3 and shows peaks for Ti, Al and N, i.e., the elements composing the TiAlN coating. This indicates that this region on the flank face of the tool was completely coated with the TiAlN coating as expected. The second region was the area where the TiAlN coating was partly worn through. This partly worn area was observed as a darker area on the flank face without grinding lines from tungsten carbide substrate of the tool. It was the transition between the completely worn through area and unworn area, area (b) in Figure 6.2. The result of EDS analysis for this partly worn area is presented in Figure 6.4 and shows that peaks for elements composing the TiAlN coating were still presented. However, in addition to the peaks for Ti, Al and N peaks for W and Co were also observed in contrast to in Figure 6.3. This indicates that the TiAlN coating on this region had been partly worn through, resulting in thinner layer of the coating. As a

consequence, tungsten carbide substrate underneath the coating was detected. Finally, the third region was the area where the TiAlN coating was completely worn through which was observed as a bright area along the cutting edge, area (c) in Figure 6.2. The result of EDS analysis for this completely worn through area is presented in Figure 6.5 where only peaks for the elements composing tungsten carbide substrate (W, Co and C) were observed indicating that the coating had been completely worn through in this region.

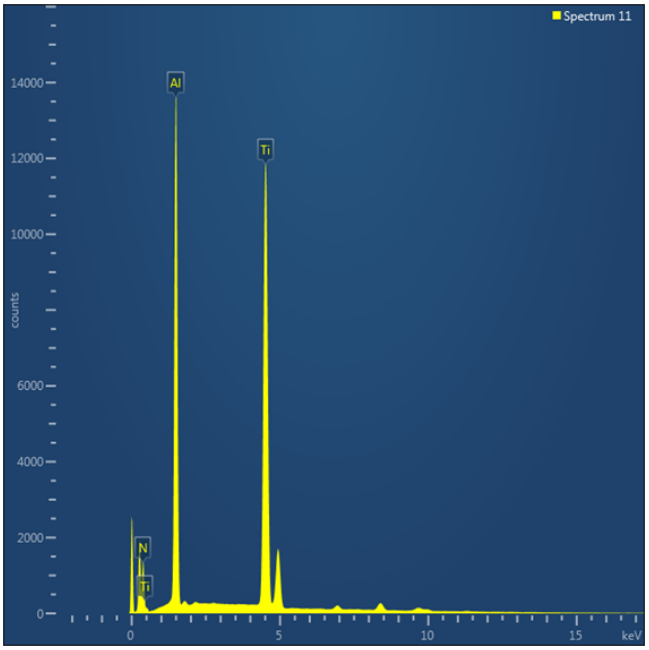

Figure 6.3: Energy dispersive spectroscopy (EDS) X-ray analysis at 30 KV of the unworn area on flank face of the tool (area (a) in Figure 6.2) used for the drilling experiment with a tool pre-cooled in LN_2 showing the evidence of complete coating of TiAlN on the tool

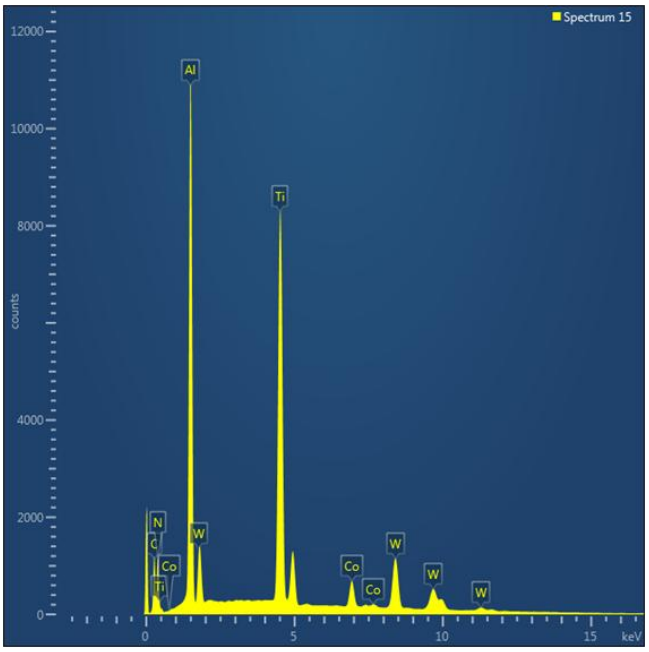

Figure 6.4: Energy dispersive spectroscopy (EDS) X-ray analysis at 30 KV of the partly worn through area on the flank face of the tool (area (b) in Figure 6.2) used for the drilling experiment with a tool pre-cooled in LN_2 showing the evidence of TiAlN coating on the flank face together with the peaks for the elements composing the tungsten carbide substrate (W,Co and C)

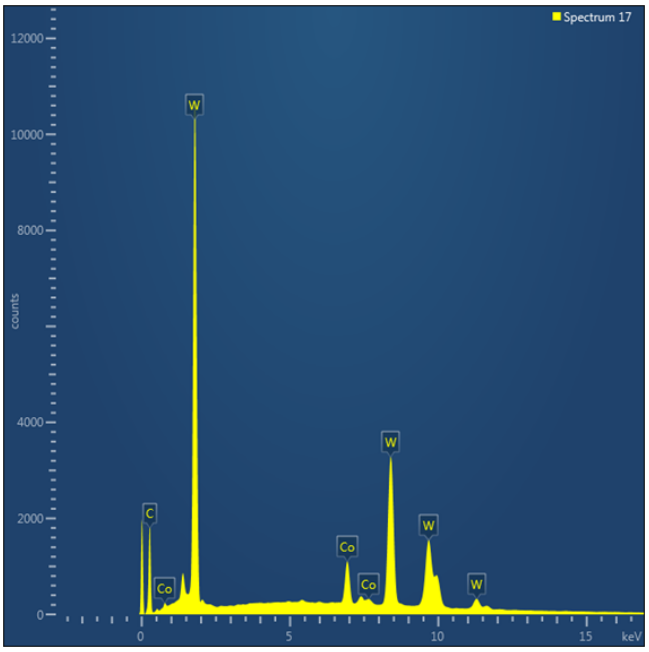

Figure 6.5: Energy dispersive spectroscopy (EDS) X-ray analysis at 30 KV of the completely worn through area on the flank face of the tool (area (c) in Figure 6.2) used for (b) the drilling experiment with a tool pre-cooled in LN_2 showing the evidence of tungsten carbide substrate of the tool without presence of the peaks for the elements composing the TiAlN coating

In addition, it is shown in Figure 6.2 that there were fine lines of abrasive wear in the completely worn area on the flank face, which were observed as fine grooves at 90° to the

cutting edge on the flank face. This indicates that abrasive wear was the major mechanism of tool wear when machining CFRPs as previously reported by other researchers [9, 99, 109, 112, 116]. As discussed in Chapter 3, other researchers have proposed that abrasive wear on carbide tools when drilling CFRPs was resulting from removal of Co binder from the surface of the tool by abrasive fractured carbon fibres and direct abrasion by the fractured and dislodged particles of WC grains as they moved along the flank face under cutting pressure [109, 111, 112]. The removal of Co binder resulted in an increase in exposed area of WC grains to dynamic cutting stress due to fracture dominated cutting mechanism in CFRP machining, causing fracture and dislodging of WC grains which then caused direct abrasion on the cutting edge [109, 111, 112]. As previously discussed in Chapter 3, the author considers this proposed mechanism of abrasive wear to be plausible because the hardness of carbon fibres was higher compared to that of Co binders, while it was lower compared to that of WC grains. Based on this wear mechanism, the fine grooves at 90° to the cutting edge shown in Figure 6.2 would result from abrasion by the fractured and dislodged particles of WC grains rather than from the workpiece material. More detailed investigation of the mechanism of abrasive wear of the tool in drilling carbon/epoxy composites will be discussed in Chapter 7.

6.1.1.2 Average Flank Wear

The results for average flank wear with number of holes drilled are presented in Figure 6.6.

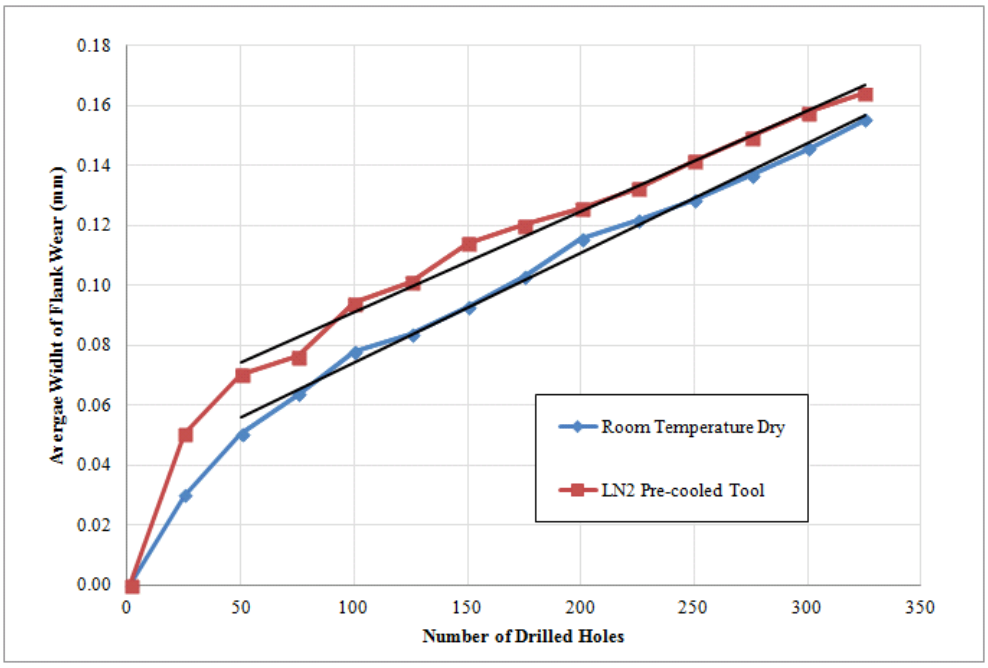

Figure 6.6: Variation of average flank wear with number of holes drilled in a CFRP plaque when machined dry at room temperature and with a tool pre-cooled in LN_2

From the results in Figure 6.6, two stages of tool wear can be observed; 1) initial tool wear and 2) steady state tool wear. During initial tool wear, a rapid increase of average flank wear was observed. During this stage, the tool/workpiece contact area was small because the cutting edge of the tool was sharp. This resulted in high cutting pressure on the tool and hence a rapid rate of tool wear. In some cases, chipping of the cutting edge could also be observed. The initial stage or the stage of rapid tool wear occurred from the first hole until the 50^{th} hole during which average flank wear increased at a rate of 1 µm/hole for room temperature dry drilling and 1.4 µm/hole for cryogenic drilling. The rate of tool wear was determined from a slope of the graph from the first hole to the 50^{th} hole in Figure 6.6. During steady state tool wear, a gradual increase in average flank wear was observed. During this stage, the tool/workpiece contact area was larger compared to that during initial tool wear as the sharpness of the cutting edge was reduced. As consequence, this resulted in lower cutting pressure on the tool and more gradual increase in tool wear during this stage of the process. Steady state tool wear occurred from the 50^{th} hole until the 325^{th} hole during which average flank wear increased at a rate of 0.4 µm/hole and 0.3 µm/hole for room temperature dry and cryogenic drilling respectively. The rate of tool wear was determined from a slope of the graph from the 50^{th} hole to the 325^{th} hole in Figure 6.6. This trend of the progressive tool wear when drilling CFRPs has previously been demonstrated by other researchers [87, 108, 109, 116, 117]. It can also be noted from Figure 6.6 that no sign of the final stage of tool wear, during which a rapid rate of tool wear would occur as a result of

rapid increase of cutting forces and temperature until reaching the end of tool life when machining CFRPs [108, 109], was shown for this drilling trial.

In Figure 6.6, it is shown that cryogenic drilling produced higher average flank wear as compared to room temperature dry drilling from the first hole to the 325th hole. The average difference between average flank wear produced from the two drilling tests was 20%. As a consequence, it can be stated that the application of cryogenic (LN_2) cooling of the tool did not improve drilling performance with respect to amount of tool wear or tool life even though the application of cryogenic cooling has been shown to provide such benefits in metal machining [28, 34, 41, 140, 145, 147, 185].

During initial tool wear (1st to 50th hole), it was observed that cryogenic drilling produced 39-69% higher average flank wear compared to room temperature dry drilling. From 75th to 175th hole, which entered steady state tool wear, it was observed that the difference between the values of average flank wear for the two drilling tests had decreased to 17-23%. Finally, this difference was reduced to less than 10% beyond the 175th hole drilling. These observations indicate that the effect of cryogenic cooling of the tool on tool wear was most dominant during initial stage of tool wear, when the cutting edge was sharp. After entering steady state tool wear, the effect of cryogenic cooling was reduced and finally became less dominant as the drilling processes continued. During initial tool wear, the tool/workpiece contact area was smaller due to the sharpness of the tool and the cutting forces were lower compared to those in the steady state where tool wear was higher. This resulted in lower cutting heat generated in the initial stage compared to that in steady state tool wear. As a consequence, it is proposed that cryogenic drilling could remove heat from the cutting zone more effectively in the initial stage than in the steady state of wear due to the lower cutting heat. It is proposed that the removal of cutting heat by the cryogenic drilling resulted in retention of more abrasiveness and higher strength in the workpiece material during the drilling which caused higher tool wear as will be discussed later in Section 6.4. Consequently, the more significant difference in average flank wear was produced for the two drilling tests in the initial stage than in the steady state of wear. As the drilling process continued, the tool/workpiece contact area and cutting forces increased due to larger tool wear resulting in higher cutting heat. This would result in less effectiveness in removing cutting heat by the cryogenic drilling. As a consequence, less difference in average flank wear was produced for the two drilling tests in the steady state of tool wear compared to that during the initial stage, and this difference decreased as the number of holes increased. The decrease in difference between average flank wear for the two drilling tests as the number of holes increased in the steady state tool wear is shown by the trend lines in Figure 6.6. It is shown from the trend lines in Figure 6.6 that the values of average flank wear for room temperature dry and cryogenic drilling tended to converge as the number of

holes increased. It is predicted from this trend that the two drilling experiments would produce the same average flank wear of approximately 0.24 mm after drilling approximately 600 holes.

As previously described in Section 5.1, the time for submerging the tool in LN_2 was changed from 10 s to 30 s from the 11^{th} to the 13^{th} drilling cycle, i.e. from drilling the 251^{st} until the 325^{th} hole. From the results in Figure 6.6, it can be seen that the change of cooling time did not affect the variation of tool wear for cryogenic drilling test. Steady state tool wear, during which average flank wear increased gradually, occurred from the 50^{th} hole until the 325^{th} hole for the cryogenic drilling test regardless of the change of cooling time. However, an increase rate of average flank wear during steady state tool wear for the cryogenic drilling test tended to reduce as the cooling time was changed. From the 50^{th} hole until the 250^{th} hole, for which the cooling time was 10 s, average flank wear increased at a rate of 0.4 µm/hole (determined from a slope of the graph from the 50^{th} hole to the 205^{th} hole in Figure 6.6). From the 251^{st} hole until the 325^{th} hole, for which the cooling time was 30 s, average flank wear increased at a rate of 0.3 µm/hole (determined from a slope of the graph from the 250^{th} hole to the 325^{th} hole in Figure 6.6). It is proposed that this reduction in an increase rate of average flank wear was due to higher level of strength of the tool that was retained during drilling as a result of lower temperature of the tool. The measured temperature of the tool after submerging in LN_2 for 10 s and 30 s was -22°C and -70°C respectively. Since the tool was cooled to a lower temperature, strength of the tool was retained at a higher level during drilling with the cooling time of 30 s compared to that with the cooling time of 10 s. This resulted in higher wear resistance of the tool, thus a lower increase rate of tool wear for the drilling with the cooling time of 30 s. Although a reduction in temperature of the tool would also result in more abrasiveness and higher strength of the workpiece material being retained, which will be discussed in Section 6.4, the author suggests that the increased abrasiveness and strength of the workpiece material would be compensated by the retention of higher strength of the tool, resulting in a lower increase rate of tool wear as the cooling time increased.

In addition, it is shown in Figure 6.6 that the change of cooling time did not affect the results with respect to the difference between the values of average flank wear for room temperature dry and cryogenic drilling tests. As previously mentioned, cryogenic drilling produced higher average flank wear compared to room temperature dry drilling from the first hole drilling until the end of the test regardless of the change of cooling time. Although it is expected that effectiveness in removing cutting heat by the cryogenic drilling would increase due to lower temperature of the cooled tool as the cooling time was changed to 30 s from the 11^{th} drilling cycle, the difference between average flank wear for the two drilling tests was reduced to less than 10% beyond the 175^{th} hole drilling until the end of the test. It

is proposed that this would be because of a more dominant effect of increased cutting heat that was generated combined with a reduction in the effect of cryogenic cooling as the drilling process continued. As previously discussed, higher cutting heat was generated as the drilling process continued due to larger tool/workpiece contact area and higher cutting forces, which were resulting from an increase in tool wear. The effect of increased cutting heat would compensate the effect of higher effectiveness in cutting heat removal by cryogenic drilling due to a reduction in temperature of the cooled tool as a result of longer cooling time, hence resulting in less dominant effect of cryogenic cooling.

6.1.2 Thrust Force

The average and maximum values of thrust force were determined during the period between when the chisel edge and the main cutting edges engaged in the cutting to the moment when the main cutting edges penetrated through the last laminate of the CFRP plaque for which the thrust force was relatively steady, Figure 6.7. This period of cutting action contributes to the major proportion of total thrust force of drilling process [3, 4]. The moment when only the chisel edge started to engage the plaque was not considered because there might be fluctuation in thrust force due to vibration and instability of the drill as it started to engage (impact) first laminates of the plaque as can be seen in Figure 6.7. This fluctuation would cause variations in performance evaluation. The moment when only minor cutting edges involved in cutting (the moment after chisel edge and major cutting edges penetrated through the plague) also was not considered because frictional force between the minor cutting edges and the hole surface did not contribute to significant proportion of total thrust force as discussed in Chapter 3 [3, 4]. Results showing the increase in thrust force with the number of holes drilled when machined dry at room temperature and with a pre-cooled tool are presented in Figures 6.8 and 6.9.

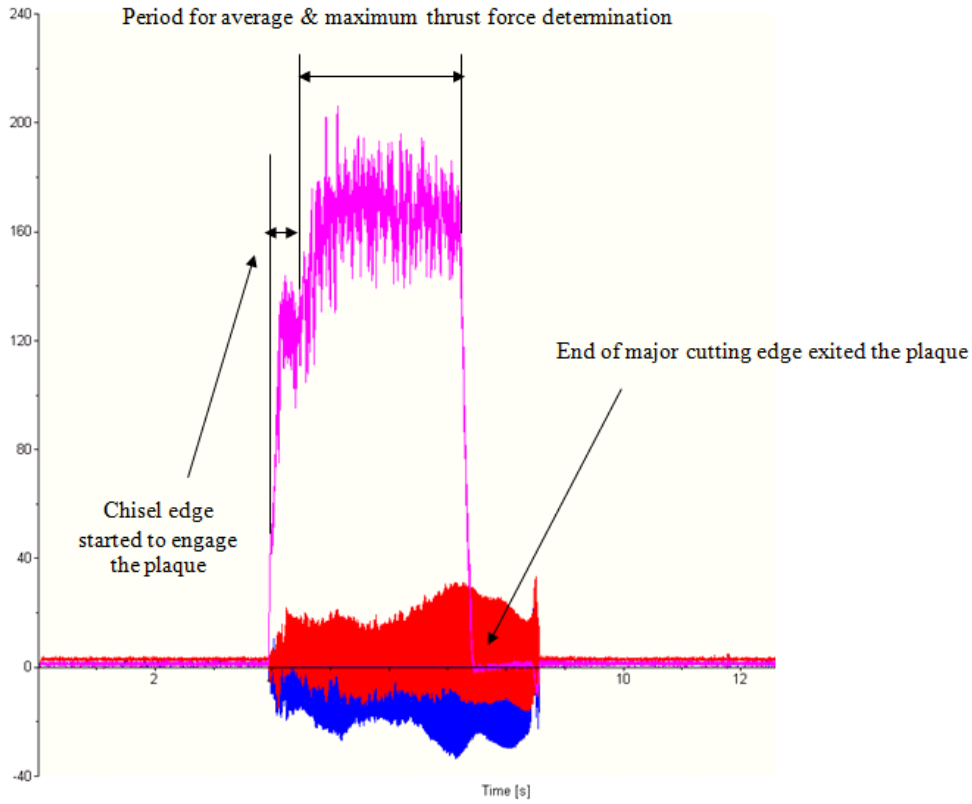

Figure 6.7: Screenshot showing the profile of thrust force for drilling of CFRP plaque with the demonstration of the period where the average and maximum values of thrust force were determined

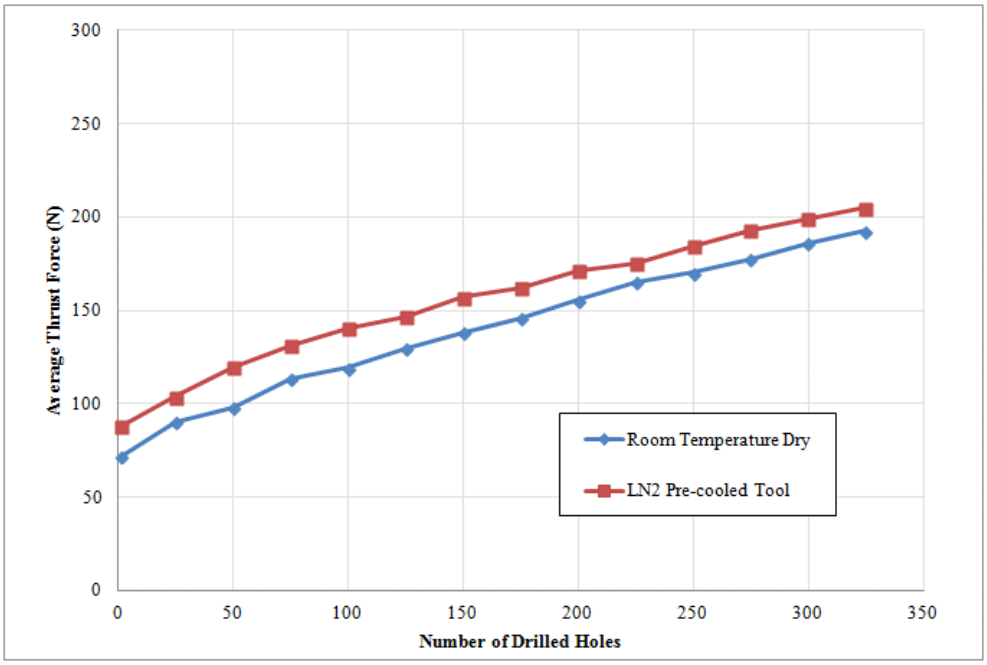

Figure 6.8: Variation of average thrust force with the number of holes drilled for drilling of CFRP plaque when machined room temperature dry and with a tool pre-cooled in LN_2

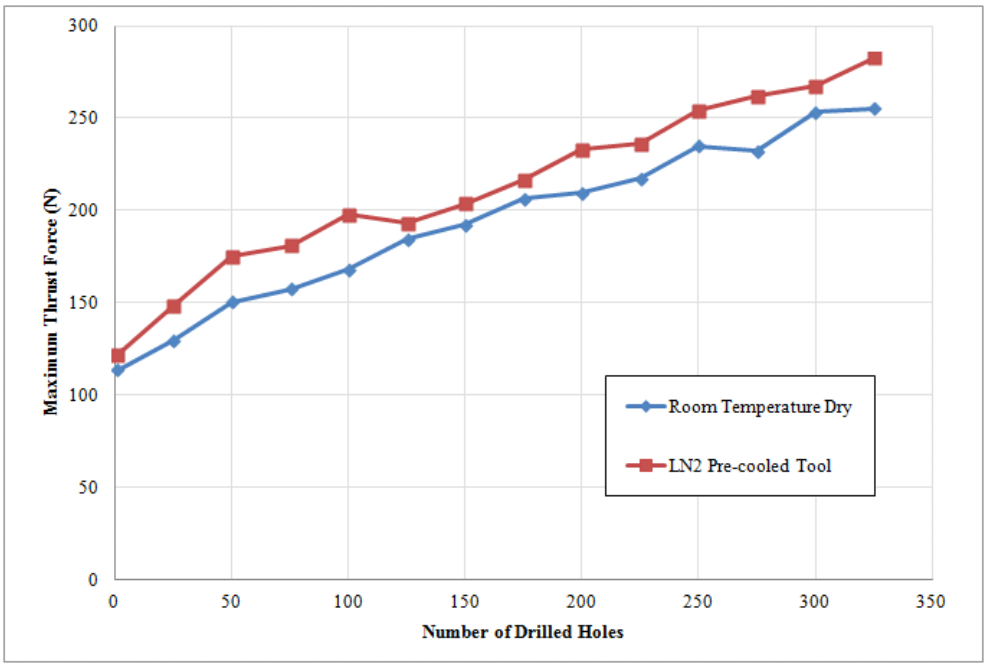

Figure 6.9: Variation of maximum thrust force with the number of holes drilled for drilling of CFRP plaque when machined dry at room temperature and with a tool pre-cooled in LN_2

It is shown in Figure 6.8 that cryogenic drilling produced higher average thrust force compared to room temperature dry drilling. A similar trend was also produced in the case of maximum thrust force, Figure 6.9. The average difference between thrust forces produced from cryogenic and room temperature dry drilling was 13% for the average values and 10% for the maximum values. This difference between thrust forces produced from the two drilling tests makes a significant contribution to different exit delamination damage produced by the two tests which will be discussed in Section 6.1.3.2. This indicates that cryogenic (LN_2) pre-cooling of the tool did not provide a benefit of thrust force reduction when drilling CFRPs. The reason for higher thrust force produced when drilling with a cryogenically cooled tool will be discussed in Section 6.4. Despite the different values of thrust force, it is shown in Figure 6.8 and 6.9 that thrust forces increased as the number of holes increased for both drilling tests due to progressive increase in tool wear with the number of holes drilled.

From the results in Figures 6.8 and 6.9, it can be seen that the change of cooling time did not affect trend of the comparison between thrust forces for room temperature dry and cryogenic drilling tests. As previously mentioned, cryogenic drilling produced higher thrust force (both average and maximum values) compared to room temperature dry drilling regardless of the change of cooling time from the 11^{th} drilling cycle. Although it is expected that average difference between thrust forces for the two drilling process would increase as the cooling time was increased to 30 s due to increased effectiveness in removing cutting

heat by cryogenic cooling, the average difference between average values of thrust force for the two drilling tests tended to reduce as the cooling time was changed. From the first to the 10^{th} drilling cycle, for which the cooling time 10 s, cryogenic drilling produced higher average thrust force with an average difference of 14%. However, from the 11^{th} to the 13^{th} drilling cycle, for which the cooling time was 30 s, the average difference between average values of thrust force for the two drilling tests was reduced to 7%. The author suggests that this would be because of a less dominant effect of cryogenic cooling plus a more dominant effect of increased cutting heat being generate as the drilling process continued as previously discussed in Section 6.1.1.2. An increase in cutting heat being generated due to increasing tool wear and cutting forces as the drilling process continued would compensate an increase in effectiveness in cutting heat removal by the cryogenic cooling as a result of longer cooling time. In case of maximum thrust force, average difference between maximum values of thrust force for the two drilling tests was not affected by the change of cooling time. The average difference between maximum values of thrust force for the two drilling tests during the first to the 10^{th} drilling cycle, i.e. submerging time of 10 s, and during the 11^{th} to the 13^{th} drilling cycle, i.e. submerging time of 30 s, was 10%.

6.1.3 Surface Delamination

Results showing the evaluation of entry and exit delamination damage in terms of delamination factor (F_d) for room temperature dry and cryogenic drilling of CFRP plaque are presented in Figure 6.10.

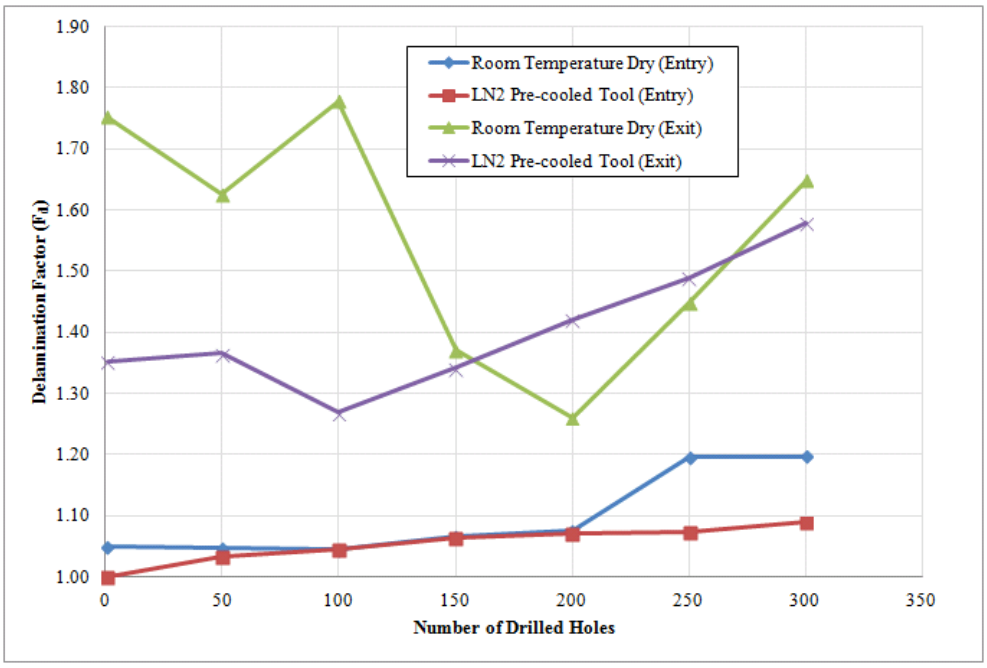

Figure 6.10: Variation of entry and exit delamination damage in terms of delamination factor ($F_d = D_{max}/D_{hole}$) with the number of holes produced from drilling of CFRP plaque when machined room temperature dry and with a tool pre-cooled in LN_2

6.1.3.1 Entry Delamination

It is shown in Figure 6.10 that entry delamination damage was significantly lower than exit delamination damage for both cryogenic and room temperature dry drilling. The entry F_d was in the range 1.04-1.20, while the exit F_d was in the range 1.26-1.78. This indicates that exit delamination damage as a result of push-down force is more severe and critical to the quality of drilled holes when drilling CFRPs, which has also been reported by other researchers [3, 4, 7, 9, 117]. Although it was not discussed by other researchers [3, 4, 7, 9, 117], the author suggests that accumulated cutting heat as the drill approaches the exit side of CFRP plaque is the factor contributing to more severe delamination at the exit than at the entry. At the entry, the drill engages and cut only few laminates at the top of the plaque. As the drill approaches the exit of the plaque, it has cut through more laminates resulting in accumulated cutting heat. This accumulated cutting heat would decrease the interlamina fracture strength of the CFRP plaque, which dominates the resistance to delamination damage [4, 5, 8], which will increase the possibility of delamination damage. The effect of heat during the cutting process on the strength of CFRP plaque will be discussed later in Section 6.4. In addition to accumulated heat, the author also suggests that push-down force acting on the last laminates would result in more possibility of delamination damage than peel-up force acting on the first laminates. This is because push-down force is more attributed to indentation by the chisel edge while peel-up force is more attributed to cutting by the cutting edges and peeling up by the flutes. As can be seen in Figures 6.11 and 6.12,

no significant delamination damage could be observed at the entry as compared to that at the exit for the first hole and 300th hole.

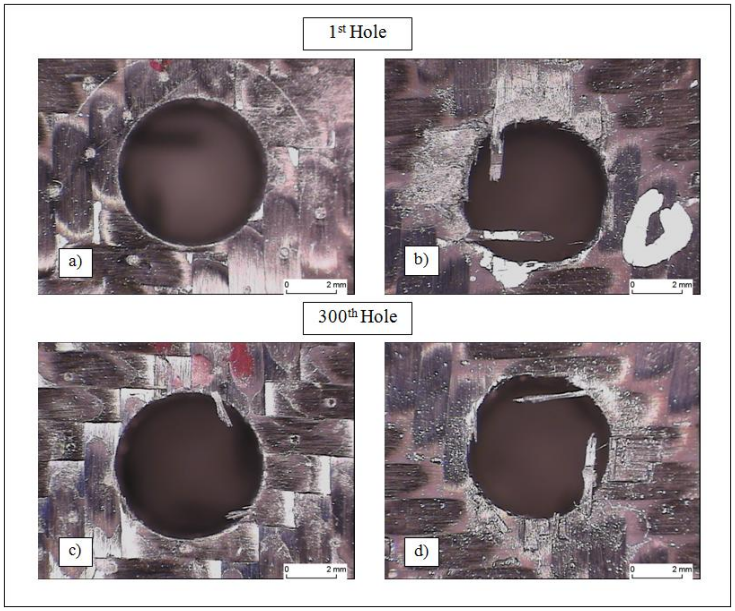

Figure 6.11: Optical microscope images showing the entry ((a) and (c)) and exit delamination ((b) and (d)) produced from room temperature dry drilling of the 1st hole and 300th hole in CFRP plaque

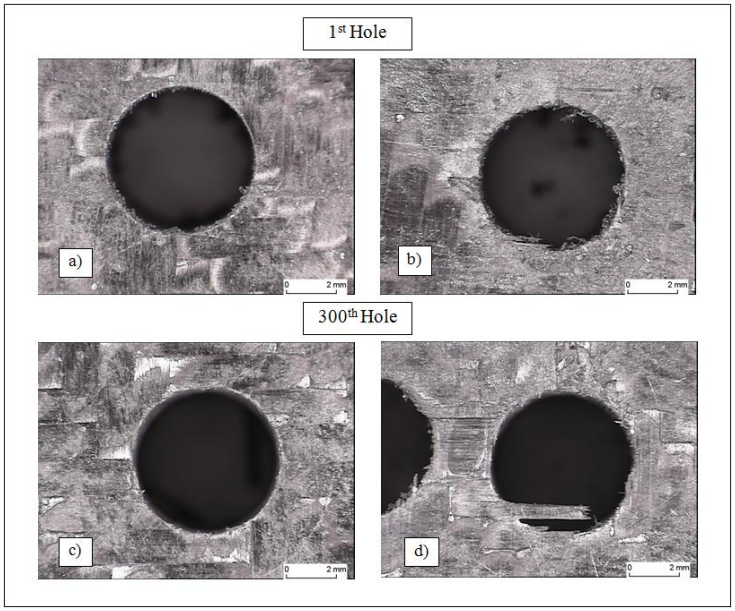

Figure 6.12: Optical microscope images showing the entry ((a) and (c)) and exit delamination produced from drilling of the 1st hole and 300th hole in CFRP plaque with a tool pre-cooled in LN_2

It is also shown in Figure 6.10 that there was no significant difference between the entry F_d of cryogenic and room temperature dry drilling from the first hole until the 200th hole. The author suggests that the difference in the tool wear and thrust force between the

two drilling tests was not sufficient to produce significant difference in entry delamination damage. However, it is shown in Figure 6.10 that cryogenic drilling produced less entry F_d as compared to room temperature dry drilling from 200^{th}-300^{th} hole at which the cutting tool was severely worn. The drilling experiments should be carried on further to confirm this trend of less entry delamination when drilling with the cryogenically cooled tool.

6.1.3.2 Exit Delamination

As previously discussed, it can be seen in Figures 6.10-6.12 that exit delamination damage was significantly higher and more obvious than entry delamination damage. Therefore, the exit delamination damage is more critical to the quality of the drilled holes when drilling CFRP composites [4, 7, 9, 117].

However, it is shown in Figure 6.10 that there were large variations in the results of exit delamination damage in term of F_d such that the trend of drilling performance could not be determined. As a consequence, use of the results for exit delamination F_d, which considered only the maximum diameter of the damaged area, were not considered suitable for evaluation of drilling performance in this research. Due to the anisotropy of the material, the shape of delamination when drilling CFRPs was irregular and, in some cases, consisted of fine cracks from the fibres being pushed down around the edge of the hole [116, 125], Figure 6.11 and 6.12. Consequently, high variations in the results showing the evaluation of delamination damage in terms of F_d could occur as a result of these fine cracks. The example of possible variations in evaluation of delamination in terms of F_d was previously demonstrated and discussed in Section 5.1.2.3. Exit delamination damage was, therefore, also evaluated in terms of area-delamiantion factor (F_{da}), which considered the actual delaminated area around the edge of the hole. The results showing evaluation of exit delamination in terms of F_{da} for cryogenic and room temperature dry drilling are presented in Figure 6.13.

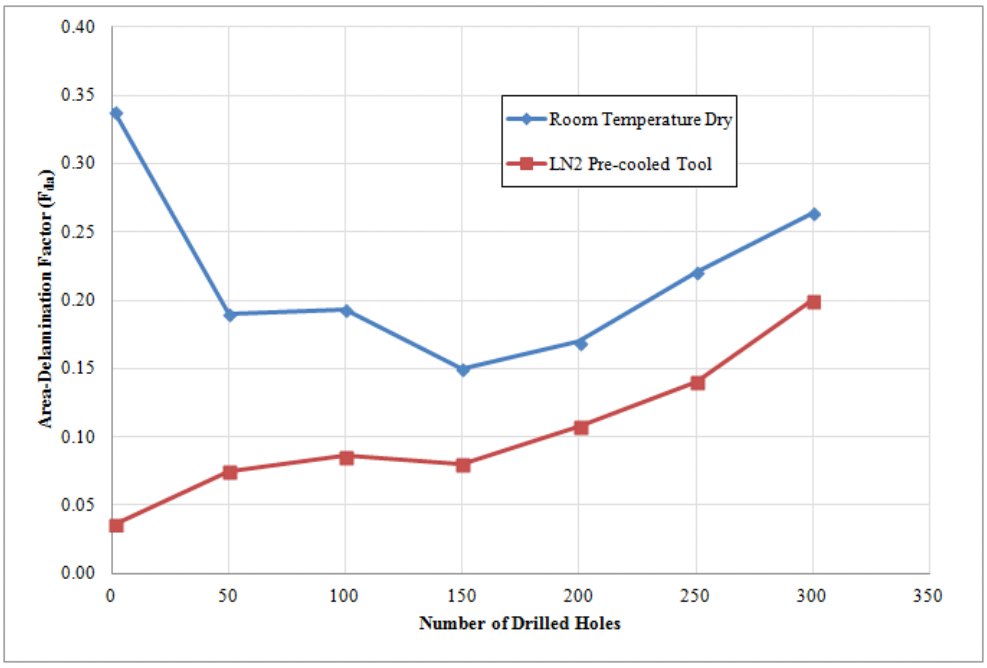

Figure 6.13: Variation of exit delamination damage in terms of area-delamination factor ($F_{da} = A_{max}/A_{hole}$) with the number of drilled holes produced from drilling of CFRP plaque when machined dry at room temperature and with a tool pre-cooled in LN_2

It is shown in Figure 6.13 that cryogenic drilling produced less exit F_{da} from the first hole to 300th hole as compared to room temperature dry drilling. The average reduction of exit F_{da} when drilling with cryogenic cooling as compared with room temperature dry drilling was 0.08 of F_{da} or 43%, excluding the extreme value of F_{da} of the first hole for room temperature dry drilling. This indicates that the application of LN_2 pre-cooling of the tool could improve drilling performance of CFRPs with respect to the quality of the drilled holes by reducing exit delamination damage as compared to room temperature dry machining. The reason for a reduction of exit delamination damage when drilling with cryogenic pre-cooling will be discussed in Section 6.4.

It is suggested that this extreme value of F_{da} for the first hole drilling when machined dry at room temperature was resulting from the variations of material properties within the plaque, which was manufactured in-house by WMG. The bonding strength between the laminates would be lower at the area where the first hole was drilled, contributing to more susceptibility to delamination damage. In addition, it is demonstrated in Figure 6.13 that the exit delamination damage for both drilling tests tended to increase as the number of drilled holes increased. This was due to the progressive increase of tool wear and thrust force with the number of drilled holes.

As the cooling time was changed from 10 s to 30 s, it is expected that the reduction of F_{da} when drilling with cryogenic cooling as compared with room temperature dry drilling would increase due to higher effectiveness in cutting heat removal as a result of lower

temperature of the cooled tool. However, it is shown in Figure 6.13 that the change of cooling time did not result in an increase in reduction of exit F_{da}. The reduction of exit F_{da} by cryogenic drilling reduced from 36% for the 250th hole drilling, for which cooling time was 10 s, to 24% for the 300th hole drilling, for which cooling time was 30 s. This indicates that an increase in effectiveness of cutting heat removal by cryogenic cooling due to longer cooling time was not sufficient to contribute an increase in benefit of exit F_{da} reduction at the end of drilling test. It is proposed that this would be because of a more dominant effect of increase in cutting heat due to progressive increase of tool wear and cutting forces at the end of drilling test compared to the increase in effectiveness of cutting heat removal by cryogenic drilling. The more dominant effect of increased cutting heat with the progress of drilling test was previously discussed in Sections 6.1.1.2 and 6.1.2. In addition, it can be seen that the reduction of exit F_{da} decreased as the drilling process continued. It reduced from 61% for the 50th hole drilling (excluding the extreme value of F_{da} of the first hole for room temperature dry drilling) to 24% for the 300th hole drilling. This indicates that the effect of cryogenic cooling became less dominant with progress of the drilling process. It is proposed that this was also because of an increase in cutting heat being generated as the drilling process continued which reduced the effectiveness in removing cutting heat by cryogenic drilling.

6.1.4 Internal Damage

In addition to delamination damage at entry and exit of the plaque, internal damage in the form of material chip-out, fibre pull-out and internal delamination was observed on the machined surface of the drilled hole, Figure 6.14. These types of damage on the machined surface, which are typical damage induced from drilling of CFRPs, were observed for both room temperature dry and cryogenic drilling tests. This damage could also be used to indicate the quality of drilled holes for each drilling process. It can also be seen in Figure 6.14 that characteristics of the machined surface vary between different laminates of the plaque due to different fibre orientation between laminates, refer to Figure 5.1. As discussed in Section 3.2.1, cutting mechanism when machining CFRPs varies based on fibre orientation relative to cutting edges resulting in different characteristics of the machined surface. The author suggests that the machined surface with material chip-out and fibre pull-out in Figure 6.14 was resulting from machining at fibre orientation greater than 90° but less than 180° which involved severe bending and compression of the laminates resulting in macro fracture and fibre pull-out [4, 8, 75, 77, 78].

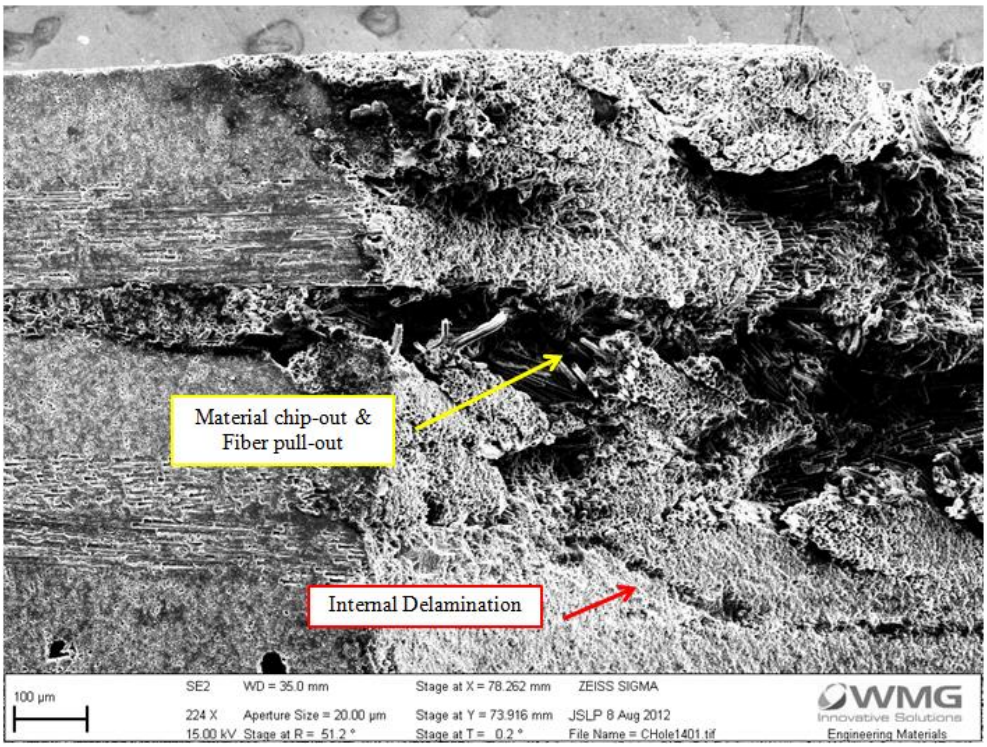

Figure 6.14: SEM image showing material chip-out, fibre pull-out and internal delamination on the machined surface produced from drilling of CFRP plaque with a pre-cooled tool

To evaluate drilling performance with respect to internal damage, values of total internal damage along the edge of drilled holes produced for the 1st hole and 325th hole when machined dry at room temperature and with a cryogenically cooled tool were compared. As previously described in Section 5.1.2.4, the drilled sample was cross-sectioned through the diameter of the hole and mounted in epoxy resin for examination under the optical microscope, refer to Figure 5.8. The total internal damage was determined by calculating the summation of the material chip-out and delamination along the edge of the hole. Results showing evaluation of the internal damage for the 1st hole and 325th hole of both drilling experiments are presented in Figure 6.15.

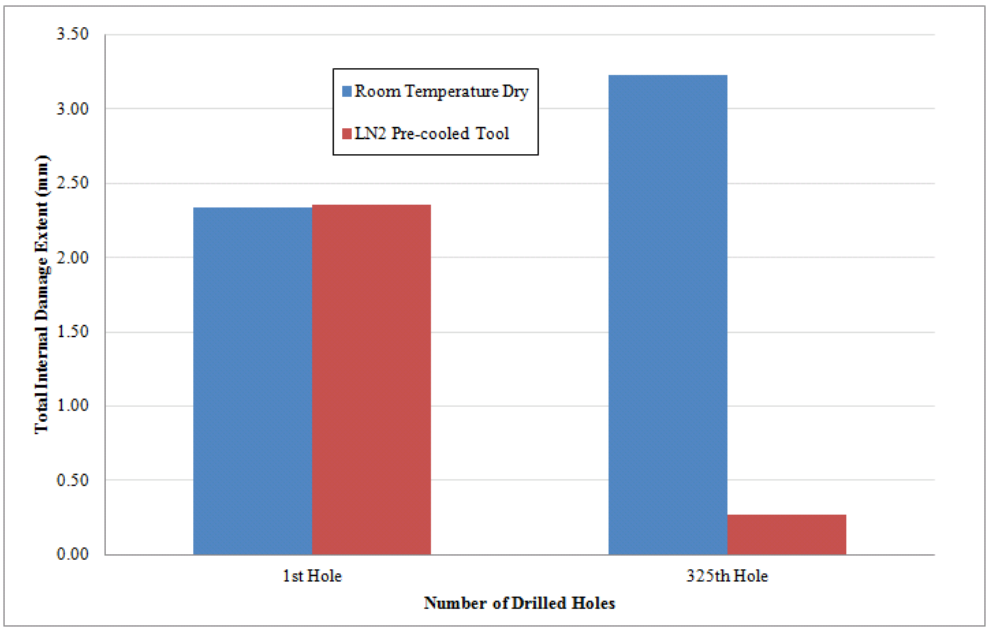

Figure 6.15: Total internal damage produced from drilling the 1st hole and 325th hole in CFRP plaque when machined dry at room temperature and with a tool pre-cooled in LN_2

It is shown in Figure 6.15 that a similar level of internal damage, of which the difference was 0.02 mm (1%), was observed for the 1st hole of cryogenic and room temperature dry drilling. However, for the 325th hole, cryogenic drilling produced significantly lower total internal damage compared to room temperature dry drilling. The total internal damage was reduced by 2.97 mm (92%) when drilling with cryogenic cooling compared to room temperature dry drilling. Referring to the methodology described in Chapter 5, the time of pre-cooling the tool in LN_2 was 10 s from the 1st to 10th drilling cycle, and was changed to 30 s from the 11th to 13th drilling cycle. Therefore, it is justified to state that cryogenic pre-cooling of the tool in LN_2 could improve the quality of the drilled holes by reducing internal damage provided that the pre-cooling time was sufficient. The results in Figure 6.15 indicate that the time of pre-cooling the tool by LN_2 for 10 s was not sufficient to provide the benefit of internal damage reduction in this case. The measured temperature after submerging the tool in LN_2 for 10 s was -22°C, while it was -70°C after submerging for 30 seconds. A reduction in internal damage by the application of cryogenic pre-cooling will be discussed in Section 6.4.

6.2 Evaluation of Drilling Performance of Carbon Fibre Reinforced Plastics when Using a CO_2 Cooling System

In this section, the evaluation of drilling performance of CFRPs when machined with a CO_2 cooling system, which will refer as "CO_2 drilling" in this research, will be discussed and compared with room temperature dry drilling. The performance evaluation will be based on results for thrust force, entry and exit delamination. The effect of cutting speed and feed rate will also be discussed. The methodology of the drilling trials and the evaluation of drilling performance in this section were previously described in Section 5.2. As mentioned in Section 5.2, drilling test with CO_2 cooling was carried out at constant volume flow rate of 3.37 l/min, for all machining conditions. Raw data of the results of drilling trials discussed in Section 6.2 is presented in Appendix B.

The plaques used for the drilling trial with CO_2 cooling in this section were manufactured from a different type of CFRP from those used for the drilling trial with cryogenic LN_2 cooling in Section 6.1. These CFRP plaques, which were aerospace-grade CFRPs supplied by BAE Systems, were autoclave-cured CFRP manufactured from uni-directional IM7 and woven AS4 carbon fibres reinforced in Hexply 8552 toughened epoxy matrix with copper mesh layer on the entry side of the plaque. The reason for changing the workpiece material to aerospace-grade CFRP was to demonstrate the effect of CO_2 cooling on drilling of actual material that will be used in aerospace industry.

6.2.1 Thrust Force

6.2.1.1 Effect of Feed Rate

Results showing variation of thrust force with feed rate for room temperature dry and CO_2 drilling are presented in Table 6.1 and Figures 6.16-6.19. The data in Table 6.1 is going to be used for discussion in this section. Similar to the drilling trial for the investigation of cryogenic cooling in Section 6.1, average and maximum values of thrust force were determined during the period between when the chisel edge and the main cutting edges engaged in the cutting to the moment when the main cutting edges penetrated through the last laminate of the plaque, refer to Figure 6.7.

Table 6.1: Variation of thrust force with feed rate for room temperature (RT) dry and CO_2 drilling of CFRP plaques at a cutting speed of 75, 100, 115, 130 and 150 m/min

Cutting Speed (m/min)	Feed Rate (mm/rev)	Avg. Thrust Force (N)		Max. Thrust Force (N)		Increase of Average Thrust Force (0.03-0.15 mm/rev)		Increase of Maximum Thrust Force (0.03-0.15 mm/rev)		Difference of Thrust Force (RT Dry/CO_2 Cooling)	
		RT Dry	CO_2 Cooling	RT Dry	CO_2 Cooling	RT Dry	CO_2 Cooling	RT Dry	CO_2 Cooling	Average Force	Maximum Force
75	0.03	69	76	81	89	55%	45%	53%	43%	9%	9%
75	0.06	84	90	97	103					7%	6%
75	0.09	94	97	108	110					3%	2%
75	0.12	102	105	116	120					3%	3%
75	0.15	108	110	125	127					2%	2%
100	0.03	68	79	83	97	59%	43%	57%	35%	15%	17%
100	0.06	86	90	103	104					4%	1%
100	0.09	94	99	111	114					5%	2%
100	0.12	104	106	121	124					2%	2%
100	0.15	109	112	129	131					3%	1%
115	0.03	70	73	81	85	55%	50%	59%	52%	5%	5%
115	0.06	88	88	102	102					1%	0%
115	0.09	95	97	113	113					2%	0%
115	0.12	103	104	122	122					1%	0%
115	0.15	109	110	129	129					1%	0%
130	0.03	72	74	84	86	55%	52%	57%	52%	3%	3%
130	0.06	88	90	103	103					2%	1%
130	0.09	98	100	115	117					2%	1%
130	0.12	105	107	124	125					2%	1%
130	0.15	112	113	131	132					1%	0%
150	0.03	76	84	88	97	55%	42%	56%	46%	12%	10%
150	0.06	92	98	106	110					6%	4%
150	0.09	103	106	119	121					3%	2%
150	0.12	110	114	128	131					3%	2%
150	0.15	117	120	137	141					2%	3%

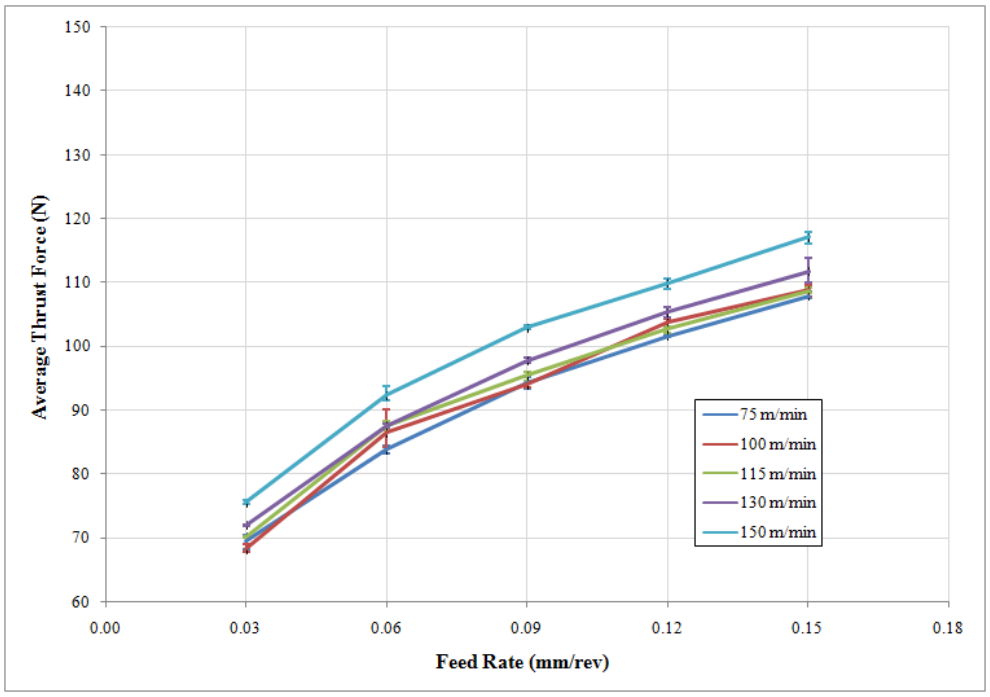

Figure 6.16: Variation of average thrust force with feed rate for room temperature dry drilling of CFRP plaques at a cutting speed of 75, 100, 115, 130 and 150 m/min

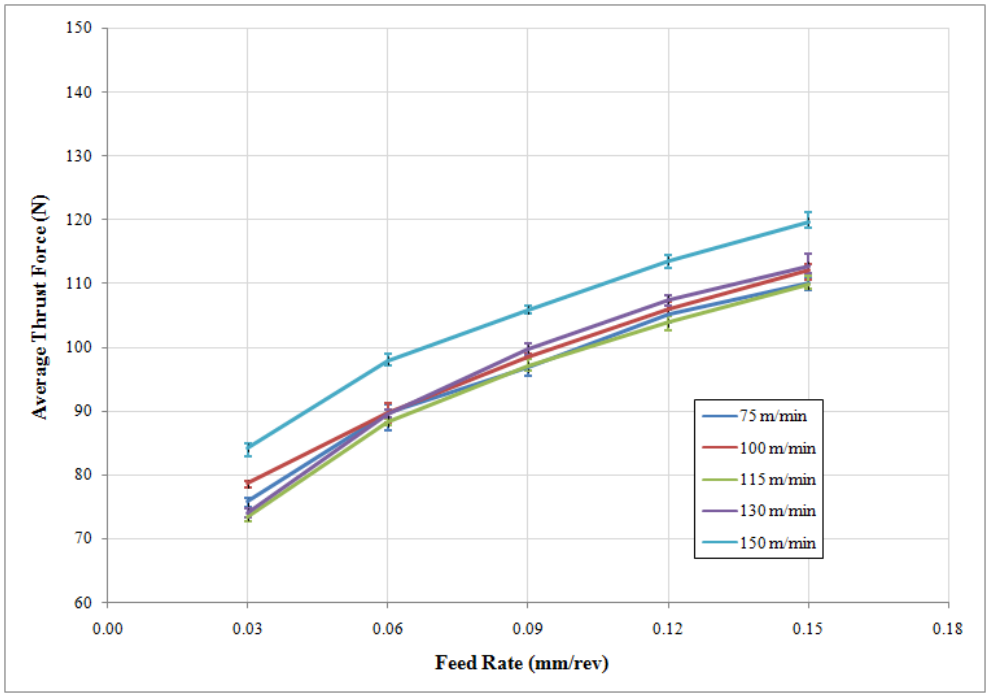

Figure 6.17: Variation of average thrust force with feed rate for drilling of CFRP plaques with CO_2 cooling at a cutting speed of 75, 100, 115, 130 and 150 m/min

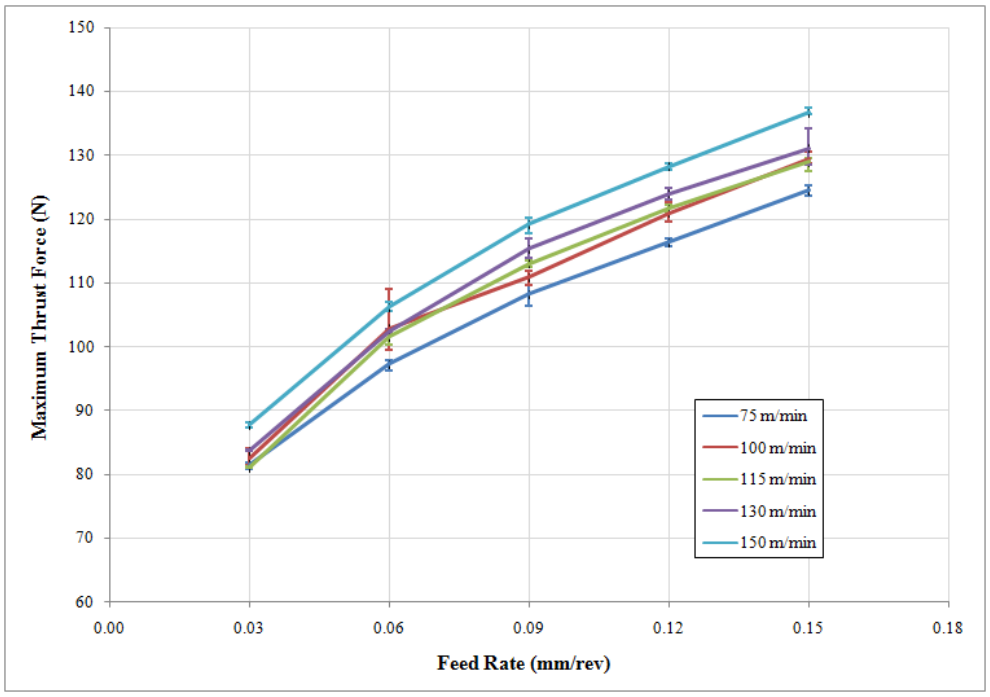

Figure 6.18: Variation of maximum thrust force with feed rate for room temperature dry drilling of CFRP plaques at a cutting speed of 75, 100, 115, 130 and 150 m/min

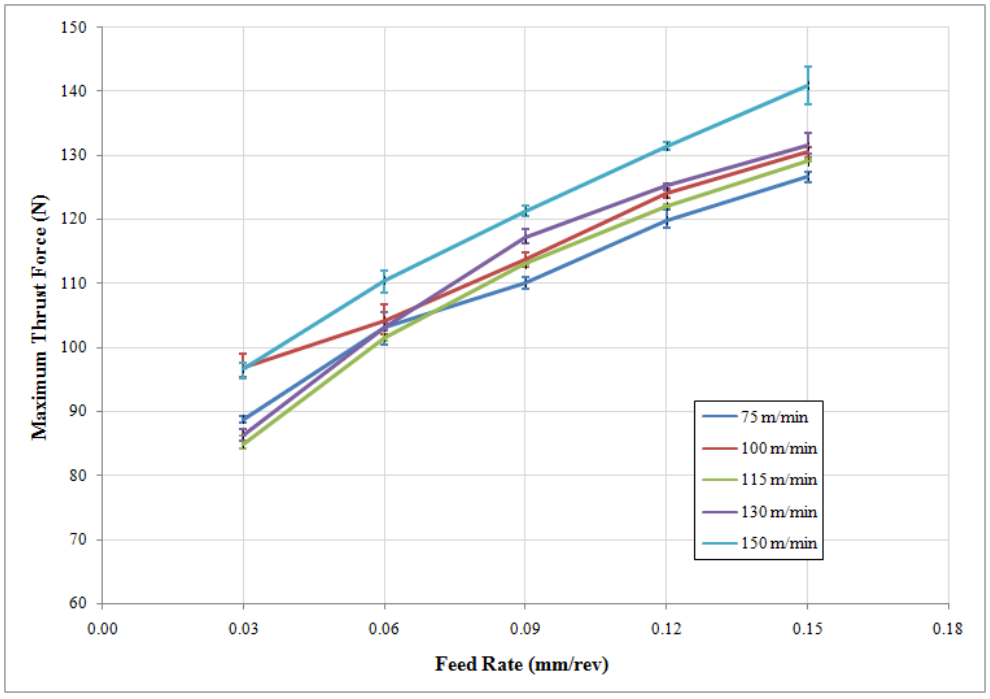

Figure 6.19: Variation of maximum thrust force with feed rate for drilling of CFRP plaques with CO_2 cooling at a cutting speed of 75, 100, 115, 130 and 150 m/min

In Figures 6.16 and 6.17, it is shown that average thrust force for room temperature dry and CO_2 drilling tended to increase as the feed rate was increased for all cutting speeds. The increase in average thrust force as the feed rate was increased from 0.03 to 0.15 mm/rev was in the range 55-59% for room temperature dry drilling and 42-52% for CO_2 drilling.

Similarly, it is shown in Figures 6.18 and 6.19 that maximum thrust force tended to increase as the feed rate was increased for all cutting speeds. The increase in maximum thrust force for room temperature dry drilling as the feed rate was increased from 0.03 to 0.15 mm/rev was it was in the range 53-59% and it was in the range 35-52% for CO_2 drilling. This trend of the results showing an increase in thrust force with increasing feed rate has also been reported by other researchers [16, 24, 63, 84, 96, 97, 99]. This was due to the amount of material to be cut per revolution of the drill increases as the feed rate was increased [16, 24, 79].

To consider the effect of CO_2 cooling on thrust force at various feed rates, the results of average and maximum thrust forces for room temperature dry and CO_2 drilling were compared, refer to Table 6.1 from which data will be used for the following discussion. Comparison of variation of average and maximum thrust force with feed rate for room temperature dry and CO_2 drilling at cutting speeds of 75-150 m/min is presented in Figures 6.20-6.24. It is shown in Figures 6.20-6.24 that CO_2 drilling produced higher average and maximum thrust forces compared to room temperature dry drilling at the lowest feed rate (0.03 mm/rev) for all cutting speeds. The difference between thrust forces for the two drilling tests at a feed rate of 0.03 mm/rev and cutting speeds of 75, 100 and 150 m/min was 9-17%. However it was 3-5% at cutting speeds of 115 and 130 m/min, which was less significant when compared to at cutting speeds of 75, 100 and 150 m/min. This difference between thrust forces for the two drilling tests at cutting speeds of 115 and 130 m/min would be considered a significant difference because it is greater than variability range in measurements (maximum value of 2%) at these cutting speeds and feed rate. As feed rate was increased to 0.06 mm/rev, the difference between thrust forces was reduced to 4-7% at cutting speeds of 75 and 150 m/min, but it was only 1-4% at a cutting speed of 100 m/min and 0-2% at cutting speeds of 115 and 130 m/min. Finally, the difference between thrust forces was reduced to within 3% as feed rate was increase from 0.06 to 0.15 mm/rev for all cutting speeds, which is within variability in measurements at a feed rate of 0.15 mm/rev (maximum value of 3.5%), resulting in a similar level of thrust forces for room temperature dry and CO_2 drilling as the feed rate was increased as can be seen in Figures 6.20-6.24. The reason for higher thrust force produced by CO_2 cooling compared to room temperature dry drilling will be discussed in Section 6.4.

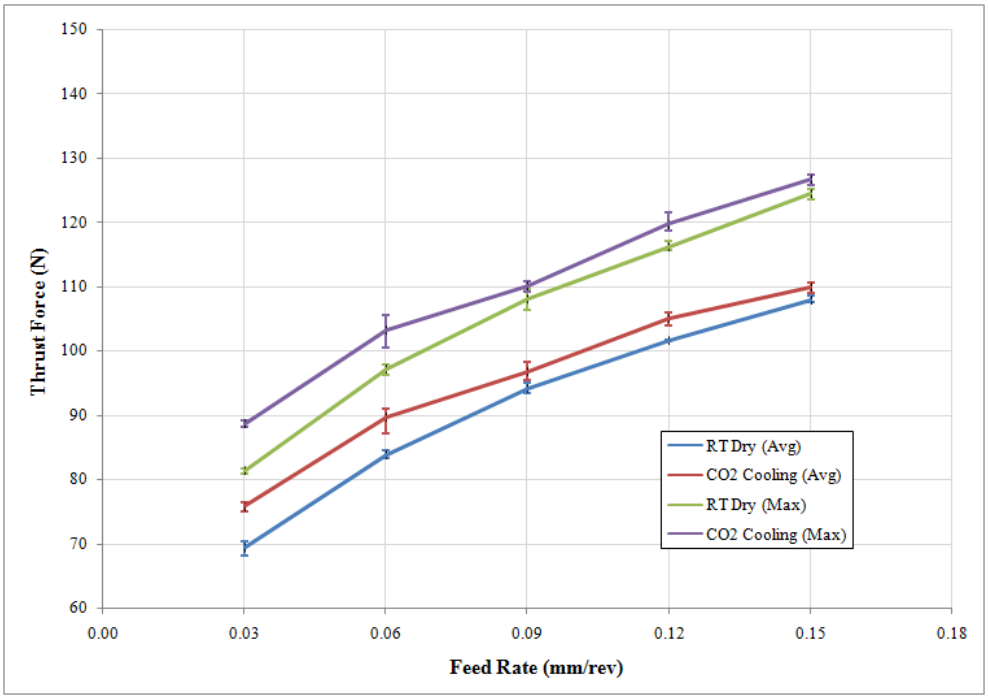

Figure 6.20: Comparison of average and maximum thrust force for room temperature (RT) dry and CO_2 drilling of CFRP plaques at a cutting speed of 75 m/min

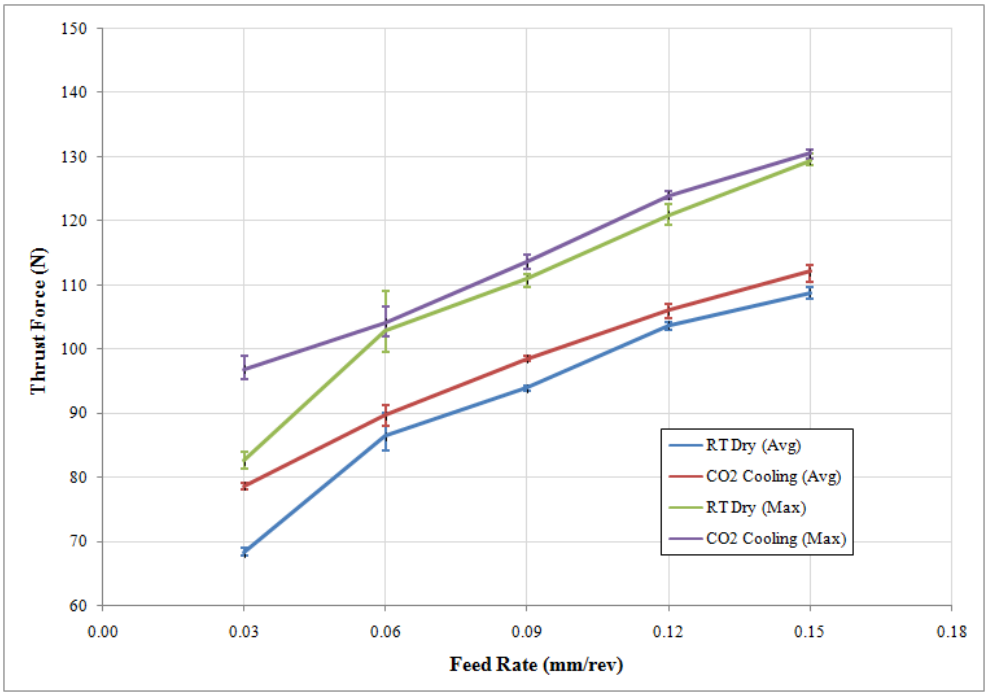

Figure 6.21: Comparison of average and maximum thrust force for room temperature (RT) dry and CO_2 drilling of CFRP plaques at a cutting speed of 100 m/min

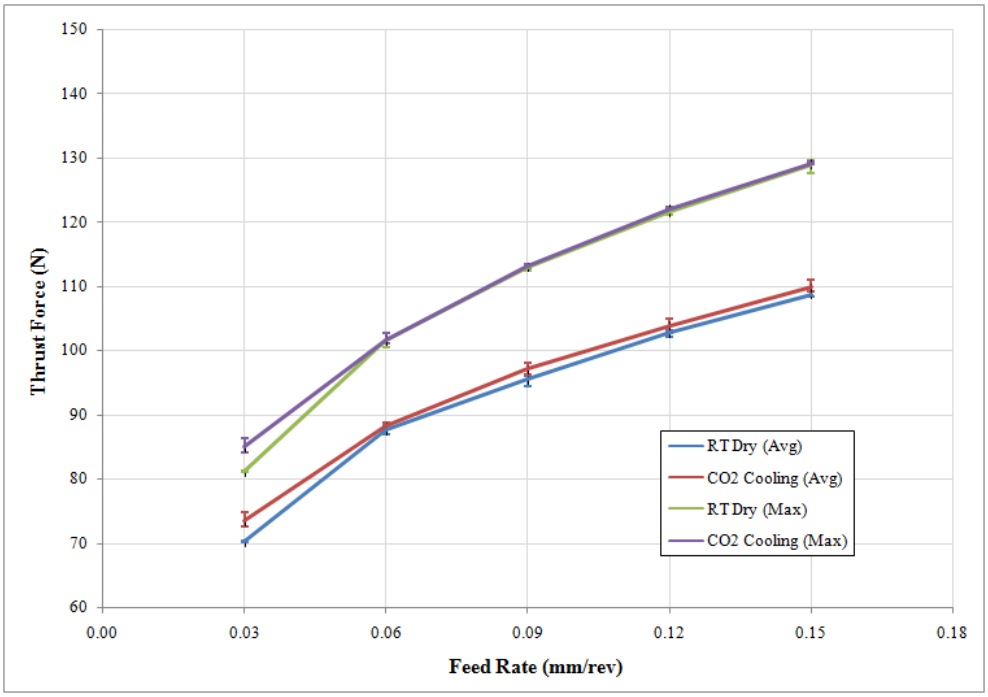

Figure 6.22: Comparison of average and maximum thrust force for room temperature (RT) dry and CO_2 drilling of CFRP plaques at a cutting speed of 115 m/min

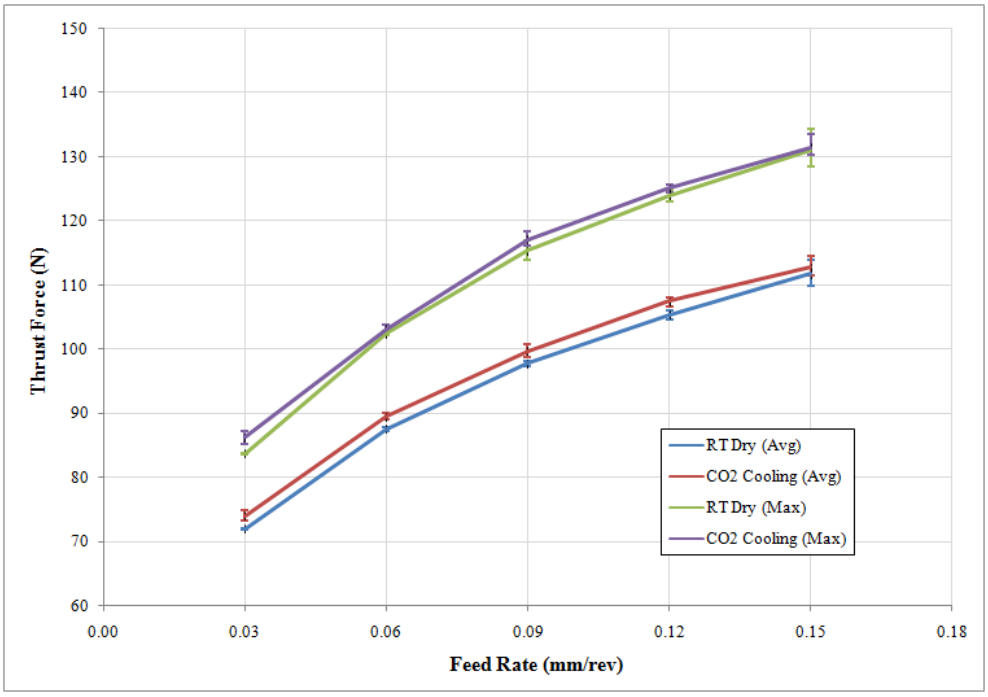

Figure 6.23: Comparison of average and maximum thrust force for room temperature (RT) dry and CO_2 drilling of CFRP plaques at a cutting speed of 130 m/min

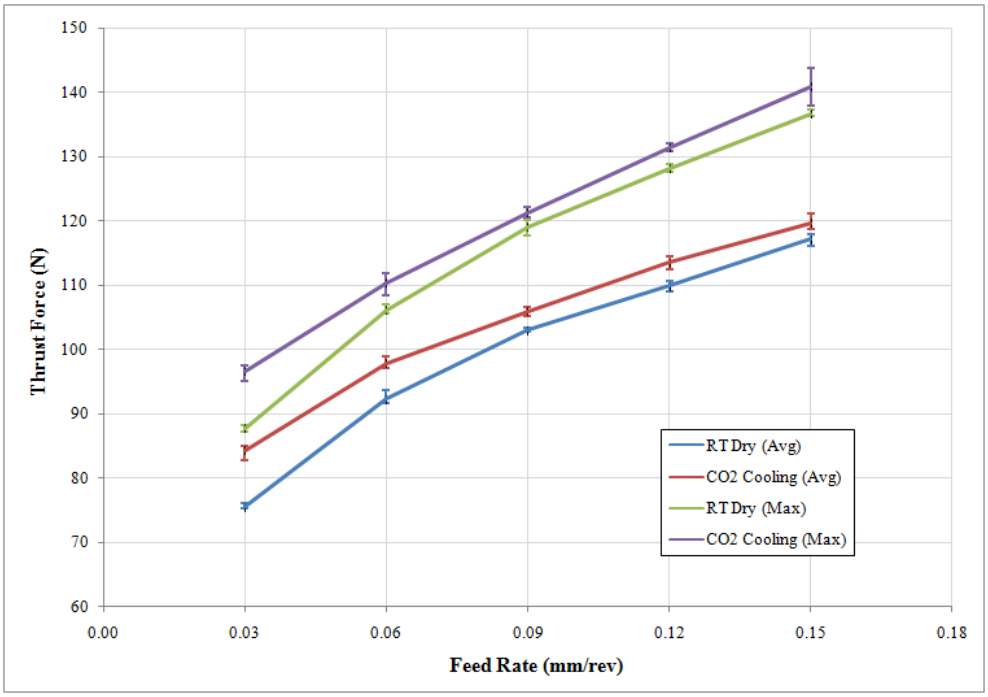

Figure 6.24: Comparison of average and maximum thrust force for room temperature (RT) dry and CO_2 drilling of CFRP plaques at a cutting speed of 150 m/min

From the results in Table 6.1 and Figures 6.20-6.24, it can be inferred that, in this research, the effect of CO_2 cooling on the increase in thrust force compared to room temperature dry drilling was more significant at low feed rates (0.03-0.06 mm/rev). As feed rate was increased, this effect was less significant, finally resulting in similar level of thrust forces being produced for CO_2 and room temperature dry drilling at high feed rate (0.09-0.15 mm/rev). It is proposed that this was because cooling ability by the CO_2 cooling system was reduced as feed rate increased due to more heat generated and shorter drilling time. As feed rate was increased, more heat would be generated in the cutting zone due to the greater quantity of material being deformed per revolution of the drill and the fact that time for drilling through the plaque was reduced. As drilling time was reduced, the amount of CO_2 directed into the cutting area also reduced, resulting in less cooling ability. As a consequence of less cooling ability and more heat generated, effect of CO_2 cooling on the increase in thrust force was less significant at higher feed rates. At lower feed rates, the amount of CO_2 directed into the area would increase because of the longer drilling time. Also, less heat would be generated in the cutting zone due to less amount of material to be deformed. Due to greater cooling ability and less heat generated, the effect of the CO_2 cooling on the increase in thrust force was more significant at lower feed rates. The reduction in cooling effect of CO_2 cooling as feed rate increased will be shown by the investigation of fracture behaviour of the epoxy matrix discussed in Section 7.2.1.1.

6.2.1.2 Effect of Cutting Speed

In this section, the data in Table 6.1 is re-presented to determine the effect of cutting speed on thrust force for room temperature dry and CO_2 drilling. Results showing variation of thrust force with cutting speed for room temperature dry and CO_2 drilling are presented in Table 6.2 and Figures 6.25-6.28. The data in Table 6.2 will be used for discussion in this section.

Table 6.2: Variation of thrust force with cutting speed for room temperature (RT) dry and CO_2 drilling of CFRP plaques at feed rates of 0.03, 0.06, 0.09, 0.12 and 0.15 mm/rev

Feed Rate (mm/rev)	Cutting Speed (m/min)	Avg. Thrust Force (N)		Max. Thrust Force (N)		Increase of Average Thrust Force (75-150 m/min)		Increase of Maximum Thrust Force (75-150 m/min)		Difference of Thrust Force (RT Dry/CO_2 Cooling)	
		RT Dry	CO_2 Cooling	RT Dry	CO_2 Cooling	RT Dry	CO_2 Cooling	RT Dry	CO_2 Cooling	Average Force	Maximum Force
0.03	75	69	76	81	89	9%	11%	8%	9%	9%	9%
0.03	100	68	79	83	97					15%	17%
0.03	115	70	73	81	85					5%	5%
0.03	130	72	74	84	86					3%	3%
0.03	150	76	84	88	97					12%	10%
0.06	75	84	90	97	103	10%	9%	9%	7%	7%	6%
0.06	100	86	90	103	104					4%	1%
0.06	115	88	88	102	102					1%	0%
0.06	130	88	90	103	103					2%	1%
0.06	150	92	98	106	110					6%	4%
0.09	75	94	97	108	110	9%	9%	10%	10%	3%	2%
0.09	100	94	99	111	114					5%	2%
0.09	115	95	97	113	113					2%	0%
0.09	130	98	100	115	117					2%	1%
0.09	150	103	106	119	121					3%	2%
0.12	75	102	105	116	120	8%	8%	10%	10%	3%	3%
0.12	100	104	106	121	124					2%	2%
0.12	115	103	104	122	122					1%	0%
0.12	130	105	107	124	125					2%	1%
0.12	150	110	114	128	131					3%	2%
0.15	75	108	110	125	127	9%	9%	10%	11%	2%	2%
0.15	100	109	112	129	131					3%	1%
0.15	115	109	110	129	129					1%	0%
0.15	130	112	113	131	132					1%	0%
0.15	150	117	120	137	141					2%	3%

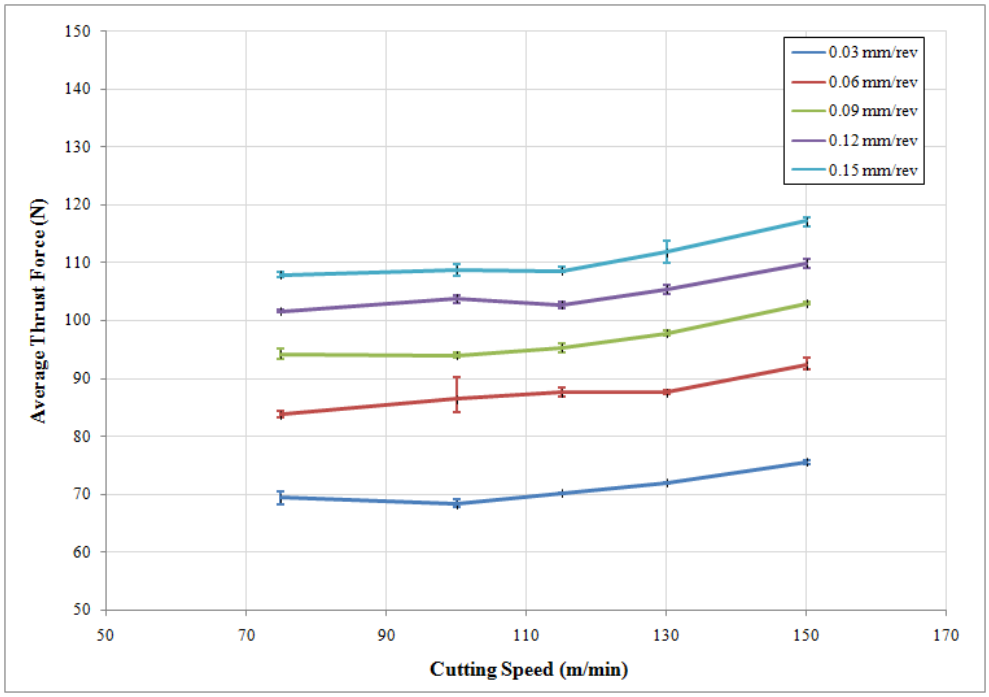

Figure 6.25: Variation of average thrust force with cutting speed for room temperature dry drilling of CFRP plaques at a feed rates of 0.03, 0.06, 0.09, 0.12, 0.15 mm/rev

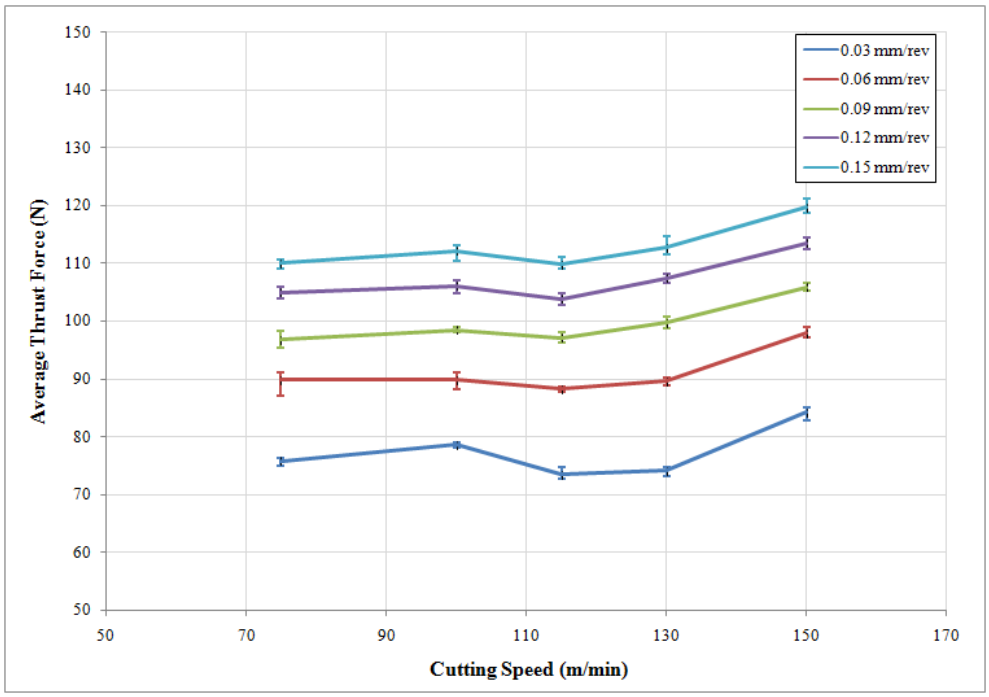

Figure 6.26: Variation of average thrust force with cutting speed for CO_2 drilling of CFRP plaques at a feed rates of 0.03, 0.06, 0.09, 0.12, 0.15 mm/rev

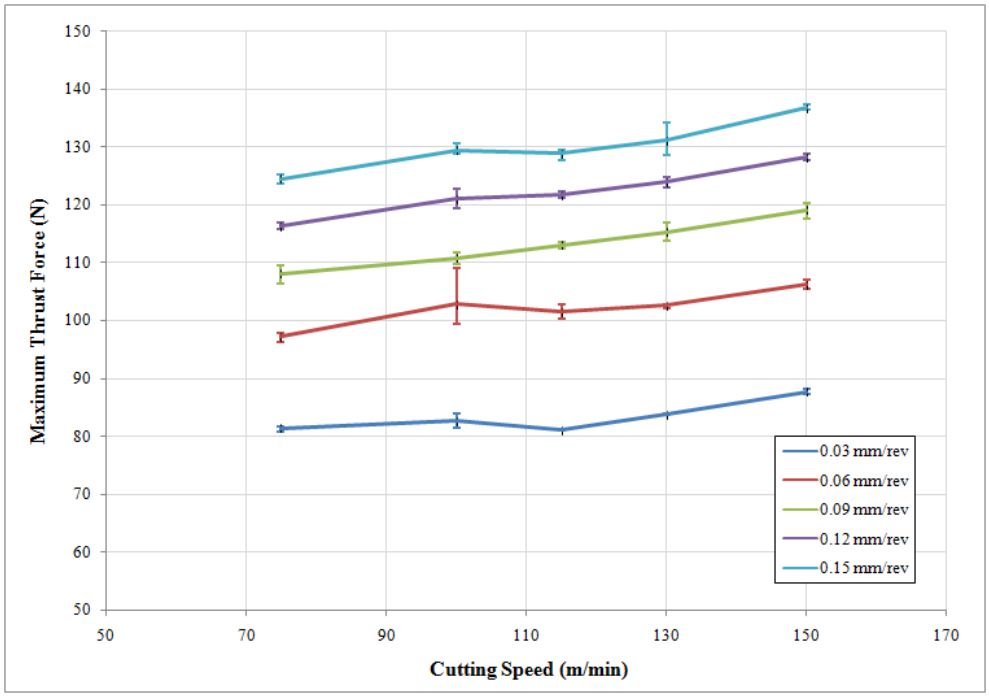

Figure 6.27: Variation of maximum thrust force with cutting speed for room temperature dry drilling of CFRP plaques at a feed rates of 0.03, 0.06, 0.09, 0.12, 0.15 mm/rev

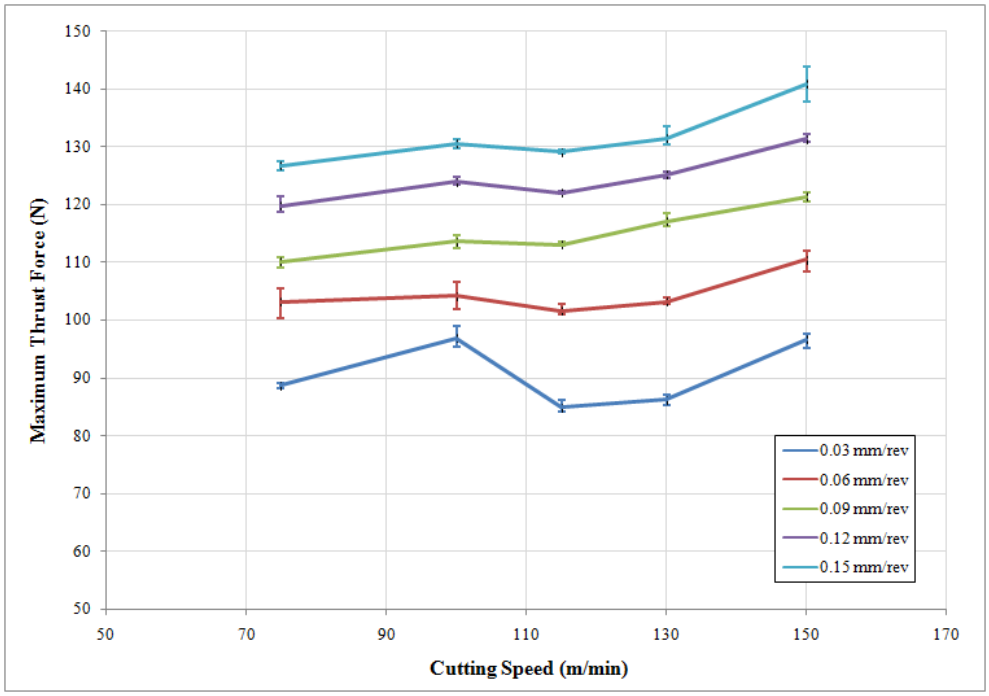

Figure 6.28: Variation of maximum thrust force with cutting speed for CO_2 drilling of CFRP plaques at a feed rates of 0.03, 0.06, 0.09, 0.12, 0.15 mm/rev

In Figures 6.25-6.28, it is shown that average and maximum thrust forces for room temperature dry and CO_2 drilling tended to increase slightly as cutting speed was increased from 75 to 150 m/min. The increase in average thrust force for room temperature dry drilling was in the range 8-10% and it was in the range 8-11% for CO_2 drilling. The increase of

maximum thrust force was in the range 8-10% and 7-11% for room temperature dry and CO_2 drilling respectively. The results in Table 6.2 and Figures 6.25-6.28 indicate that the influence of cutting speed on variations in thrust force (7-11% increase) was less significant than that of feed rate (28-59% increase). It has been reported by other researchers that thrust force in drilling CFRPs decreased as cutting speed was increased as a result of the increase in cutting heat with increasing cutting speed which caused thermal softening of the polymer in CFRPs [94, 95, 101, 103, 104]. However, it is suggested that thermal softening of epoxy with increasing cutting speed would not significantly affect the variation in thrust force because the accumulated cutting and frictional heat would not be sufficient when drilling thin plaques. In this instance, it is shown that thrust force tended to increase with increasing cutting speed, which has also been reported by other researchers [15, 99]. It was suggested by Lin and Chen [15] that the increase in thrust force with increasing cutting speed was due to progressive wear of the tool as cutting speed was increased. However, it is suggested that the increase in thrust force in the work reported here was not due to the increase of tool wear with cutting speed because the range of cutting speeds used in drilling trial in this section was lower than that used in the work of Lin and Chen (210-850 m/min for a 7 mm diameter drill) [15]. For this reason, the increase in thrust force in the work reported here would be because of the increase in material to be cut at a given time as cutting speed increased resulting in higher thrust force required.

The results of the thrust force for room temperature dry and CO_2 drilling were compared in order to consider the effect of CO_2 cooling on thrust force at various cutting speeds, Table 6.2 and Figures 6.29-6.33. Data from Table 6.2 and Figures 6.29-6.33 is going to be used for the following discussion. It is shown that CO_2 drilling produced 6-9% higher average and maximum values of thrust force at a cutting speed of 75 m/min with range of low feed rates (0.03-0.06 mm/rev). At a cutting speed of 100 m/min, CO_2 drilling produced higher average and maximum thrust forces by 15% and 17% respectively compared to room temperature dry drilling at a feed rate of 0.03 mm/rev. For feed rates of 0.03-0.06 mm/rev, this effect of CO_2 cooling on the increase in thrust force compared to room temperature dry drilling was reduced becoming less significant (within 5%) as cutting speed was increased from 100 to 130 m/min. However, this difference between thrust forces for the two drilling tests increased to 10-12% and 6-4% at a feed rate of 0.03 and 0.06 mm/rev respectively as cutting speed was increased from 130 to 150 m/min. At higher feed rates (0.09-0.15 mm/rev), the difference between thrust forces for CO_2 and room temperature dry drilling was less significant (within 5%) when compared to that at lower feed rates (0.03-0.06 mm/rev) for all cutting speeds.

From the results in Table 6.2 and Figures 6.29-6.33, it can be inferred that the effect of CO_2 cooling on the increase in thrust force as compared to room temperature dry drilling was more significant at lower cutting speeds (75 and 100 m/min) and lower feed rates (0.03 and 0.06 mm/rev) and became less significant at higher cutting speeds (115-150 m/min) and feed rates (0.09-0.15 mm/rev). Similar to the effect of feed rate that had been discussed in Section 6.2.1.1, it is proposed that this was because of reduced cooling ability of the CO_2 cooling system with increasing cutting speed as a result of more heat being generated combined with a shorter drilling time. As cutting speed was increased, more heat would be generated as more material was deformed in a given period of time. Drilling time was also reduced with an increase in cutting speed resulting in fewer amount of CO_2 directed into the cutting zone hence less cooling ability. Due to reduced cooling ability and more heat generated, effect of the CO_2 cooling on the increase in thrust force was less significant at higher cutting speeds. At lower cutting speeds, less heat was generated due to less material deformed in a given period of time and cooling ability of CO_2 cooling was higher due to greater amount of CO_2 supply to the cutting zone in longer drilling time. Therefore, the effect of CO_2 cooling on the increase in thrust force was more significant. The reduced cooling effect of CO_2 cooling at higher cutting speeds will be shown by the investigation of behaviour of the epoxy matrix discussed in Section 7.2.1.2.

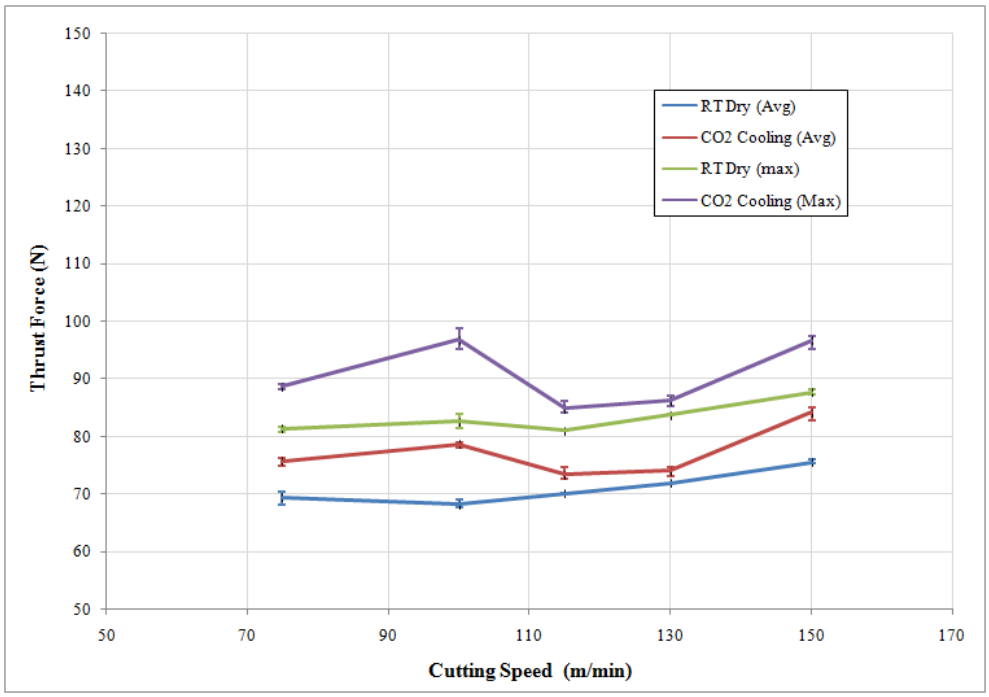

Figure 6.29: Comparison of average and maximum thrust force for room temperature (RT) dry and CO_2 drilling of CFRP plaques at a feed rate of 0.03 mm/rev

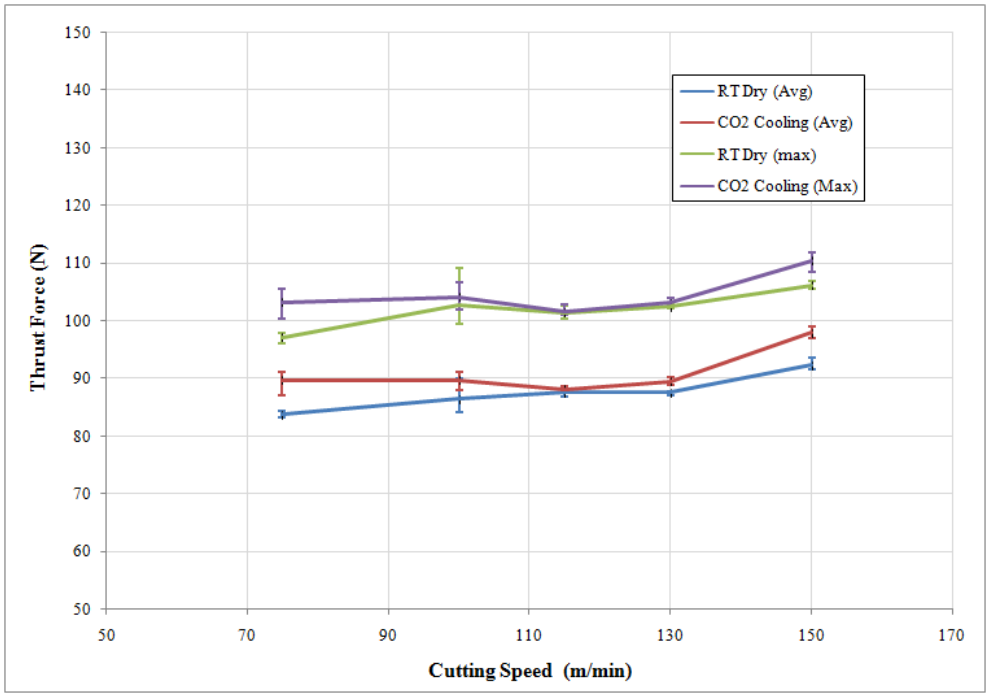

Figure 6.30: Comparison of average and maximum thrust force for room temperature (RT) dry and CO_2 drilling of CFRP plaques at a feed rate of 0.06 mm/rev

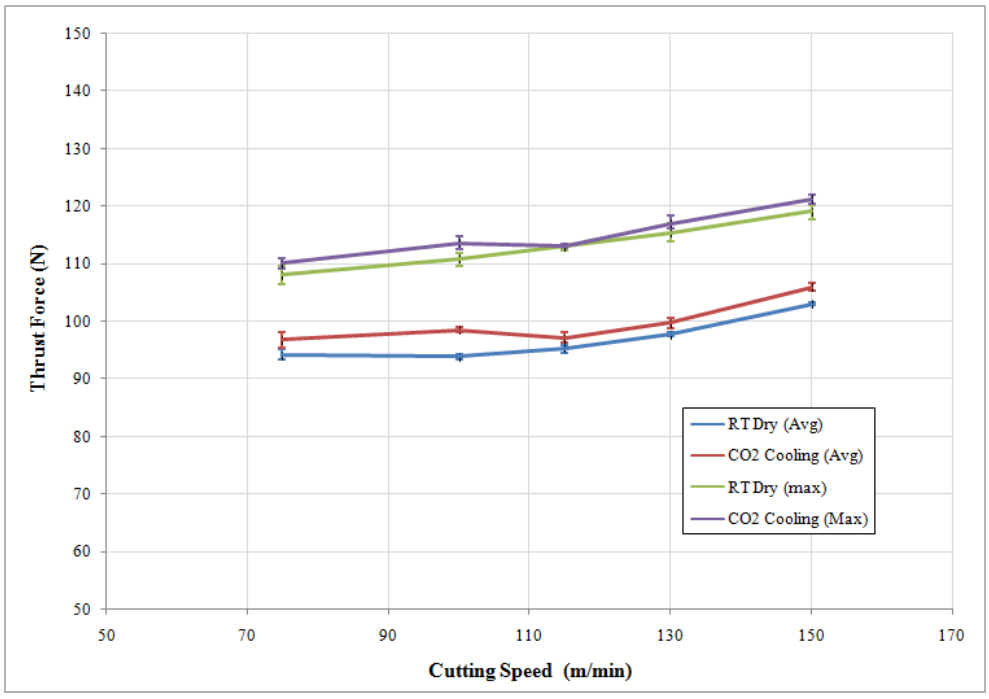

Figure 6.31: Comparison of average and maximum thrust force for room temperature (RT) dry and CO_2 drilling of CFRP plaques at a feed rate of 0.09 mm/rev

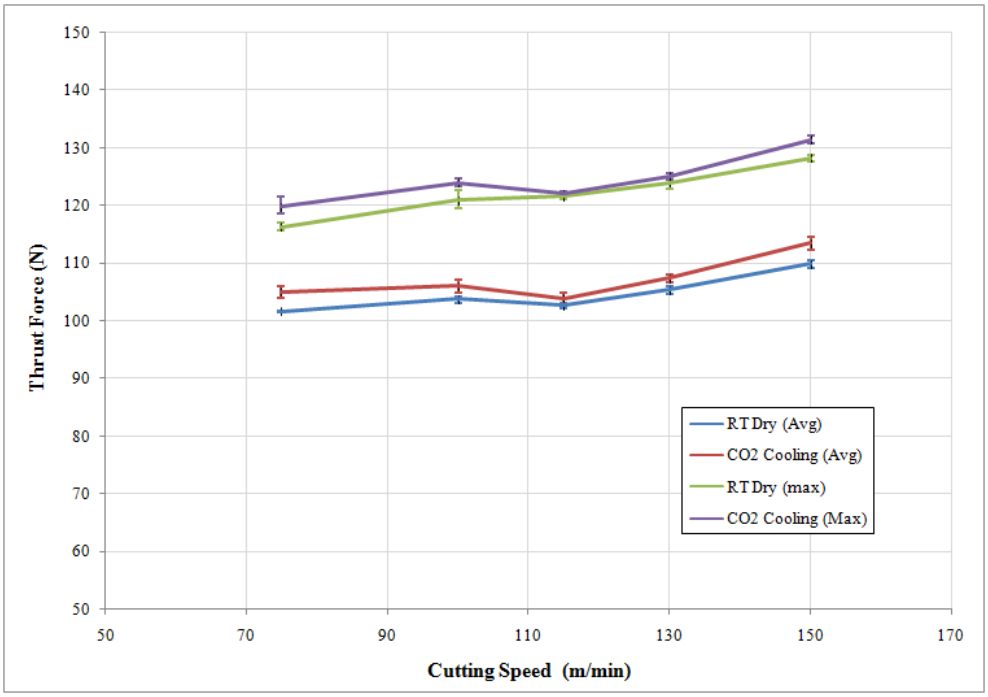

Figure 6.32: Comparison of average and maximum thrust force for room temperature (RT) dry and CO_2 drilling of CFRP plaques at a feed rate of 0.12 mm/rev

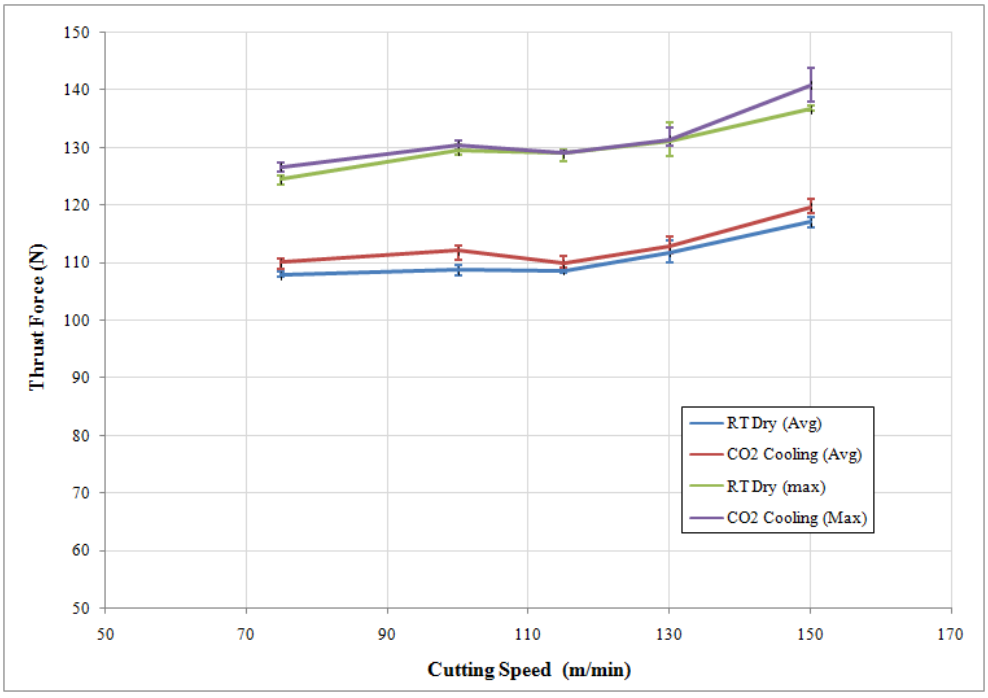

Figure 6.33: Comparison of average and maximum thrust force for room temperature (RT) dry and CO_2 drilling of CFRP plaques at a feed rate of 0.15 mm/rev

6.2.2 Entry Delamination

There was no significant delamination damage observed from the visual inspection using low magnification optical microscope at the entry compared to at the exit for room temperature dry or CO_2 drilling, Figure 6.34. Therefore, the entry delamination damage could not be quantified by visual inspection using the optical microscope analysis.

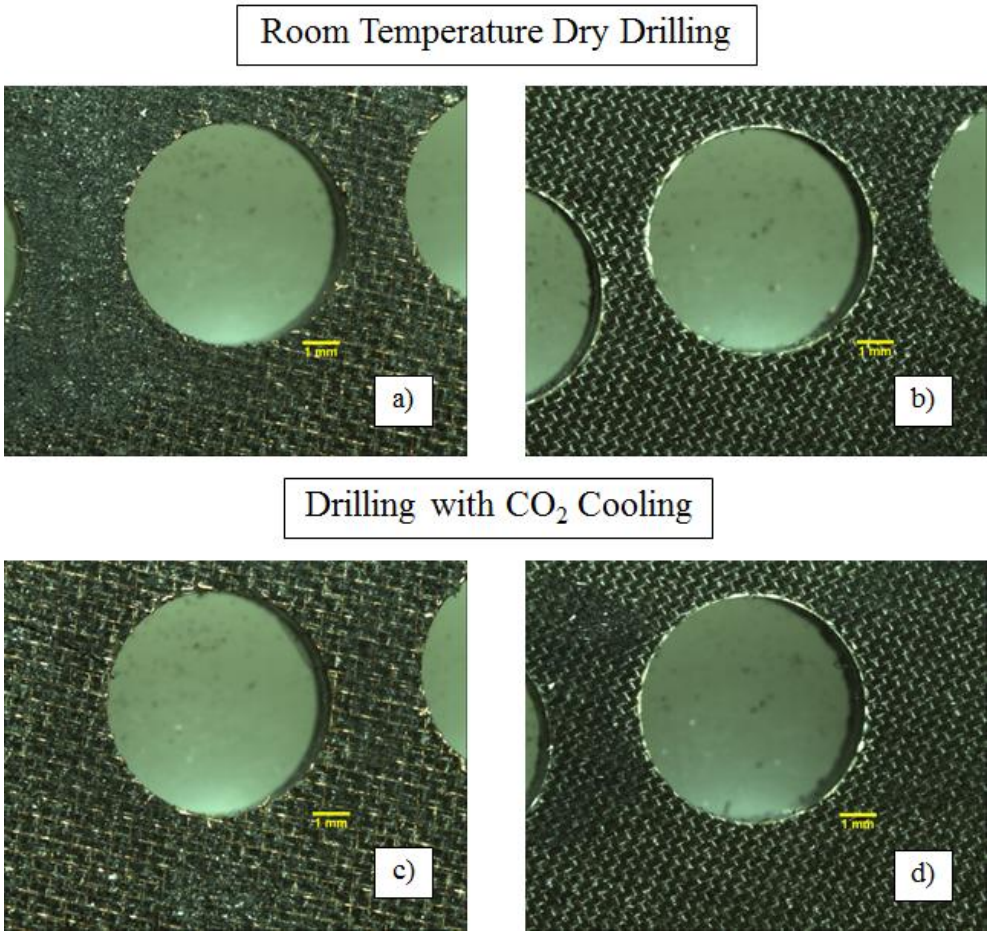

Figure 6.34: Optical microscope images showing entry ((a) and (c)) and exit ((b) and (d)) after drilling dry at room temperature ((a) and (b)) and with CO_2 cooling ((C) and (d)) at a cutting speed of 100 m/min and a feed rate of 0.06 mm/rev

6.2.3 Exit Delamination

6.2.3.1 Effect of Feed Rate

Results showing variation of total delamination area (A_{del}) at exit of the plaque with feed rate for room temperature dry and CO_2 drilling are presented in Table 6.3 and Figures 6.35 and 6.36. Data that will be used for discussion in this section is from Table 6.3. It can be seen in Figures 6.35 and 6.36 that variability in the measurements of total

delamination area is higher than variability in the measurements of thrust force, which is shown in Figures 6.16-6.33. Variability in the measurements of total delamination area was in the range 2.5-62.7%, while variability in the measurements of thrust force was in the range 0.3-9.3%. It is proposed that high variation in the measurements of delamination area was attributed to anisotropic nature of CFRPs, which could cause variations in delamination damage being produced for different drilling trial, plus variations due to dependence on contrast and visibility of damage in microscopic examination.

Table 6.3: Variation of total delamination area (A_{del}) at the exit with feed rate produced by room temperature (RT) dry and CO_2 drilling of CFRP plaques at cutting speeds of 75, 100, 115, 130 and 150 m/min

Cutting Speed (m/min)	Feed Rate (mm/rev)	Total A_{del} (mm²)		Increase of Total A_{del} (0.03-0.15 mm/rev)		Reduction of Total A_{del}
		RT Dry	CO_2 Cooling	RT Dry	CO_2 Cooling	RT Dry/CO_2 Cooling
75	0.03	1.49	1.25	52%	17%	16%
75	0.06	1.63	1.40			14%
75	0.09	1.69	1.44			15%
75	0.12	2.15	1.48			31%
75	0.15	2.27	1.46			36%
100	0.03	2.02	1.60	27%	54%	21%
100	0.06	2.06	1.92			7%
100	0.09	2.23	2.05			8%
100	0.12	2.41	2.26			6%
100	0.15	2.56	2.46			4%
115	0.03	2.11	1.87	20%	31%	11%
115	0.06	2.19	2.11			4%
115	0.09	2.32	2.21			5%
115	0.12	2.49	2.39			4%
115	0.15	2.53	2.45			3%
130	0.03	2.21	1.94	16%	28%	12%
130	0.06	2.39	2.23			7%
130	0.09	2.48	2.35			5%
130	0.12	2.52	2.40			5%
130	0.15	2.56	2.48			3%
150	0.03	2.27	1.97	9%	11%	14%
150	0.06	2.41	2.23			7%
150	0.09	2.58	2.39			7%
150	0.12	2.68	2.45			8%
150	0.15	2.48	2.18			12%

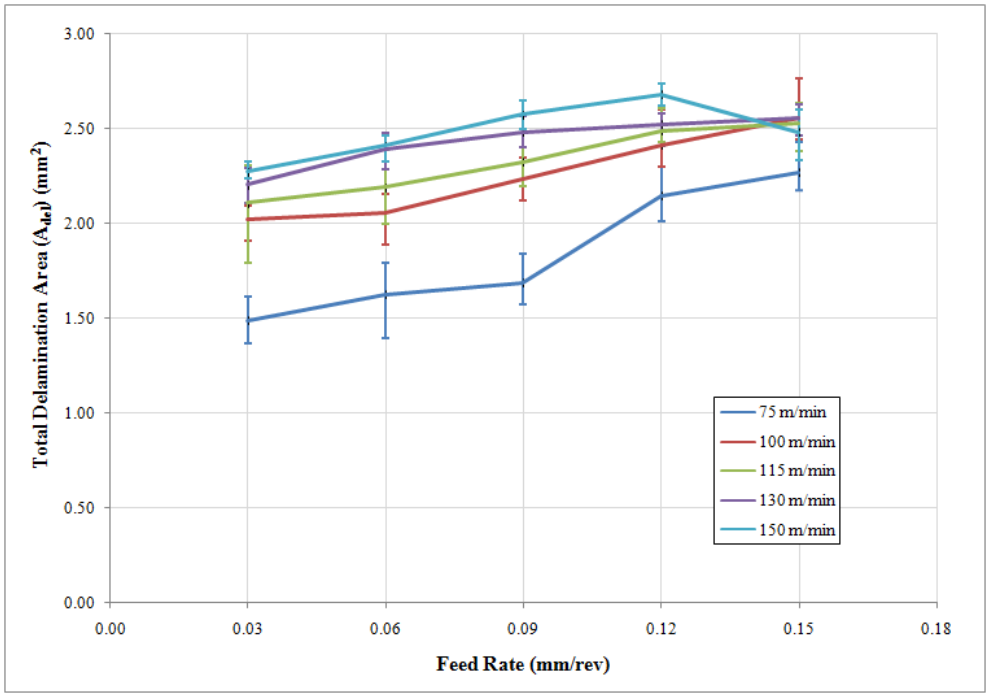

Figure 6.35: Variations of total delamination area (A_{del}) at the exit with feed rate produced from room temperature dry drilling of CFRP plaques at cutting speeds of 75, 100, 115, 130 and 150 m/min

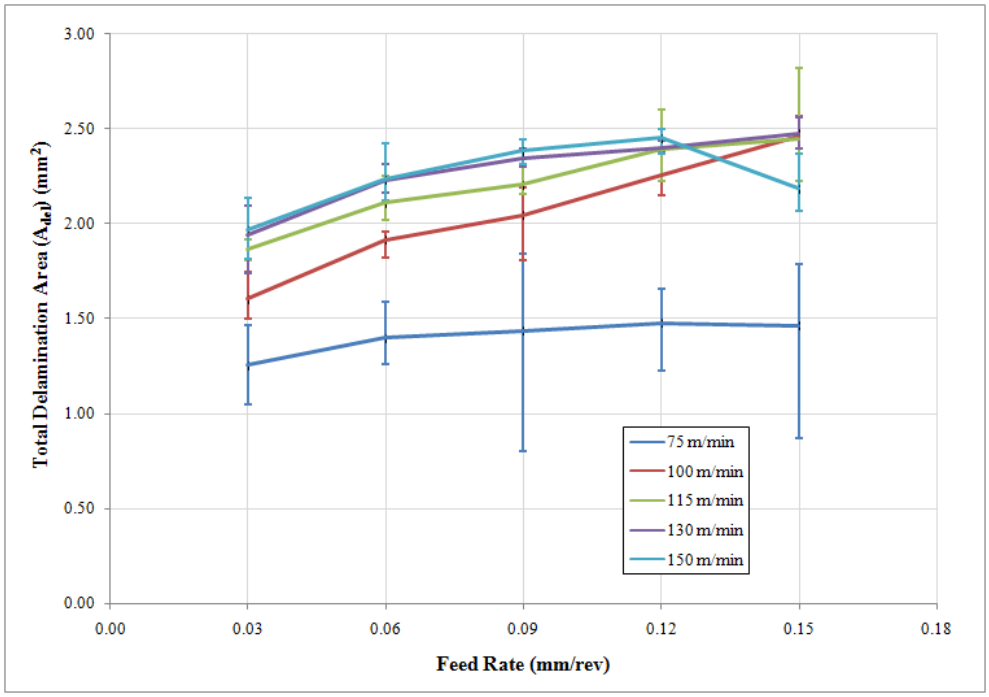

Figure 6.36: Variation of total delamination area (A_{del}) at the exit with feed rate produced from CO_2 drilling of CFRP plaques at cutting speeds of 75, 100, 115, 130 and 150 m/min

It is shown in Figures 6.35 and 6.36 that exit A_{del} for room temperature dry and CO_2 drilling tended to increase as feed rate was increased from 0.03 to 0.15 mm/rev for all cutting speeds. The increase in delamination damage as feed rate was increased was due to

the increase in thrust force with increased feed rate, which has been reported by other researchers [19, 20, 89, 107]. For room temperature dry drilling, the increase in exit A_{del} as feed rate was increased from 0.03 to 0.15 mm/rev was highest at the lowest cutting speed for which exit A_{del} increased by 52% at a cutting speed of 75 m/min. As cutting speed was increased, the increase in exit A_{del} reduced to 27%, 20%, 16% and 9% at a cutting speed of 100, 115, 130 and 150 m/min respectively. This indicates that the effect of feed rate on the variations of exit A_{del} for room temperature dry drilling was less dominant as cutting speed increased. This would be because, at higher cutting speeds, the effect of cutting heat on a reduction of resistance to delamination of the plaque was more dominant than the effect of the increase in thrust force due to increasing feed rate, which would increase size of delamination. However, for CO_2 drilling, the increase in exit A_{del} was only 17% at a cutting speed of 75 m/min, which was much lower than at a cutting speed of 100 m/min (54%). The author suggests that this was because the amount of CO_2 supplied to the cutting area increased due to a longer drilling time at low cutting speed and was sufficient to show the benefit of CO_2 cooling in removing the cutting heat generated process. The removal of cutting heat by CO_2 cooling is proposed to result in an increase in resistance to delamination due to a reduction in cutting temperature, which will be discussed later in Section 6.4. Due to sufficient amount of CO_2 and less heat being generated at low cutting speed, CO_2 cooling could effectively remove heat from the cutting zone resulting in lower increase rate of exit A_{del} as resistance to delamination could be effectively maintained at a higher level. As cutting speed increased, greater amount of heat was generated, which would reduce resistance to delamination due to an increase in cutting temperature. Combined with the increase in thrust force with increasing feed rate, this resulted in greater increase in exit A_{del} as feed rate was increased from 0.03 to 0.15 mm/rev at cutting speed of 100 m/min (54%) compared to at a cutting speed of 75 m/min (17%). Similar to room temperature dry drilling, the increase in exit A_{del} as feed rate was increased from 0.03 to 0.15 mm/rev reduced as cutting speed was increased, for which it reduced to 31%, 28% and 11% at a cutting speed 115, 130 and 150 m/min respectively. Similarly, this indicates that the effect of feed rate on the variations of exit A_{del} for CO_2 drilling was also becoming less significant as cutting speed was increased as occurred for room temperature dry drilling, which is proposed to be because of the same reason.

Considering the effect of CO_2 cooling on exit A_{del} with changing feed rate, the results of exit A_{del} for CO_2 drilling at various feed rates were compared with room temperature dry drilling, Table 6.3 and Figures 6.37-6.41. It is shown in Figures 6.27 and 6.28 that less exit A_{del} was produced for CO_2 drilling compared to room temperature dry drilling for all cutting speeds and feed rates. It is shown in Figures 6.38-6.41 that the highest percentage reduction

of exit A_{del} with the use of CO_2 cooling for cutting speeds 100, 115, 130 and 150 m/min could be observed at the lowest feed rate (0.03 mm/rev). The percentage reduction at a feed rate of 0.03 mm/rev for cutting speeds of 100-150 m/min was in the range 11-21%. As feed rate was increased, the percentage reduction of the exit A_{del} decreased and it was reduced to 3-4% at the highest feed rate (0.15 mm/rev) for cutting speeds of 100-150 m/min. Similar to the effect of machining parameters on thrust force which was discussed in Section 6.2.1, a decrease in benefit of CO_2 cooling in reducing exit A_{del} as feed rate was increased is proposed to be due to reduced cooling ability as the amount of CO_2 supply to the cutting zone was decreased because of shorter drilling time combined with the more heat being generated as feed rate was increased. As previously discussed, the use of CO_2 cooling for drilling at the cutting speed of 75 m/min resulted in less increase in exit A_{del} at high feed rates compared to other cutting speeds (100-150 m/min). As a consequence, it is shown in Figure 6.37 that the percentage reduction of exit A_{del} when drilling with CO_2 cooling at a cutting speed of 75 m/min was still high (31-36% at a feed rate of 0.12 and 0.15 mm/rev) even at the high feed rates.

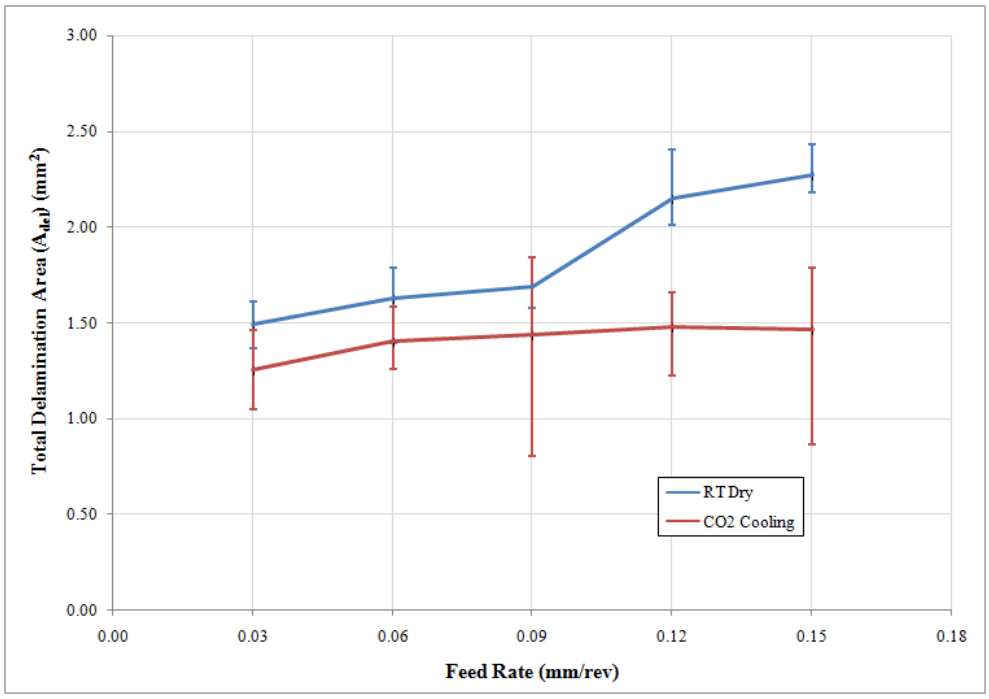

Figure 6.37: Comparison of total delamination area (A_{del}) at the exit produced from room temperature (RT) dry and CO_2 drilling of CFRP plaques at a cutting speed of 75 m/min

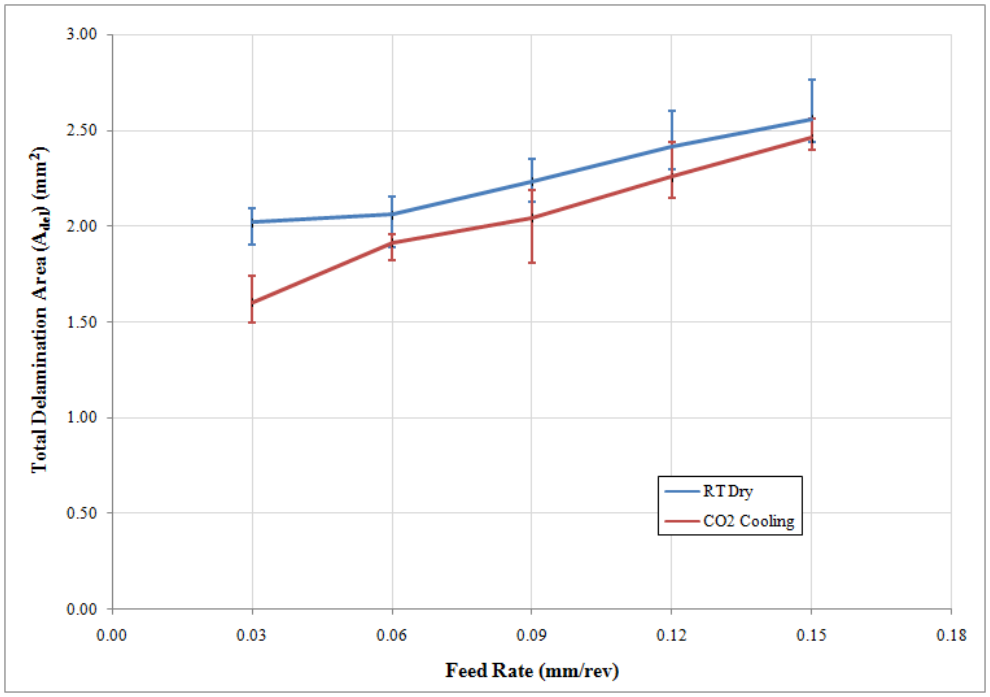

Figure 6.38: Comparison of total delamination area (A_{del}) at the exit produced from room temperature (RT) dry and CO_2 drilling of CFRP plaques at a cutting speed of 100 m/min

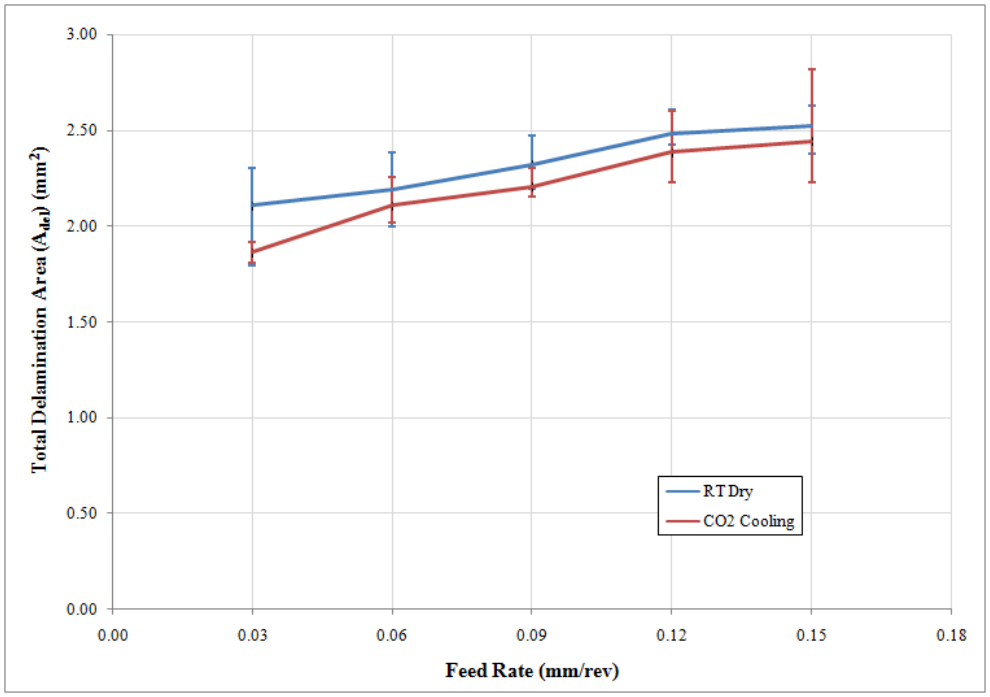

Figure 6.39: Comparison of total delamination area (A_{del}) at the exit produced from room temperature (RT) dry and CO_2 drilling of CFRP plaques at a cutting speed of 115 m/min

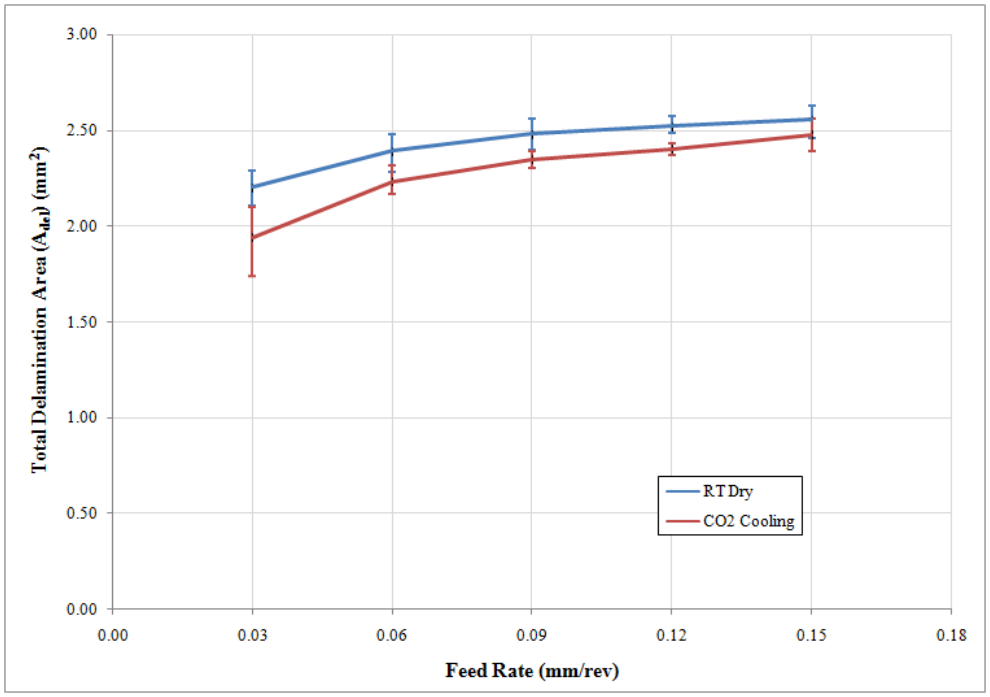

Figure 6.40: Comparison of total delamination area (A_{del}) at the exit produced from room temperature (RT) dry and CO_2 drilling of CFRP plaques at a cutting speed of 130 m/min

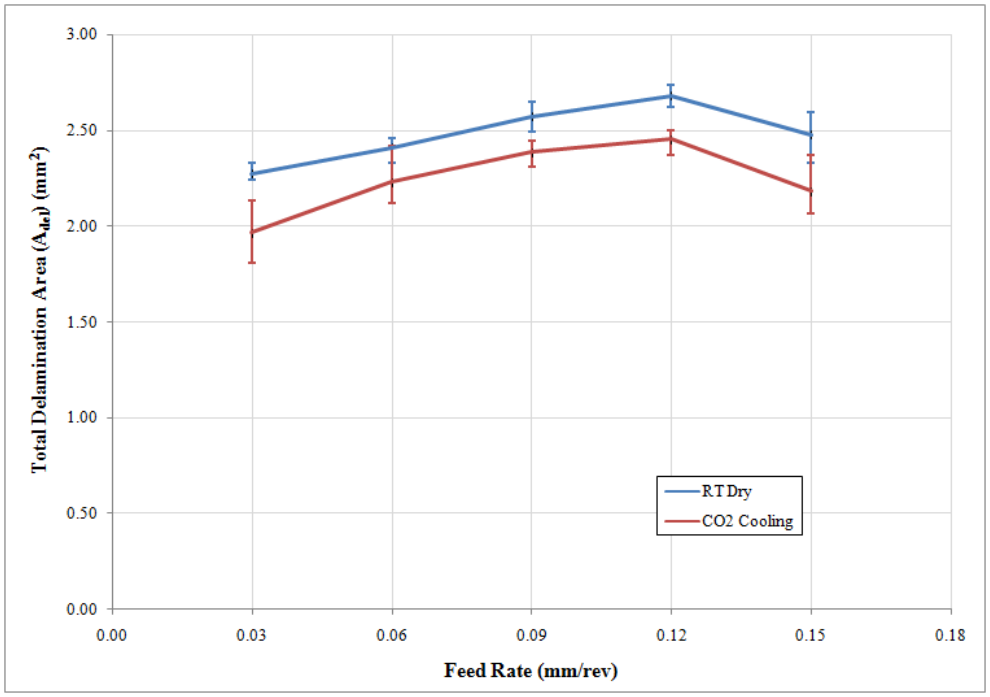

Figure 6.41: Comparison of total delamination area (A_{del}) at the exit produced from room temperature (RT) dry and CO_2 drilling of CFRP plaques at a cutting speed of 150 m/min

It can be concluded from the results in Table 6.3 and Figures 6.27 and 6.28 that CO_2 drilling produced less A_{del} at the exit compared to room temperature dry drilling for all cutting speeds and feed rates. However, the percentage reduction of exit A_{del} tended to

decrease as feed rate was increased. The reasons for a reduction of exit A_{del} by the use of CO_2 cooling will be discussed in Section 6.4.

6.2.3.2 Effect of Cutting Speed

Results showing the variations of exit A_{del} with cutting speed for room temperature dry and CO_2 drilling are presented in Table 6.4 and Figures 6.42 and 6.43. The results in Table 6.4 and Figures 6.42 and 6.43 were from the same set of data presented in Table 6.3 in Section 6.2.3.1 but re-presented to show the effect of cutting speed on the variations of exit A_{del}. Data from Table 6.4 is going to be used for discussion in this section.

Table 6.4: Variation of total delamination area (A_{del}) at the exit with cutting speed produced from room temperature (RT) dry and CO_2 drilling of CFRP plaques at feed rates of 0.03, 0.06, 0.09, 0.12 and 0.15 mm/rev

Feed Rate (mm/rev)	Cutting Speed (m/min)	Total A_{del} (mm^2)		Increase of Total A_{del} (75-150 m/min)		Reduction of Total A_{del}
		RT Dry	CO_2 Cooling	RT Dry	CO_2 Cooling	RT Dry/CO_2 Cooling
0.03	75	1.49	1.25	53%	57%	16%
0.03	100	2.02	1.60			21%
0.03	115	2.11	1.87			11%
0.03	130	2.21	1.94			12%
0.03	150	2.27	1.97			14%
0.06	75	1.63	1.40	48%	59%	14%
0.06	100	2.06	1.92			7%
0.06	115	2.19	2.11			4%
0.06	130	2.39	2.23			7%
0.06	150	2.41	2.23			7%
0.09	75	1.69	1.44	53%	66%	15%
0.09	100	2.23	2.05			8%
0.09	115	2.32	2.21			5%
0.09	130	2.48	2.35			5%
0.09	150	2.58	2.39			7%
0.12	75	2.15	1.48	25%	66%	31%
0.12	100	2.41	2.26			6%
0.12	115	2.49	2.39			4%
0.12	130	2.52	2.40			5%
0.12	150	2.68	2.45			8%
0.15	75	2.27	1.46	9%	49%	36%
0.15	100	2.56	2.46			4%
0.15	115	2.53	2.45			3%
0.15	130	2.56	2.48			3%
0.15	150	2.48	2.18			12%

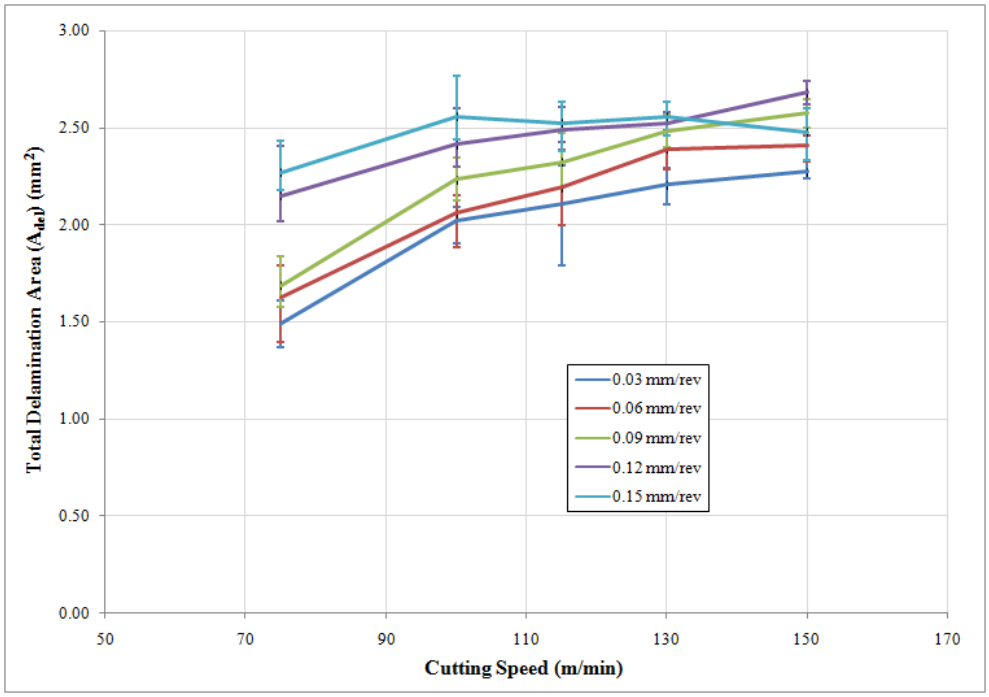

Figure 6.42: Variation of total delaminated area (A_{del}) at the exit with cutting speed produced from room temperature dry drilling of CFRP plaques at feed rates of 0.03, 0.06, 0.09, 0.12, 0.15 mm/rev

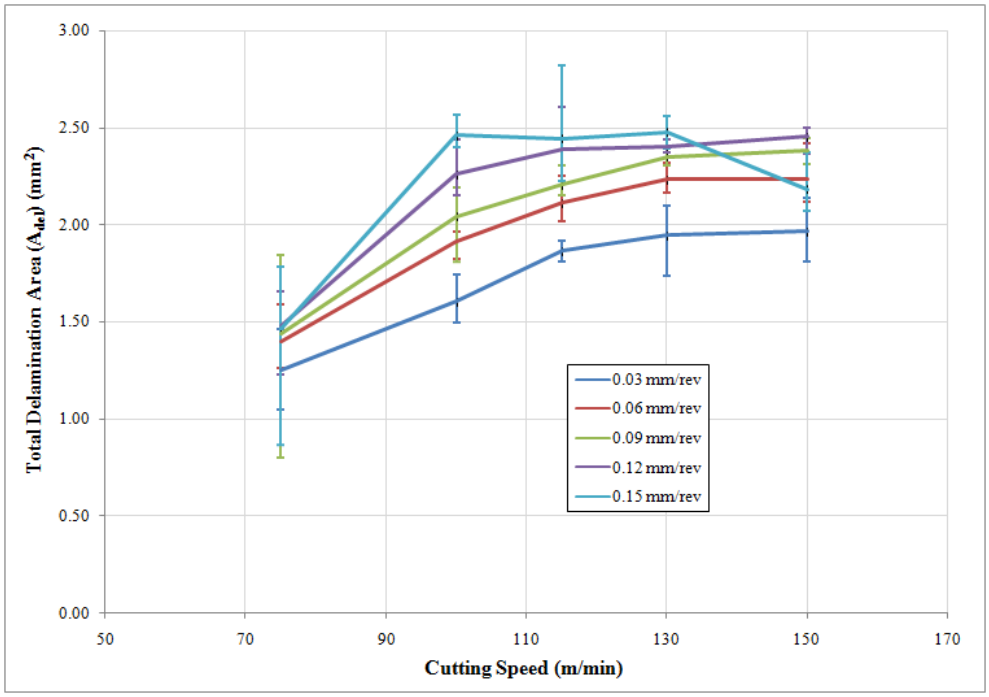

Figure 6.43: Variation of total delaminated area (A_{del}) at the exit with cutting speed produced from CO_2 drilling of CFRP plaques at feed rates of 0.03, 0.06, 0.09, 0.12, 0.15 mm/rev

It is shown in Figures 6.42 and 6.43 that exit A_{del} for room temperature dry and CO_2 drilling increased as cutting speed was increased from 75 to 150 m/min. It has been reported by other researchers [16, 19, 20] that the size of delamination damage increased as cutting

speed was increased due to the progressive wear of the tool. However, the author suggests that it was also due to the higher cutting temperature produced by the increase in cutting heat as cutting speed was increased. An increase in cutting temperature would result in lower resistance to delamination damage of the workpiece material and hence larger delamination damage (discussed in Section 6.4). The increase in exit A_{del} as cutting speed was increased from 75 to 150 m/min for CO_2 drilling was in the range 57-66% for feed rates of 0.03-0.12 mm/rev. This indicates the less dominant effect of feed rate on the increase of exit A_{del} compared to that of cutting speed for CO_2 drilling. It is suggested that this was due to the more dominant effect of the increase of cutting temperature with increasing cutting speed when compared to the effect of the increase of thrust force with increasing feed rate. However, this increase in exit A_{del} with increasing cutting speed for CO_2 drilling was reduced to 49% for a feed rate of 0.15 mm/rev, which is lowest compared to other feed rates. Similarly, the increase in exit A_{del} with increasing cutting speed for room temperature dry drilling was reduced to 9% for a feed rate of 0.15 mm/rev. This was a result of a decrease in exit A_{del} as cutting speed was changed from 130 to 150 m/min at a feed rate of 0.15 mm/rev for both experiments. This is contradictory to expectation that exit A_{del} with would be higher as cutting speed and feed rate increased because of more heat being generated, which would result in a reduction in resistance to delamination damage. Repetition of drilling experiment for a feed rate of 0.15 mm/rev would be needed to validate this trend of the results.

The results of exit A_{del} for room temperature dry CO_2 drilling at various cutting speeds were compared to investigate the effect of CO_2 cooling on exit A_{del} at changing cutting speed, Table 6.4 and Figures 6.44-6.48. It is shown in Figures 6.44-6.48 that drilling with CO_2 cooling produced less exit A_{del} when compared to room temperature dry drilling for feed rates of 0.03, 0.06, 0.09, 0.12 and 0.15 m/rev at all cutting speeds. The reduction of exit A_{del} when drilling with CO_2 cooling was in the range 11-21%, 4-14%, 5-15%, 4-31% and 3-36% with feed rates of 0.03, 0.06, 0.09, 0.12 and 0.15 mm/rev respectively. Similar to the effect of feed rate, the reduction of exit A_{del} when drilling with CO_2 cooling decreased as cutting speed was increased from 75 to 150 m/min. It is proposed that this was due to more heat generated and reduced cooling ability because of shorter drilling time to supply CO_2 to the cutting area at higher cutting speeds, similar to that had been discussed for thrust force in Section 6.2.1.

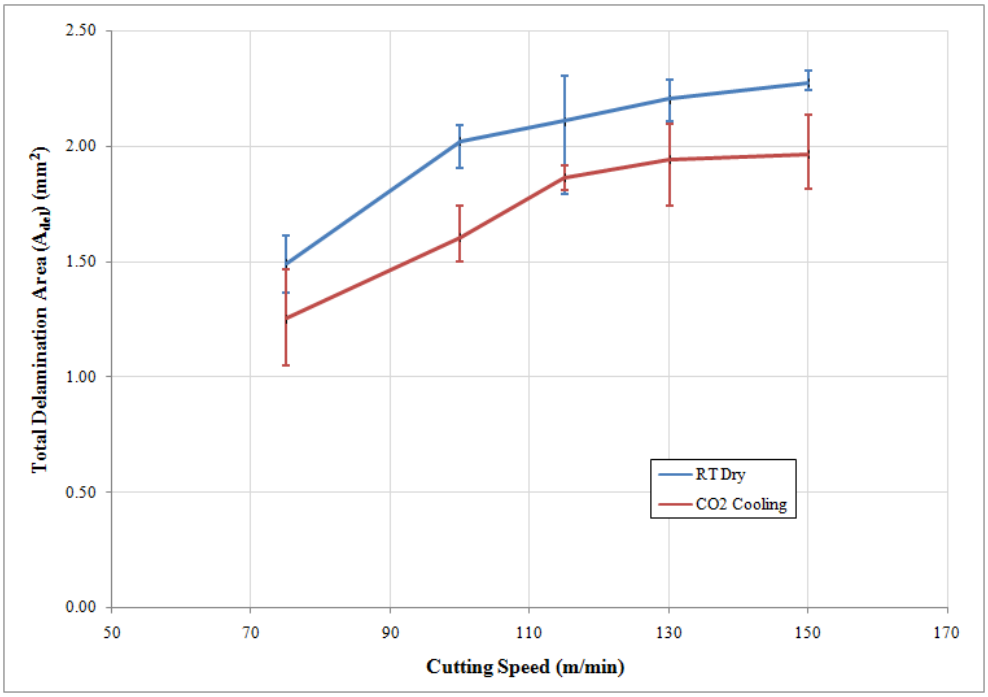

Figure 6.44: Comparison of total delamination area (A_{del}) at the exit produced from room temperature (RT) dry and CO_2 drilling of CFRP plaques at a feed rate of 0.03 mm/rev

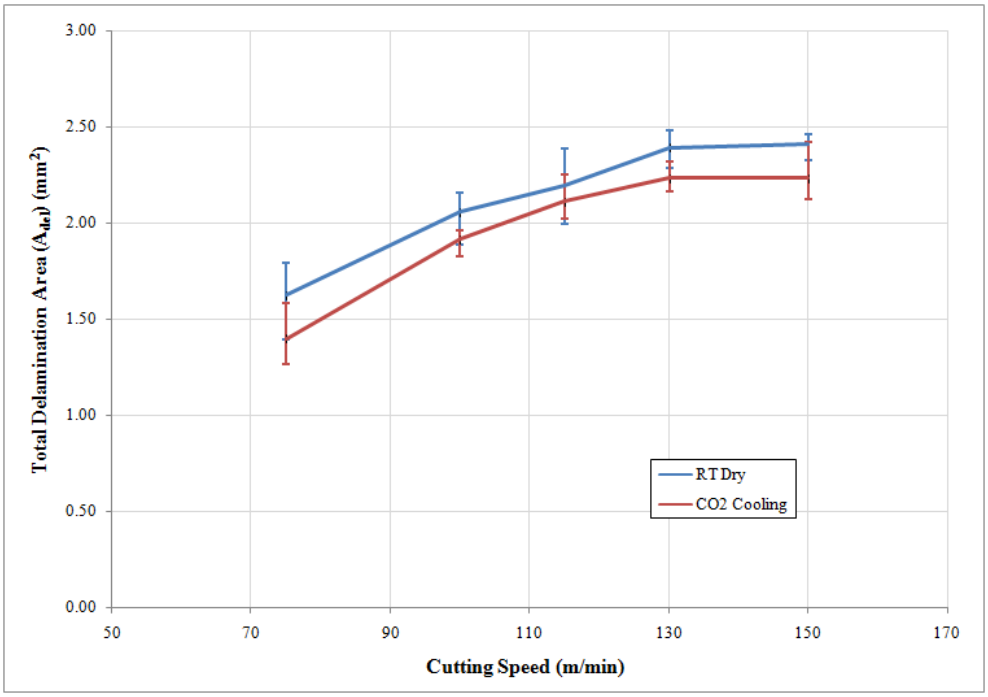

Figure 6.45: Comparison of total delamination area (A_{del}) at the exit produced from room temperature (RT) dry and CO_2 drilling of CFRP plaques at a feed rate of 0.06 mm/rev

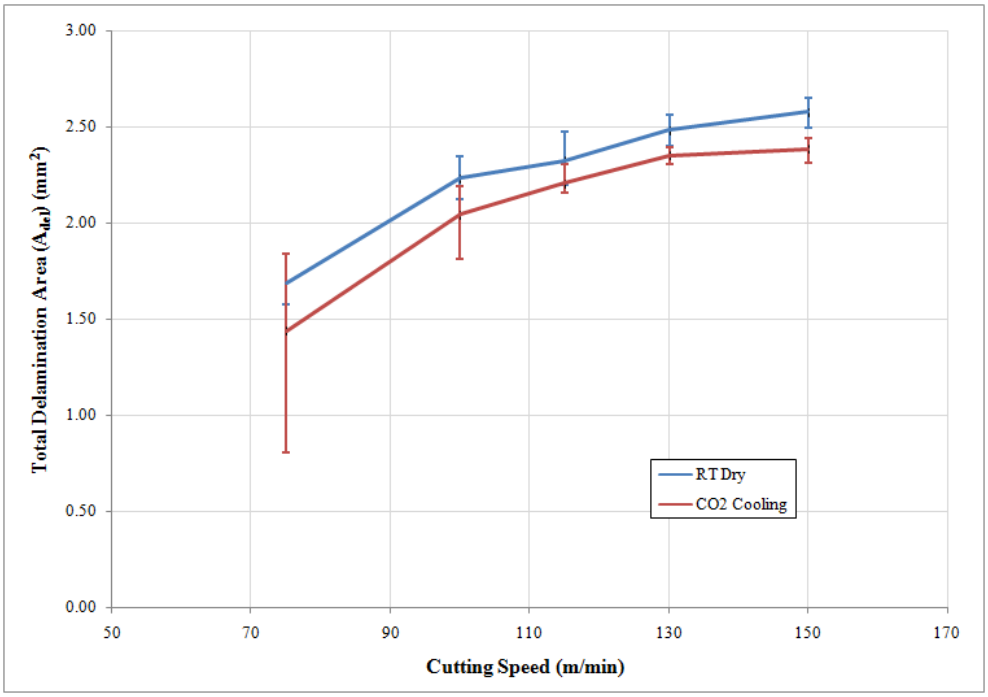

Figure 6.46: Comparison of total delamination area (A_{del}) at the exit produced from room temperature (RT) dry and CO_2 drilling of CFRP plaques at a feed rate of 0.09 mm/rev

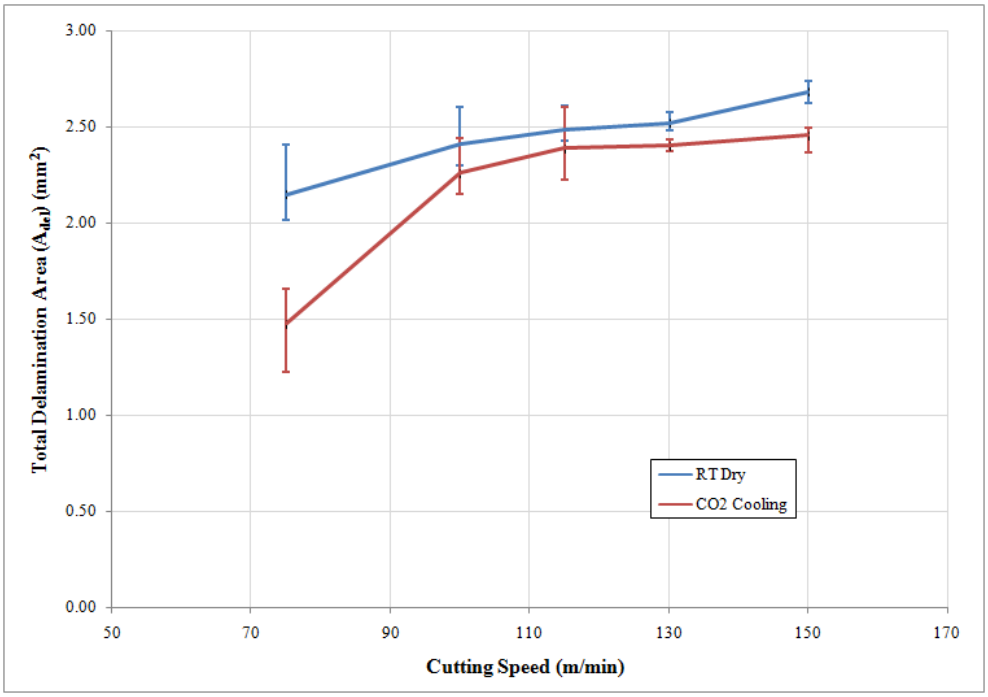

Figure 6.47: Comparison of total delamination area (A_{del}) at the exit produced from room temperature (RT) dry and CO_2 drilling of CFRP plaques at a feed rate of 0.12 mm/rev

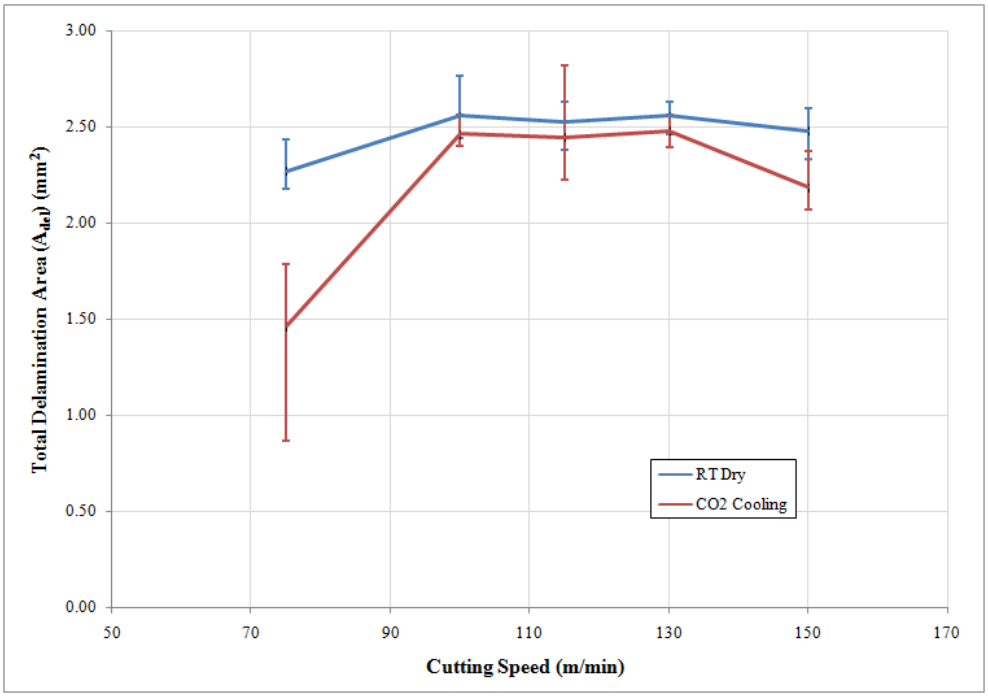

Figure 6.48: Comparison of total delamination area (A_{del}) at the exit produced from room temperature (RT) dry and CO_2 drilling of CFRP plaques at a feed rate of 0.15 mm/rev

6.3 X-ray CT-Scanning Analysis of Damage in Drilling of Carbon Fibre Reinforced Plastics with Cryogenically Pre-cooled Tools, with CO_2 Cooling and when Machined Dry at Room Temperature

It has previously been shown in Sections 6.1 and 6.2 that drilling with cryogenically pre-cooled tools and drilling with CO_2 cooling had similar effect on the drilling performance by producing higher thrust force but less damage to the hole compared to room temperature dry drilling. However, the effect of the two cooling methods on drilling performance have not been examined and compared at the same machining condition. For this reason, the evaluation of drilling performance with respect to thrust force and damage to the hole in drilling of CFRP plaques with cryogenically pre-cooled tools and with CO_2 cooling will be discussed and compared with room temperature dry drilling in this section. The CFRP plaques used for the drilling trials in this section were the same type and from the same batch as those used for the drilling trials with CO_2 cooling in Section 6.2. This type of CFRP was used in order to demonstrate the effect of CO_2 cooling and cryogenic pre-cooling of the tool on the actual material that will be used in aerospace industry [186]. For the drilling trials in this section, the analysis of the damage to the drilled hole was performed by using the X-ray CT-scanning technique. The methodology for the drilling trials was previously

described in Section 5.3. Raw data of the results of thrust force for drilling trials discussed in Section 6.3 is presented in Appendix C.

6.3.1 Thrust Force

Results showing average and maximum thrust forces for drilling of CFRP plaques when machining dry at room temperature, with the cryogenically pre-cooled tools (30 and 120 s cooling time) and with CO_2 cooling (flow rate of 3.37 l/min) are presented in Figures 6.49 and 6.50.

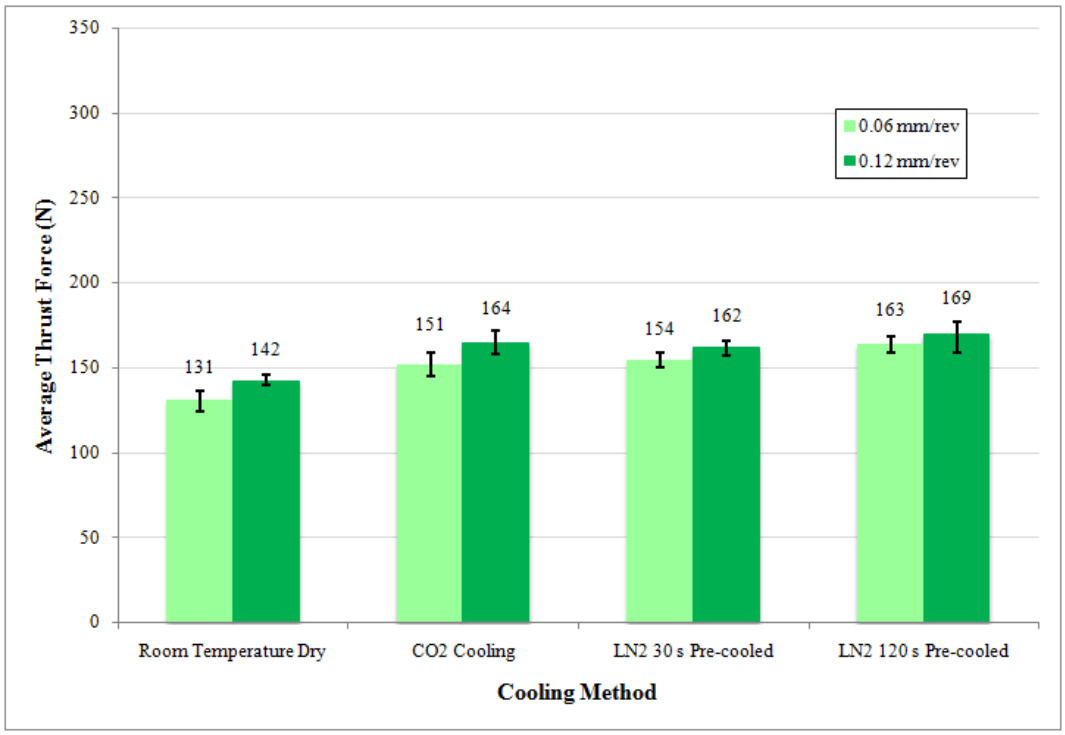

Figure 6.49: Average thrust force for drilling of CFRP plaques when machined dry at room temperature, with CO_2 cooling and with a tool pre-cooled in LN_2 for 30 s and 120 s respectively at a cutting speed of 100 m/min and feed rates of 0.06 and 0.12 mm/rev

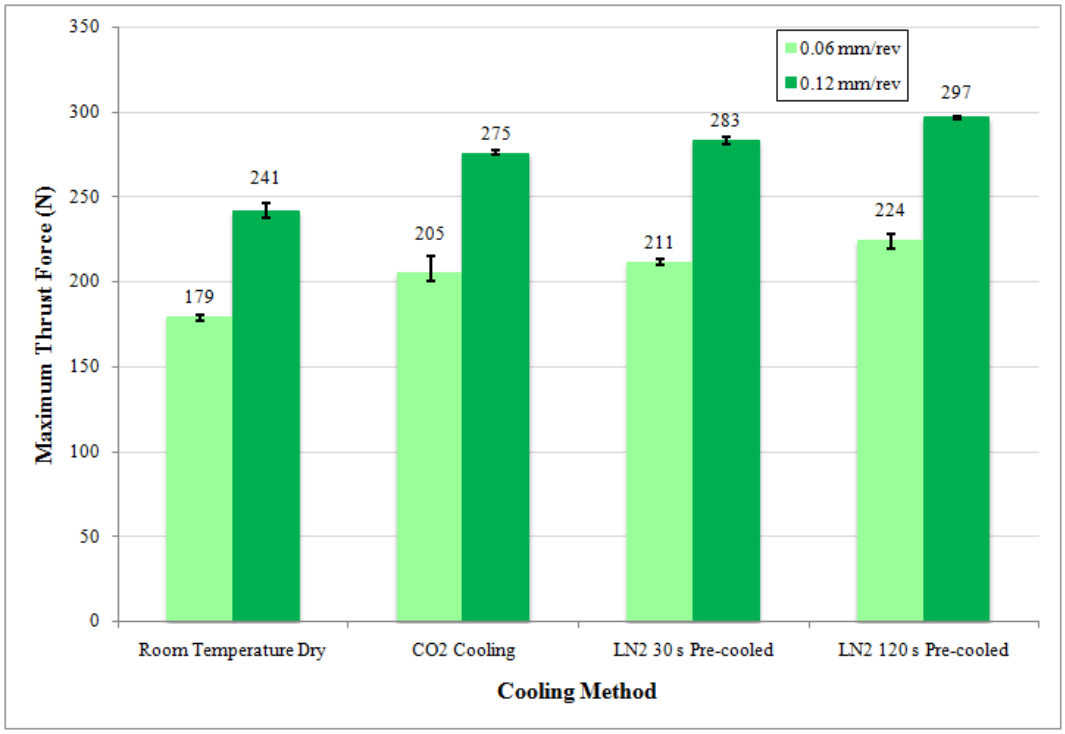

Figure 6.50: Maximum thrust force for drilling of CFRP plaques when machined dry at room temperature, with CO_2 cooling and with a tool pre-cooled in LN_2 for 30 s and 120 s respectively at a cutting speed of 100 m/min and feed rates of 0.06 and 0.12 mm/rev

It is shown in Figures 6.49 and 6.50 that higher average and maximum thrust forces were produced when drilling with CO_2 cooling and with the tools pre-cooled in LN_2 (30 and 120 s cooling time) compared to room temperature dry drilling for feed rates of 0.06 and 0.12 mm/rev. CO_2 drilling produced 16% and 15% higher average thrust force and 15% and 14% higher maximum thrust force than room temperature dry drilling at feed rates of 0.06 and 0.12 mm/rev respectively. The drilling with a 30 s cryogenically pre-cooled tool produced 18% and 14% higher average thrust force and 18% and 17% higher maximum thrust force compared to drilling dry at room temperature at feed rates of 0.06 and 0.12 mm/rev respectively. As pre-cooling time was changed to 120 s, the increase in thrust force as compared to the room temperature dry drilling was increased to 25% and 19% for average thrust force and to 25% and 23% for maximum thrust force at feed rates of 0.06 an 0.12 mm/rev respectively. This trend of the higher thrust forces produced when drilling with CO_2 cooling or the cryogenically pre-cooled tools compared to those when machining dry at room temperature has previously been shown from the results in Sections 6.1 and 6.2. In addition, it can be noticed that the effect of CO_2 cooling or LN_2 pre-cooling of the tool on the increase in thrust force tended to decrease as feed rate was increased from 0.06 mm/rev to 0.12 mm/rev. This trend of less significant effect of CO_2 cooling on the increase in thrust force as feed rate increased has previously been shown with

discussion of the reason of this trend in Section 6.2.1.1. For cryogenic pre-cooling of the tool, it is proposed that this was because of more heat generated at higher feed rates which increased temperature of the cooled tool hence reduced the effectiveness in cutting heat removal.

From the results in Figures 6.49 and 6.50, it can be seen that significance of the effect of CO_2 cooling on the increase in thrust force was similar to that of 30 s cryogenic pre-cooling of the tool. The difference between thrust forces for CO_2 drilling and the drilling with a 30 s pre-cooled tool was only 2-3%. It is proposed that this was due to a similar level of temperature of CO_2 gas exiting the nozzle and the temperature of the tool after submerging in LN_2 for 30 seconds. As previously discussed in Section 6.1, the temperature of the drill was decreased to -70°C after pre-cooling for 30 s in LN_2. Similarly, according to SGS, Ltd UK, the temperature of CO_2 at the nozzle end could reach -60 to -70°C [166]. As pre-cooling time was changed to 120 s, the difference between thrust forces for CO_2 drilling and drilling with a cryogenically pre-cooled tool was increased to 5-6%, indicating only 2-3% increase as the cooling time was increased from 30 to 120 seconds. This small difference in thrust force indicates that change of the cooling time from 30 to 120 s did not contribute to an increase in the effect of cryogenic pre-cooling on the increase in thrust force even though temperature of the drill could reach cryogenic temperature (-196°C) after being submerged in LN_2 for 120 s, for which it was observed that there was no bubbling of LN_2 in the polystyrene cups. Based on this inspection of the results in Figures 6.49 and 6.50, it is therefore justified to state CO_2 drilling and drilling with the cryogenically pre-cooled tools produced similar level of thrust force despite the change of the pre-cooling time.

6.3.2 Maximum Depth of Internal Damage Measured by X-ray CT-Scanning Analysis

As previously described in Section 5.3.2.2, the maximum depth of damage to the hole at various positions through-the-thickness was determined by calculating the difference between the maximum radius of the profile in each slice image of the hole, which was obtained by CT-scanning, and the "ideal" radius (3 mm) produced by a 6-mm diameter drill, Figure 5.16. The results showing the maximum depth of internal damage to the hole at various distances (h) from the top laminate of the plaque resulting from room temperature dry, CO_2 drilling and drilling with the LN_2 pre-cooled tools are shown in Figures 6.51 and 6.52 with average and total values of depth of damage shown in Table 6.5. As described in Section 5.3.2.2, the top laminates of the plaque were machined off with 0.7 mm depth of cut to remove the copper-mesh layer on the entry of the plague. Therefore, it should be noted that the top laminate of the plaque discussed in this section was the top

laminate after 0.7 mm of the plaque had been machined off rather than the actual top of the plaque as drilled; hence entry delamination damage will not be considered.

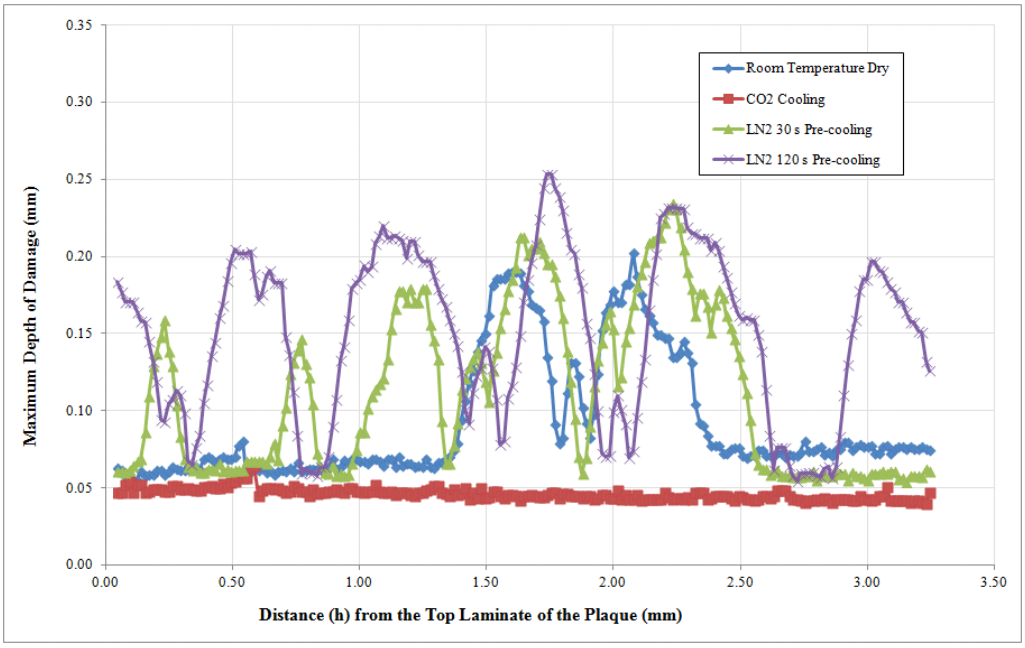

Figure 6.51: Maximum depth of internal damage at various distance (h) from the top laminate of the plaque produced by drilling of CFRP dry at room temperature, with CO_2 cooling and with a tool pre-cooled in LN_2 for 30 s and 120 s respectively at a cutting speed of 100 m/min and a feed rate of 0.06 mm/rev

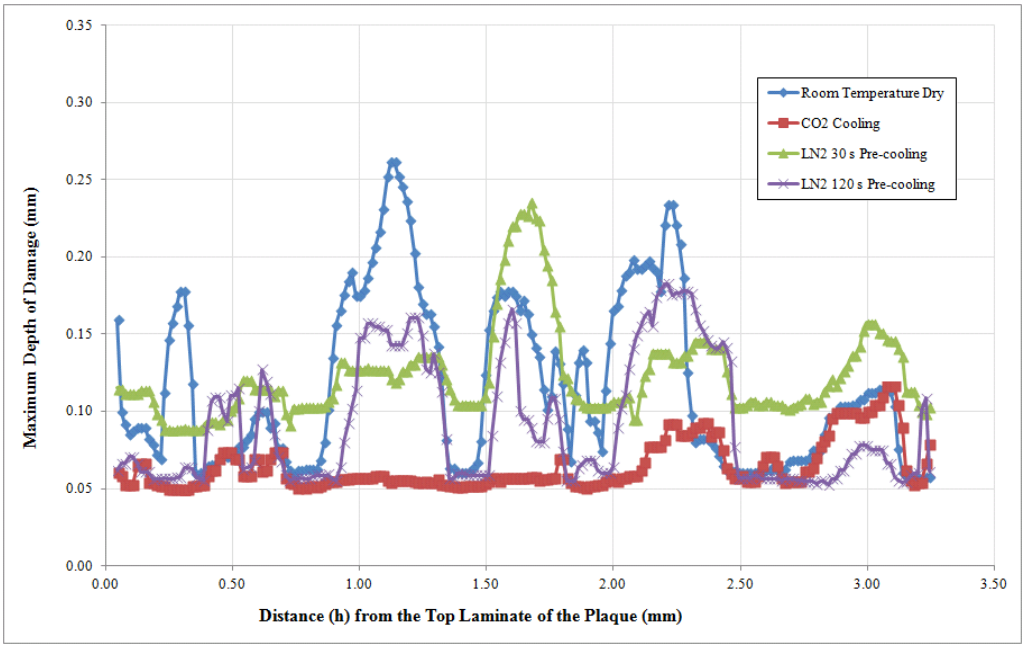

Figure 6.52: Maximum depth of internal damage at various distance (h) from the top laminate of the plaque produced by drilling of CFRP dry at room temperature, with CO_2 cooling and with a tool pre-cooled in LN_2 for 30 s and 120 s respectively at a cutting speed of 100 m/min and a feed rate of 0.12 mm/rev

Table 6.5: Results showing maximum depth of internal damage to the hole produced by drilling of CFRP plaque dry at room temperature, with CO_2 cooling and with the tools pre-cooled in LN_2 (30 s and 120 s cooling time) at a cutting speed of 100 m/min and feed rates of 0.06 and 0.12 mm

Machining Conditions	Maximum Depth of Internal Damage (mm)			
	Average		Total	
	0.06 mm/rev	0.12 mm/rev	0.06 mm/rev	0.12 mm/rev
Room Temperature Dry	0.09	0.12	19.29	24.33
CO_2 Cooling	0.05	0.06	9.70	13.46
30 s LN_2 Pre-Cooling	0.11	0.12	23.30	25.77
120 s LN_2 Pre-Cooling	0.15	0.09	31.40	19.13

In Table 6.5, it is shown that the use of CO_2 cooling resulted in a reduction of internal damage compared to machining dry at room temperature for feed rates of 0.06 and 0.12 mm/rev. Drilling with CO_2 cooling produced 44-50% and 45-50% less internal damage in terms of average and total depth of damage respectively compared to room temperature dry drilling. In Figures 6.51 and 6.52, the quality of the machined surface can be indicated from the variations of maximum depth damage through the thickness of the hole. It was found that drilling with CO_2 cooling produced better quality of the machined surface as measured by a lower depth of internal damage and lower variations in the edge profile through the thickness of the hole compared to room temperature dry drilling for the two feed rates tested. The reason for better quality of the machined surface through the thickness of the hole when drilling with CO_2 cooling will be discussed in Section 6.4.

However, there was inconsistency in the performance of LN_2 pre-cooling compared to room temperature dry drilling. In Table 6.5, it is shown that drilling with a cryogenically cooled tool produced higher average and total depth of internal damage, 21-22% for the 30 s pre-cooling and 63-67% for the 120 s pre-cooling, compared to room temperature dry drilling at a feed rate of 0.06 mm/rev. At a feed rate of 0.12 mm/rev, drilling with a 30 s LN_2 pre-cooled tool produced similar level of internal damage compared to room temperature dry drilling, while drilling with a 120 s LN_2 pre-cooled tool produced less internal damage, 25% and 21% lower average and total depth of damage respectively, compared to room temperature dry drilling. Considering the quality of machined surface through the thickness of the hole, it is shown in Figures 6.51 and 6.52 that the use of LN_2 pre-cooling did not result in a better quality of the machined surface compared to machining dry at room temperature, which is contradictory to the results obtained from CO_2 cooling. High roughness of the hole edge, which can be seen by high values of depth of damage through the thickness, could be observed for drilling with the cryogenically cooled tools and room

temperature dry drilling. In fact, room temperature dry drilling tended to produce lower depth of damage through the thickness of the hole compared to drilling with the cooled tools at a feed rate of 0.06 mm/rev, Figure 6.34. These results in Table 6.5 and Figures 6.51 and 6.52 were contradictory to what has been shown and discussed previously in Section 6.1 that a reduction of internal damage was achieved by the use of LN_2 pre-cooling. As previously described in Section 5.3, the results of the CT-scanning analysis were obtained from only one repetition of each machining condition. For this reason, the author suggests that the contradictory results and variations in the performance of cryogenic pre-cooling in terms of internal damage to the hole in this drilling trial could be due to the anisotropic nature of CFRP plus a different type of CFRP was used. Further investigation with more repetitions of each machining condition will be required to validate this trend in the results.

Despite variations in the results for drilling with cryogenic pre-cooling, it can be seen from the results in Table 6.5 and Figures 6.51 and 6.52 that the drilling with CO_2 cooling produced less internal damage and hence better quality of the machined surface through the thickness of the hole compared to drilling with LN_2 pre-cooled tools for feed rates of 0.06 and 0.12 mm/rev. Drilling with CO_2 cooling produced 50-55% and 48-58% less average and total depth of internal damage compared to drilling with a 30 s LN_2 pre-cooled tool, while it produced 33-67% and 30-69% less average and total depth of damage compared to drilling with a 120 s LN_2 pre-cooled tool. Since a reduction of cutting temperature would result in higher resistance to damage (discussed in Section 6.4), this indicates that application of external CO_2 cooling was more effective in reducing cutting temperature in the drilling process than LN_2 pre-cooling. This higher effectiveness in reducing cutting temperature is proposed to be resulting from continuous cooling of the cutting zone in drilling with external CO_2 cooling method as opposed to cooling of the tool only before performing the drilling process in drilling with LN_2 pre-cooling method. As previously described in Section 5.3, the tool and the workpiece were continuously cooled during the drilling process by external supply of CO_2 gas. However, when drilling with the cryogenically cooled tools, the tool was only cooled by submerging in LN_2 before the drilling process was performed without further cooling of the tool or the workpiece during the drilling process. In addition, it is suggested that the temperature of the cryogenically cooled tool would increase while traveling from the LN_2 to the cutting zone, resulting in a reduced capability for removing the cutting heat. As a consequence, it is proposed that the effectiveness of cutting heat removal by drilling with CO_2 cooling was higher than that by drilling using the LN_2 pre-cooled tools even though LN_2 was much colder than CO_2. The investigation of cutting temperature for drilling of

CFRP plaques with CO_2 cooling and cryogenically cooled tools showing the different effectiveness in removing the cutting heat will be discussed in Chapter 7.

6.3.3 Cross-sectioning of CT-scanned samples

As discussed in Section 5.3.2.2, the scale of damage which is detectable within CT-scanning in this research is 15 µm. However, it can be seen from visual inspection analysis of the cross-sectioned sample resulting from drilling with CO_2 cooling, Figure 6.53, that there is internal damage to the edge of the hole of which the scale is smaller than 15 µm. The internal damage with the scale of damage less than 15 µm was also observed in the cross-sectioned samples resulting from room temperature dry drilling and drilling with LN_2 pre-cooling. The internal damage with scale of damage less than 15 µm would not be detected within CT-scanning technique used in this research. This would not affect the analysis of internal damage by CT-scanning in term of maximum depth of damage for each slice through the thickness of the plaque, which are presented and discussed in Section 6.3.2, as only the maximum values of depth of damage for each slice were used for the analysis. However, this would affect the results of damage analysis by CT-scanning in terms of total area of damage for each slice, which is suggested for further work. This is because all scale of damage will be considered as contribution to the total area of internal damage for each slice rather than considering only the contribution from internal damage with the maximum depth. The results of total area of internal damage by the CT-scanning would not represent the actual value of total area of internal damage if the internal damage of which the scale is smaller than 15 µm, Figure 6.53, could not be detected. In addition, a crack with the scale smaller than 15 µm into the workpiece material could be observed in the cross-sectioned sample resulting from drilling CO_2 cooling and with 120 s LN_2 pre-cooling, Figures 6.54 and 6.55. This crack would not be detected within CT-scanning used in this research; hence information on the crack propagation and its contribution to depth of internal damage could not be obtained by the CT-scanning technique.

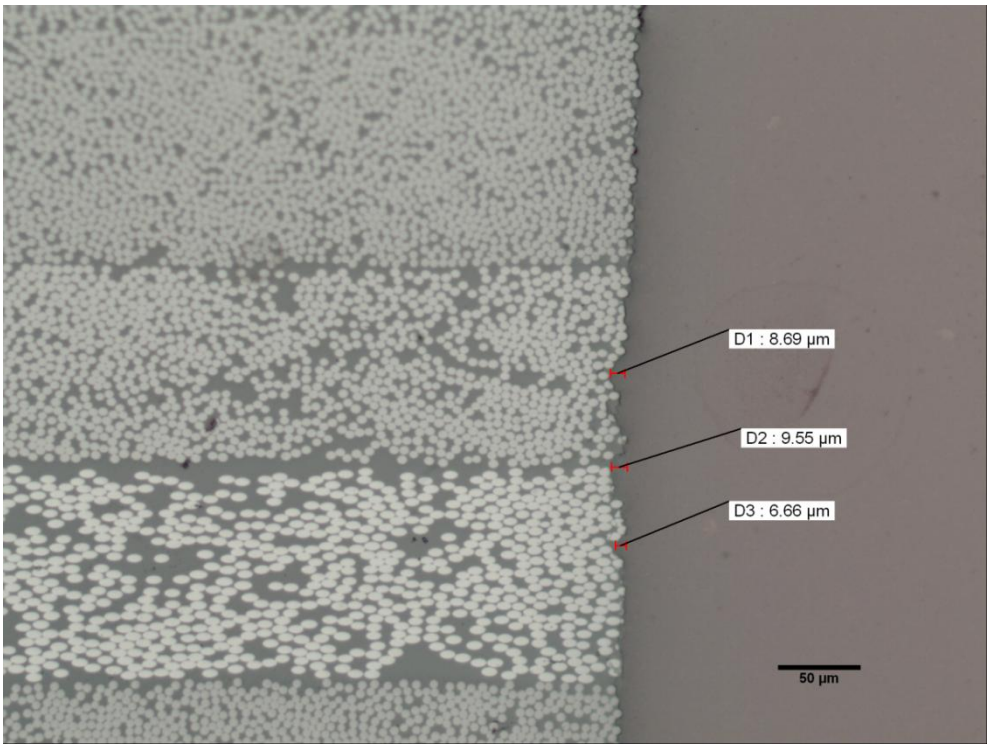

Figure 6.53: Optical microscope image of a cross-sectioned CFRP sample showing internal damage to the machined surface of the hole with the scale of damage of less than 15 µm when drilling with CO_2 cooling at a cutting speed and feed rate of 100 m/min and 0.12 mm/rev respectively

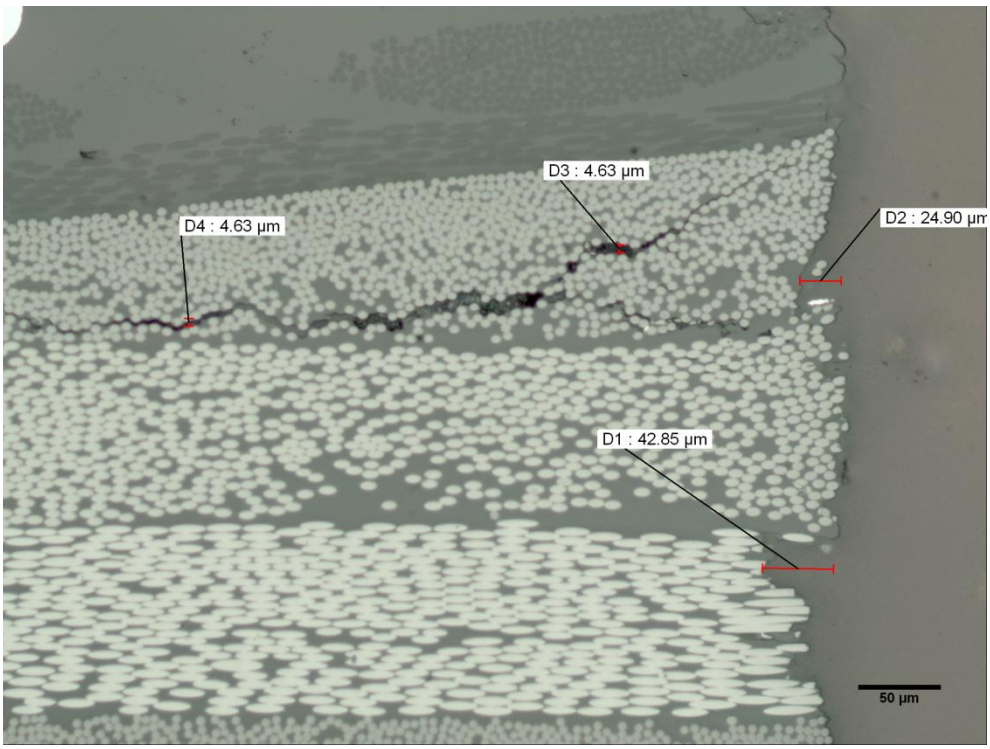

Figure 6.54: Optical microscope image of a cross-section CFRP sample showing cracks into the workpiece material with the scale less than 15 µm when drilling with CO_2 cooling at a cutting speed and feed rate of 100 m/min and 0.12 mm/rev respectively

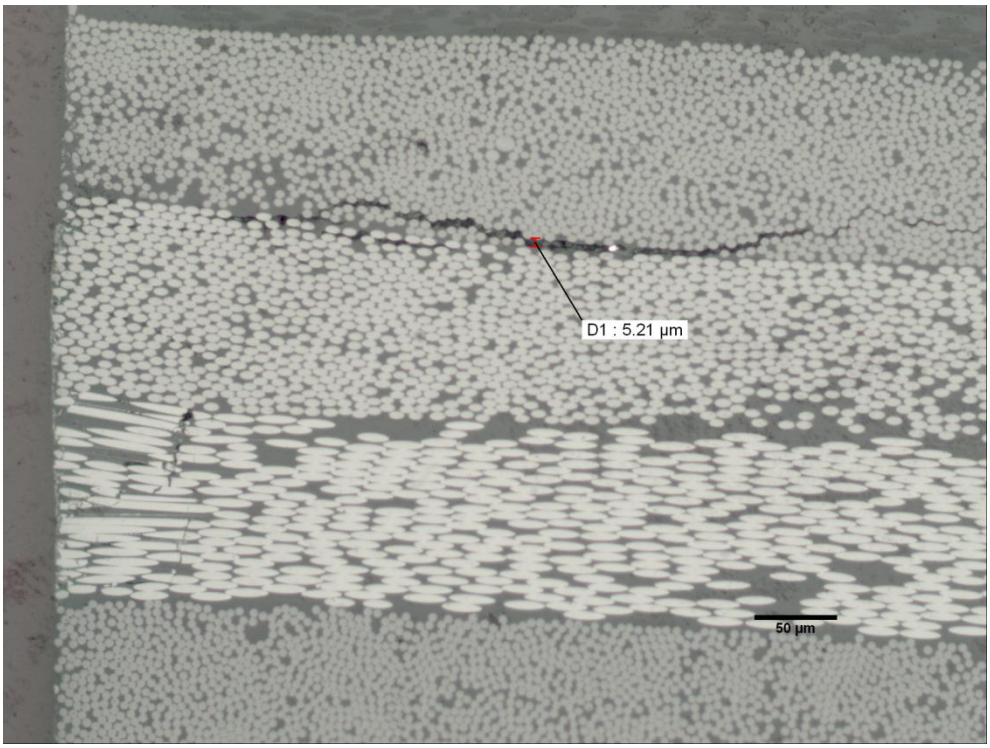

Figure 6.55: Optical microscope image of a cross-section CFRP sample showing cracks into the workpiece material with the scale less than 15 µm when drilling with 120 s LN_2 pre-cooling cooling at a cutting speed and feed rate of 100 m/min and 0.12 mm/rev respectively

Although CT-scanning analysis technique can eliminate the possibility of additional damage resulting from sectioning and preparation of the samples for the cross-sectioning and visual inspection analysis technique, it cannot detect internal damage with the scale of damage smaller than 15 µm as observed by visual inspection of the cross-sectioned samples. In order to reduce the scale of damage which is detectable within CT-scanning, it would take longer time for scanning and analysis of each hole. As mentioned in Section 5.3, scanning and analysis of each hole with the detectable scale of damage of 15 µm already took three to six hours [179]. Therefore, this considerable amount of time for scanning and analysis by CT-scanning analysis technique would limit the use of this technique in case the analysis of larger size of samples (more repetitions of drilling trials) is required to minimise variation in the results due to anisotropic nature of CFRP. It is proposed that the analysis technique by cross-sectioning and visual inspection of the samples is more practical for quality control process in industry due to shorter process time and hence ability to analyse larger size of samples compared to CT-scanning technique. It is suggested that the possibility of additional damage to the sample by cross-sectioning and visual inspection analysis technique as previously mentioned could be minimised if sectioning and preparation of the samples are done properly. However, there would still be variation in the results of internal damage due to the position of cross-sectioning. The sample might be cross-sectioned at the position

where the maximum depth of internal damage is not revealed. It is proposed that this variation in the results due to dependence on the position of cross-sectioning could be minmised by examining the damage from large number of samples using various positions of cross-sectioning.

6.4 Discussion

6.4.1. Effect of Cryogenic Pre-Cooling and CO_2 Cooling on Thrust Force

From the results in Sections 6.1-6.3, it was found that application of cryogenic pre-cooling by LN_2 and CO_2 cooling resulted in higher thrust force compared to machining dry at room temperature when drilling CFRPs. This is contradictory to the results found in metal machining which it has been reported by other researchers that application of cryogenic cooling provided a benefit in reducing cutting forces compared to room temperature dry machining [43, 45, 144, 145, 167] as discussed in Chapter 4. It was shown that application of cryogenic cooling to metal machining resulted in improved condition at the tool/workpiece interface, i.e., lower coefficient of friction and shorter tool/workpiece contact length, which consequently resulted in larger shear plane angle, compared to machining dry at room temperature and with conventional cutting fluid [43, 45, 144, 145, 167]. This was attributed to the higher effectiveness in removing heat from the cutting zone, resulting in lower cutting temperature and lubrication effect at the tool/workpiece interface [43, 45, 144, 145, 167]. The lubrication effect by cryogenic cooling was proposed to be due to the presence of a cushion layer of evaporating cryogen at the tool/workpiece interface which reduced friction and tool/workpiece contact length [40, 145, 146]. A reduction in cutting temperature as a result of more effective cutting heat removal also resulted in an increase in strength of the workpiece material which would increase cutting force. However, it is proposed that the effect of improved condition at the tool/workpiece interface was more dominant and compensated for the effect of increased strength of the workpiece material, hence resulting in a reduction in cutting forces. This is because cutting force in metal machining is dominantly influenced by conditions at the tool/workpiece interface in the secondary shear zone and shear plane angle in the primary shear zone as the mechanism of cutting is dominated by extensive shearing and plastic deformation in the primary shear zone and secondary shear zone where seizure at the tool/workpiece interface on the rake face usually occurs [72].

However, mechanism of cutting associated with CFRPs is dominated by a series of brittle fractures of workpiece material and limited shearing at the fibre/matrix interface rather than extensive shearing and plastic deformation in the shear zones [4, 75, 77, 78].

This indicates less influence of conditions at the tool/workpiece interface on cutting forces when machining CFRPs. For this reason, it is proposed that the effect of reduced friction and shorter contact length at the tool/workpiece interface due to lubrication effect would be less dominant and compensated by the effect of increased strength of the workpiece material due to cooling effect when machining CFRPs. As a consequence, the application of cryogenic cooling would not result in lower cutting forces when machining CFRPs. It is proposed that higher cutting forces would be produced when machining CFRPs with cryogenic cooling due to an increase in strength of the workpiece material as cutting temperature is reduced. An increase in cutting forces due to increased strength of the workpiece material by the cooling effect of cryogenic machining was reported by Hong *et al.* [148] when machining titanium alloy and by Bhattacharrya *et al.* [187] when machining Kevlar composites.

Based on the discussion in this section, the author proposes that variation in strength and stiffness of CFRPs with temperature was the major factor contributing to higher thrust force produced when drilling with LN_2 pre-cooling or CO_2 cooling compared to room temperature dry drilling as reported in this research. It has been reported by other researchers that tensile strength and stiffness and such matrix-dominant properties as the transverse and in-plane shear strength and stiffness and bending fracture strength, of CFRPs increased with decreased temperature [5, 188-191]. This indicates an increase in strength and stiffness of CFRPs with decreasing temperature. It was also reported by Alauddin *et al*. [192], that an increase in drilling temperature (from room temperature to 125°C) resulted in lower thrust force due to thermal softening of epoxy matrix. Based on these findings by other researchers, it is proposed that drilling with LN_2 cooling of the tool or CO_2 cooling would result in a higher level of strength and stiffness of the workpiece material that could be retained during drilling compared to machining dry at room temperature due to the expected lower cutting temperature. In cryogenic pre-cooling, cutting temperature was reduced because heat was more effectively removed from the cutting zone by the cryogenically cooled tool. In CO_2 cooling, a reduction in cutting temperature was resulting from more effective cutting heat removal by continual supply of low-temperature CO_2 gas (-70°C) to the cutting zone during drilling. Due to a higher level of strength and stiffness of CFRP being retained, drilling with a cryogenically pre-cooled tool or with CO_2 cooling would therefore produce higher thrust force compared to room temperature dry drilling.

6.4.2. Effect of Cryogenic Pre-cooling on Tool Wear

It was found from the results in Section 6.1 that application of cryogenic (LN_2) pre-cooling resulted in higher rate of tool wear compared to machining dry at room temperature when drilling CFRPs. This is again contradictory to what has been reported by other

researchers that improved tool life (lower rate of tool wear) compared to machining dry at room temperature was achieved by application of cryogenic cooling when machining metals with carbide tools [35, 40, 140, 145, 147] as discussed in Chapter 4. It was shown that application of cryogenic cooling resulted in improved interaction at the tool/workpiece interface, i.e., reduced coefficient of friction, shorter tool/workpiece contact length and reduced chemical reactivity between the tool and the workpiece hence resulting in a reduction of adhesion-dissolution-diffusion wear, which is temperature-dependent wear mechanism, when machining metals [40, 140, 147]. This was attributed to a combination of cooling effect by effective removal of cutting heat, which resulted in less plastic deformation of the workpiece material [147], and lubrication effect by the presence of a cushion layer of cryogen [40, 146]. The application of cryogenic cooling also resulted in an increase in wear resistance of the tool as cutting temperature was reduced by more effective cutting heat removal [35, 40, 140, 145, 147]. Combined with lower friction and contact length at the tool/workpiece interface, this resulted in a reduction in mechanical wear such as abrasive wear and notch wear on flank face. Based in these findings by other researchers, it indicates that a benefit of tool wear reduction by the application of cryogenic cooling in metal machining was resulting from a reduction in adhesion-diffusion-dissolution wear (temperature-dependent wear mechanism) as a result of improved interaction at the tool/workpiece interface and a reduction in mechanical wear due to higher retention of wear resistance of the tool.

However, the author proposes that the benefit of reducing temperature-dependent wear due to improved tool/workpiece interaction by cryogenic cooling would not be applied when machining CFRPs. This is because less heat and hence lower cutting temperature was produced when machining CFRPs due to brittle-fracture dominated mechanism of cutting with significantly less amount of shearing and plastic deformation and lower material strength compared to when machining metals [4, 5, 16] as discussed in Chapter 3. Due to the fracture dominated mechanism of cutting and lower cutting temperature, adhesion-diffusion-dissolution wear was not a major wear mechanism when machining CFRPs [111, 112]. Although cryogenic cooling would also result in an increase in wear resistance of the tool due to lower cutting temperature, it is proposed that the effect of higher retention of wear resistance of a carbide tool would not be dominant when machining CFRPs. It was reported that the hardness of a carbide tool was reduced by only 10% of the hardness at room temperature at 300°C and was reduced to one sixth at 700°C [72, 73]. However, it has been reported that the cutting temperature produced when drilling CFRPs was could reach 200-400°C depending on the machining conditions [16, 32, 108, 110]. Therefore, the hardness of

a carbide tool would not be affected at this range of cutting temperature when drilling of CFRPs.

Based on the discussion in this section, it proposed that the variation in strength and abrasiveness of CFRP with temperature is the major factor contributing to higher tool wear produced when drilling with cryogenic pre-cooling compared to machining dry at room temperature. Since carbon fibres can maintain their strength and hardness up to 510°C [1, 5], it is proposed that strength of the epoxy matrix had the dominant effect on the variation of the strength and abrasiveness of CFRPs with temperature in this drilling trial. It was demonstrated by Yamini *et al.* [193] that a more ductile fracture of epoxy resin could be observed at the temperature close to the glass transition temperature (63°C for epoxy resin used in their work), while a more brittle failure mode was observed at lower temperatures. Similarly, it was also demonstrated in by Kinloch *et al*. [194, 195] that the fracture behaviour of epoxy resin was described as ductile failure with localised shear yielding at the crack initiation zone at the temperature approaching the glass transition temperature (100°C for epoxy resin used in their work). At room temperature and below, fracture behaviour was described as brittle failure with limited localised plastic deformation ahead of the crack tip [194, 195]. In addition, the degree of brittle failure of epoxy resin increased as the temperature decreased due to lower allowable localised shear yielding of epoxy resin [194]. Due to the more brittle fracture mode observed with the decrease of temperature, it is proposed that epoxy resin in the CFRP plaque would be stronger, which results in a more rigid support holding the abrasive carbon fibres in the plaque, as the temperature was lowered. It was shown by Kim *et al.* [191] that transverse and in-plane shear properties (strength and stiffness) of CFRPs (carbon/epoxy), which were the matrix-dominant properties, increased as the temperature was decreased from room temperature to -150°C. This increase in the matrix-dominant properties also indicates an increase in strength of epoxy matrix and the provision of a more rigid support for the fibres by the epoxy matrix as temperature is reduced. As a result of a more rigid support holding the abrasive carbon fibres, higher flank wear by abrasion would be produced as the flank face rubbed against the better supported carbon fibres. In addition, it was reported by other researchers that a reduction of cutting temperature resulted in an increase in strength and stiffness of CFRPs [5, 188-191] as discussed in Section 6.4.1. Based on these findings by other researchers, it is proposed that the cutting tool would encounter more abrasive and stronger workpiece material during cryogenic drilling compared to during room temperature dry drilling. As mentioned in Section 6.4.1, cutting temperature was reduced because heat was more effectively removed from the cutting zone by the cryogenically cooled tool, resulting in expected lower cutting temperature. As a consequence of higher strength and abrasiveness of

CFRPs combined with higher thrust force, this resulted in higher flank wear when drilling with cryogenic cooling compared to drilling dry at room temperature.

6.4.3. Effect of Cryogenic Pre-cooling and CO_2 Cooling on Delamination, Internal Damage and Quality of the Machined Surface

From the results in Sections 6.1-6.3, it was found that a reduction in exit delamination was achieve by application of cryogenic cooling when drilling CFRPs even though higher thrust force was produced compared to room temperature dry drilling. This correlation between thrust force and exit delamination observed in the work reported here was opposite to the findings by other researchers. It has been reported by other researchers [16, 22, 23, 85, 120, 126] that the thrust force produced when drilling CFRPs has a positive correlation with the size of push-down (exit) delamination showing that the higher the thrust force the larger the diameter or area of delamination was produced. For this reason, it is proposed that the different amount of thrust force would not be the factor contributing to the different amount of exit delamination damage produced for cryogenic and room temperature dry drilling. The author proposes that the variation in strength and stiffness of CFRPs with temperature, which will affect the resistance to delamination damage of the plaque, would be the factor that mainly contributed to a reduction in delamination observed when drilling with cryogenic cooling as compared to the room temperature dry drilling.

It has been proposed by other researchers [3, 85, 88, 120, 127] that exit delamination produced when drilling CFRPs dominantly occurred by a mode I (opening) fracture mechanism as a result of plate bending due to push-down thrust force. From a delamination model proposed by Hocheng and Dharan [120], Tsao and Chen [127], and Jain and Yang [88], it can be stated that an increase in resistance to bending fracture of CFRP plaque would result in more resistance to delamination damage due to higher critical thrust force for the onset of delamination. In addition to bending strength, interlamina fracture strength in bending-opening mode also determines resistance to delamination damage [3, 4, 8]. Sheikh-Ahmad [4] and Di Paolo *et al.* [196] proposed that exit delamination occurred in mode I (opening) and mode III (shearing) fracture modes as a result of bending, tearing and twisting of the laminates. As a consequence, interlamina shear fracture strength of the plaque also determines the resistance to delamination damage [4, 196]. As discussed in detail in Section 6.4.1, matrix-dominant properties such as bending fracture strength and interlamina shear strength and stiffness of CFRPs increased as temperature decreased [5, 189-191]. This increase in matrix-dominant properties of CFRPs with decreasing temperature indicates an increase in strength of epoxy matrix as temperature decreased. The stronger epoxy matrix would provide a more rigid support for the plaque to withstand load acting between

laminates, hence results in an increase in interlamina fracture strength as reported by other researchers [190, 194, 195]. The higher bending fracture strength, interlamina fracture strength and interlamina shear strength and stiffness of CFRP plaque would result in higher resistance to delamination damage as mentioned previously. Based on these findings by other researchers, it is proposed that a higher level of mechanical properties controlling resistance to delamination of CFRP plaque was retained during drilling with cryogenic pre-cooling and CO_2 cooling compared to during room temperature dry drilling as a result of lower cutting temperature. As a consequence, less exit delamination would be produced when drilling with cryogenic pre-cooling and CO_2 cooling compared to room temperature dry drilling.

From the results in Sections 6.1 and 6.3 (despite the variations in the results for drilling with cryogenic pre-cooling in Section 6.3), it was found that the application of cryogenic pre-cooling and CO_2 cooling produced less internal damage and hence better quality of the machined surface compared to room temperature dry drilling while producing higher thrust force. Similar to the case of exit delamination, it is proposed that the variation in strength and stiffness of CFRPs with temperature was the main factor contributing to a reduction in internal damage observed for cryogenic drilling and better quality of the machined surface for CO_2 drilling compared to room temperature dry drilling. As previously discussed in this section, it was reported that the mechanical properties controlling resistance to delamination damage such as bending strength, interlamina fracture strength, interlamina shear strength and stiffness increased as temperature decreased [5, 188-191, 194, 195]. Since internal damage was in the form of delamination and material chip-out, which resulting from mode I (bending) and III (tearing and twisting) fracture, this indicates that resistance to internal damage increased as temperature decreased. Since cutting heat was more effectively removed by the cryogenically cooled drill and continual supply of low-temperature CO_2 gas, lower cutting temperature would be produced when drilling with cryogenic pre-cooling and CO_2 cooling compared to room temperature dry drilling. As a consequence, it is proposed that a higher level of resistance to internal damage of the plaque was retained during drilling with cryogenic cooling resulting in less internal damage and hence better quality of the machined surface compared to room temperature dry drilling.

From the opposite correlation between thrust force and drilling-induced damage reported in this research, it can be stated that application of cryogenic cooling contributed to a reduction in drilling-induced damage when drilling CFRPs by increasing the resistance to delamination and internal damage, which resulted in higher critical thrust force at which damage occurs, rather than by a reduction in thrust force. This mechanism contributing to damage reduction is similar to drilling with an exit back-up plate or with a support structure

which was reported by other researchers [26, 27, 126]. As discussed in Chapter 3, drilling with a back-up plate or support structure at the exit of the plaque resulted in higher thrust force compared to drilling without a support structure due to increased strength and stiffness of the plaque [26, 27]. However, an increase in strength and stiffness of the plaque resulted in higher critical thrust force at which delamination occurs because of higher resistance to delamination damage which was attributed to support during drilling restriction of bending and deflection of the plaque by a back-up plate or support structure at the exit. In drilling with cryogenic cooling, the higher resistance to drilling-induced damage was attributed to the retention of strength and stiffness of CFRPs at a higher level during drilling as a result of lower cutting temperatures.

6.5 Conclusion

In conclusion, drilling performance with respect to quality was improved by application of cryogenic (LN_2) pre-cooling of the tool and application of external CO_2 cooling. Less exit delamination and internal damage was produced when drilling with CO_2 cooling and with cryogenically cooled tools compared to machining dry at room temperature. This is attributed to the higher strength and stiffness of CFRP plaque that was retained, which resulted in higher resistance to delamination and internal damage, as cutting temperature was lower because cutting heat was more effectively removed. However, application of cryogenic (LN_2) pre-cooling of the tool and application of external CO_2 cooling did not improve drilling performance with respect to thrust force and tool life. They resulted in higher thrust force and tool wear compared to machining dry at room temperature. This is also attributed to higher strength, stiffness and abrasiveness of CFRP plaque that was retained when drilling with CO_2 cooling or with a cryogenically cooled tool due to the lower cutting temperature. This indicates that a reduction of drilling induced damage by application of LN_2 pre-cooling and CO_2 cooling was resulting from an increase in resistance to damage, which would result in higher critical thrust force at which damage occurs, rather than by reducing thrust force. The investigation of cutting temperature produced for drilling with CO_2 cooling and with cryogenically cooled tools and variation of behaviour and properties of CFRPs with changing cutting temperature will be discussed in Chapter 7.

In addition, it was found that the effect of CO_2 cooling on the increase in thrust force and reduction in delamination damage compared to room temperature dry drilling was more significant at lower cutting speeds and feed rates. This effect became less significant as cutting speed and feed rate increased. This is proposed to be due to the shorter time of drilling as cutting speed and feed rate increased due to the thickness of the workpiece, which

reduced the amount of CO_2 supply to the cutting zone hence reducing cooling ability, combined with more heat generated with increasing cutting speed and feed rate.

At the same machining parameters (cutting speed of 100 m/min, feed rate of 0.06 and 0.12 mm/rev), it was found that drilling with CO_2 cooling produced similar levels of thrust force compared to drilling with LN_2 pre-cooling with difference of 2-6%. However, the results of maximum depth of internal damage through the thickness of the hole show that the lowest internal damage through the thickness of the hole and hence the best quality of the machined surface were produced by drilling with CO_2 cooling compared to other drilling processes at the same machining parameters. This indicates that drilling with CO_2 cooling was more effective in removing cutting heat compared to drilling with cryogenically cooled tools. This was due to continuous cooling of the tool and the workpiece during drilling process by continual supply of the CO_2 gas as opposed to cooling the tool only before performing the drilling process in drilling with LN_2 pre-cooling of the tool. Since the X-ray CT-scanning analysis method used in this research was still in the initial development stage, it was used to obtain only the data of maximum depth of damage through the thickness of the hole. Further development of the analysis method is suggested to be done for the analysis of damage in terms of area of damage.

Finally, abrasion was observed to be the major wear mechanism in drilling CFRP plaques with carbide tools when drilling with cryogenically cooled tools and when machining dry at room temperature. This was attributed to removal of cobalt binders between tungsten carbide grains by the abrasive carbon fibres and debris, resulting in fracture of the grains next to the cobalt removal area, which further caused direct abrasion on cutting edge by these grains [109, 111, 112]. Detailed investigation of wear mechanisms for carbide tools when drilling CFRPs will be discussed in Chapter 7.

7 Discussion of the Effect of CO_2 Cooling on the Cutting Mechanism and Material Behaviour in Drilling of Carbon Fibre Reinforced Plastics

In this chapter, the effect of CO_2 cooling on the cutting mechanism and behaviour of CFRPs during conventional drilling will be discussed. The cutting mechanism and material behaviour with CO_2 cooling will be considered in relation to the results of drilling trials with cryogenic cooling, which were presented in Chapter 6. In Section 7.1, results of the measured cutting temperature when drilling CFRP plagues with CO_2 cooling and a LN_2 pre-cooled tool will be discussed in comparison to those for room temperature dry drilling to confirm a reduction in the cutting temperature. In Section 7.2, cutting mechanism and fracture behaviour of the epoxy matrix in CFRP plaques when drilling with CO_2 cooling will be investigated and compared to those when machining dry at room temperature. The effect of cutting speed and feed rate on the fracture behaviour will also be considered. In Section 7.3, variations in the hardness of epoxy matrix in CFRP plaques with temperature will be discussed to determine the effect of cryogenic cooling on the properties of workpiece material, especially resistance to delamination and drilling-induced damage. Finally, the detailed investigation of the wear mechanism observed with carbide tools during drilling of CFRPs will be discussed in Section 7.4. The evidence supporting the specific mechanism of abrasive wear, which was previously discussed in Chapter 6, will be presented.

7.1 Cutting Temperature when Drilling Carbon Fibre Reinforced Plastics with Cryogenically Pre-cooled Tools, with CO_2 Cooling and Dry at Room Temperature

From the literature, the main objective for the application of cryogenic LN_2 or CO_2 cooling is to provide a reduction in the cutting temperature of the machining process [34, 38, 39, 41, 140, 145, 149, 185]. In addition, it has been proposed from the results in Chapter 6 that the lower cutting temperature when drilling with cryogenically pre-cooled tools and with CO_2 cooling was the major factor contributing to the higher tool wear and thrust force, but reduced delamination and internal damage compared to machining dry at room temperature. Therefore, the investigation of the actual cutting temperature during drilling of CFRPs with cryogenic LN_2 and CO_2 cooling was performed to confirm a reduction in the cutting temperature. In this section, results from the measurement of cutting temperature during drilling of CFRP plaques with the tools pre-cooled in LN_2, with the CO_2 cooling and room temperature dry, will be presented. The cutting temperature was measured by using the "cement-on" K-type thermocouple, which were attached on the exit side of a CFRP plaque,

as previously described in Section 5.4. The CFRP plaques used were the same type and from the same batch of those used for the drilling trial in Section 6.2 and for the analysis of damage by X-ray CT-scanning technique in Section 6.3.

Results showing the cutting temperature when drilling CFRP plaques at room temperature, with CO_2 cooling and when pre-cooled in LN_2 for 30 and 120 s at a cutting speed and feed rate of 100 m/min and 0.06 mm/rev respectively are presented in Table 7.1 and Figure 7.1. As described in Section 5.4, temperature of the drilling process for this drilling trial was measured at a distance of 1 mm away from the edge of the hole. As a consequence, it should be noted that the measured cutting temperatures for these drilling trials, which are presented in Table 7.1 and Figure 7.1, did not represent the actual temperatures at the cutting edges of the drill. It is expected that the actual cutting temperatures at the cutting edges of the drill will be higher than the measured values presented in Table 7.1 and Figure 7.1 which were measured 1 mm away from the edge of the hole. Although the results of measured cutting temperatures in Table 7.1 and Figure 7.1 do not represent the actual temperatures at the cutting edge of the drill, the author proposes that the results of the measured cutting temperatures in Table 7.1 and Figure 7.1 was still justified to be used for the evaluation and comparison of the cutting temperatures for different drilling processes. This is because the distance between the edge of the hole and the tip of thermocouple was constant for all drilling processes. The results in Table 7.1 and Figure 7.1 were used as an indication of the effect of CO_2 cooling and cryogenic pre-cooling of the tool on cutting temperatures as compared with room temperature dry drilling.

Table 7.1: Results showing the maximum cutting temperature generated by room temperature dry drilling, CO_2 drilling, and drilling with cryogenic LN_2 cooling of the tool for 30 and 120 s of CFRP plaque

Drilling Temperature at a Cutting Speed of 100 m/min and Feed rate of 0.06 mm/rev		
Machining Condition	Max. Cutting Temp. (°C)	Reduction of Temp. (compared to room temperature dry)
Room Temperature Dry	85	
CO_2 Cooling	62	27%
LN_2 Pre-Cooling (30 s)	73	14%
LN_2 Pre-Cooling (120 s)	65	24%

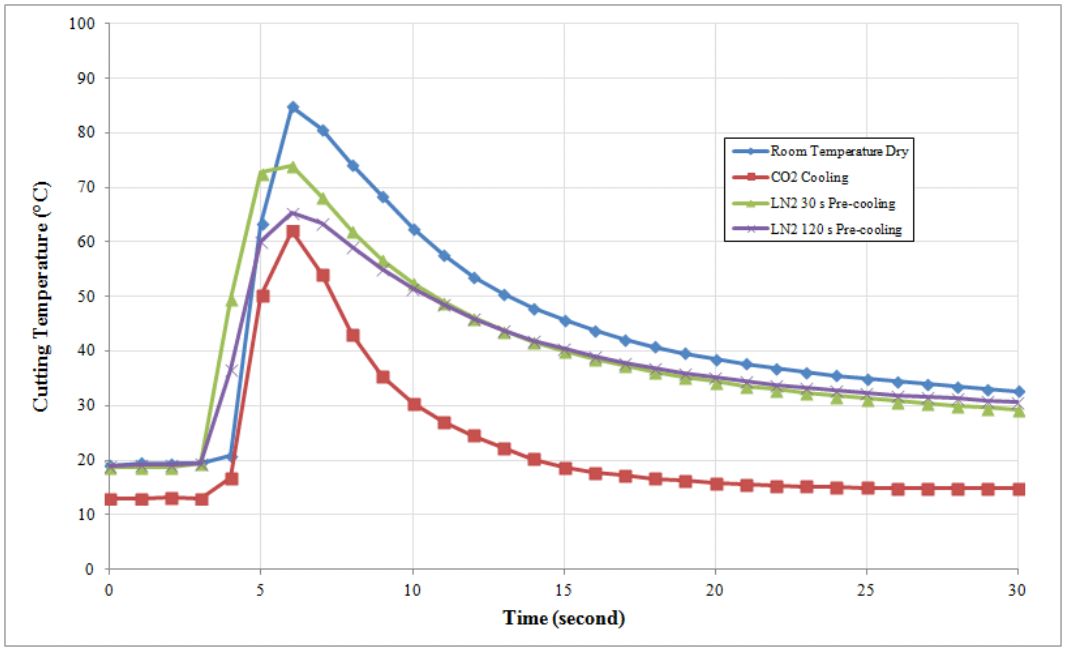

Figure 7.1: Variation of cutting temperature generated by room temperature dry drilling, CO_2 drilling and drilling with cryogenic LN_2 cooling of the tool for 30 and 120 s of CFRP plaque at a cutting speed of 100 m/min and feed rate of 0.06 mm/rev

In Figure 7.1, it is shown that the highest maximum cutting temperature was produced when drilling dry at room temperature, followed by cryogenic LN_2 drilling (30 and 120 s cooling time respectively) and the lowest by CO_2 drilling. The maximum cutting temperature for room temperature dry drilling was 85°C, while it was reduced to 73°C, 65°C and 62°C when drilling with a tool pre-cooled in LN_2 for 30 and 120 s and with CO_2 cooling respectively, Table 7.1. This shows that the maximum cutting temperature could be reduced by 14%, 24% and 27% when drilling with cryogenically pre-cooled tools (30 and 120 s cooling time) and with CO_2 cooling respectively compared to room temperature dry drilling, indicating a more effectiveness in removing cutting heat by application of CO_2 cooling or LN_2 pre-cooling compared to room temperature dry drilling. As previously discussed, the measured maximum cutting temperatures for these drilling trials do not represent the actual temperatures at the cutting edge of the drill. Hence, the results showing percentage reduction of cutting temperature by application of cryogenic cooling as compared with room temperature dry drilling which are discussed in this section, Table 7.1, do not represent the actual reduction of cutting temperature by cryogenic cooling. These results are used as an indication of a benefit in cutting temperature reduction by application of cryogenic cooling when drilling CFRPs rather than providing data of the actual quantity of a reduction in cutting temperature as a result of cryogenic cooling.

From the results in Table 7.1 and Figure 7.1, it was found that application of external CO_2 cooling was more effective in reducing cutting temperature than cryogenic pre-cooling

of the tool with LN_2. As discussed previously in Chapter 6, the tool could be cooled down to -70°C after submerging in LN_2 for 30 s, which was similar to temperature of the CO_2 gas exiting the nozzle of the CO_2 cooling system [166]. However, it is shown in Table 7.1 that drilling with CO_2 cooling produced 15% lower maximum cutting temperature than drilling with a 30 s cryogenically pre-cooled tool, indicating the increased effectiveness of the CO_2 cooling in removing the cutting heat as compared to cryogenic pre-cooling of the tool for 30 seconds. As previously discussed in Section 6.3.2, it is proposed that this was because of the different methods of cooling the cutting zone between the two cooling processes. In cryogenic pre-cooling in this research, the tool was cooled by submerging in LN_2 before the drilling process was performed. After being cooled for a certain time, the tool was used to perform the drilling without further cooling during the drilling process. From this method of cooling, the temperature of the pre-cooled tool would increase while the tool travelled from the cooling liquid (polystyrene cups filled with LN_2) to the cutting zone, resulting in lower capability to remove the cutting heat. In addition, there was no cooling of the workpiece during the cutting process. In contrast, the CO_2 cooling system removed the cutting heat by continually supplying low-temperature CO_2 gas to the cutting zone, which cooled the tool and the workpiece during the drilling process. This continued cooling of the drill and workpiece during the cutting process by CO_2 gas can be seen from the progress of the measured cutting temperature in Figure 7.1 showing that the temperature of the plaque when drilling with CO_2 cooling was already lower than when drilling with cryogenically cooled tools before the drill engaged the plaque and after the drilling process was completed. This cooling of the workpiece during the cutting process contributed to the higher capability to remove the cutting heat with CO_2 cooling compared to cryogenic pre-cooling of the tool hence resulting in a lower maximum cutting temperature.

However, it is shown in Table 7.1 and Figure 7.1 that the effectiveness in reducing the cutting temperature for cryogenic pre-cooling of the tool could approach that for CO_2 cooling as the submerging time was increased to 120 seconds. The difference between the maximum cutting temperatures for CO_2 drilling and the drilling with a cryogenically pre-cooled tool was decreased to 5% as a result of increased cooling time. This higher capability to reduce the cutting temperature as compared to the 30 s cryogenic pre-cooling was due to the lower temperature of the drill as it was submerged longer in LN_2. After being submerged in LN_2 for 120 s, the drill was cooled to LN_2 temperature (-196°C) as it was observed that there was no bubbling of LN_2 in the polystyrene cups. Although increasing pre-cooling time to 120 s could reduce the maximum cutting temperature to similar levels for that of the CO_2 cooling, it is still suggested that the application of external CO_2 cooling was more cost-effective and more practical to be used in the production process in industry than the

cryogenic LN_2 pre-cooling of the tool. The pre-cooling of the tool for 120 s before drilling would result in additional time for drilling process and hence additional cost for producing the final CFRP components when compared to the in-process CO_2 cooling.

Using through-tool LN_2 cooling would be a more cost-effective and more practical option than LN_2 pre-cooling of the tool due to an in-process and more precise cooling of the cutting zone with reduced quantity of LN_2. Low-temperature LN_2 (-196°C) supplied through the cutting tool will turn the tool into a heat sink which effectively removes heat from the cutting zone. In addition, the author proposes that through-tool CO_2 cooling would be more effective in reducing the cutting temperature compared to external CO_2 cooling used in this research. This is because cooling would be carried out more precisely and continuously to the cutting zone by liquid CO_2 or CO_2 gas which expands near the cutting edges when cooling with through-tool method. In external CO_2 cooling, CO_2 gas was supplied to the cutting zone from the top of the laminate which would result in inconsistent cooling through the thickness of the plaque, especially at the exit where maximum temperature is produced. The variation in cooling effect through the thickness of the plaque which affects fracture mode of CFRP through the thickness will be discussed in Section 7.2. A disadvantage of inconsistent cooling through the thickness would be more pronounced when drilling a thicker plaque. Due to the lower temperature of LN_2 compared to CO_2 which results in a colder cutting tool (heat sink), it is proposed that through-tool LN_2 cooling would provide higher capability in reducing cutting temperature than through-tool CO_2 cooling. Evaluation of drilling performance of CFRPs using through-tool LN_2 is suggested to be done and compare with through-tool CO_2 cooling. In addition, the effect of the extremely low temperature of LN_2 on the properties of the cutting tool and workpiece material is suggested to be investigated due to the concern of possible damage to the cutting tool and workpiece material when they are exposed to the extreme temperature of LN_2.

Considering the results of thrust forces previously presented in Figures 6.33 and 6.34 in Section 6.3.1, it is shown that drilling with CO_2 cooling produced only 5-6% difference of thrust forces as compared to drilling with 120 s cryogenic pre-cooling at a cutting speed and feed rate of 100 m/min and 0.06 mm/rev. It is proposed that this insignificant difference of thrust forces result from a similar level cutting temperature produced for CO_2 drilling and drilling with 120 s cryogenic pre-cooling, for which the difference was 5%, at the same machining parameters. It is also shown in Figures 6.33 and 6.34 that there was no significant difference between thrust forces for CO_2 drilling and drilling with a 30 s cryogenically pre-cooled tool, for which the difference was only 2-3%. However, the maximum cutting temperature for the CO_2 drilling was measured to be 15% lower than that for drilling with a 30 s cryogenically pre-cooled tool. This indicates that the difference between the capability

to reduce the cutting temperature of CO_2 drilling and drilling with the 30 s cryogenic cooling was minimal in terms of its effect on thrust force produced by the two drilling processes (3 N of 151-154 N for the average thrust force and 6 N of 205-211 N for the maximum thrust force).

However, it was found that the difference between the capability of reducing the cutting temperature of CO_2 drilling and drilling with the 30 s LN_2 pre-cooling was more dominant in terms of its effect on the internal damage produced from the two drilling processes. In Table 6.5 and Figure 6.35 in Section 6.3.2, it is shown that less internal damage (55% less average and 58% less total depth of damage) was produced when drilling with CO_2 cooling compared to that when drilling with a 30 s cryogenically cooled tool at a cutting speed and feed rate of 100 m/min and 0.06 mm/rev. Although it is shown in Table 7.1 and Figure 7.1 that increasing pre-cooling time to 120 s could increase the capability in reducing the cutting temperature to be approaching that of the CO_2 cooling, it is shown in Table 6.5 and Figure 6.35 that drilling with CO_2 cooling produced 67% and 69% less internal damage in terms of the average and total depth of damage respectively compared to drilling with 120 s cooled tool. However, further investigation with more repetitions of the drilling trial for each machining condition will be required to minimise the possible variations in the results due to the anisotropic nature of CFRPs as previously discussed in Section 6.3.

In addition, it can be seen that the maximum cutting temperature produced by dry drilling at room temperature in this drilling trial was much lower compared to that has been reported in the literature by other researchers (200-400°C depending on machining parameters and thickness of the workpiece) [32, 108, 110]. It is proposed that this was because of less thickness of CFRP plaque and lower cutting speed and feed rate used in this drilling trial. It was reported that maximum cutting temperature of 387°C was produced when dry drilling a 20 mm thick CFRP plaque with an 8 mm diameter drill at a cutting speed of 180 m/min and feed rate of 0.3 mm/rev at room temperature [32]. Brinksmeier *et al.* [110] reported that maximum temperature of 196°C was produced when drilling a 10 mm thick CFRP plaque at a cutting speed and feed rate of 120 m/min and 0.08 mm/rev respectively with a 16 mm diameter drill without cutting fluid. This indicates that the amount of heat generated and hence cutting temperature decrease as thickness of the workpiece, cutting speed and feed rate reduce as discussed in Chapter 3. Due to the thinness of the plaque (4 mm) and lower cutting speed and feed rate (100 m/min and 0.06 mm/rev), maximum cutting temperature produced by room temperature dry drilling in this trial would be lower compared to that has been reported in the literature. In addition, the lower cutting temperature measured in this drilling trial was also because the distance between cutting edge and measuring point in this drilling trial was greater than that in other researchers'

work. Cutting temperature was measured at 0.2 and 0.6 mm away from the cutting edge for the technique used by Brinksmeier *et al.* [110] and Weinert and Kempmann [32] respectively, which was closer compared to 1 mm distance for the technique used in this drilling trial. As measurement was carried out closer to the cutting zone, cutting temperature would be measured at higher value even with the same thickness of the workpiece and machining parameters.

7.2 Fracture Behaviour of Carbon Fibre Reinforced Plastics when Drilling with Cryogenically Pre-cooled Tools, with CO_2 Cooling and Dry at Room Temperature

Having confirmed a reduction in the cutting temperature by CO_2 cooling and cryogenic pre-cooling of the tool in Section 7.1, it is also important to determine how the fracture behaviour of CFRPs during the drilling process will be affected by the difference in cutting temperature. This is because material behaviour during drilling will have an effect on thrust force, tool wear and drilling-induced damage produced from the drilling process. In this section, the fracture behaviour of the carbon fibres and epoxy matrix in the plaques when drilling with CO_2 cooling and cryogenically cooled tools will be discussed and compared to that when machining dry at room temperature. The machined surface of the samples, which were produced from the drilling trials in Sections 6.2 and 6.3, were examined in the SEM. The effect of machining parameters (cutting speed and feed rate) and the change of pre-cooling time by LN_2 on the fracture behaviour of the plaque will also be discussed.

7.2.1 Effect of LN_2 Pre-cooling on Behaviour of CFRPs

It has previously been shown in Section 7.1 that the maximum cutting temperature produced when drilling CFRP plaques of the type used in Sections 6.2 and 6.3 of Chapter 6 with cryogenic pre-cooling of the tool and dry at room temperature was in the range 65-85°C at a cutting speed and feed rate of 100 m/min and 0.06 mm/rev. With this range of temperature, the fracture mechanism of carbon fibres in the plaques would not vary between room temperature dry drilling and drilling with cryogenically cooled tools. This is because it was reported that carbon fibres can maintain their strength and stiffness up to 510°C [1, 5]. Although it has been reported by other researchers that the cutting temperature produced by drilling of CFRPs could reach 200-400°C depending on the machining conditions [7, 9, 15, 16, 32], the fracture behaviour of the carbon fibres would still not be affected. The similar fracture appearance of carbon fibres on the machined surface when drilling with cryogenically cooled tools and when drilling dry at room temperature is shown in Figures 7.2-7.4. In Figures 7.2-7.4, the brittle fracture mode at the end of fibres was

observed for room temperature dry drilling and drilling with cryogenic pre-cooling. It is also shown that increasing pre-cooling time from 30 to 120 s did not produce any variation in the fracture behaviour of the fibres, Figures 7.3 and 7.4. The brittle failure mode of carbon fibres from the machining process, which was due to the graphitic crystalline structure of the fibres [1, 2, 4, 5], has also been shown by other researchers [4, 10, 76, 197]. In addition, it can be observed that increasing feed rate from 0.06 mm/rev (Figures 7.2a-7.4a) to 0.12 mm/rev (Figures 7.2b-7.4b) did not change the fracture mechanism of the fibres. This indicates that difference in thrust force, tool wear, delamination and internal damage produced by room temperature dry drilling and drilling with cryogenically cooled tools was not result of variation in behaviour of carbon fibres.

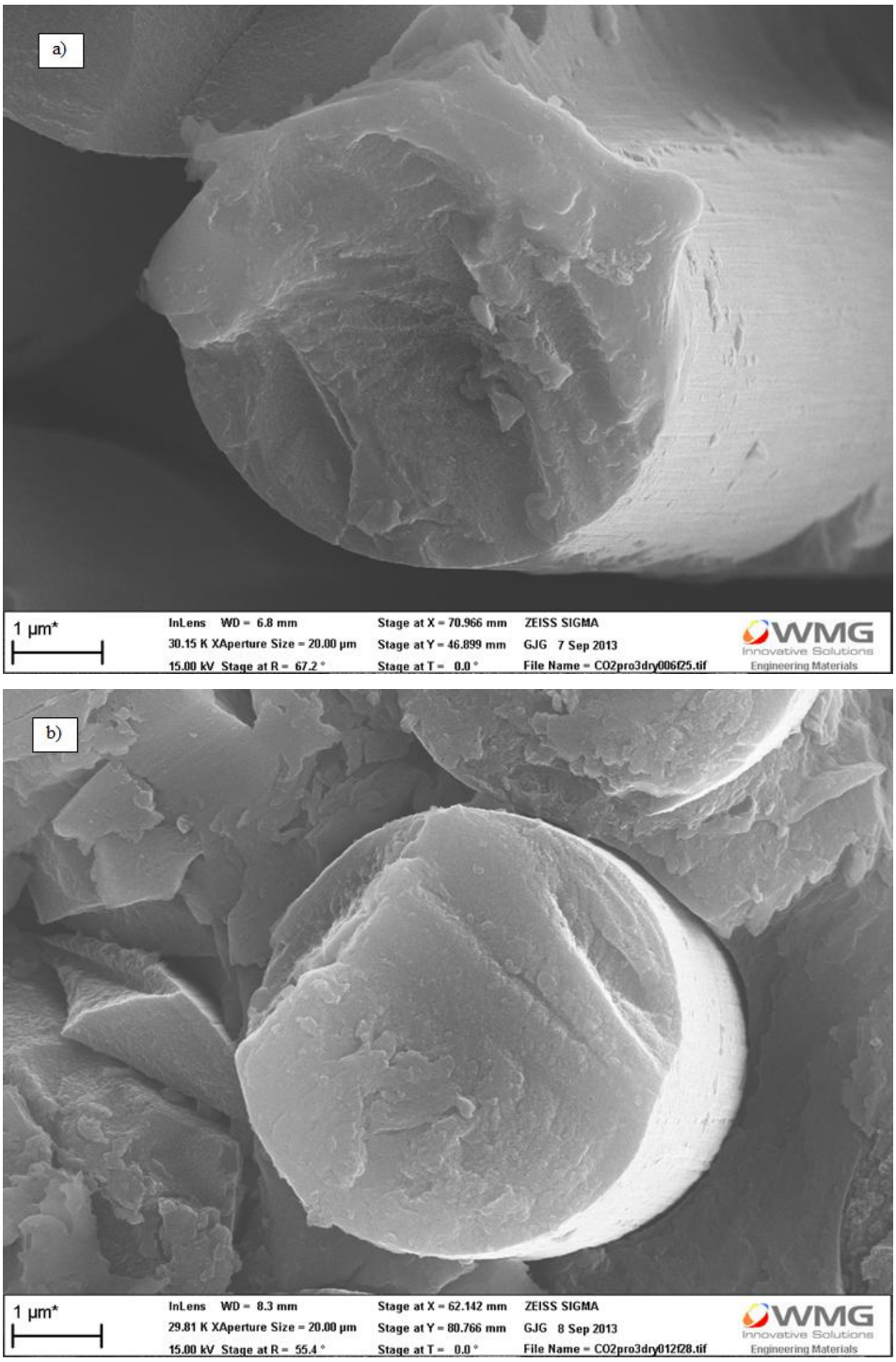

Figure 7.2: SEM images showing the brittle fracture mode of carbon fibres resulting from room temperature dry drilling at a cutting speed of 100 m/min and a feed rate of (a) 0.06 mm/rev and (b) 0.12 mm/rev

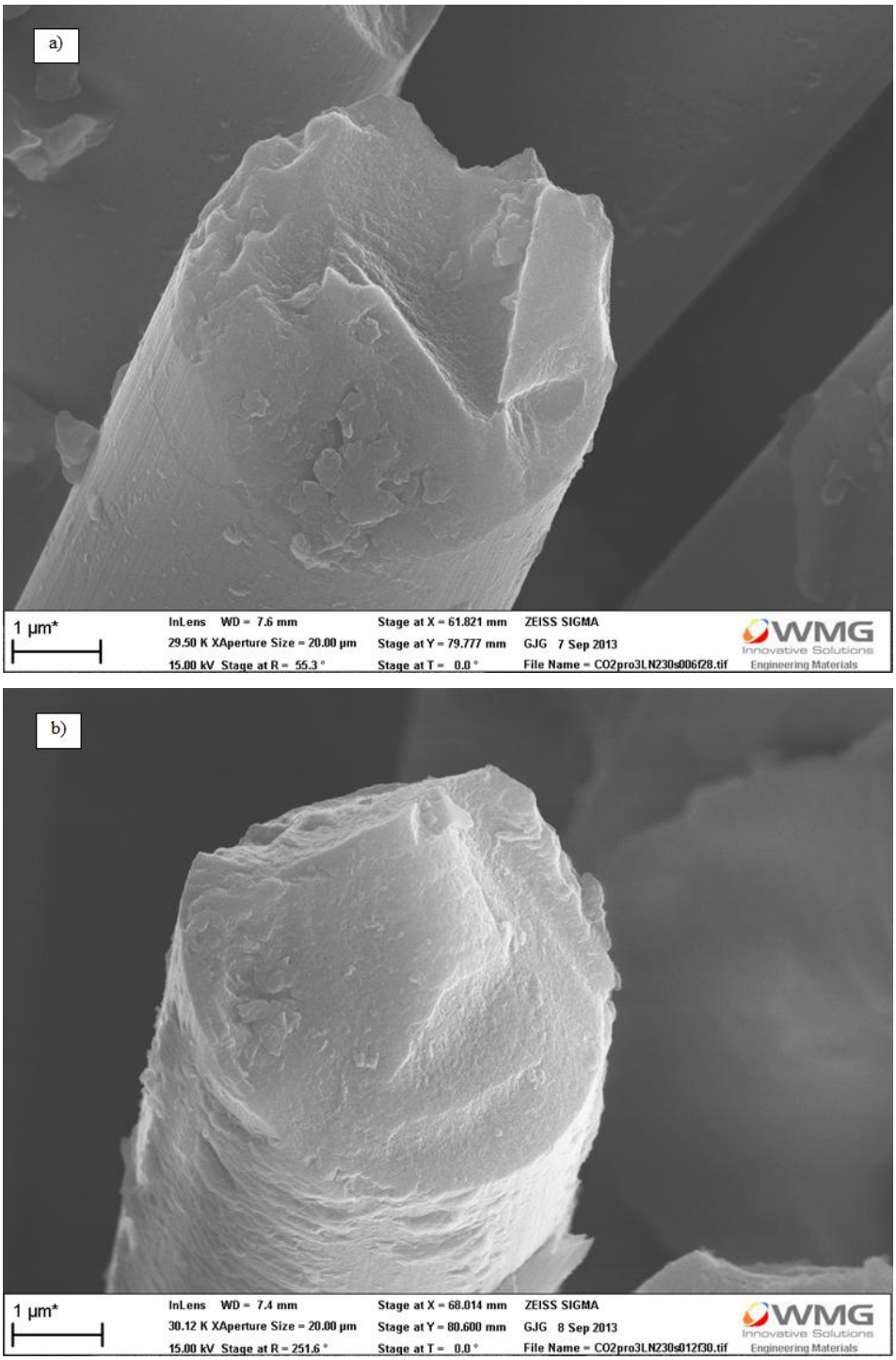

Figure 7.3: SEM images showing the brittle fracture mode of carbon fibres resulting from drilling with a LN_2 pre-cooled tool for 30 s at a cutting speed of 100 m/min and a feed rate of (a) 0.06 mm/rev and (b) 0.12 mm/rev

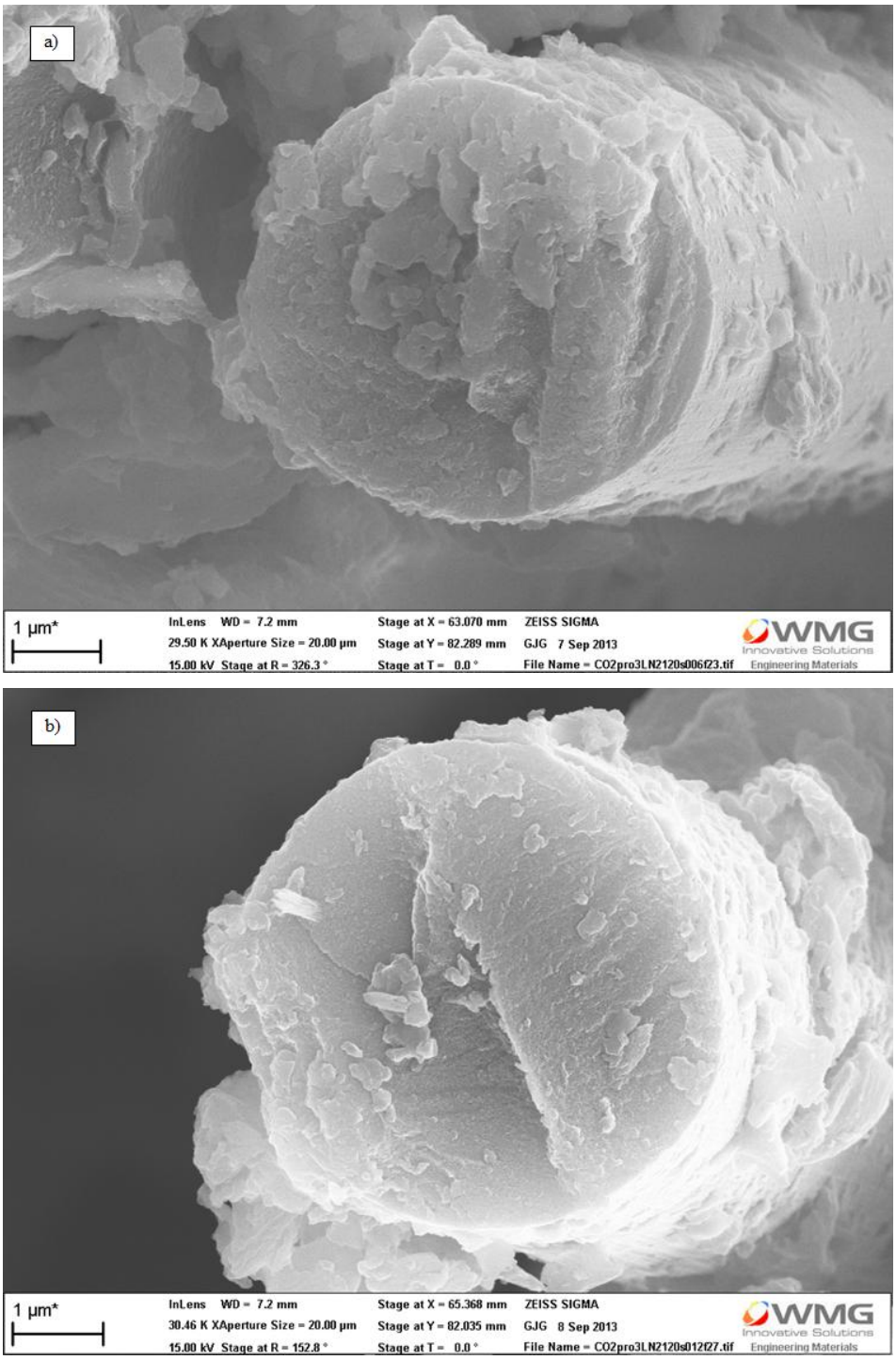

Figure 7.4: SEM images showing the brittle fracture mode of carbon fibres resulting from drilling with a LN_2 pre-cooled tool for 120 s at a cutting speed of 100 m/min and a feed rate of (a) 0.06 mm/rev and (b) 0.12 mm/rev

However, different fracture surfaces of epoxy matrix between drilling with cryogenically cooled tools and dry at room temperature can be seen, Figures 7.5-7.7. In Figure 7.5, the more rounded shape of the fractured epoxy and smooth surface as a result of smearing of epoxy on the machined surface was observed when machined dry at room temperature. This indicates that epoxy matrix underwent more ductile failure and that more

thermal softening of the epoxy had taken place when the plaque was machined dry at room temperature. In contrast, it can be seen that epoxy matrix was fractured into more angular pieces when drilling with 30 and 120 s LN_2 pre-cooled tools compared to when machined dry at room temperature, Figures 7.6 and 7.7. In addition, the smooth surface of epoxy as a result of smearing as observed in Figure 7.5 for room temperature dry drilling was not observed for drilling with cryogenically cooled tools, Figures 7.6 and 7.7. This indicates a more brittle fracture and less thermal softening of the epoxy matrix when drilling with cryogenically pre-cooled tools. More brittle fracture surface with less thermal softening of the epoxy matrix when drilling with cryogenic pre-cooling was also observed on the machined surface of CFRP plaque used for the drilling trial in Section 6.1. The more brittle behavior of epoxy during cryogenic drilling was a result of a reduction in cutting temperature by the cooled tool as it has been reported by other researchers that higher degree of brittle and glassy behaviour of epoxy occurred as temperature decreased [193-195]. However, it can be seen in Figures 7.6 and 7.7 that no significant difference between the fracture surface of epoxy for cryogenic drilling with 30 and 120 s cooling time could be observed even though the drill was cooled down to a lower temperature as cooling time was increased.

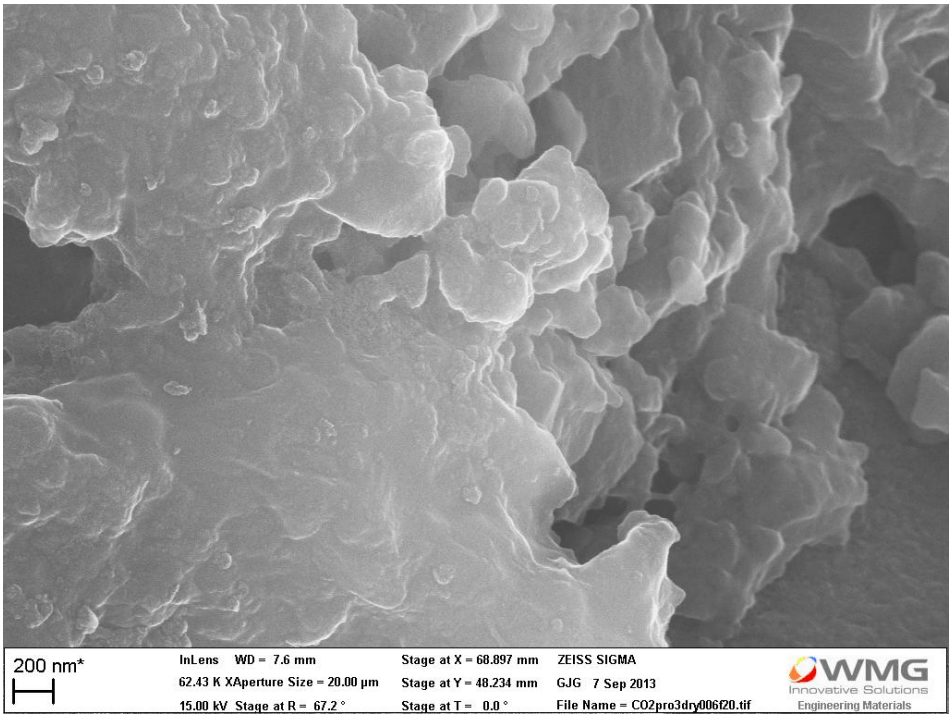

Figure 7.5: SEM image showing the more ductile fracture surface and more thermal softening of epoxy matrix on the machined surface resulting from room temperature dry drilling at a cutting speed and feed rate of 100 m/min and 0.06 mm/rev respectively

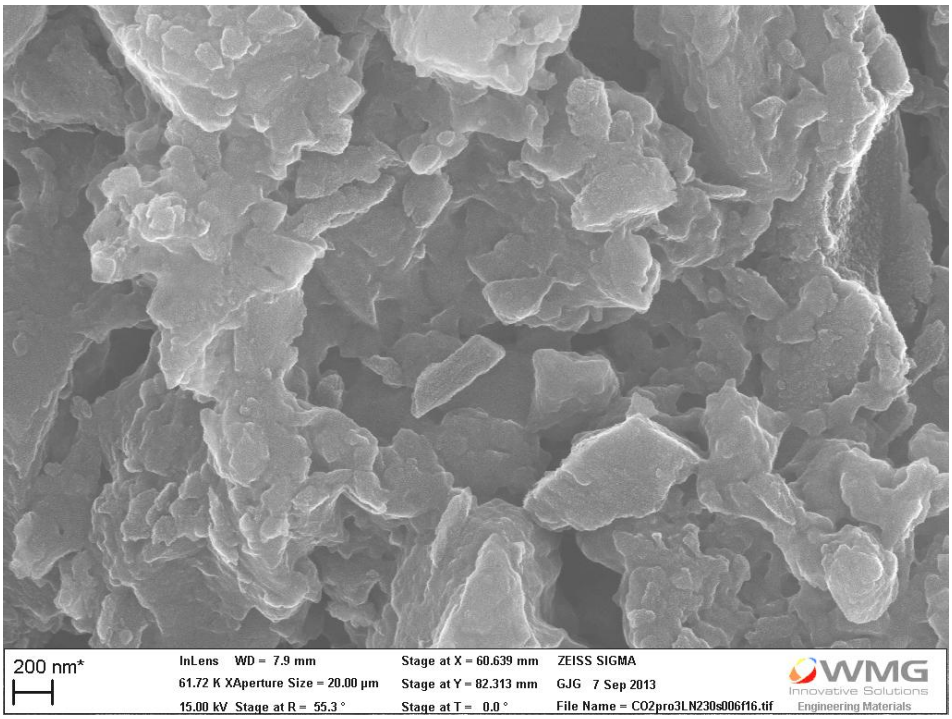

Figure 7.6: SEM image showing the more brittle fracture surface and less thermal softening of epoxy matrix on the machined surface resulting from drilling with a tool pre-cooled in LN_2 for 30 s at a cutting speed and feed rate of 100 m/min and 0.06 mm/rev respectively

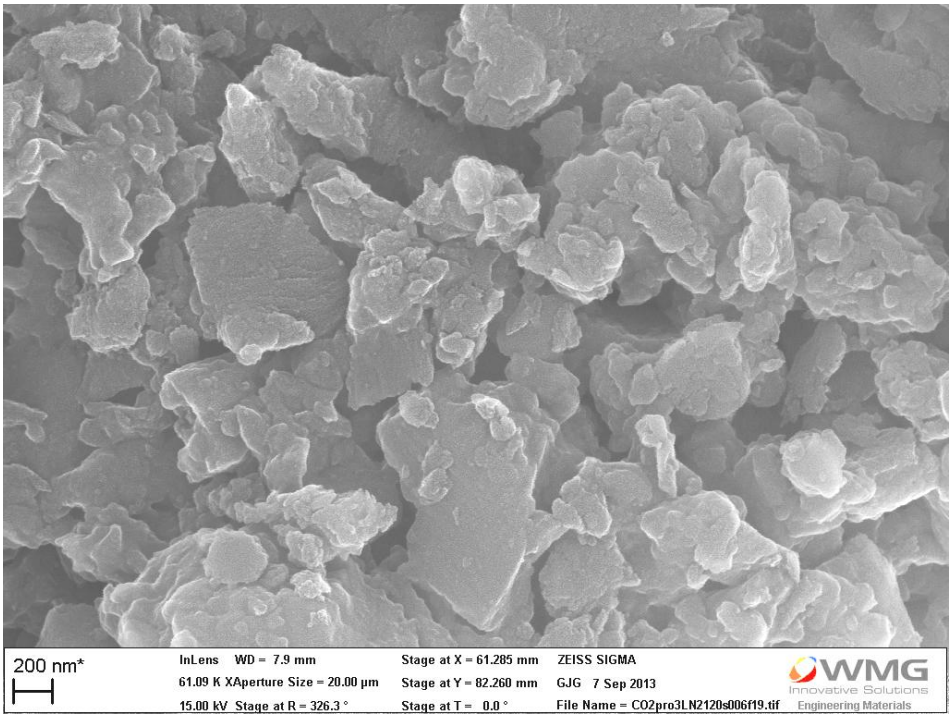

Figure 7.7: SEM image showing the more brittle fracture surface and less thermal softening of epoxy matrix on the machined surface resulting from drilling with a tool pre-cooled in LN_2 for 120 s at a cutting speed and feed rate of 100 m/min and 0.06 mm/rev respectively

As feed rate was increased from 0.06 to 0.12 mm/rev, difference in fracture surface of epoxy matrix on the machined surface between room temperature dry drilling and drilling with cryogenically cooled tools can still be seen, Figures 7.8-7.10. Again, more brittle fracture mode and less thermal softening of epoxy matrix was observed for drilling with cryogenically cooled tools, Figures 7.9 and 7.10, compared to room temperature dry drilling, Figure 7.8. Similar to a feed rate of 0.06 mm/rev, no significant difference in fracture mode of epoxy was observed for cryogenic drilling even though pre-cooling time was increased from 30 to 120 s for a feed rate of 0.12 mm/rev.

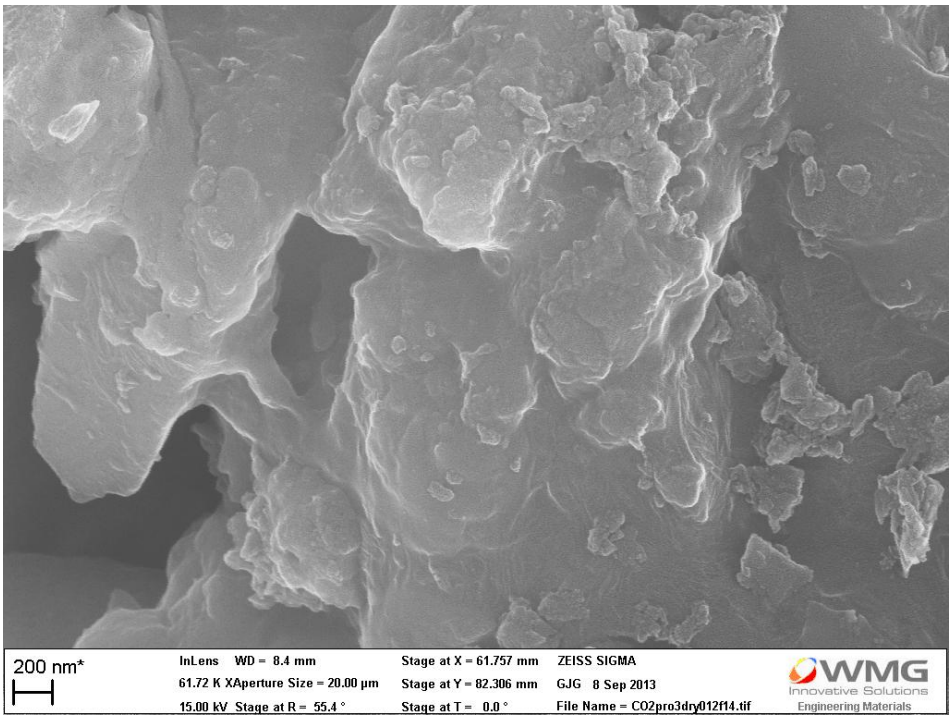

Figure 7.8: SEM image showing the more ductile fracture surface and more thermal softening of epoxy matrix on the machined surface resulting from room temperature dry drilling at a cutting speed and feed rate of 100 m/min and 0.12 mm/rev respectively

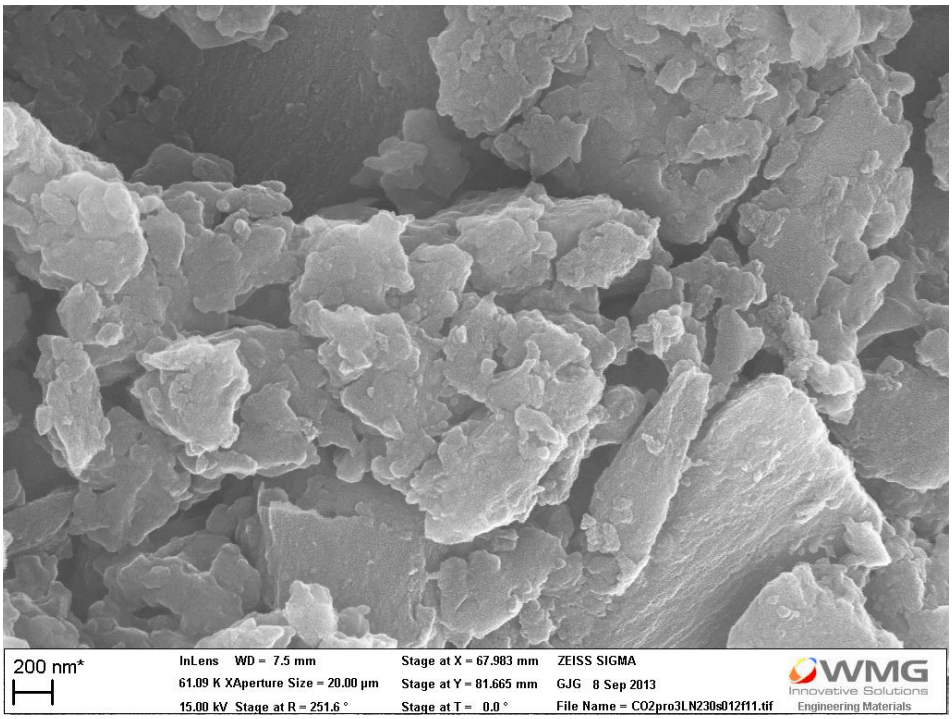

Figure 7.9: SEM image showing the more brittle fracture surface and less thermal softening of epoxy matrix on the machined surface resulting from drilling with a tool pre-cooled in LN_2 for 30 s at a cutting speed and feed rate of 100 m/min and 0.12 mm/rev respectively

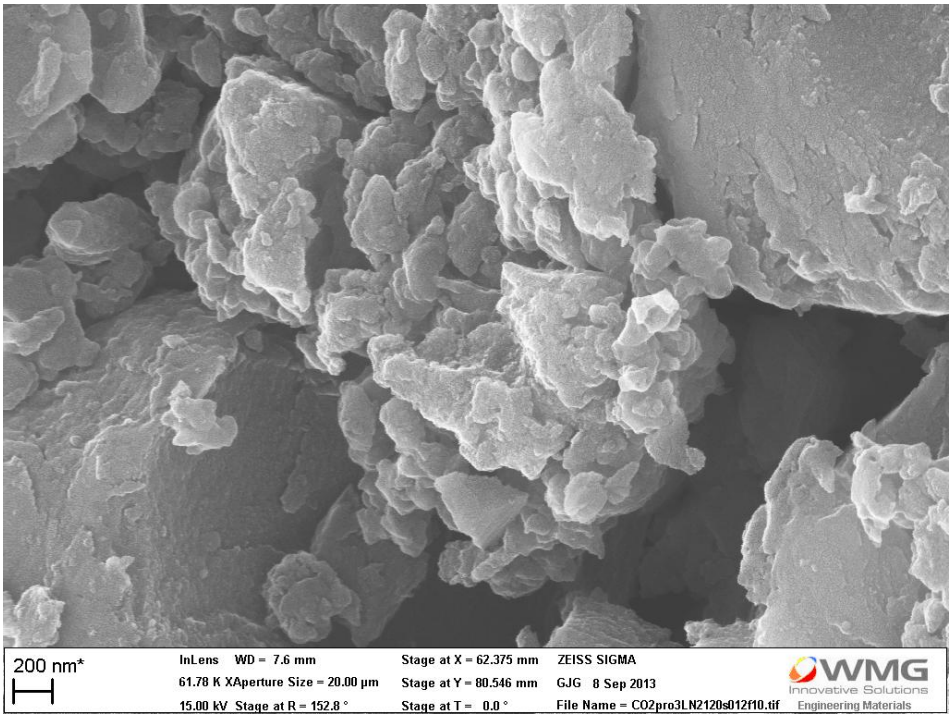

Figure 7.10: SEM image showing the more brittle fracture surface and less thermal softening of epoxy matrix on the machined surface resulting from drilling with a tool pre-cooled in LN_2 for 120 s at a cutting speed and feed rate of 100 m/min and 0.12 mm/rev respectively

Based on the findings in Figures 7.2-7.10, it can be stated that a reduction in the cutting temperature by cryogenic pre-cooling did not produce any variation in fracture mode of carbon fibres but resulted in variation in behaviour of epoxy matrix during drilling. Regardless of the increase in feed rate, more brittle fracture mode and less softening of epoxy matrix occurred during drilling with cryogenic pre-cooling as cutting temperature was reduced due to more effective heat removal by the cooled tools. The more brittle fracture surface with less thermal softening indicates that the epoxy matrix underwent more brittle and glassy behaviour and that strength and stiffness of epoxy was retained at a higher level during drilling. This justifies the proposed argument discussed in Section 6.4 that variation in strength and stiffness of epoxy with temperature was the major factor contributing to an increase in thrust force and tool wear but a reduction in delamination and internal damage when drilling with cryogenically cooled tools compared to drilling dry at room temperature. Since it was found that no significant variation in fracture behaviour of epoxy for drilling with 30 and 120 s pre-cooled tool for feed rates of 0.06 and 0.12 mm/rev, strength and stiffness of epoxy would be maintained at a similar level in the two drilling processes. This can be justified as the reason for an insignificant increase in thrust force produced as the time for submerging the tool in LN_2 was increased from 30 to 120 s for feed rates of 0.06 and 0.12 mm/rev as discussed in Section 6.3.1.

Although more brittle fracture appearance of epoxy on the machined surface was observed for the sample produced by drilling with cryogenic pre-cooling, it was found that the machined surface at a distance closer to the exit of the same sample showed brittle fracture surface with more ductile-like characteristics, Figure 7.11. It can be seen in Figure 7.11 that epoxy matrix was fractured into small pieces but more rounding and greater amount of epoxy smearing was observed compared to that of the sample shown in Figure 7.6. This shows more ductile behaviour of epoxy in Figure 7.11 compared to that in Figure 7.6 even though the behaviour of epoxy matrix in this sample was observed as more brittle and glassy than that in the sample produced by room temperature dry drilling, Figure 7.5. This indicates a variation in the cooling effect of the application of LN_2 cooling through the thickness of the plaque for which capability in cutting heat removal by the cooled tool decreased as the drill proceeded towards the exit of the plaque. As the drill proceeds through the thickness of the plaque, more heat was generated and accumulated in the process due to the greater amount of material which had been deformed. Recall that there was no cooling of the drill or the workpiece during drilling in the application of LN_2 pre-cooling, the temperature of the drill would increase as it proceeded through the thickness of the plaque due to the greater amount of accumulated heat in the process. This resulted in a decrease in effectiveness in cutting heat removal hence more ductile fracture and smearing

of epoxy was observed on some of the machined surface closer to the exit of the plaque. This variation in cooling effect of cryogenic pre-cooling was also found when drilling with pre-cooling time of 120 s and at feed rates of 0.06 and 0.12 mm/rev. In addition, it is proposed that the decrease in effectiveness in cutting heat removal through the thickness of the plaque was one of the reasons for more severe delamination at the exit compared to the entry as resistance to delamination would decrease due to more accumulated heat when the drill proceeded towards the exit as discussed in Section 6.1.3.1.

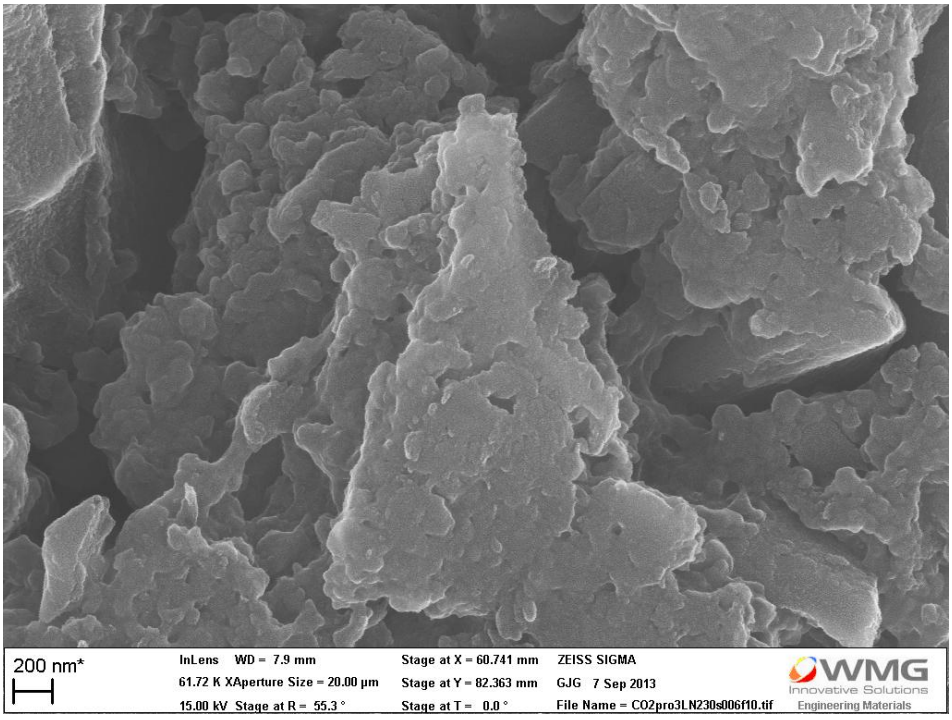

Figure 7.11: SEM image showing more ductile fracture surface of epoxy matrix on the machined surface examined at greater distance from the entry (close to the exit) of the same sample in Figure 7.6

7.2.2 Effect of CO_2 Cooling on Behaviour of CFRPs

As previously discussed in the case of LN_2 pre-cooling in Section 7.2.1, fracture mechanism of the carbon fibres would not vary between room temperature dry and CO_2 drilling since the cutting temperature for drilling CFRPs would not reach the temperature at which the strength and stiffness of the carbon fibres degrade [1, 5, 7, 9, 15, 16, 32]. The fracture appearance of carbon fibres on the machined surface resulting from CO_2 drilling is shown in Figure 7.12. Similar to that for room temperature dry drilling previously shown in Figure 7.2, the brittle fracture mode of carbon fibres could be observed on the machined surface resulting from drilling with CO_2 cooling. It was also observed that there was no difference between the fracture mode of carbon fibres on the machined surface when drilling at a feed rate of 0.06 mm/rev (Figure 7.2a and 7.12a) and at a feed rate of 0.12 mm/rev

(Figures 7.2b and 7.12b). However, some deformed epoxy adhering to the end of the machined fibre could be observed at a feed rate of 0.06 mm/rev, Figure 7.12a. This would be due to more frictional heat generated when drilling at a lower feed rate.

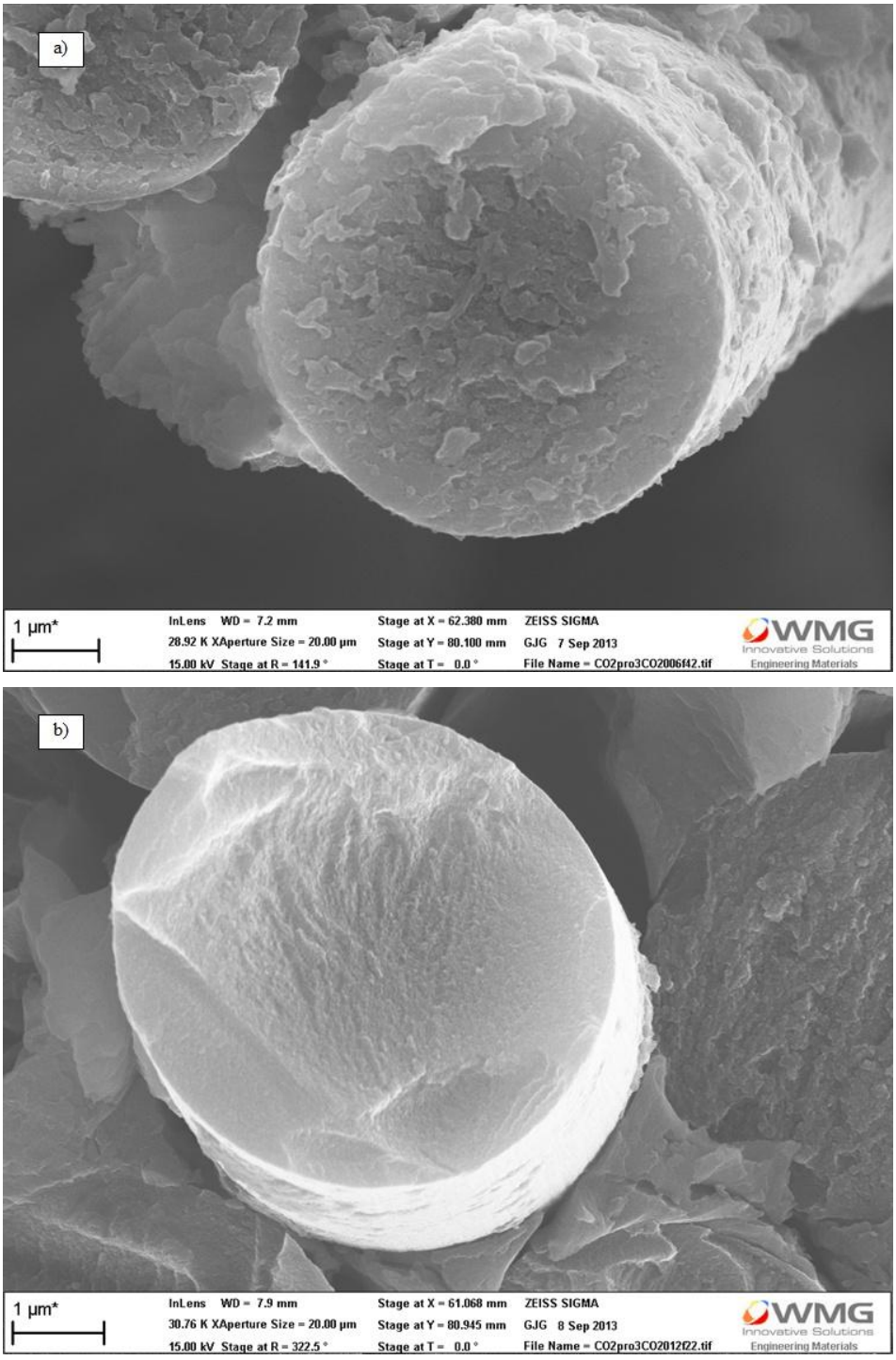

Figure 7.12: SEM images showing the brittle fracture mode of carbon fibres resulting from drilling with CO_2 cooling at a cutting speed of 100 m/min and a feed rate of (a) 0.06 mm/rev and (b) 0.12 mm/rev

The fracture behavior of the epoxy matrix on the machined surface resulting from the drilling with CO_2 cooling is presented in Figure 7.13. Comparing to room temperature dry drilling, Figure 7.5, more angular shape of fractured epoxy and less smooth surface due to smearing of epoxy was observed for CO_2 drilling, Figure 7.13, showing a more brittle fracture mode and less thermal softening of epoxy as a result of a reduction in cutting temperature similar to the effect of LN_2 pre-cooling. As discussed for cryogenic pre-cooling, the more brittle fracture appearance and less thermal softening of epoxy indicates that a higher level of strength and stiffness of epoxy matrix was retained during drilling with CO_2 cooling. This justifies the proposed argument discussed in Section 6.4 that higher thrust force and less delamination and internal damage were produced by CO_2 drilling compared to drilling dry at room temperature as a result of higher strength and stiffness of CFRPs being retained. It can also be seen that no significant difference in the fracture surface of epoxy matrix between drilling with LN_2 pre-cooling (30 and 120 s cooling time) and CO_2 cooling at the same machining parameter was observed, Figures 7.6 and 7.13. It is proposed that this was a reason for a similar level of thrust force for drilling with CO_2 cooling and LN_2 pre-cooling despite the difference in cooling ability between the two cooling techniques as shown in Sections 6.3 and 7.1.

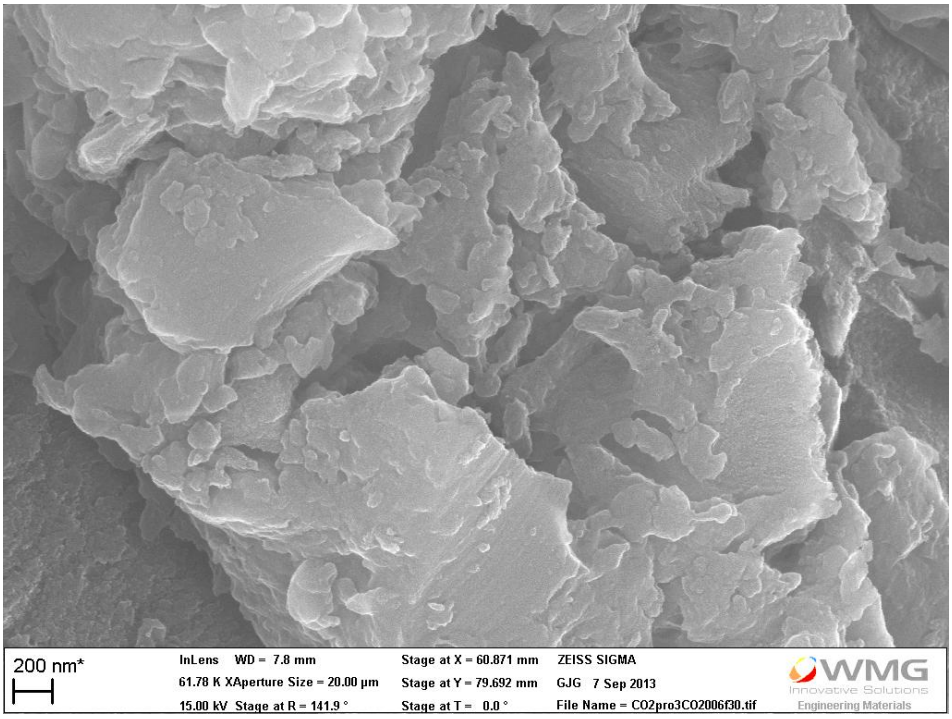

Figure 7.13: SEM image showing the more brittle fracture appearance and less thermal softening of epoxy matrix on the machined surface resulting from drilling with CO_2 cooling at a cutting speed and feed rate of 100 m/min and 0.06 mm/rev respectively

Similar to LN_2 pre-cooling, variation in behaviour of epoxy matrix through the thickness within the same sample when drilling with CO_2 cooling could be observed. The fracture surface of epoxy on the machined surface examined at a distance closer to the exit of the same sample shown in Figure 7.13 is presented in Figure 7.14. In Figure 7.14, it can be seen that epoxy matrix was fractured into small pieces without significant smooth surface of epoxy smearing. However, the shape of fractured epoxy was more rounded compared to that in Figure 7.13. This shows brittle fracture surface with more ductile-like characteristics compared to that in Figure 7.13. The variation of the fracture surface through the thickness of the plaque could also be observed in CO_2 drilling with other machining parameters. This indicates a variation in cooling ability of the application of CO_2 cooling through the thickness of the plaque for which effective in cutting heat removal reduced as the drill approached the exit of the plaque similarly to the application of LN_2 pre-cooling as discussed in Section 7.2.1. Since CO_2 gas was supplied from the entry of the plaque in the application of external CO_2 cooling in this research, the tool and the workpiece would be cooled to a lower temperature in the closer to the entry compared to that closer to the exit of the plaque. Combined with the more accumulated heat as the drill proceeded through the thickness of the plaque, this resulted in lower capability in cutting heat removal during drilling at the exit compared to that at the entry and hence resulted in more ductile fracture appearance on some of the machined surface close to the exit of the plaque.

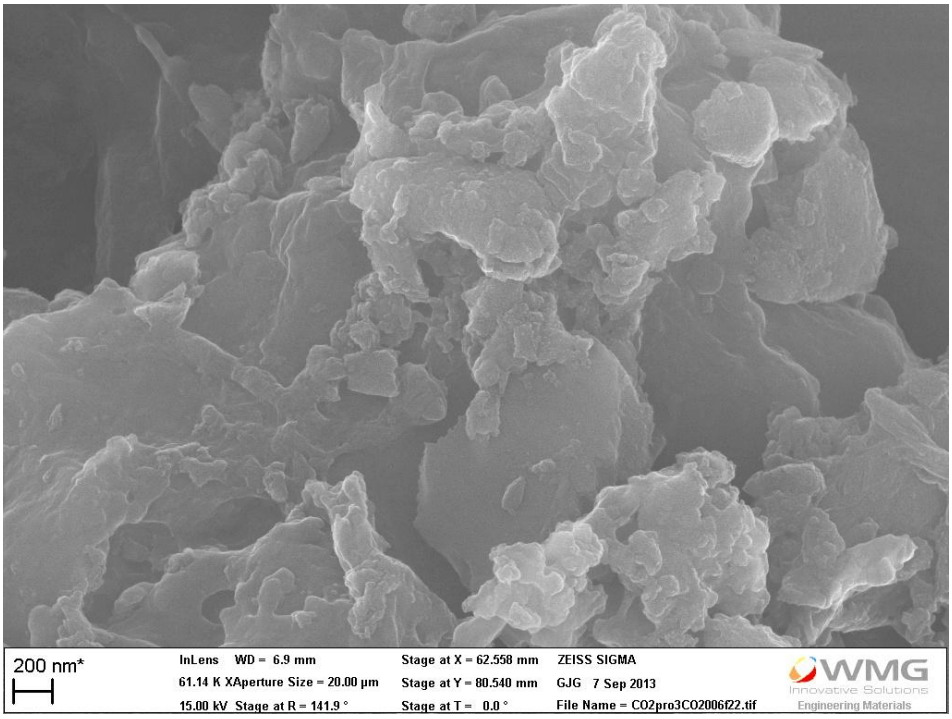

Figure 7.14: SEM image showing the more ductile fracture surface of epoxy matrix on the machined surface examined at greater distance from the entry (close to the exit) of the same sample in Figure 7.13

As proposed in Section 7.1, the variation in cooling effect through the thickness of the plaque in the application of external CO_2 cooling and LN_2 pre-cooling in the work reported here would be reduced by using through-tool CO_2 or LN_2 cooling. In through-tool cryogenic cooling, the drill is continuously cooled by the supply of cryogen through the tool to the cutting zone during drilling. This would result in more consistent cooling effect through the thickness of the plaque compared to external CO_2 cooling which directs cryogen from the top laminate and pre-cooling of the tool by LN_2 before drilling.

7.2.2.1 Influence of Feed Rate on the Effect of CO_2 Cooling on Behaviour of Epoxy

Comparison of fracture surface of the machined surface resulting from room temperature dry drilling and drilling with CO_2 cooling at a cutting speed of 100 and 150 m/min and feed rates of 0.03 and 0.09 mm/rev are presented in Figures 7.15-7.18. At a feed rate of 0.03 mm/rev, significant difference between the fracture surfaces of epoxy matrix resulting from drilling with CO_2 cooling and dry at room temperature could be observed at both cutting speeds (100 and 150 m/min), Figures 7.15 and 7.17, showing more brittle behaviour and less thermal softening of epoxy when drilling with CO_2 cooling. As the feed rate was increased to 0.09 mm/rev, the difference between the fracture surfaces of epoxy matrix resulting from the two drilling processes could still be observed, but the difference was less obvious compared to that at a feed rate of 0.03 mm/rev. It can be seen in Figures 7.16b and 7.18b that the epoxy matrix was fractured into small pieces with less smearing of epoxy (smooth surface) when drilling with CO_2 cooling. However, the shape of fractured epoxy was more rounded compared to that at a feed rate of 0.03 mm/rev showing more “ductile-like” fracture behaviour hence more similar characteristics of the machined surface resulting from room temperature dry drilling, Figures 7.16a and 7.18a. This trend of less obvious difference between fracture surfaces of epoxy matrix resulting from room temperature dry and CO_2 drilling also occurred as the feed rate was increased to 0.15 mm/rev.

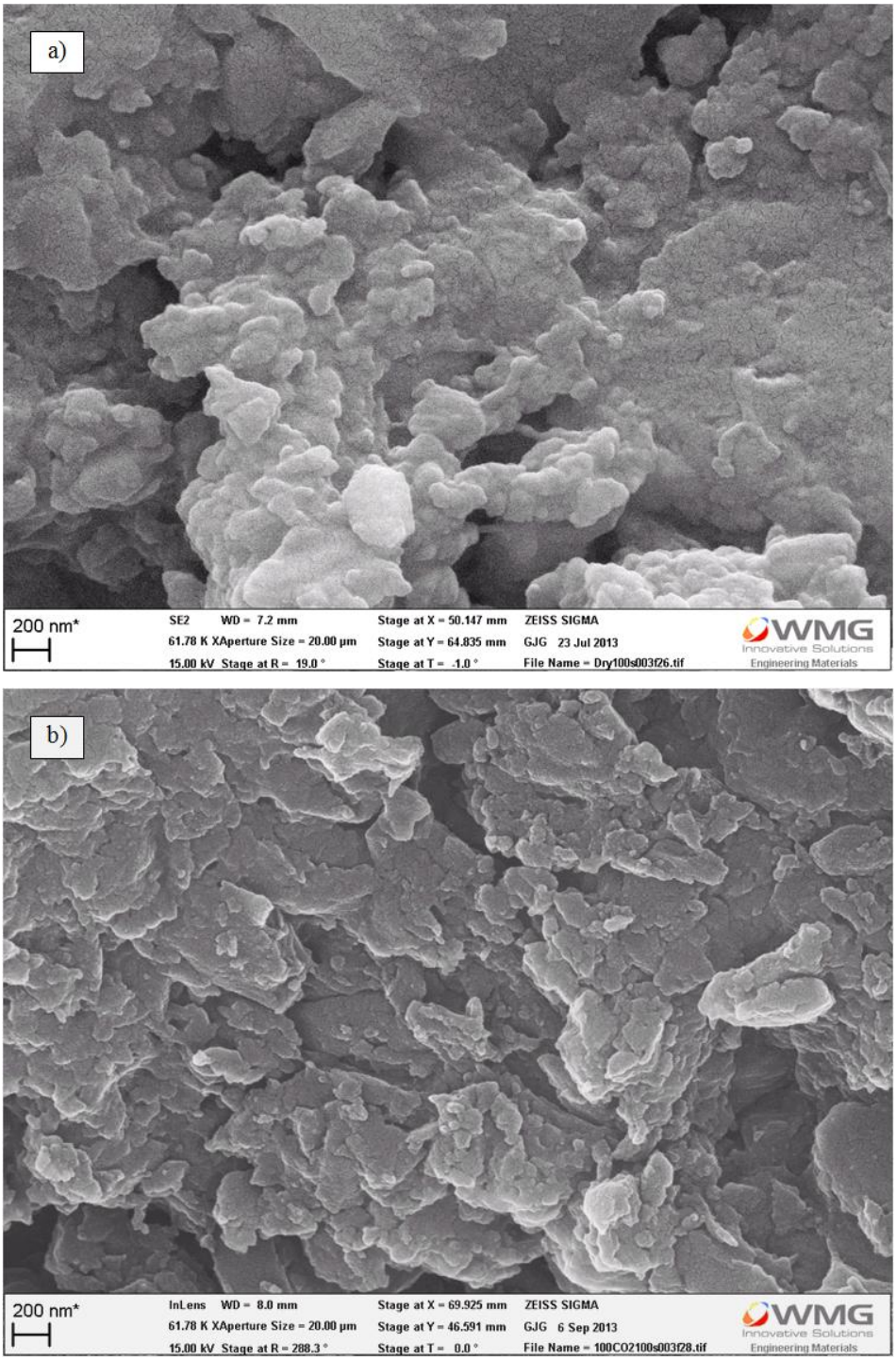

Figure 7.15: SEM images showing the fracture surface of epoxy matrix on the machined surface of CFRP plaque resulting from (a) room temperature dry drilling and (b) drilling with CO_2 cooling at a cutting speed of 100 m/min and feed rate of 0.03 mm/rev

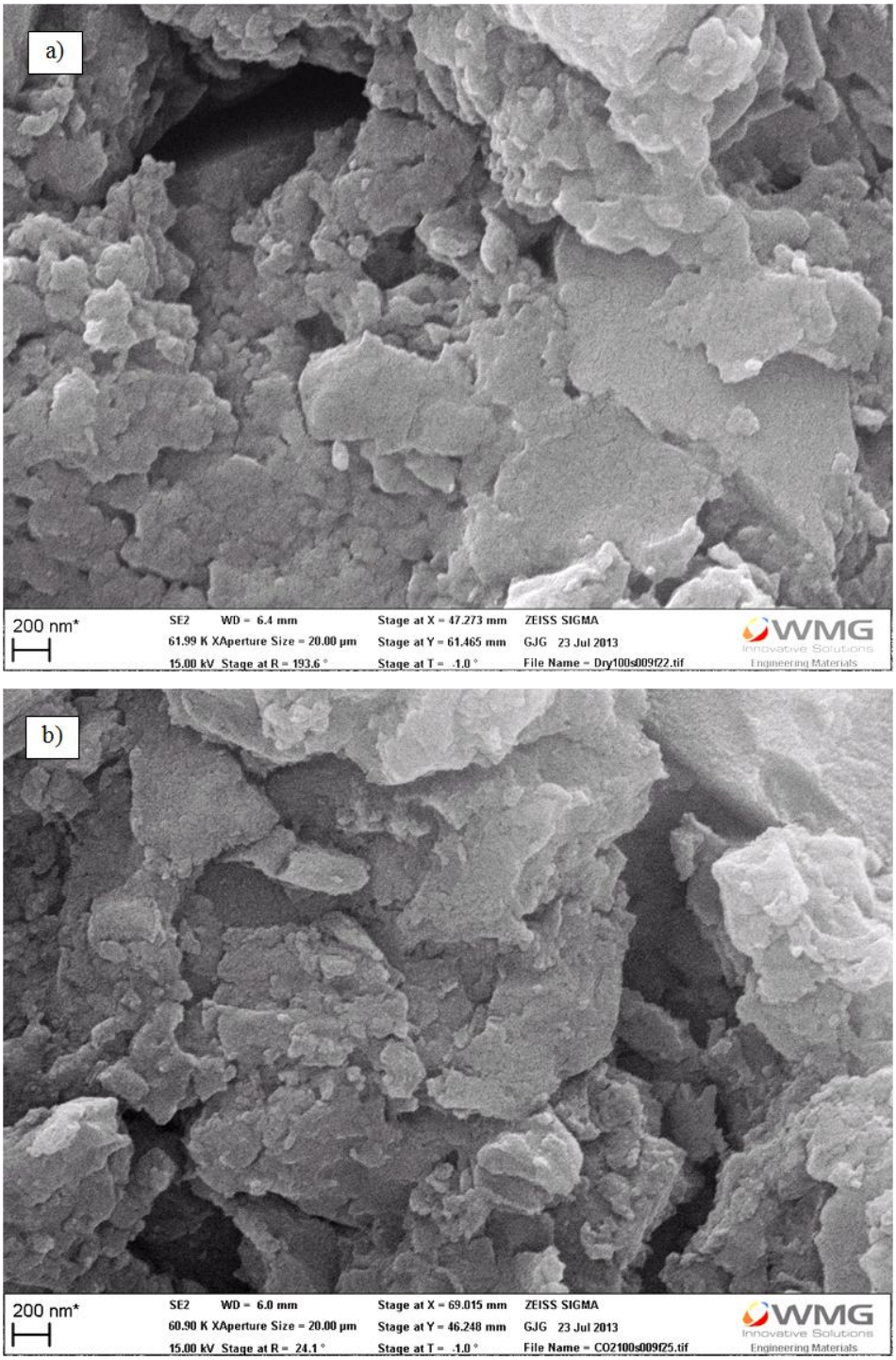

Figure 7.16: SEM images showing the fracture surface of epoxy matrix on the machined surface of CFRP plaque resulting from (a) room temperature dry drilling and (b) drilling with CO_2 cooling at a cutting speed of 100 m/min and feed rate of 0.09 mm/rev

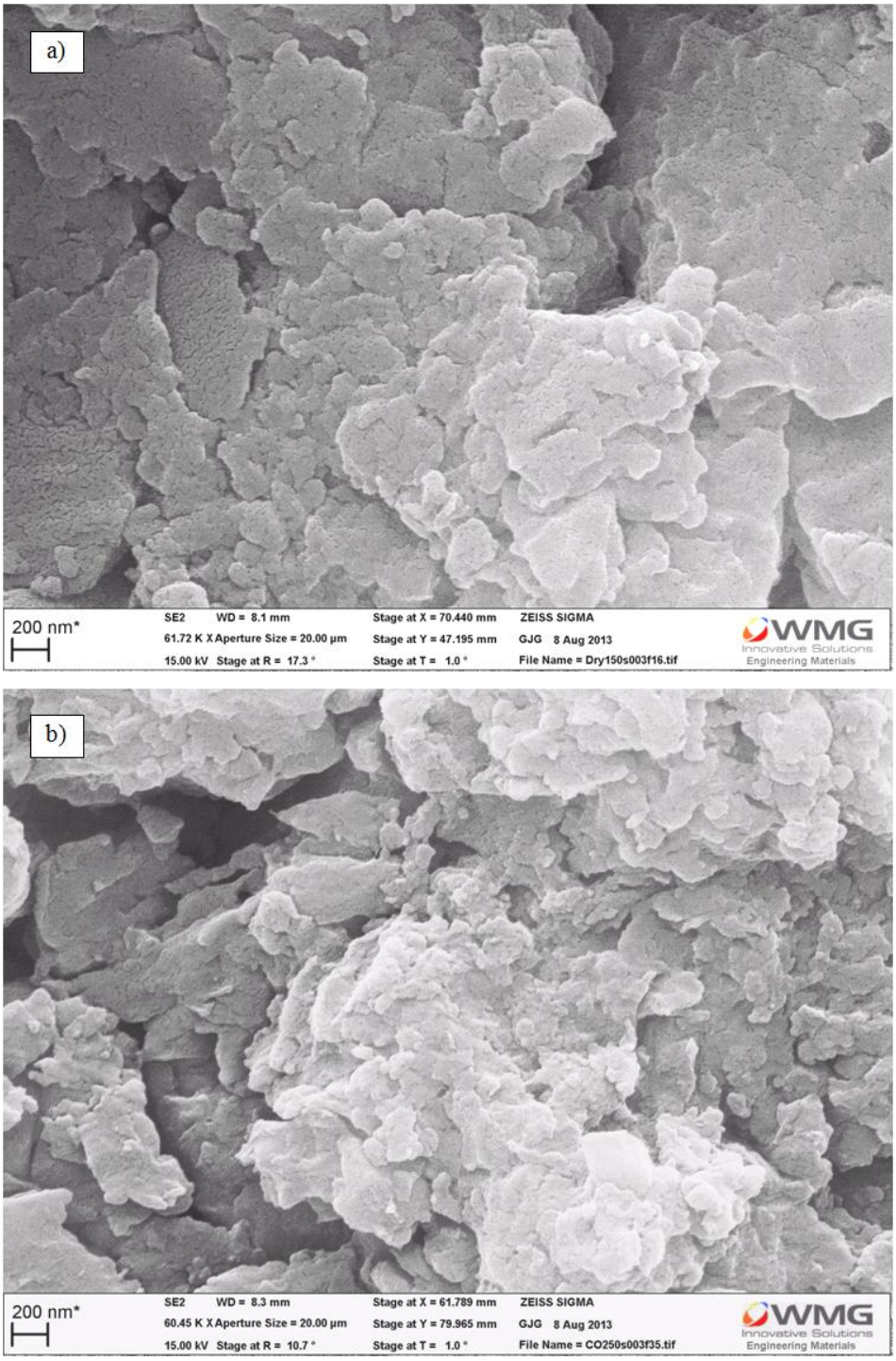

Figure 7.17: SEM images showing the fracture surface of epoxy matrix on the machined surface of CFRP plaque resulting from (a) room temperature dry drilling and (b) drilling with CO_2 cooling at a cutting speed of 150 m/min and feed rate of 0.03 mm/rev

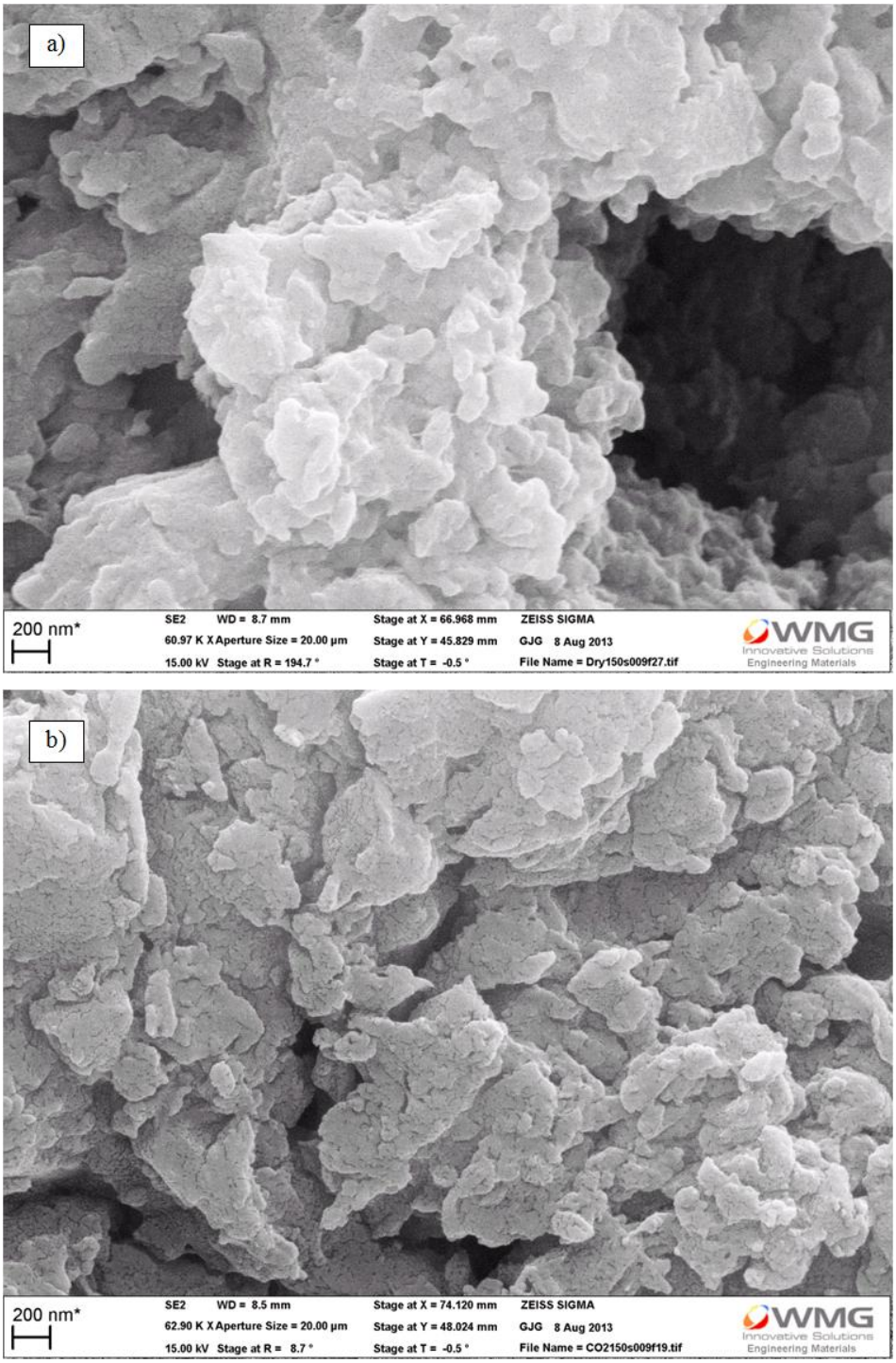

Figure 7.18: SEM images showing the fracture surface of epoxy matrix on the machined surface of CFRP plaque resulting from (a) room temperature dry drilling and (b) drilling with CO_2 cooling at a cutting speed of 150 m/min and feed rate of 0.09 mm/rev

As previously discussed in Sections 7.2.1 and 7.2.2, the difference in behaviour and fracture surfaces of epoxy matrix indicates the different level of strength and stiffness of the epoxy matrix being retained during drilling. As a consequence, the more obvious difference in the fracture surfaces of machined epoxy matrix at low feed rate would result in a greater

difference in thrust force and delamination damage produced when drilling dry at room temperature and with CO_2 cooling at low feed rate compared to that at higher feed rates, which was shown in Section 6.2. As feed rate was increased, the difference in the fracture surfaces was less obvious resulting in less difference in thrust force and delamination damage produced for the two drilling processes. The less obvious difference in fracture surface of epoxy matrix for the two drilling processes at high feed rates was due to lower capability in reducing the cutting temperature by CO_2 cooling with increasing feed rate. As discussed in Section 6.2, an increase in feed rate resulted in shorter drilling time, hence the amount of CO_2 directed to the cutting zone decreased. The reduction in the amount of CO_2 supply to the cutting area resulted in lower capability in reducing the cutting temperature. Due to less cooling effect by CO_2 cooling, brittle fracture surface of the epoxy matrix with more "ductile-like" characteristics (more rounding of fractured epoxy), which was more similar to when drilling dry at room temperature, was resulted. At low feed rate, the amount of CO_2 supply to the cutting zone was sufficient to show the cooling effect as the drilling time was longer. Due to increased cooling effect, brittle fracture surface of the epoxy matrix showing more angular shape of the broken pieces without epoxy smearing compared to that at high feed rates was observed.

7.2.2.2 Influence of Cutting Speed on the Effect of CO_2 Cooling on Behaviour of Epoxy

The following discussion will be based on the fracture surfaces of epoxy matrix shown in Figures 7.15-7.18. Similar to the effect of feed rate, the increase in cutting speed resulted in less obvious difference between the fracture surfaces of epoxy matrix resulting from room temperature dry drilling and drilling with CO_2 cooling. At a feed rate of 0.03 mm/rev, the more brittle fracture and less thermal softening of epoxy matrix when drilling with CO_2 cooling compared to room temperature dry drilling could still be observed for cutting speeds of 100 and 150 m/min, Figures 7.15 and 7.17. However, the evidence indicating the different behaviours of epoxy matrix was less obvious as the cutting speed was increased from 100 to 150 m/min. At a cutting speed of 150 m/min, when drilling with CO_2 cooling, Figure 7.17b, the epoxy matrix was fractured into small pieces similar to at a cutting speed of 100 m/min but more rounding and smearing of the fractured epoxy could be observed. This shows brittle fracture surface with more "ductile-like" characteristic, which was more similar to room temperature dry drilling, Figure 7.17a. This trend of the results showing less obvious difference in fracture surface of epoxy between room temperature dry and CO_2 drilling as cutting speed was increased from 100 to 150 m/min also occurred at feed rates of 0.09 (Figures 7.16 and 7.18) and 0.15 mm/rev.

As discussed in Section 7.2.1.1, more obvious difference in fracture surfaces of epoxy matrix for room temperature dry and CO_2 drilling at lower cutting speed result in a greater difference in thrust force and delamination damage produced by the two drilling processes as a result of different levels of strength and stiffness of CFRPs being retained, as shown in Section 6.2. As cutting speed was increased, the difference in fracture surfaces of epoxy matrix for the two drilling processes was less obvious, indicating a similar level of strength and stiffness of CFRPs and resulting in a smaller difference in thrust force and delamination damage as shown in Section 6.2. Similar to the effect of feed rate discussed in Section 7.2.1.1, the less obvious difference in fracture surface and behaviour of epoxy matrix for room temperature dry and CO_2 drilling at high cutting speeds was also due to lower capability in reducing the cutting temperature by CO_2 cooling with increasing cutting speed. The reduction in cooling effect of CO_2 cooling was a result of the lower amount of CO_2 directed to the cutting zone as drilling time was reduced with increasing cutting speed.

7.3 Variations of Hardness of Epoxy Matrix in Carbon Fibre Reinforced Plastic Plaques with Changing Temperature

From the results in Section 7.2, it has been shown that drilling with CO_2 cooling or with cryogenically cooled tools resulted in a variation in fracture surface and behaviour of the epoxy matrix in CFRP plaque, indicating a variation in material properties of the epoxy matrix. As a consequence, the variation in material properties of epoxy matrix in CFRP plaques with changing temperature was investigated to find evidence supporting the discussion in Section 7.2. Micro-hardness testing of CFRP plaques was carried out to examine the hardness of epoxy matrix in the plaque at different temperatures. Although strength of the epoxy matrix was not directly examined, it is justified that the results of hardness testing are an indication of strength of the material. This is because hardness of the material is the resistance to indentation, suggesting resistance to deformation of the material due to the applied load. The methodology for the micro-hardness testing of the epoxy in the plaque was previously described in Section 5.5. The CFRP plaques used in this test were the same type and from the same batch as the plaques being used for the drilling trials in Sections 6.2 and 6.3.

Results showing the hardness of CFRP (measured at various points on the sample) with changing temperature are presented in Table 7.2. As discussed in Section 5.5, the lowest hardness value of CFRP plaque at each temperature were used to represent the variation of hardness of epoxy matrix in the plaque with changing temperature because it is expected to yield the hardness value of epoxy matrix without any contribution from carbon fibres. Therefore, the points that yielded the lowest hardness value of CFRP plaque at each

temperature in Table 7.2 were plotted against temperature to show the variation of hardness of the epoxy matrix with changing temperature, Figure 7.19. It is shown in Figure 7.19 that hardness of the epoxy decreased with a rate of 0.6 HV/°C as temperature increased from -60°C to 100°C. Referred to the results in Section 7.1, the maximum cutting temperature produced by drilling the CFRP plaque was measured at 85°C for room temperature dry drilling, 62°C for CO_2 drilling, 73°C for cryogenic drilling with 30 s pre-cooling time and 65°C for cryogenic drilling with 120 s pre-cooling time at a cutting speed of 100 m/min and a feed rate of 0.06 mm/rev. By using the rate of variation from the results in Figure 7.19, hardness of the epoxy matrix in the plaque would be 45.6 HV, 59.4 HV, 52.8 HV and 57.6 HV for room temperature dry drilling, CO_2 drilling, drilling with 30 s cryogenic pre-cooling and drilling with 120 s cryogenic pre-cooling respectively at the cutting temperature measured for each drilling process. It is shown that, during drilling with CO_2 cooling, 30 and 120 s cryogenic pre-cooling, the epoxy matrix would be able to maintain 30%, 16% and 26% higher hardness respectively as compared to that when machined room temperature dry. This supports the discussion in Section 7.2 that the epoxy matrix could maintain strength and stiffness at a higher level during drilling with CO_2 cooling or with LN_2 pre-cooled tools compared to during room temperature dry drilling as observed by the more brittle fracture surface with less thermal softening of epoxy. Since the measured cutting temperatures in Table 7.1 do not represent the actual temperatures at the cutting of the drill for different drilling processes, it should also be noted that the results of the hardness of epoxy matrix in the plaque for different drilling processes being discussed in this section do not represent the actual hardness values of the epoxy matrix during different drilling process. They are used as an indication of the higher retention of strength of the CFRP plaque during drilling with cryogenic cooling compared to when drilling dry at room temperature.

Table 7.2: Results showing the hardness of CFRP plaque (measured at various points on the sample) with changing temperature

Temperature (°C)	Vickers Hardness (0.5 kg load) HV				
	Point 1	Point 2	Point 3	Point 4	Point 5
-60	352.4	174.6	198.7	240.6	132.5
-40	380.3	178.1	161.6	179.3	121.8
-20	282.5	143.8	128.8	134.8	116.6
0	250.1	133.3	240.6	110	113.5
27 (RT)	106.7	86.9	72.4	97.4	80.4
100	87.3	62.8	35.3	87.3	48.1

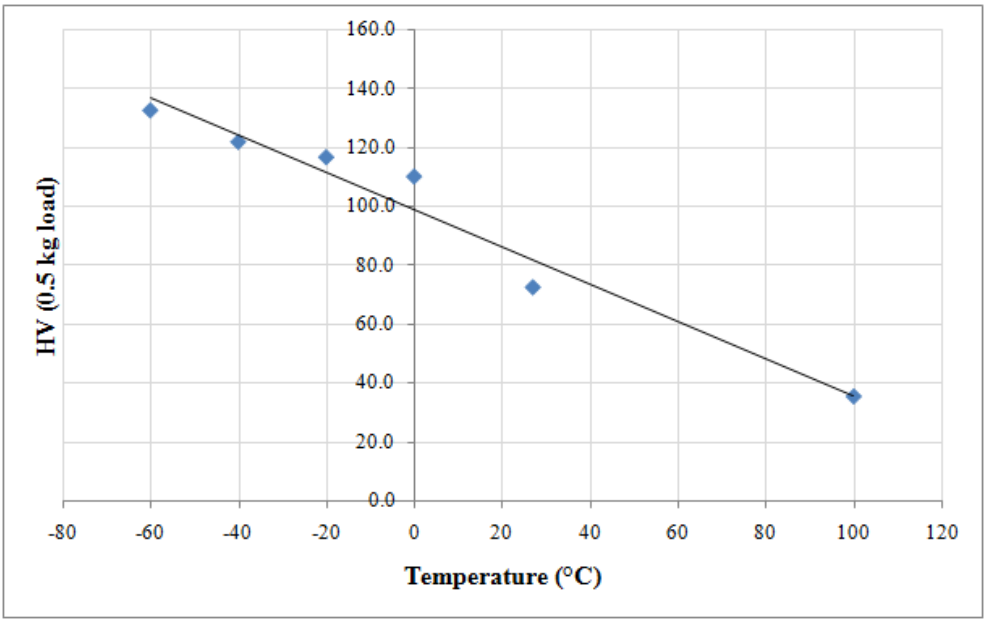

Figure 7.19: Variations of epoxy matrix hardness in the CFRP plaque with temperature

7.4 Investigation of the Wear Mechanism for Carbide Tools when Drilling Carbon Fibre Reinforced Plastics

From the results in Section 6.1.1.1 in Chapter 6, abrasive wear was observed as the major wear mechanism for carbide tools when drilling CFRPs dry at room temperature and with cryogenic pre-cooling of the tool. As discussed in Section 5.6, a detailed investigation of wear mechanism for carbide tools when drilling CFRPs was performed to find clear evidence supporting the proposed abrasive wear mechanism by other researchers [109, 111, 112]. The methodology for this investigation as described in Section 5.6.

From the investigation of the solid carbide twist drill with DK 460 UF grade of carbides (0.55 µm grain size) in the SEM, some voids between the WC grains on the worn surface of the flank face of the tool could be observed, area (a) in Figure 7.20. This indicates that evidence showing that Co binders between the WC grains on the worn surface of the tool had been removed. The removal of Co binders was a result of the flank face of the tool rubbing against the highly abrasive carbon fibres on the machined surface of the CFRP plaque as proposed by other researchers [109, 111, 112] due to the higher hardness of carbon fibres compared to that of Co binders as previously discussed in Section 3.2.4.1. It is also shown in Figure 7.20 that there were voids, area (b), on the worn surface of the tool which were larger than the voids between WC grains, which indicates the removal of cobalt binders (area (a)). Since the size of these voids was larger than the possible size of the WC grains observed in Figure 7.20, these voids indicate the evidence of dislodging of WC grains next to the area where Co binder had been removed. At higher magnification of this worn

area, cracks initiating from the sharp edges of the WC grains next to the voids where the cobalt binder had been removed could be observed, Figure 7.21. Since the grain size of the solid carbide tool being investigated was reported to be 0.55 µm [182, 183], it is justified that the lines across the grains observed in the square in Figure 7.21 were cracks of the grains rather than the boundary of the grains. This is because the size of the grains would be too small (much smaller than 0.55 µm) if these lines were considered as the grain boundaries. In addition, it was observed that some of the lines in the square in Figure 7.21 would not make a complete grain if they were considered as grain boundaries. These cracks occurred because the WC grains had increased exposure to dynamic cutting stress as a result of the removal of cobalt binders between the grains as proposed by other researchers [109, 111, 112]. It could also be observed that some cracks have propagated from the sharp edge across the WC grains, which will result in fracture and dislodging of the grains. As proposed by Rawat and Attia [109] and Wang *et al.* [112], the fractured and dislodged WC grains then caused abrasive wear by direct abrasion on the carbide tool as they moved along the flank face under cutting pressure. The direct abrasion by these fractured and dislodged grains can be observed as fine grooves at 90° to the cutting edge on the flank face of the tool in Figure 6.2.

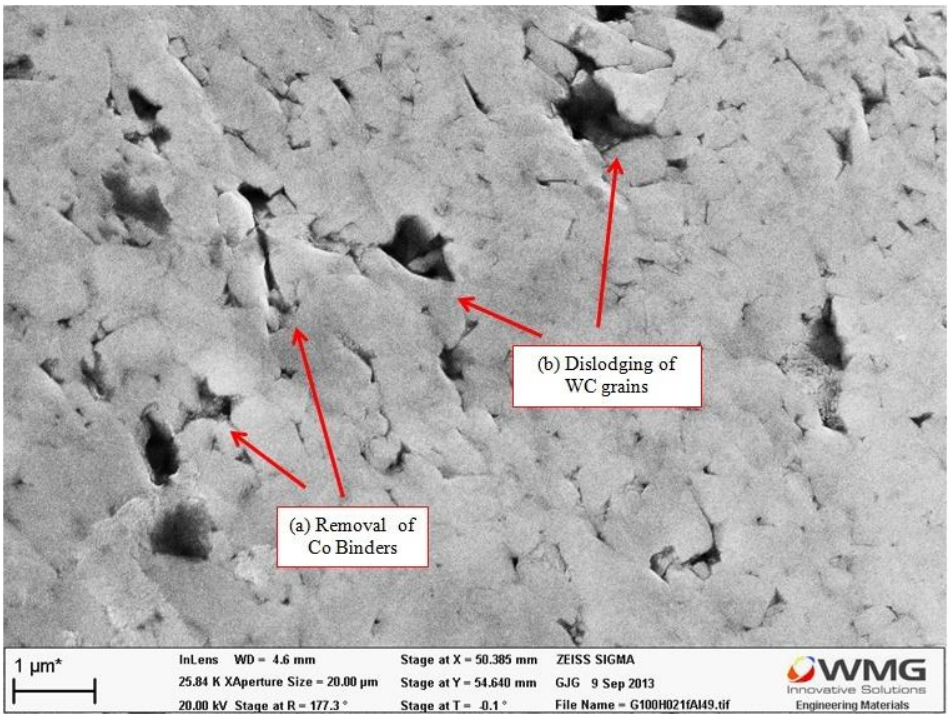

Figure 7.20: SEM image showing the worn surface on the flank face of the solid carbide twist drill with DF 460 UF grade of carbide (0.55 µm grain size) with evidence of cobalt binder removal and grain dislodging after drilling 100 through-holes in CFRP plaque at a cutting speed and feed rate of 75.4 m/min (8,000 RPM) and 0.12 mm/rev respectively

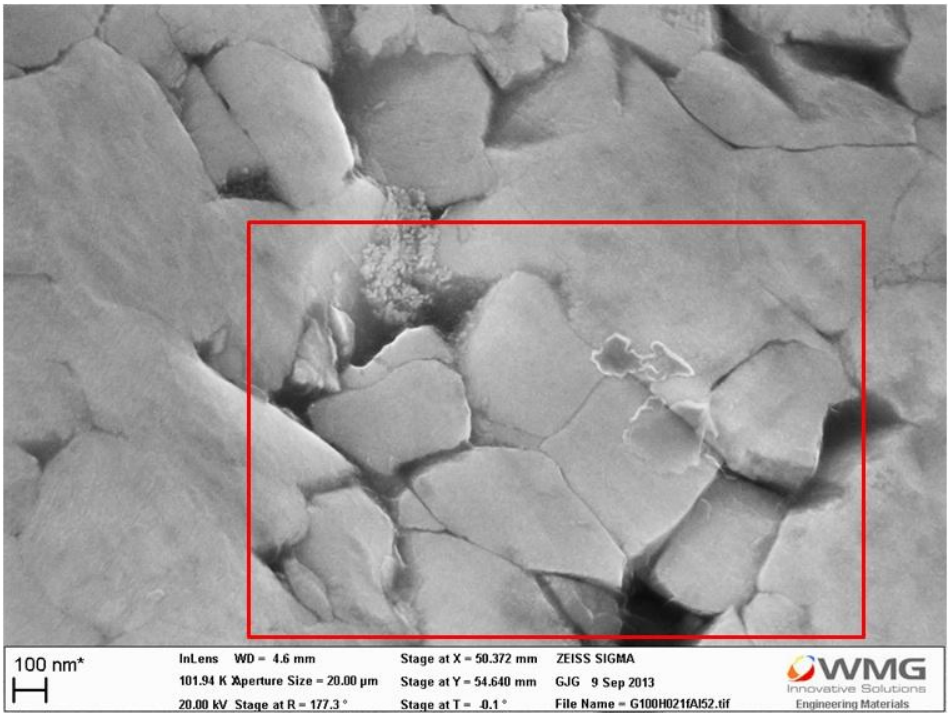

Figure 7.21: SEM image showing a higher magnification of the worn surface of the flank face of the drill in Figure 7.20 with evidence of cracks initiating from the sharp edge and across the WC grains next to the area where the cobalt binders have been removed (inside the square)

From evidence in Figures 7.20 and 7.21 supporting the proposed mechanism of abrasive wear, the following possible solutions to minimise the disadvantage of higher tool wear from cryogenic drilling of CFRPs as compared to room temperature dry drilling, which was discussed in Section 6.1.1, have been proposed.

1. Use a carbide drill with lower cobalt binder content

In the work of Blombery *et al.* [198], it was also proposed that the removal of cobalt binders of the carbide tool is the factor controlling the rate of abrasive wear of the tool when drilling sandstone. It was shown in their work that etching of the tool, which removed 3-4 µm of the cobalt binders from the tool surface, resulted in higher rate of abrasive wear compared to the unetched tool [198]. Although it was for the drilling of sandstone, it is justified that this could be applied to drilling of CFRPs due to the abrasiveness of CFRP and sandstone debris. Blombery *et al.* [198] also showed that the area with high Co content was more susceptible to damage and fracture of the WC grains. This proposed argument is similar to that from Masuda *et al.* [111]. It was demonstrated by Masuda *et al.* [111] that the rate of abrasive wear of the carbide tool when turning CFRPs increased as the Co content increased [111]. As a consequence, a carbide tool with low Co content is justified to be more suitable to decrease tool wear when drilling with cryogenic cooling.

2. Use a "mixed-crystal grade" carbide drill

It is shown in Figure 7.21 that fracture of the WC grains was resulted from the cracks initiating from the sharp edges of the grains next to the voids. For this reason, it is proposed that using a "mixed-crystal grade" carbide drill would be able to reduce the possibility of cracking at the sharp edges of the grains because of the inclusion of more rounded grains of mixed carbides containing Ti and Ta [73, 113], which reduces the stress concentration points compare to the more angular WC grains. In addition, hardness of the "mixed-crystal grade" carbide tool is reported to be higher than the "straight-grade" WC tool [113], which would increase the resistance to direct abrasion by the fractured and dislodged grains.

3. Use a diamond coated carbide drill

Since it is shown that the fractured and dislodegd WC grains also cause tool wear by direct abrasion on the cutting edge, it is proposed that using the diamond coated carbide drill instead of the TiAlN coated drill, which was used in the drilling trial with cryogenic LN_2 cooling, would provide a benefit in reducing the abrasive wear. This is due to higher resistance to abrasive wear of the diamond coating compared to the TiAlN coating [87, 99, 112]. It has been shown that use of diamond coated carbide drill could reduce the amount of tool wear produced when drilling CFRPs compared to using TiAlN coated and uncoated drill [87, 112]. Due to the higher resistance to abrasive wear of the diamond coating, the coating on the cutting edge of the tool would be worn through at slower rate when compared to the use of TiAlN coating resulting in slower rate of Co binder removal. After the coating on the cutting edge had been worn through, the tool would still be more effectively protected by the diamond coating from direct abrasion by the fractured and dislodged grains on the flank face of the tool, resulting in lower rate of flank wear when compared to the uncoated or TiAlN coated drill.

7.5 Conclusion

From the results and discussion in this chapter, it has been shown that drilling with CO_2 cooling or with a tool pre-cooled in LN_2 (30 and 120 s cooling time) results in a significant reduction in the cutting temperature as compared to room temperature dry drilling of CFRPs at the same cutting speed and feed rate. However, drilling with CO_2 cooling was shown to be more effective in reducing the cutting temperature as compared to drilling with a tool pre-cooled in LN_2 for 30 s despite the similar temperatures of the tool after submerged in LN_2 for 30 s and the CO_2 gas exiting the nozzle. Increasing the pre-cooling time to 120 s, for which the tool was cooled to a lower temperature (-196°C), could increase the effectiveness of temperature reduction, approaching that of drilling with CO_2 cooling. However, drilling with external CO_2 cooling is still proposed to be more cost-effective due to shorter process

time and more practical to be applied for industrial production than drilling with LN_2 pre-cooling of the tool. Nevertheless, using through-tool CO_2 or LN_2 cooling is proposed to be more effective than application of external CO_2 cooling and LN_2 pre-cooling of the tool in reducing the cutting temperature because of continual supply of cryogen more precisely to the cutting zone during drilling.

The use of CO_2 or cryogenic cooling of the tool did not result in variations in the behaviour of carbon fibres in CFRP plaque, showing brittle fracture mode of fibres, the same as when drilling dry at room temperature. It resulted in different behaviours of the epoxy matrix in the plaque during drilling compared to room temperature dry drilling. For drilling with CO_2 cooling or with a cryogenically cooled tool, a more brittle fracture mode and less thermal softening of the epoxy matrix was observed on the machined surface as indicated by the more angular broken pieces of fractured epoxy due to lower cutting temperature. In contrast, a more ductile failure mode and more thermal softening of the epoxy matrix were observed for room temperature dry drilling. The more brittle behaviour of the epoxy matrix indicates that CFRP plaque would be able to maintain strength and stiffness at a higher level and the plaque would become more abrasive when drilling with CO_2 cooling or cryogenic pre-cooling of the tool as compared to room temperature dry drilling.

Within the same sample, the variation in cooling effect by application of CO_2 cooling and cryogenic pre-cooling was found. Brittle fracture surface with more ductile-like characteristics was observed on the machined surface at a distance closer to the exit of the plaque compared to that at a distance closer to the entry. This is attributed to inconsistency in cooling ability through the thickness of the plaque by application of external CO_2 cooling, which directed cryogen from the entry of the plaque, and application of cryogenic pre-cooling, which only cooled the tool before performing the drilling process. This variation in cooling effect through the thickness of the plaque would be eliminated by using through-tool LN_2 or CO_2 cooling due to the continual supply of cryogen close to the cutting edge during drilling.

At lower cutting speeds and feed rates, a more significant difference between the fracture behaviours of epoxy matrix resulting from room temperature dry drilling and drilling with CO_2 cooling was observed. As the cutting speed and feed rate were increased, the difference was less obvious showing more similar characteristics of machined surface of epoxy matrix for room temperature dry and CO_2 drilling. This indicates a similar level of strength and stiffness of the plaque being retained when drilling with CO_2 cooling and dry at room temperature at higher cutting speeds and feed rates, resulting in insignificant difference in thrust force and delamination damage as discussed in Section 6.2. The less significant difference between the fracture behaviours of epoxy matrix for room temperature dry and

CO_2 drilling at higher cutting speeds and feed rates was due to a reduction in cooling effect by CO_2 cooling as a result of lower amount of CO_2 directed to the cutting zone with shorter drilling time.

From an examination of the hardness of epoxy matrix in CFRP plaque, it was shown that hardness of the epoxy matrix increased as temperature decreased from 100°C to -60°C. This indicates that hardness of the epoxy matrix would be retained at a higher level during drilling with CO_2 cooling or with cryogenically cooled tools compared to room temperature dry drilling, suggesting higher strength and stiffness of CFRP plaque being retained and higher abrasiveness of CFRP plaque. This results in more brittle fracture behaviour and less thermal softening of the epoxy matrix during drilling with CO_2 cooling or with a cryogenic cooled tool.

Abrasive wear was observed as the major wear mechanism for carbide tools when drilling CFRPs, as previously proposed in Chapter 6. The evidence indicating the removal of cobalt binders between WC grains on the worn surface by the highly abrasive carbon fibres was presented. Evidence showing the cracks on WC grains initiating from the sharp edges and fracture of WC grains next to the void was also presented. This evidence supports the abrasive wear mechanism for carbide tools when drilling CFRPs proposed by other researchers [109, 111, 112]. From this proposed mechanism of abrasive wear, possible solutions to minimise the disadvantage of higher tool wear from cryogenic drilling of CFRPs as compared to room temperature dry drilling: 1) Use a carbide drill with low cobalt content, 2) Use a “mixed-crystal grade” carbide drill and 3) Use a diamond-coated drill, have been proposed.

8 Conclusions

Referring to the objectives of this research stated in Chapter 1, the overall objectives were 1) evaluate the performance of cryogenic cooling for conventional drilling of carbon fibre reinforced plastics, 2) present a detailed explanation of the mechanisms associated with cryogenic machining of these materials and 3) explain mechanism of wear on carbide tools when drilling CFRPs with cryogenic cooling. According to these objectives, the conclusions from the results of this research can be stated as follows.

8.1 Effect of the Application of CO_2 Cooling and LN_2 Pre-cooling of the Tool on Performance of Conventional Drilling of Carbon Fibre Reinforced Plastics

1. Improvement in drilling performance with respect to quality of drilled hole, i.e. drilling-induced delamination and internal damage to the machined surface, which is critical to the quality of the drilled hole and hence performance of the CFRP components [4, 7, 9, 12, 13], was achieved by application of CO_2 cooling and LN_2 pre-cooling, indicating the potential benefit of CO_2 and LN_2 cooling in conventional drilling of CFRPs.
    - Area of exit delamination was decreased by an average reduction of 43% (0.08 F_{da}) and total depth of internal damage through the thickness of the hole was reduced by 92% (2.97 mm) when drilling with a cryogenically cooled tool at a cutting speed and feed rate of 94 m/min and 0.065 mm/rev with a TiAlN coated carbide twist drill.
    - Drilling with CO_2 cooling produced 11-21% less exit A_{del} than room temperature dry drilling at a feed rate of 0.03 mm/rev and cutting speeds of 75-150 m/min with a diamond coated eight facet double angle carbide drill.
    - 44-50% and 45-50% less internal damage in terms of average and total depth of damage respectively was produced when drilling with CO_2 cooling compared to room temperature dry drilling at a cutting speed of 100 m/min and feeds rate of 0.06 and 0.12 mm/rev with a TiAlN coated carbide twist drill.
2. Application of CO_2 cooling and LN_2 pre-cooling resulted in higher thrust force and higher rate of tool wear (indicating shorter tool life) compared to room temperature dry drilling.
    - Drilling with LN_2 pre-cooled tool produced 13% and 10% higher average and maximum thrust force respectively compared to room temperature dry drilling at a cutting speed of 94 m/min and feed rate of 0.065 mm/rev with a TiAlN coated carbide twist drill.

- At a cutting speed of 100 m/min and feed rates of 0.06 and 0.12 mm/rev, drilling with LN_2 pre-cooled tools produced 14-18% and 19-25% higher thrust force than room temperature dry drilling when cooling time was 30 s and 120s respectively.
- Using a diamond coated eight facet double angle carbide drill, 9-17% higher thrust force compared to room temperature dry drilling was produced when drilling with CO_2 cooling at a feed rate of 0.03 mm/rev for cutting speeds of 75, 100 and 150 m/min and 3-5% for cutting speeds of 115 and 130 m/min.
- Using a TiAlN coated carbide twist drill, application of CO_2 cooling resulted in 14-16% higher thrust force compared to machining dry at room temperature at a cutting speed of 100 m/min and feed rates of 0.06 and 0.12 mm/rev.
- Drilling with LN_2 pre-cooling produced higher average flank wear by 39-69% during initial stage of wear and by 17-23% during steady state of wear compared to room temperature dry drilling at a cutting speed and feed rate of 94 m/min and 0.065 mm/rev.
- The investigation of tool life when drilling with CO_2 cooling was not performed due to limited availability of drills and workpiece material.

3. At the same machining parameter, drilling with CO_2 cooling was shown to produce less internal damage compared to drilling with LN_2 pre-cooling due to a higher effectiveness in reducing the cutting temperature as compared with LN_2 pre-cooling.
    - At a cutting speed of 100 m/min and feed rates of 0.06 and 0.12 mm/rev, drilling with CO_2 cooling produced 50-55% and 33-67% less average depth of internal damage than drilling with 30 and 120 s LN_2 pre-cooled tools respectively, while it produced 48-58% and 30-69% less total depth of internal damage compared to drilling with 30 and 120 s LN_2 pre-cooled tools respectively.
4. The effect of CO_2 cooling on a reduction in exit delamination and an increase in thrust force as compared with room temperature dry drilling was found to become less dominant as cutting speed and feed rate increased.
    - The increase in thrust force was reduced from 9-17% to within 3% as feed rate was increased from 0.03 to 0.15 mm/rev and it was decreased from 6-17% to within 5% as cutting speed was increased from 75 to 150 m/min.
    - The reduction in exit delamination was decreased from 11-21% to 3-4% as feed rate was increased from 0.03 to 0.15 mm/rev for cutting speeds of 100-150 m/min.
    - As cutting speed was increased from 75 to 150 m/min, the reduction in exit delamination was reduced from 14-36% to 7-14%.

5. The reduction in damage to the hole, while producing higher thrust force and tool wear, by application of CO_2 cooling and LN_2 pre-cooling was found to be attributed to the higher strength and stiffness of CFRPs that was retained, hence increasing resistance to drilling-induced damage, during drilling process by CO_2 cooling or by cooled tool due to the lower cutting temperature compared to room temperature dry drilling.

8.2 Effect of the Application of CO_2 Cooling and LN_2 Pre-cooling of the Tool on the Behaviour of Carbon Fibre Reinforced Plastics in Relation to Cutting Mechanism

1. Brittle fracture surface at the end of carbon fibres was observed for room temperature dry and cryogenic drilling.
2. Application of CO_2 cooling and LN_2 pre-cooling resulted in more brittle behaviour of epoxy matrix in the CFRP plaque, i.e. more brittle fracture and less thermal softening of epoxy, compared to when machining dry at room temperature as a result of lower cutting temperature. This indicates that strength and stiffness of the epoxy matrix were retained at a higher level when drilling with cryogenic cooling, resulting in more abrasiveness and higher strength and stiffness of CFRP plaque due to a more rigid support from the epoxy matrix.
    - More angular shape of fractured epoxy and less smooth surface of epoxy smearing on the machining surface was observed when drilling with cryogenic cooling, in contrast to more rounded shape of fractured epoxy with more obvious smooth surface of epoxy smearing observed when machining dry at room temperature.
    - Results of micro-hardness testing indicate an increase in the hardness of epoxy with decreasing temperature.
        - 16-30% higher hardness of epoxy matrix in CFRP plaque would be retained during drilling with cryogenic cooling compared to machining dry at room temperature at a cutting speed of 100 m/min and feed rate of 0.06 mm/rev.
3. An increase of cutting speed and feed rate resulted in less obvious difference between fracture behaviours of the epoxy matrix for room temperature dry and CO_2 drilling, contributing to less difference in thrust force and delamination produced for the two drilling processes.
    - When drilling with CO_2 cooling at higher cutting speeds and feed rates, the epoxy matrix was fractured in to small pieces without significant smooth surface of epoxy smearing, but more rounding of epoxy was observed compared to

when drilling at lower cutting speeds and feed rates, showing more ductile-like fracture characteristics similarly to room temperature dry drilling.

4. It was found that there was variation in cooling effect by CO_2 cooling and LN_2 pre-cooling through the thickness of CFRP plaque, showing a reduction in effectiveness in cutting heat removal as drilling approached the exit of the plaque.
    - More ductile-like characteristics, i.e., more rounded shape of fractured epoxy and more epoxy smearing, were observed on the brittle fracture surface of epoxy matrix on the machined surface close to the exit of the plaque compared to the machined surface closer to the entry of the same plaque resulting from cryogenic drilling.

8.3 Capability of Reducing the Drilling Temperature by Application of CO_2 Cooling and LN_2 Pre-cooling of the Tool

1. The highest capability of reducing the cutting temperature produced in drilling of CFRPs was achieved by the application of external CO_2 cooling, followed by LN_2 pre-cooling of the tool with 120 s and 30 s of cooling time respectively. This indicates the highest effectiveness in cutting heat removal by CO_2 cooling as a result of continuous cooling of the tool and the workpiece during drilling process by the continual supply of CO_2 gas.
    - At cutting speed of 100 m/min and feed rate of 0.06 mm/rev, the maximum drilling temperature was reduced by 27%, 24% and 14% when drilling with the CO_2 cooling, with 120 s and 30 s LN_2 cooled tools respectively compared to that when machined dry at room temperature.
2. Increasing pre-cooling time to 120 s could increase the capability of reducing cutting temperature to be approaching CO_2 cooling because the tool was cooled to a lower temperature. However, application of external CO_2 cooling is suggested to be more cost-effective and more practical to be used in the production process in industry than cryogenic LN_2 pre-cooling of the tool due to shorter process time and in-process cooling of the cutting zone by cryogen.
    - The difference between cutting temperature produced from drilling with CO_2 cooling and with LN_2 pre-cooled tools was reduced from 15% to 5% as pre-cooling time was increased from 30 to 120 seconds.

8.4 Characteristics and Mechanism of Tool Wear

1. Two stages of tool wear could be observed in variation of tool wear with number of holes drilled when drilling CFRPs with LN_2 pre-cooled tools and dry at room temperature.
    - The initial stage of wear occurred during drilling the first hole to 50^{th} hole during which average flank wear increased at a rate of 1 µm/hole for room temperature dry drilling and 1.4 µm/hole for drilling with LN_2 pre-cooled tools.
    - The steady state of wear occurred during drilling 51th hole to 325^{th} hole during which average flank wear increased gradually at a rate of 0.4 µm/hole and 0.3 µm/hole for room temperature dry and cryogenic drilling respectively.
2. Abrasion was observed as the major wear mechanism for carbide tools when drilling CFRPs dry at room temperature and with cryogenic cooling, contributing to a uniform wear band along the cutting edge and fine grooves at 90° to the cutting edge on the flank face of the tool.
3. The removal of cobalt binder between tungsten carbide grains by the highly abrasive carbon fibres and direct abrasion by the fractured and dislodged carbide grains as they move along the cutting edge under pressure were found to be the main factors contributing to abrasive wear mechanism for carbide tools when drilling CFRPs. Clear evidence with better quality of images, which was lacking in other researchers' work [109, 111, 112], was presented in this research.
    - Evidence showing the removal of cobalt binder between tungsten carbide grains on the worn surface was presented.
    - Evidence showing cracks in carbide grains next to the area of cobalt binder removal and voids with the size larger than the size of carbide grains on the worn surface was also presented, indicating the fracture and dislodging of carbide grains due to increasingly exposed area of the grains to cutting force after cobalt binder had been removed.
4. From this proposed mechanism of abrasive wear, the possible solutions to minimise the disadvantage of higher tool wear resulting from the cryogenic drilling have been proposed:
    - Use a carbide drill with low cobalt content
    - Use a "mixed-crystal grade" carbide drill
    - Use a diamond-coated drill

8.5 Evaluation of Damage to the Drilled Hole

1. Exit delamination was found to be more critical to drilling performance with respect to quality in this research.
    - Entry delamination in terms of F_d was in the range 1.04-1.20 while exit delamination in terms of F_d was in the range 1.26-1.78, Figure 6.10.
    - No obvious delamination at the entry was observed from the visual inspection using low magnification optical microscope compared to at the exit for room temperature dry drilling and drilling with CO_2 cooling, Figure 6.24.
2. Evaluation of damage in terms of total area of delamination was more suitable for the evaluation of exit delamination in this research because it considered the actual area of damage to the hole rather than only the maximum diameter of damage which could be resulted from only fine cracks as a result of fibres being pushed down at the exit of the hole.
3. From the collaboration with Product Evaluation Technologies Group, X-ray CT-scanning analysis method was used to examine damage through the thickness of the drilled hole.
    - X-ray CT-scanning technique can eliminate the disadvantages of the visual analysis of damage using the optical microscope of exit delamination area, which was due to the dependence of the contrast on illumination and visibility of the defects, and destructive (cross-sectioning) analysis technique to examine internal damage.
    - Since this technique was in the initial stage of development, only internal damage in terms of maximum depth of damage through the thickness of the hole was used for the evaluation of the drilling performance.
    - Internal damage in terms of average depth of damage through the thickness of the hole produced from room temperature dry drilling, drilling with CO_2 cooling and with 30 s and 120 s LN_2 pre-cooled tools was 0.09, 0.05, 0.11 and 0.15 mm respectively at a cutting speed of 100 m/min and a feed rate of 0.06 mm/rev and 0.12, 0.06, 0.12 and 0.09 mm respectively at a feed rate of 0.12 mm/rev.
    - However, internal damage and crack of which the scale smaller than 15 µm, which was observed by cross-sectioning analysis technique, would not be detected by CT-scanning in this research.
    - Cross-sectioning analysis technique is proposed to be more suitable for quality control process in industry due to shorter process time and ability to examine larger size of samples compared to CT-scanning technique.

8.6 Overall Summary

Based on the conclusions discussed in Sections 8.1-8.5, overall summary and contributions to knowledge of this research are:

- Application of CO_2 cooling and LN_2 pre-cooling resulted in an improvement in drilling performance with respect to quality of holes by reducing exit delamination and internal damage to the machined surface in conventional drilling of CFRPs, indicating the potential benefit of cryogenic cooling in drilling of CFRPs in industry.
- Application of CO_2 cooling and LN_2 pre-cooling did not improve drilling performance with respect to machining performance, for which higher thrust force and higher rate of tool wear was produced, in conventional drilling of CFRPs.
- As a result of a reduction in cutting temperature, application of cryogenic cooling resulted in more brittle behaviour and less thermal softening of the epoxy matrix, hence a higher retention of abrasiveness, strength and stiffness of CFRP plaque during drilling due to a more rigid support of the epoxy matrix during drilling. This was found to be major factors contributing to a reduction in drilling-induced damage while producing higher thrust force and tool wear.
- An increase of cutting speed and feed rate resulted in less dominant effect of CO_2 cooling on a reduction in exit delamination, an increase in thrust force and a more brittle behaviour of the epoxy matrix.
- Application of external CO_2 cooling provided higher capability in reducing cutting temperature as compared with application of LN_2 pre-cooling because of continuous cooling of the tool and the workpiece by the continual supply of CO_2 gas as opposed to cooling the tool only before performing the drilling process as was the case for drilling with the LN_2 pre-cooled tools.
- Removal of cobalt binder by carbon fibres and direct abrasion by fractured and dislodged tungsten carbide grains are the major factors contributing to abrasive wear mechanism of tungsten carbide tools when drilling CFRPs dry at room temperature and with cryogenic cooling.
- X-ray CT-scanning analysis technique was used to examine drilling-induced damage through the thickness of the drilled hole with detectable scale of damage of 15 µm without causing additional damage due to cross-sectioning and polishing of the samples. However, visual inspection and cross-sectioning analysis technique is proposed to be more practical for industrial quality control process because of shorter process time and hence ability to examine larger size of samples.

9 Suggestions for Further Work

The suggestions for further work can be stated as follows:

- Although the work in this research has shown a benefit of damage reduction by application of cryogenic cooling, the effect of the reduction in drilling-induced damage on mechanical properties of CFRP parts is not presented. For this reason, investigation of mechanical properties of CFRP sample produced from drilling with cryogenic cooling and dry at room temperature is suggested to be performed to determine the effect of damage reduction by cryogenic drilling on improvement of mechanism properties and performance of CFRP parts compared to machining dry at room temperature. Data on the improvement of mechanical properties of CFRP parts will indicate the actual benefit of cryogenic cooling when applied in conventional drilling of CFRPs in industry for which end-performance of the machined parts is also critical. Bolt bearing strength test is suggested for examining strength of the drilled samples under actual application of CFRP parts in which they will be assembled to other parts.
- In this research, investigation of tool wear when drilling with LN_2 pre-cooling compared to room temperature dry drilling (Section 6.1.1.2) has been done using one tool for each drilling experiment, i.e., one repetition for room temperature dry drilling and drilling with cryogenically cooled tool. This was due to limited availability of drill and workpiece material. For this reason, more repetitions of each drilling process is suggested to be done to determine consistency in the results showing higher rate of tool wear when drilling with LN_2 pre-cooling compared to room temperature dry drilling. In addition, investigation of tool wear has been done only for drilling with LN_2 pre-cooling and compare to machining dry at room temperature. Therefore, investigation of tool wear produced from drilling with CO_2 cooling is suggested to be performed to confirm the results showing increased rate of tool wear observed when drilling with LN_2 pre-cooling.
- Since it was not possible with the CO_2 cooling system used in this research, investigation of the effect of flow rate of CO_2 on drilling performance of CFRPs is suggested to be done for further work.
- As mentioned in Section 5.3.2, only data of internal damage in terms of maximum depth of damage was obtained for evaluation of drilling performance in this research because the CT-scanning analysis method was in the initial stage of development when this thesis was completed. Since maximum depth of damage could be resulting from fine cracks of irregular shape of damage around the hole due to anisotropy of

CFRPs, actual area of damage would not be presented by evaluation of damage in terms of maximum depth of damage. As a consequence, development of CT-scanning analysis method for obtaining data of internal damage through the thickness in terms of area of damage is suggested for further work.

- Since only one repetition of drilling was performed for every machining condition for evaluation of damage by CT-scanning method (Section 6.3.2), drilling experiments with three repetitions at each machining condition (room temperature dry drilling, drilling with CO_2 cooling and with LN_2 pre-cooled tools) is suggested to be performed for further work. This is suggested to be done to obtain consistency in the results of drilling performance of every drilling process and to validate variations in the performance of LN_2 pre-cooling and contradictory results showing increased internal damage compared to room temperature dry drilling.
- In this research, investigation and comparison of cutting temperature produced by room temperature dry drilling and drilling with cryogenic cooling was carried out only when drilling at a cutting speed of 100 m/min and feed rate of 0.06 mm/rev due to limited availability of workpiece material. Therefore, it is suggested that measurement of cutting temperature produced by room temperature dry drilling and drilling with cryogenic cooling at various cutting speeds and feed rates should be performed. This is to determine the effect of variation in cutting speed and feed rate on cutting temperature produced by each drilling process and on the capability of reducing cutting temperature by cryogenic cooling.
- Performance evaluation of cryogenic cooling when drilling CFRPs using various drill geometries is suggested to be done in order to determine the effect of tool geometry on drilling performance with cryogenic cooling, hence optimising the tool which is suitable for drilling CFRPs with cryogenic cooling.
- Evaluation of performance of through-tool CO_2 and LN_2 cooling, which is used in commercial machine tools by MAG [153] and Starrag Group [168], when drilling CFRPs is suggested to be carried out and compare to drilling performance of application of external CO_2 cooling and LN_2 pre-cooling of the tool used in this research. As discussed in Section 7.1, the use of through-tool cryogenic cooling is more practical for industrial application than LN_2 pre-cooling of the tool and is proposed to be more effective in reducing the cutting temperature than application of external CO_2 cooling used in this research. The objectives of evaluation of drilling performance of CFRPs using through-tool cryogenic cooling are;

  - To determine a reduction in drilling-induced damage and capability of reducing the cutting temperature by through-tool cryogenic cooling and compare to that by external CO_2 cooling and LN_2 pre-cooling of the tool.
  - To determine whether a reduction in cooling effect through the thickness of the hole which was observed in the application of external CO_2 cooling and LN_2 pre-cooling as discussed in Section 7.2 would be reduced or eliminated by the use of through-tool cryogenic cooling when drilling CFRP plaque with the same or more thickness as that being used in this research.
- For application of through-tool cryogenic cooling in conventional drilling of CFRPs, it is suggested that evaluation of performance of through-tool cooling using CO_2 should be carried out and compare with that using LN_2 to determine which cryogen provides better performance in terms of damage reduction and increase in mechanical properties of CFRP parts. This is also to determine which range of temperature (-70°C for CO_2 or -196°C for LN_2) is most effective and suitable for improving performance in drilling of CFRPs.
- Investigation of the effect of cryogenic temperature of LN_2 on property of workpiece and cutting tool is also suggested to be done for further work since there has been concern on damage to the workpiece material and cutting tool cause by extremely low temperature of LN_2 (-196°C). Investigation of possible thermal fatigue damage to the cutting tool when drilling with through-tool LN_2 cooling should be performed.
- As mentioned in Chapter 1, drilling of CFRPs in industry is aiming to improve productivity while maintaining "dry machining" condition to avoid material degradation and additional cost of cleaning due to contamination of conventional cutting fluid or cutting oil [10, 13, 32]. However, it is suggested that using minimum quantity of cutting oil in addition to cryogenic cooling CFRPs would improve drilling performance of CFRPs compared to the use of cryogenic cooing alone particularly when drilling at higher cutting speeds and feed rates, which generates larger amount of heat. As shown in this research, a reduction in exit delamination by cryogenic cooling decreases as cutting speed and feed rate increase due to more heat generated and lower amount of cryogen directed to the cutting zone in a shorter drilling time. As a result of lubrication effect by MQL in addition to cooling effect by cryogenic cooling, significance of reduction in delamination at higher cutting speeds and feed rates would be increased. Therefore, performance evaluation and comparison of application of through-tool cryogenic cooling, a mixture of through-tool cryogenic cooling and minimum quantity lubrication (MQL) and MQL without

cryogenic cooling in drilling of CFRPs is suggested to be performed. The objectives of this investigation are;

- To determine an “improvement” in drilling performance by the use of MQL in addition to through-tool cryogenic cooling compared to the use of cryogenic cooling alone
- To determine whether a benefit of the “improvement” in drilling performance achieved by the addition of MQL can compensate disadvantages of possible material degradation and additional cost of cleaning due to contamination of cutting oil
- To determine the effect of application of MQL alone on drilling performance and determine the effect of lubrication by MQL on the associated cutting mechanism

Reference

[1] Chung, D. D. L., 1994, Carbon Fiber Composites, Butterworth-Heinemann, Newton. ISBN 0750691697.

[2] Schwartz, M. M., 1997, Composite Materials Volume I: Properties, Nondestructive Testing, and Repair, Prentice-Hall, Inc., New Jersey. ISBN 0133000478.

[3] Davim, J. P., 2008, Machining: Fundamentals and Recent Advances, Springer-Verlag London Limited, London. ISBN 978-1-84800-212-8.

[4] Sheikh-Ahmad, J. Y., 2009, Machining of Polymer Composites, Springer Science and Business Media, New York. ISBN 978-0-387-68619-6.

[5] Campbell, F. C., 2010, Structural Compoiste Materials, ASM International, Ohio, United States of America. ISBN 9781615030378.

[6] Soutis, C., 2005, "Carbon fiber reinforced plastics in aircraft construction," Mat Sci Eng a-Struct, **412**(1-2), pp. 171-176.

[7] Abrao, A. M., Faria, P. E., Campos Rubio, J. C., Reis, P., and Davim, J. P., 2007, "Drilling of fiber reinforced plastics: A review," Journal of Materials Processing Technology, **186**, pp. 1-7.

[8] Davim, J. P., 2010, Machining composite materials, Wiley, London. ISBN 9781848211704.

[9] Liu, D. F., Tang, Y. J., and Cong, W. L., 2012, "A review of mechanical drilling for composite laminates," Compos Struct, **94**(4), pp. 1265-1279.

[10] Teti, R., 2002, "Machining of Composite Materials," CIRP Annals-Manufacturing Technology, Elsevier.

[11] Che, D. M., Saxena, I., Han, P. D., Guo, P., and Ehmann, K. F., 2014, "Machining of Carbon Fiber Reinforced Plastics/Polymers: A Literature Review," J. Manuf. Sci. Eng.-Trans. ASME, **136**(3).

[12] Persson, E., Eriksson, I., and Zackrisson, L., 1997, "Effects of hole machining defects on strength and fatigue life of composite laminates," Compos Part a-Appl S, **28**(2), pp. 141-151.

[13] Private communication with Austin Cook, Senior Manufacturing Development Engineer at BAE Systems, 2013.

[14] DiPaolo, G., Kapoor, S. G., and DeVor, R. E., 1996, "An experimental investigation of the crack growth phenomenon for drilling of fiber-reinforced composite materials," J. Eng. Ind.-Trans. ASME, **118**(1), pp. 104-110.

[15] Lin, S. C., and Chen, I. K., 1996, "Drilling carbon fiber-reinforced composite material at high speed," Wear, **194**(1-2), pp. 156-162.

[16] Chen, W. C., 1997, "Some experimental investigations in the drilling of carbon fiber-reinforced plastic (CFRP) composite laminates," Int J Mach Tool Manu, **37**(8), pp. 1097-1108.

[17] Piquet, R., Ferret, B., Lachaud, F., and Swider, P., 2000, "Experimental analysis of drilling damage in thin carbon/epoxy plate using special drills," Compos Part a-Appl S, **31**(10), pp. 1107-1115.

[18] Zhang, H. J., Chen, W. Y., Chen, D. C., and Zhang, L. C., 2001, "Assessment of the exit defects in carbon fibre-reinforced plastic plates caused by drilling," Key Eng Mat, **196**, pp. 43-52.

[19] Davim, J. P., and Reis, P., 2003, "Study of delamination in drilling carbon fiber reinforced plastics (CFRP) using design experiments," Compos Struct, **59**(4), pp. 481-487.

[20] Davim, J. P., and Reis, P., 2003, "Drilling carbon fiber reinforced plastics manufactured by autoclave - experimental and statistical study," Mater Design, **24**(5), pp. 315-324.

[21] Hocheng, H., and Tsao, C. C., 2003, "Comprehensive analysis of delamination in drilling of composite materials with various drill bits," Journal of Materials Processing Technology, **140**, pp. 335-339.
[22] Hocheng, H., and Tsao, C. C., 2006, "Effects of special drill bits on drilling-induced delamination of composite materials," Int J Mach Tool Manu, **46**(12-13), pp. 1403-1416.
[23] Hocheng, H., and Tsao, C. C., 2007, "Computerized tomography and C-scan for measuring drilling-induced delamination in composite material using twist drill and core drill," Progress of Precision Engineering and Nano Technology, **339**, pp. 16-20.
[24] Won, M. S., and Dharan, C. K. H., 2002, "Chisel edge and pilot hole effects in drilling composite laminates," J. Manuf. Sci. Eng.-Trans. ASME, **124**(2), pp. 242-247.
[25] Tsao, C. C., and Hocheng, H., 2003, "The effect of chisel length and associated pilot hole on delamination when drilling composite materials," Int J Mach Tool Manu, **43**(11), pp. 1087-1092.
[26] Capello, E., 2004, "Workpiece damping and its effect on delamination damage in drilling thin composite laminates," Journal of Materials Processing Technology, **148**(2), pp. 186-195.
[27] Tsao, C. C., and Hocheng, H., 2005, "Effects of exit back-up on delamination in drilling composite materials using a saw drill and a core drill," Int J Mach Tool Manu, **45**(11), pp. 1261-1270.
[28] Ezugwu, E. O., 2005, "Key improvements in the machining of difficult-to-cut aerospace superalloys," Int J Mach Tool Manu, **45**(12-13), pp. 1353-1367.
[29] Clarens, A. F., Zimmerman, J. B., Keoleian, G. A., Hayes, K. F., and Skerlos, S. J., 2008, "Comparison of Life Cycle Emissions and Energy Consumption for Environmentally Adapted Metalworking Fluid Systems," Environ Sci Technol, **42**(22), pp. 8534-8540.
[30] Skerlos, S. J., Hayes, K. F., Clarens, A. F., and Zhao, F., 2008, "Current advances in sustainable metalworking fluids research," International Journal of Sustainable Manufacturing, **1**(1), pp. 180-202.
[31] Shokrani, A., Dhokia, V., and Newman, S. T., 2012, "Environmentally conscious machining of difficult-to-machine materials with regard to cutting fluids," Int J Mach Tool Manu, **57**, pp. 83-101.
[32] Weinert, K., and Kempmann, C., 2004, "Cutting temperatures and their effects on the machining behaviour in drilling reinforced plastic composites," Adv Eng Mater, **6**(8), pp. 684-689.
[33] Pusavec, F., Krajnik, P., and Kopac, J., 2010, "Transitioning to sustainable production–Part I: application on machining technologies," Journal of Cleaner Production, **18**(2), pp. 174-184.
[34] Yildiz, Y., and Nalbant, M., 2008, "A review of cryogenic cooling in machining processes," Int J Mach Tool Manu, **48**(9), pp. 947-964.
[35] Machai, C., and Biermann, D., 2011, "Machining of β-titanium-alloy Ti–10V–2Fe–3Al under cryogenic conditions: Cooling with carbon dioxide snow," Journal of Materials Processing Technology, **211**(6), pp. 1175-1183.
[36] Shokrani, A., Dhokia, V., Munoz-Escalona, P., and Newman, S., 2013, "State-of-the-art cryogenic machining and processing," International Journal of Computer Integrated Manufacturing, **26**(7), pp. 616-648.
[37] Hong, S. Y., and Ding, Y., 2001, "Cooling approaches and cutting temperatures in cryogenic machining of Ti-6Al-4V," International Journal of Machine Tools and Manufacture, **41**(10), pp. 1417-1437.
[38] Clarens, A. F., Hayes, K. F., and Skerlos, S. J., 2006, "Feasibility of Metalworking Fluids Delivered in Supercritical Carbon Dioxide," Journal of Manufacturing Processes, **8**(1), pp. 47-53.

[39] De Chiffre, L., Andreasen, J. L., Lagerberg, S., and Thesken, I.-B., 2007, "Performance Testing of Cryogenic CO_2 as Cutting Fluid in Parting/Grooving and Threading Austenitic Stainless Steel," Cirp Annals-Manufacturing Technology, **56**(1), pp. 101-104.
[40] Venugopal, K. A., Paul, S., and Chattopadhyay, A. B., 2007, "Tool wear in cryogenic turning of Ti-6Al-4V alloy," Cryogenics, **47**(1), pp. 12-18.
[41] Khan, A. A., and Ahmed, M. I., 2008, "Improving tool life using cryogenic cooling," Journal of Materials Processing Technology, **196**(1–3), pp. 149-154.
[42] Dhananchezian, M., and Pradeep Kumar, M., 2011, "Cryogenic turning of the Ti–6Al–4V alloy with modified cutting tool inserts," Cryogenics, **51**(1), pp. 34-40.
[43] Bermingham, M. J., Palanisamy, S., Kent, D., and Dargusch, M. S., 2012, "A comparison of cryogenic and high pressure emulsion cooling technologies on tool life and chip morphology in Ti–6Al–4V cutting," Journal of Materials Processing Technology, **212**(4), pp. 752-765.
[44] Dilip Jerold, B., and Pradeep Kumar, M., 2012, "Experimental comparison of carbon-dioxide and liquid nitrogen cryogenic coolants in turning of AISI 1045 steel," Cryogenics, **52**(10), pp. 569-574.
[45] Dilip Jerold, B., and Pradeep Kumar, M., 2011, "Experimental investigation of turning AISI 1045 steel using cryogenic carbon dioxide as the cutting fluid," Journal of Manufacturing Processes, **13**(2), pp. 113-119.
[46] Chung, D. D. L., 2010, Composite Materials : Science and Applications, Springer-Verlag, London. ISBN 9781848828315.
[47] Abrate, S., and Walton, D. A., 1992, "Machining of composite materials. Part I: Traditional methods," Composite mAnufacturing, **3**(2), pp. 75-83.
[48] Chawla, N., and Chawla, K. K., 2006, Metal Matrix Composites, Springer Science+Business Media, Inc., United States of America.
[49] Clyne, T. W., and Withers, P. J., 1993, An Intorduction to Metal Matrix Composites, Cambridge University Press, Cambridge. ISBN 0521418089.
[50] Chawla, K. K., 1993, Ceramic Matrix Composites, Chapman & Hall, London. ISBN 0412367408
[51] Bernd, C., 2008, "Fibres for Ceramic Matrix Composites," Ceramic Matrix Composites, W. Krenel, ed., WILEy-VCH Verlag GmbH & Co., Weinheim. ISBN 9783527313617.
[52] Schwartz, M. M., 1997, Composite Materials Volume II: Processing, Fabrications, and Applications, Prentice-Hall, Inc., New Jersey. ISBN 0133000397.
[53] Mallick, P. K., 1997, "Introduction: Definitions, Classifications, and Applications," Composites Engineering Handbook, P. K. Mallick, ed., Marcel Dekker, Inc., New York, pp. 1-48. ISBN 0824793048.
[54] AB Sandvik Coromant, 2010, "User's Guide: Machining Carbon Fibre Materials," AB Sandvik Coromant Web site. (Accessed March 2012). URL http://www2.coromant.sandvik.com/coromant/downloads/users_guide/eng/C-2920-30.pdf
[55] Konig, W., Wulf, C., Grab, P., and Willerscheid, H., 1985, "Machining of fibre reinforced plastics," Annals of CIRP, pp. 537-547.
[56] Zhang, L., 2010, "Mechanics and Modeling of Machining Polymer Matrix Composites Reinforced by Long Fibers," Machining Composite Materials, P. J. Davim, ed., ISTE Ltd, London, pp. 1-35.
[57] Jones, F. R., 1994, "Epoxy Resins," Handbook of Polymer-Fibre Composites, F. R. Jones, ed., Longman Scientific & Technical, Essex, pp. 86-96. ISBN 0582065542.
[58] Hay, J. N., 1994, "High Temperature Resins- Thermosetting Polyimides," Handbook of Polymer-Fibre Composites, F. R. Jones, ed., Longman Scientific & Technical, Essex, pp. 96-101. ISBN 0582065542.

[59] Hay, J. N., 1994, "High Temperature Resins-Other Thermosets," Handbook of Polymer-Fibre Composites, F. R. Jones, ed., Longman Scientific & Technical, Essex, pp. 101-106. ISBN 0582065542.
[60] Parvizi-Majidi, A., 1993, "Fibers and Whiskers," Materials Science and Technology Volume 13: Structure and properties of composites, T. W. Chou, ed., VCH Verlagsgesellschaft mbH, Weinheim. ISBN 352726826X
[61] Jones, F. R., 1994, "Glass fibre-type and form," Handbook of Polymer-Fibre Composites, F. R. Jones, ed., Longman Scientific & Technical, Essex, pp. 38-42. ISBN 0582065542
[62] Penn, L. S., 1994, "Aramid fibres," Handbook of Polymer-Fibre Composites, F. R. Jones, ed., Longman Scientific & Technical, Essex, pp. 12-15. ISBN 0582065542.
[63] Won, M. S., and Dharan, C. K. H., 2002, "Drilling of aramid and carbon fiber polymer composites," J. Manuf. Sci. Eng.-Trans. ASME, **124**(4), pp. 778-783.
[64] Edie, D. D., 1998, "The Effect of Processing on Structure and Properties of Carbon Fibers," Carbon, **36**(4), pp. 345-362.
[65] Kumar, S., and Wang, Y., 1997, "Fibers, Fabrics, and Fillers," Composites Engineering Handbook, P. K. Mallick, ed., Marcel Dekker, Inc., New York, p. 58. ISBN 0824793048.
[66] agy Inc., 2006, "High Strength Glass Fibers," High Strength Glass Fibers Technical Paper. (Accessed March 2012). URL http://www.agy.com/technical_info/graphics_PDFs/HighStrengthTechPaperEng.pdf
[67] DuPont Inc., "Kevlar: Aramid Fiber," Kevlar Technical Guide, DuPont, Inc. (Accessed March 2012). URL http://www2.dupont.com/Kevlar/en_US/assets/downloads/KEVLAR_Technical_Guide.pdf
[68] Jones, F. R., 1994, "Carbon fibres from PAN-preparation and properties," Handbook of Polymer-Fibre Composites, F. R. Jones, ed., Longman Scientific & Technical, Essex. ISBN 0582065542.
[69] Johnson, D. J., 1994, "Carbon fibres from PAN-structure," Hnadbook of Polymer-Fibre Composites, F. R. Jones, ed., Longman Scientific & Technical, Essex. ISBN 0582065542.
[70] Fitzer, E., and Frohs, W., 1988, "The influence of carbonization and post treatment conditions on the properties of PAN-based carbon fibers," Carbon '88, Proceedings of the International Carbon ConferenceNewcastle upon Tyne, pp. 298-300.
[71] Rand, B., and Turpin, M., 1994, "Carbon fibres from pitch," Handbook of Polymer-Fibre Composites, F. R. Jones, ed., Longman Scientific & Technical, Essex. ISBN 0582065542.
[72] Trent, E. M., and Wright, P. K., 2000, Metal Cutting, Butterworth-Heinemann, Massachusetts. ISBN 075067069X.
[73] Shaw, M. C., 2005, Metal cutting principles, Oxford University Press, New York. ISBN 0195142063.
[74] Wang, X. M., and Zhang, L. C., 2003, "An experimental investigation into the orthogonal cutting of unidirectional fibre reinforced plastics," Int J Mach Tool Manu, **43**(10), pp. 1015-1022.
[75] Iliescu, D., Gehin, D., Iordanoff, I., Girot, F., and Gutierrez, M. E., 2010, "A discrete element method for the simulation of CFRP cutting," Compos Sci Technol, **70**(1), pp. 73-80.
[76] Koplev, A., Lystrup, A., and Vorm, T., 1983, "The Cutting Process, Chips, and Cutting Forces in Machining Cfrp," Composites, **14**(4), pp. 371-376.
[77] Wang, D. H., Ramulu, M., and Arola, D., 1995, "Orthogonal cutting mechanisms of graphite/epoxy composite. Part II: multi-directional laminate," International Journal of Machine Tools and Manufacture, **35**(12), pp. 1639-1648.

[78] Wang, D. H., Ramulu, M., and Arola, D., 1995, "Orthogonal cutting mechanisms of graphite/epoxy composite. Part I: unidirectional laminate," International Journal of Machine Tools and Manufacture, **35**(12), pp. 1623-1638.
[79] Hocheng, H., and Puw, H. Y., 1992, "On Drilling Characteristics of Fiber-Reinforced Thermoset and Thermoplastics," Int J Mach Tool Manu, **32**(4), pp. 583-592.
[80] Bhatnagar, N., Ramakrishnan, N., Naik, N. K., and Komanduri, R., 1995, "On the Machining of Fiber-Reinforced Plastic (Frp) Composite Laminates," Int J Mach Tool Manu, **35**(5), pp. 701-716.
[81] Santiuste, C., Soldani, X., and Miguélez, M. H., 2010, "Machining FEM model of long fiber composites for aeronautical components," Compos Struct, **92**(3), pp. 691-698.
[82] Wang, X., and Zhang, L., 2003, "An experimental investigation into the orthogonal cutting of unidirectional fibre reinforced plastics," International Journal of Machine Tools and Manufacture, **43**(10), pp. 1015-1022.
[83] Arola, D., Ramulu, M., and Wang, D., 1996, "Chip formation in orthogonal trimming of graphite/epoxy composite," Composites Part A: applied science and manufacturing, **27**(2), pp. 121-133.
[84] Dharan, C. K. H., and Won, M. S., 2000, "Machining parameters for an intelligent machining system for composite laminates," Int J Mach Tool Manu, **40**(3), pp. 415-426.
[85] Jain, S., and Yang, D. C. H., 1994, "Delamination-Free Drilling of Composite Laminates," J. Eng. Ind.-Trans. ASME, **116**(4), pp. 475-481.
[86] Lazar, M.-B., and Xirouchakis, P., 2011, "Experimental analysis of drilling fiber reinforced composites," International Journal of Machine Tools and Manufacture, **51**(12), pp. 937-946.
[87] Murphy, C., Byrne, G., and Gilchrist, M. D., 2002, "The performance of coated tungsten carbide drills when machining carbon fibre-reinforced epoxy composite materials," P I Mech Eng B-J Eng, **216**(2), pp. 143-152.
[88] Jain, S., and Yang, D. C. H., 1993, "Effects of Feedrate and Chisel Edge on Delamination in Composites Drilling," J. Eng. Ind.-Trans. ASME, **115**(4), pp. 398-405.
[89] Enemuoh, E. U., El-Gizawy, A. S., and Okafor, A. C., 2001, "An approach for development of damage-free drilling of carbon fiber reinforced thermosets," Int J Mach Tool Manu, **41**(12), pp. 1795-1814.
[90] Tsao, C. C., and Hocheng, H., 2004, "Taguchi analysis of delamination associated with various drill bits in drilling of composite material," Int J Mach Tool Manu, **44**(10), pp. 1085-1090.
[91] Tsao, C. C., and Hocheng, H., 2007, "Parametric study on thrust force of core drill," Journal of Materials Processing Technology, **192**, pp. 37-40.
[92] Durao, L. M. P., Goncalves, D. J. S., Tavares, J. M. R. S., de Albuquerque, V. H. C., Vieira, A. A., and Marques, A. T., 2010, "Drilling tool geometry evaluation for reinforced composite laminates," Compos Struct, **92**(7), pp. 1545-1550.
[93] Tsao, C. C., and Hocheng, H., 2005, "Computerized tomography and C-Scan for measuring delamination in the drilling of composite materials using various drills," Int J Mach Tool Manu, **45**(11), pp. 1282-1287.
[94] Tsao, C. C., 2008, "Experimental study of drilling composite materials with step-core drill," Mater Design, **29**(9), pp. 1740-1744.
[95] Tsao, C. C., 2008, "Comparison between response surface methodology and radial basis function network for core-center drill in drilling composite materials," Int J Adv Manuf Tech, **37**(11-12), pp. 1061-1068.
[96] Marques, A. T., Durao, L. M., Magalhaes, A. G., Silva, J. F., and Tavares, J. M. R. S., 2009, "Delamination analysis of carbon fibre reinforced laminates: Evaluation of a special step drill," Compos Sci Technol, **69**(14), pp. 2376-2382.

[97] Shyha, I., Soo, S. L., Aspinwall, D., and Bradley, S., 2010, "Effect of laminate configuration and feed rate on cutting performance when drilling holes in carbon fibre reinforced plastic composites," Journal of Materials Processing Technology, **210**(8), pp. 1023-1034.
[98] Tsao, C. C., and Hocheng, H., 2008, "Evaluation of thrust force and surface roughness in drilling composite maternal using Taguchi analysis and neural network," Journal of Materials Processing Technology, **203**(1-3), pp. 342-348.
[99] Iliescu, D., Gehin, D., Gutierrez, M. E., and Girot, F., 2010, "Modeling and tool wear in drilling of CFRP," Int J Mach Tool Manu, **50**(2), pp. 204-213.
[100] Zhang, L. B., Wang, L. J., and Liu, X. Y., 2001, "A mechanical model for predicting critical thrust forces in drilling composite laminates," P I Mech Eng B-J Eng, **215**(2), pp. 135-146.
[101] Tsao, C. C., and Hocheng, H., 2008, "Analysis of delamination in drilling composite materials by core-saw drill," Int J Mater Prod Tec, **32**(2-3), pp. 188-201.
[102] Malhotra, S. K., 1990, "Some Studies on Drilling of Fibrous Composites," Journal of Materials Processing Technology, **24**, pp. 291-300.
[103] Park, K. Y., Choi, J. H., and Lee, D. G., 1995, "Delamination-Free and High-Efficiency Drilling of Carbon-Fiber-Reinforced Plastics," J Compos Mater, **29**(15), pp. 1988-2002.
[104] Tsao, C. C., and Hocheng, H., 2007, "Effect of tool wear on delamination in drilling composite materials," Int J Mech Sci, **49**(8), pp. 983-988.
[105] Gaitonde, V. N., Karnik, S. R., Rubio, J. C., Correia, A. E., Abrao, A. M., and Davim, J. P., 2008, "Analysis of parametric influence on delamination in high-speed drilling of carbon fiber reinforced plastic composites," Journal of Materials Processing Technology, **203**(1-3), pp. 431-438.
[106] Karnik, S. R., Gaitonde, V. N., Rubio, J. C., Correia, A. E., Abrao, A. M., and Davim, J. P., 2008, "Delamination analysis in high speed drilling of carbon fiber reinforced plastics (CFRP) using artificial neural network model," Mater Design, **29**(9), pp. 1768-1776.
[107] Rubio, J. C. C., Abrao, A. M., Faria, P. E., Correia, A. E., and Davim, J. P., 2008, "Delamination in high speed drilling of carbon fiber reinforced plastic (CFRP)," J Compos Mater, **42**(15), pp. 1523-1532.
[108] Rawat, S., and Attia, H., 2009, "Characterization of the dry high speed drilling process of woven composites using Machinability Maps approach," Cirp Annals-Manufacturing Technology, **58**(1), pp. 105-108.
[109] Rawat, S., and Attia, H., 2009, "Wear mechanisms and tool life management of WC-Co drills during dry high speed drilling of woven carbon fibre composites," Wear, **267**(5-8), pp. 1022-1030.
[110] Brinksmeier, E., Fangmann, S., and Rentsch, R., 2011, "Drilling of composites and resulting surface integrity," Cirp Annals-Manufacturing Technology, **60**(1), pp. 57-60.
[111] Masuda, M., Kuroshima, Y., and Chujo, Y., 1993, "Failure of tungsten carbide-cobalt alloy tools in machining of carbon materials," Wear, **169**(2), pp. 135-140.
[112] Wang, X., Kwon, P. Y., Sturtevant, C., Kim, D., and Lantrip, J., 2013, "Tool wear of coated drills in drilling CFRP," Journal of Manufacturing Processes, **15**(1), pp. 127-135.
[113] Trent, E. M., and Wright, P. K., 2000, Metal cutting, Butterworth-Heinemann, Boston. ISBN 075067069X.
[114] Wang, X., Kwon, P. Y., Sturtevant, C., Kim, D., and Lantrip, J., 2012, "Tool wear of coated drills in drilling CFRP," Journal of Manufacturing Processes.
[115] Engqvist, H., Jacobson, S., and Axen, N., 2002, "A model for the hardness of cemented carbides," Wear, **252**(5-6), pp. 384-393.

[116] Faraz, A., Biermann, D., and Weinert, K., 2009, "Cutting edge rounding: An innovative tool wear criterion in drilling CFRP composite laminates," Int J Mach Tool Manu, **49**(15), pp. 1185-1196.
[117] Shyha, I. S., Aspinwall, D. K., Soo, S. L., and Bradley, S., 2009, "Drill geometry and operating effects when cutting small diameter holes in CFRP," Int J Mach Tool Manu, **49**(12-13), pp. 1008-1014.
[118] Durão, L. M. P., Tavares, J. M. R. S., de Albuquerque, V. H. C., and Gonçalves, D. J. S., 2013, "Damage evaluation of drilled carbon/epoxy laminates based on area assessment methods," Compos Struct, **96**(0), pp. 576-583.
[119] Stone, R., and Krishnamurthy, K., 1996, "A neural network thrust force controller to minimize delamination during drilling of graphite-epoxy laminates," Int J Mach Tool Manu, **36**(9), pp. 985-1003.
[120] Hocheng, H., and Dharan, C. K. H., 1990, "Delamination during Drilling in Composite Laminates," J. Eng. Ind.-Trans. ASME, **112**(3), pp. 236-239.
[121] Durao, L. M., Tavares, J. M. R. S., de Magalhaes, A. G., Marques, A. T., and Baptista, A. P. M., 2008, "Damage analysis of carbon/epoxy plates after drilling," Int J Mater Prod Tec, **32**(2-3), pp. 226-242.
[122] Tsao, C. C., 2007, "Effect of pilot hole on thrust force by saw drill," Int J Mach Tool Manu, **47**(14), pp. 2172-2176.
[123] Tsao, C. C., 2008, "Thrust force and delamination of core-saw drill during drilling of carbon fiber reinforced plastics (CFRP)," Int J Adv Manuf Tech, **37**(1-2), pp. 23-28.
[124] Tsao, C. C., 2008, "Investigation into the effects of drilling parameters on delamination by various step-core drills," Journal of Materials Processing Technology, **206**(1-3), pp. 405-411.
[125] Davim, J. P., Rubio, J. C., and Abrao, A. M., 2007, "A novel approach based on digital image analysis to evaluate the delamination factor after drilling composite laminates," Compos Sci Technol, **67**(9), pp. 1939-1945.
[126] Hocheng, H., and Tsao, C. C., 2005, "The path towards delamination-free drilling of composite materials," Journal of Materials Processing Technology, **167**(2-3), pp. 251-264.
[127] Tsao, C. C., and Chen, W. C., 1997, "Prediction of the location of delamination in the drilling of composite laminates," Journal of Materials Processing Technology, **70**(1-3), pp. 185-189.
[128] Sardinas, R. Q., Reis, P., and Davim, J. P., 2006, "Multi-objective optimization of cutting parameters for drilling laminate composite materials by using genetic algorithms," Compos Sci Technol, **66**(15), pp. 3083-3088.
[129] Klocke, F., and Wurtz, C., 1998, "The Use of PCD Tools for Machining Fibre Reinforced Materials," ECCM-8: European Conference on Composite Materials, pp. 509-514.
[130] Tsao, C. C., 2006, "The effect of pilot hole on delamination when core drill drilling composite materials," Int J Mach Tool Manu, **46**(12-13), pp. 1653-1661.
[131] Tsao, C. C., and Chiu, Y. C., 2011, "Evaluation of drilling parameters on thrust force in drilling carbon fiber reinforced plastic (CFRP) composite laminates using compound core-special drills," Int J Mach Tool Manu, **51**(9), pp. 740-744.
[132] Knight, W. A., and Boothroyd, G., 2005, Fundamentals of Metal Machining and Machine Tools, Third Edition, Taylor & Francis.
[133] Abukhshim, N. A., Mativenga, P. T., and Sheikh, M. A., 2006, "Heat generation and temperature prediction in metal cutting: A review and implications for high speed machining," International Journal of Machine Tools and Manufacture, **46**(7–8), pp. 782-800.
[134] Byrne, G., and Scholta, E., 1993, "Environmentally clean machining processes—a strategic approach," Cirp Annals-Manufacturing Technology, **42**(1), pp. 471-474.

[135] Bhattacharyya, D., Allen, M., and Mander, S., 1993, "Cryogenic machining of Kevlar composites," MATERIAL AND MANUFACTURING PROCESS, **8**(6), pp. 631-651.
[136] Hong, S. Y., Ding, Y., and Ekkens, R. G., 1999, "Improving low carbon steel chip breakability by cryogenic chip cooling," International Journal of Machine Tools and Manufacture, **39**(7), pp. 1065-1085.
[137] Hong, S. Y., and Ding, Y., 2001, "Micro-temperature manipulation in cryogenic machining of low carbon steel," Journal of Materials Processing Technology, **116**(1), pp. 22-30.
[138] Wang, Z. Y., Rajurkar, K. P., and Murugappan, M., 1996, "Cryogenic PCBN turning of ceramic (Si3N4)," Wear, **195**(1–2), pp. 1-6.
[139] Wang, Z. Y., and Rajurkar, K. P., 1997, "Wear of CBN tool in turning of silicon nitride with cryogenic cooling," International Journal of Machine Tools and Manufacture, **37**(3), pp. 319-326.
[140] Wang, Z. Y., and Rajurkar, K. P., 2000, "Cryogenic machining of hard-to-cut materials," Wear, **239**(2), pp. 168-175.
[141] Ahmed, M. I., Ismail, A. F., Abakr, Y. A., and Amin, A. K. M. N., 2007, "Effectiveness of cryogenic machining with modified tool holder," Journal of Materials Processing Technology, **185**(1–3), pp. 91-96.
[142] Ávila, R. F., and Abrão, A. M., 2001, "The effect of cutting fluids on the machining of hardened AISI 4340 steel," Journal of Materials Processing Technology, **119**(1–3), pp. 21-26.
[143] Zurecki, Z., Frey, J., and Ghosh, R., 2003, "Finish-turning of hardened powder-metallurgy steel using cryogenic cooling," Advances in Powder Metallurgy and Particulate Materials(7), pp. 7-185.
[144] Dhar, N., Kishore, N. S., Paul, S., and Chattopadhyay, A., 2002, "The effects of cryogenic cooling on chips and cutting forces in turning AISI 1040 and AISI 4320 steels," Proceedings of the Institution of Mechanical Engineers, Part B: Journal of Engineering Manufacture, **216**(5), pp. 713-724.
[145] Kalyan Kumar, K. V. B. S., and Choudhury, S. K., 2008, "Investigation of tool wear and cutting force in cryogenic machining using design of experiments," Journal of Materials Processing Technology, **203**(1–3), pp. 95-101.
[146] Venugopal, K. A., Paul, S., and Chattopadhyay, A. B., 2007, "Growth of tool wear in turning of Ti-6Al-4V alloy under cryogenic cooling," Wear, **262**(9–10), pp. 1071-1078.
[147] Bermingham, M. J., Kirsch, J., Sun, S., Palanisamy, S., and Dargusch, M. S., 2011, "New observations on tool life, cutting forces and chip morphology in cryogenic machining Ti-6Al-4V," International Journal of Machine Tools and Manufacture, **51**(6), pp. 500-511.
[148] Hong, S. Y., Ding, Y., and Jeong, W.-c., 2001, "Friction and cutting forces in cryogenic machining of Ti–6Al–4V," International Journal of Machine Tools and Manufacture, **41**(15), pp. 2271-2285.
[149] Hong, S. Y., Markus, I., and Jeong, W.-c., 2001, "New cooling approach and tool life improvement in cryogenic machining of titanium alloy Ti-6Al-4V," International Journal of Machine Tools and Manufacture, **41**(15), pp. 2245-2260.
[150] Air Products and Chemicals Inc., 2014, "Metal Forming/Shaping," (Accessed March 2014). URL http://www.airproducts.com/industries/metals/metals-processing/metals-formingshaping/product-list/machining-metals-formingshaping.aspx?itemId=2105045D6A774F1783B913A25D359ADF.
[151] Zurecki, Z., Ghosh, R., and Frey, J. H., 2003, "Investigation of white layers formed in conventional and cryogenic hard turning of steels," ASME 2003 International Mechanical Engineering Congress and Exposition, American Society of Mechanical Engineers, pp. 211-220.

[152] Air Products and Chemicals Inc., 2003, "Process Step Elimination in Powder Metal Part Manufacturing," (Accessed March 2012). URL http://www.airproducts.com/~/media/downloads/i/icefly-machining-technology-north-america-only/data-sheets/en-icefly-machining-technology-datasheet.pdf?industryItem=industries&subIndustryItem=Metals&segment=Metals-Processing&applicationChildItem=Metals-FormingShaping&productLevel3=ICEFLY-Machining-Technology-North-America-Only.

[153] MAG Industrial Automative Systems, 2014, "Cryogenic: Breakthrough Cryogenic Design," (Accessed March 2014). URL http://www.mag-ias.com/en/mag/technologies.html.

[154] Zelinski, P., 2013, "Expanded Possibilities for Cryogenic Machining," Modern Machine Shop.

[155] Zelinski, P., 2011, "The 400° Difference," Modern Machine Shop.

[156] da Silva, F. J., Franco, S. D., Machado, Á. R., Ezugwu, E. O., and Souza Jr, A. M., 2006, "Performance of cryogenically treated HSS tools," Wear, **261**(5–6), pp. 674-685.

[157] Firouzdor, V., Nejati, E., and Khomamizadeh, F., 2008, "Effect of deep cryogenic treatment on wear resistance and tool life of M2 HSS drill," Journal of Materials Processing Technology, **206**(1–3), pp. 467-472.

[158] Das, D., Dutta, A. K., Toppo, V., and Ray, K. K., 2007, "Effect of Deep Cryogenic Treatment on the Carbide Precipitation and Tribological Behavior of D2 Steel," Materials and Manufacturing Processes, **22**(4), pp. 474-480.

[159] Seah, K., Rahman, M., and Yong, K., 2003, "Performance evaluation of cryogenically treated tungsten carbide cutting tool inserts," Proceedings of the Institution of Mechanical Engineers, Part B: Journal of Engineering Manufacture, **217**(1), pp. 29-43.

[160] Yong, A. Y. L., Seah, K. H. W., and Rahman, M., 2006, "Performance evaluation of cryogenically treated tungsten carbide tools in turning," International Journal of Machine Tools and Manufacture, **46**(15), pp. 2051-2056.

[161] Yong, A. Y. L., Seah, K. H. W., and Rahman, M., 2007, "Performance of cryogenically treated tungsten carbide tools in milling operations," Int J Adv Manuf Tech, **32**(7-8), pp. 638-643.

[162] De Chiffre, L., Andreasen, J. L., Lagerberg, S., and Thesken, I. B., 2007, "Performance Testing of Cryogenic CO2 as Cutting Fluid in Parting/Grooving and Threading Austenitic Stainless Steel," CIRP Annals - Manufacturing Technology, **56**(1), pp. 101-104.

[163] Clarens, A. F., Park, Y.-E., Temme, J., Hayes, K., Zhao, F., and Skerlos, S., 2009, "Evaluation of cooling potential and tool life in turning using metalworking fluids delivered in supercritical carbon dioxide," ASME 2009 International Manufacturing Science and Engineering Conference, American Society of Mechanical Engineers, pp. 67-75.

[164] Le, T.-S., Dau, P.-H., Vuong, Q.-T., Vuong, B.-T., and Nguyen1c, V.-C., 2012, "On the Feasibility of MQL Using a Mixture of Supercritical CO2 with Cutting Fluid for Green Machining."

[165] Stephenson, D. A., Skerlos, S. J., King, A. S., and Supekar, S. D., 2014, "Rough turning Inconel 750 with supercritical CO2-based minimum quantity lubrication," Journal of Materials Processing Technology, **214**(3), pp. 673-680.

[166] Private Communication with Niklas Lehming, Managing Director at SGS Tools, February 2013.

[167] Çakır, O., Kıyak, M., and Altan, E., 2004, "Comparison of gases applications to wet and dry cuttings in turning," Journal of Materials Processing Technology, **153–154**(0), pp. 35-41.

[168] Findley Media Ltd., 2013, "Machinery: Starrag Group CO2 coolant development is award winner.," (Accessed July 2014). URL http://www.machinery.co.uk/machinery-videos/starrag-group-co2-coolant-maschinenmarkt/57144/.
[169] Private Communication with Neil Reynolds, Senior Research Fellow at WMG, 8th November 2014.
[170] Durao, L. M. P., Magalhaes, A. G., Marques, A. T., Manuel, J., and Tavares, R. S., 2007, "Effect of drilling parameters on composite plates damage," International Conference HSIMPSenlis, France, pp. 1-8.
[171] De Chiffre, L., Andreasen, J. L., Lagerberg, S., and Thesken, I. B., 2007, "Performance testing of cryogenic CO_2 as cutting fluid in parting/grooving and threading austenitic stainless steel," Cirp Ann-Manuf Techn, **56**(1), pp. 101-104.
[172] Clarens, A. F., Park, Y. E., Temme, J., Hayes, K., Zhao, F., and Skerlos, S., 2009, "Evaluation of Cooling Potential and Tool Life in Turning Using Metalworking Fluids Delivered in Supercritical Carbon Dioxide," Proceedings of the Asme International Manufacturing Science and Engineering Conference, **1**, pp. 67-75.
[173] Jerold, D. B., and Kumar, P. M., 2011, "Experimental investigation of turning AISI 1045 steel using cryogenic carbon dioxide as the cutting fluid," Journal of Manufacturing Processes, **13**, pp. 113-119.
[174] Machai, C., and Biermann, D., 2011, "Machining of β-titanium-alloy Ti–10V–2Fe–3Al under cryogenic conditions: Cooling with carbon dioxide snow " Journal of Materials Processing Technology, **211**, pp. 1175-1183.
[175] SGS Tool UK, Ltd., "CO_2 Technology is Part of the Solution."
[176] SGS Tool UK, Ltd., "Composite Catalogue: SGS Solid Carbide Tools."
[177] Private communication with Nadia Kourra, EngD candidate at WMG, 2013.
[178] SGS Tool UK, Ltd., 2012, "SGS Solid Carbide Tools: High Performance Drilling Solutions." (Accessed March 2013). URL http://www.sgstool.com/languages/french/catalogs/PDFsections/Hi-PerCarb.pdf
[179] Private communication with Nadia Kourra, EngD candidate at WMG, 11th November 2014.
[180] Schilling, P. J., Karedla, B. R., Tatiparthi, A. K., Verges, M. A., and Herrington, P. D., 2005, "X-ray computed microtomography of internal damage in fiber reinforced polymer matrix composites," Compos Sci Technol, **65**(14), pp. 2071-2078.
[181] Omega Engineering Limited, 2013, "Omega Engineering Limted Website," (Acessed May 2013). URL http://www.omega.co.uk/pptst/CO-K.html.
[182] Private Communication with Dave Hudson, National Sales Manager at Guhring Ltd., 2013.
[183] Ultra Carbide Inc., 2007, "Carbide Grade: DK 460 UF," (Accessed July 2013). URL http://www.ultracarbide.com/pdfs/dk460uf.pdf.
[184] Private Communication with Neil Reynolds, Senior Research Fellow at WMG, 2012,
[185] Kaynak, Y., Karaca, H. E., Noebe, R. D., and Jawahir, I. S., 2013, "Analysis of Tool-wear and Cutting Force Components in Dry, Preheated, and Cryogenic Machining of NiTi Shape Memory Alloys," Procedia CIRP, **8**(0), pp. 498-503.
[186] Private Communication with Austin Cook, Senior Manufacturing Development Engineer at BAE Systems, 2012.
[187] Bhattacharyya, D., Allen, M., and Mander, S., 1991, "Cryogenic machining of Kevlar composites," Processing and Manufacturing of Composite Materials, pp. 133-147.
[188] Schutz, J. B., 1998, "Properties of composite materials for cryogenic applications," Cryogenics, **38**(1), pp. 3-12.
[189] Morioka, K., Tomita, Y., and Takigawa, K., 2001, "High-temperature fracture properties of CFRP composite for aerospace applications," Mat Sci Eng a-Struct, **319**, pp. 675-678.

[190] Kim, M.-G., Kang, S.-G., Kim, C.-G., and Kong, C.-W., 2007, "Tensile response of graphite/epoxy composites at low temperatures," Compos Struct, **79**(1), pp. 84-89.
[191] Kim, M. G., Kang, S. G., Kim, C. G., and Kong, C. W., 2010, "Tensile Properties of Carbon Fiber Composites with Different Resin Compositions at Cryogenic Temperatures," Adv Compos Mater, **19**(1), pp. 63-77.
[192] Alauddin, M., Choudhury, I. A., ElBaradie, M. A., and Hashmi, M. S. J., 1995, "Plastics and their machining: A review," Journal of Materials Processing Technology, **54**(1-4), pp. 40-46.
[193] Yamini, S., and Young, R. J., 1980, "The mechanical properties of epoxy resins," Journal of materials science, **15**(7), pp. 1823-1831.
[194] Kinloch, A. J., Shaw, S. J., and Hunston, D. L., 1983, "Deformation and Fracture-Behavior of a Rubber-Toughened Epoxy .2. Failure Criteria," Polymer, **24**(10), pp. 1355-1363.
[195] Kinloch, A. J., Shaw, S. J., Tod, D. A., and Hunston, D. L., 1983, "Deformation and Fracture-Behavior of a Rubber-Toughened Epoxy .1. Microstructure and Fracture Studies," Polymer, **24**(10), pp. 1341-1354.
[196] DiPaolo, G., Kapoor, S., and DeVor, R., 1996, "An experimental investigation of the crack growth phenomenon for drilling of fiber-reinforced composite materials," Journal of engineering for industry, **118**(1), pp. 104-110.
[197] Krishnamurthy, R., Santhanakrishnan, G., and Malhotra, S., 1992, "Machining of polymeric composites," Machining of composite materials(A 95-15178 02-37), Materials Park, OH, ASM International, 1992, pp. 139-148.
[198] Blombery, R. I., Perrot, C. M., and Robinson, P. M., 1974, "Abrasive wear of tungsten carbide-cobalt composites. I. Wear mechanisms," Materials Science and Engineering, **13**(2), pp. 93-100.

Appendix A

Raw data of drilling tests for evaluation of drilling performance of carbon fibre reinforced plastics with a tool pre-cooled in LN_2 (Section 6.1)

No. of Drilled Holes	Average Flank Wear (mm)		Average Thrust Force (N)		Maximum Thrust Force (N)		Entry F_d (D_{max}/D_{hole})		Exit F_d (D_{max}/D_{hole})		Exit F_{da} (A_{max}/A_{hole})		Total Depth of Internal Damage (mm)	
	RT Dry	LN_2 Pre-cooling	RT Dry	LN_2 Pre-cooling	RT Dry	LN_2 Pre-cooling	RT Dry	LN_2 Pre-cooling	RT Dry	LN_2 Pre-cooling	RT Dry	LN_2 Pre-cooling	RT Dry	LN_2 Pre-cooling
1	0.00	0.00	72	88	114	122	1.05	1.00	1.75	1.35	0.34	0.04	2.33	2.35
25	0.03	0.05	90	104	130	148								
50	0.05	0.07	98	120	151	175	1.05	1.03	1.63	1.37	0.19	0.07		
75	0.06	0.08	113	132	157	181								
100	0.08	0.09	119	141	168	198	1.04	1.05	1.78	1.27	0.19	0.09		
125	0.08	0.10	130	147	185	193								
150	0.09	0.11	138	157	192	204	1.07	1.06	1.37	1.34	0.15	0.08		
175	0.10	0.12	146	162	206	217								
200	0.12	0.13	156	171	209	233	1.08	1.07	1.26	1.42	0.17	0.11		
225	0.12	0.13	165	175	217	236								
250	0.13	0.14	170	185	235	255	1.20	1.07	1.45	1.49	0.22	0.14		
275	0.14	0.15	178	193	232	262								
300	0.15	0.16	186	199	253	267	1.20	1.09	1.65	1.58	0.26	0.20		
325	0.16	0.16	193	205	255	283							3.23	0.27

Appendix B

Raw data of drilling tests for evaluation of drilling performance of carbon fibre reinforced plastics with a CO_2 cooling system (Section 6.2)

No. of Hole	Cutting Speed		Feed Rate		Flow Rate of CO_2 (l/min)	Thrust Force (N)		Exit Delamination
	m/min	RPM	mm/rev	mm/min		Average	Maximum	Total A_D (mm²)
1	75	3979	0.03	119	0	70	82	1.37
2	75	3979	0.03	119	0	68	81	1.61
3	75	3979	0.03	119	0	70	82	1.49
Average	75	3979	0.03	119	0	69	81	1.49
4	75	3979	0.03	119	3.37	75	88	1.05
5	75	3979	0.03	119	3.37	76	89	1.47
6	75	3979	0.03	119	3.37	76	89	1.25
Average	75	3979	0.03	119	3.37	76	89	1.25
7	75	3979	0.06	239	0	84	98	1.69
8	75	3979	0.06	239	0	84	98	1.39
9	75	3979	0.06	239	0	83	96	1.79
Average	75	3979	0.06	239	0	84	97	1.63
10	75	3979	0.06	239	3.37	87	100	1.35
11	75	3979	0.06	239	3.37	91	104	1.26
12	75	3979	0.06	239	3.37	91	106	1.59
Average	75	3979	0.06	239	3.37	90	103	1.40
13	75	3979	0.09	358	0	95	110	1.65
14	75	3979	0.09	358	0	94	109	1.58

15	75	3979	0.09	358	0	93	106	1.84
Average	75	3979	0.09	358	0	94	108	1.69
16	75	3979	0.09	358	3.37	97	111	1.84
17	75	3979	0.09	358	3.37	95	109	0.80
18	75	3979	0.09	358	3.37	98	111	1.67
Average	75	3979	0.09	358	3.37	97	110	1.44
19	75	3979	0.12	477	0	102	117	2.02
20	75	3979	0.12	477	0	102	116	2.41
21	75	3979	0.12	477	0	102	116	2.02
Average	75	3979	0.12	477	0	102	116	2.15
22	75	3979	0.12	477	3.37	106	119	1.55
23	75	3979	0.12	477	3.37	106	122	1.66
24	75	3979	0.12	477	3.37	104	119	1.23
Average	75	3979	0.12	477	3.37	105	120	1.48
25	75	3979	0.15	597	0	109	125	2.20
26	75	3979	0.15	597	0	108	124	2.18
27	75	3979	0.15	597	0	108	125	2.43
Average	75	3979	0.15	597	0	108	125	2.27
28	75	3979	0.15	597	3.37	110	127	0.87
29	75	3979	0.15	597	3.37	111	127	1.73
30	75	3979	0.15	597	3.37	109	126	1.79
Average	75	3979	0.15	597	3.37	110	127	1.46

No. of Hole	Cutting Speed		Feed Rate		Flow Rate of CO_2 (l/min)	Thrust Force (N)		Exit Delamination
	m/min	RPM	mm/rev	mm/min		Average	Maximum	Total A_D (mm^2)
1	100	5305	0.03	159	0	69	84	1.91
2	100	5305	0.03	159	0	68	82	2.09
3	100	5305	0.03	159	0	68	81	2.06
Average	100	5305	0.03	159	0	68	83	2.02
4	100	5305	0.03	159	3.37	78	95	1.57
5	100	5305	0.03	159	3.37	79	96	1.50
6	100	5305	0.03	159	3.37	79	99	1.74
Average	100	5305	0.03	159	3.37	79	97	1.60
7	100	5305	0.06	318	0	90	109	2.13
8	100	5305	0.06	318	0	85	100	2.15
9	100	5305	0.06	318	0	84	100	1.89
Average	100	5305	0.06	318	0	86	103	2.06
10	100	5305	0.06	318	3.37	88	102	1.82
11	100	5305	0.06	318	3.37	90	104	1.96
12	100	5305	0.06	318	3.37	91	107	1.96
Average	100	5305	0.06	318	3.37	90	104	1.92
13	100	5305	0.09	477	0	94	112	2.35
14	100	5305	0.09	477	0	94	111	2.23
15	100	5305	0.09	477	0	93	110	2.12
Average	100	5305	0.09	477	0	94	111	2.23
16	100	5305	0.09	477	3.37	99	114	1.81
17	100	5305	0.09	477	3.37	98	113	2.13

18	100	5305	0.09	477	3.37	98	115	2.19
Average	100	5305	0.09	477	3.37	99	114	2.05
19	100	5305	0.12	637	0	104	123	2.30
20	100	5305	0.12	637	0	104	120	2.34
21	100	5305	0.12	637	0	103	121	2.60
Average	100	5305	0.12	637	0	104	121	2.41
22	100	5305	0.12	637	3.37	106	123	2.19
23	100	5305	0.12	637	3.37	105	124	2.15
24	100	5305	0.12	637	3.37	107	125	2.44
Average	100	5305	0.12	637	3.37	106	124	2.26
25	100	5305	0.15	796	0	109	131	2.76
26	100	5305	0.15	796	0	110	129	2.44
27	100	5305	0.15	796	0	108	129	2.47
Average	100	5305	0.15	796	0	109	129	2.56
28	100	5305	0.15	796	3.37	111	130	2.43
29	100	5305	0.15	796	3.37	113	131	2.56
30	100	5305	0.15	796	3.37	113	131	2.40
Average	100	5305	0.15	796	3.37	112	131	2.46

No. of Hole	Cutting Speed		Feed Rate		Flow Rate of CO_2 (l/min)	Thrust Force (N)		Exit Delamination
	m/min	RPM	mm/rev	mm/min		Average	Maximum	Total A_D (mm^2)
1	115	6101	0.03	183	0	70	81	1.79
2	115	6101	0.03	183	0	70	81	2.31
3	115	6101	0.03	183	0	70	81	2.23
Average	115	6101	0.03	183	0	70	81	2.11
4	115	6101	0.03	183	3.37	73	84	1.81
5	115	6101	0.03	183	3.37	73	84	1.87
6	115	6101	0.03	183	3.37	75	86	1.92
Average	115	6101	0.03	183	3.37	73	85	1.87
7	115	6101	0.06	366	0	88	103	2.00
8	115	6101	0.06	366	0	87	100	2.19
9	115	6101	0.06	366	0	88	102	2.39
Average	115	6101	0.06	366	0	88	102	2.19
10	115	6101	0.06	366	3.37	88	101	2.02
11	115	6101	0.06	366	3.37	89	103	2.06
12	115	6101	0.06	366	3.37	88	101	2.25
Average	115	6101	0.06	366	3.37	88	102	2.11
13	115	6101	0.09	549	0	96	113	2.19
14	115	6101	0.09	549	0	95	112	2.30
15	115	6101	0.09	549	0	96	114	2.47
Average	115	6101	0.09	549	0	95	113	2.32
16	115	6101	0.09	549	3.37	96	114	2.17
17	115	6101	0.09	549	3.37	98	113	2.30

18	115	6101	0.09	549	3.37	97	113	2.15
Average	115	6101	0.09	549	3.37	97	113	2.21
19	115	6101	0.12	732	0	103	122	2.43
20	115	6101	0.12	732	0	102	121	2.43
21	115	6101	0.12	732	0	103	121	2.61
Average	115	6101	0.12	732	0	103	122	2.49
22	115	6101	0.12	732	3.37	104	122	2.23
23	115	6101	0.12	732	3.37	103	122	2.61
24	115	6101	0.12	732	3.37	105	122	2.33
Average	115	6101	0.12	732	3.37	104	122	2.39
25	115	6101	0.15	915	0	109	130	2.38
26	115	6101	0.15	915	0	108	130	2.63
27	115	6101	0.15	915	0	109	128	2.57
Average	115	6101	0.15	915	0	109	129	2.53
28	115	6101	0.15	915	3.37	109	129	2.23
29	115	6101	0.15	915	3.37	109	130	2.30
30	115	6101	0.15	915	3.37	111	129	2.82
Average	115	6101	0.15	915	3.37	110	129	2.45

No. of Hole	Cutting Speed		Feed Rate		Flow Rate of CO_2 (l/min)	Thrust Force (N)		Exit Delamination
	m/min	RPM	mm/rev	mm/min		Average	Maximum	Total A_D (mm^2)
1	130	6897	0.03	207	0	72	84	2.11
2	130	6897	0.03	207	0	72	84	2.22
3	130	6897	0.03	207	0	72	84	2.29
Average	130	6897	0.03	207	0	72	84	2.21
4	130	6897	0.03	207	3.37	73	85	2.10
5	130	6897	0.03	207	3.37	74	86	1.99
6	130	6897	0.03	207	3.37	75	87	1.74
Average	130	6897	0.03	207	3.37	74	86	1.94
7	130	6897	0.06	414	0	88	102	2.28
8	130	6897	0.06	414	0	88	103	2.41
9	130	6897	0.06	414	0	87	103	2.48
Average	130	6897	0.06	414	0	88	103	2.39
10	130	6897	0.06	414	3.37	89	103	2.17
11	130	6897	0.06	414	3.37	90	104	2.22
12	130	6897	0.06	414	3.37	89	103	2.32
Average	130	6897	0.06	414	3.37	90	103	2.23
13	130	6897	0.09	621	0	97	115	2.49
14	130	6897	0.09	621	0	98	117	2.40
15	130	6897	0.09	621	0	98	114	2.56
Average	130	6897	0.09	621	0	98	115	2.48
16	130	6897	0.09	621	3.37	100	116	2.35
17	130	6897	0.09	621	3.37	99	117	2.40

18	130	6897	0.09	621	3.37	101	118	2.30
Average	130	6897	0.09	621	3.37	100	117	2.35
19	130	6897	0.12	828	0	106	125	2.48
20	130	6897	0.12	828	0	105	123	2.58
21	130	6897	0.12	828	0	106	124	2.51
Average	130	6897	0.12	828	0	105	124	2.52
22	130	6897	0.12	828	3.37	108	125	2.44
23	130	6897	0.12	828	3.37	108	126	2.37
24	130	6897	0.12	828	3.37	107	125	2.40
Average	130	6897	0.12	828	3.37	107	125	2.40
25	130	6897	0.15	1035	0	114	134	2.46
26	130	6897	0.15	1035	0	110	129	2.58
27	130	6897	0.15	1035	0	112	130	2.63
Average	130	6897	0.15	1035	0	112	131	2.56
28	130	6897	0.15	1035	3.37	112	130	2.48
29	130	6897	0.15	1035	3.37	112	131	2.56
30	130	6897	0.15	1035	3.37	115	134	2.40
Average	130	6897	0.15	1035	3.37	113	132	2.48

No. of Hole	Cutting Speed		Feed Rate		Flow Rate of CO_2 (l/min)	Thrust Force (N)		Exit Delamination
	m/min	RPM	mm/rev	mm/min		Average	Maximum	Total A_D (mm²)
1	150	7958	0.03	239	0	75	88	2.24
2	150	7958	0.03	239	0	76	87	2.33
3	150	7958	0.03	239	0	75	88	2.26
Average	150	7958	0.03	239	0	76	88	2.27
4	150	7958	0.03	239	3.37	85	97	1.95
5	150	7958	0.03	239	3.37	83	95	2.14
6	150	7958	0.03	239	3.37	85	98	1.81
Average	150	7958	0.03	239	3.37	84	97	1.97
7	150	7958	0.06	477	0	94	107	2.33
8	150	7958	0.06	477	0	92	106	2.46
9	150	7958	0.06	477	0	92	106	2.44
Average	150	7958	0.06	477	0	92	106	2.41
10	150	7958	0.06	477	3.37	97	109	2.16
11	150	7958	0.06	477	3.37	98	111	2.12
12	150	7958	0.06	477	3.37	99	112	2.42
Average	150	7958	0.06	477	3.37	98	110	2.23
13	150	7958	0.09	716	0	103	120	2.65
14	150	7958	0.09	716	0	103	120	2.50
15	150	7958	0.09	716	0	103	118	2.58
Average	150	7958	0.09	716	0	103	119	2.58
16	150	7958	0.09	716	3.37	105	121	2.31

17	150	7958	0.09	716	3.37	106	121	2.40
18	150	7958	0.09	716	3.37	107	122	2.44
Average	150	7958	0.09	716	3.37	106	121	2.39
19	150	7958	0.12	955	0	111	129	2.74
20	150	7958	0.12	955	0	110	128	2.68
21	150	7958	0.12	955	0	109	128	2.62
Average	150	7958	0.12	955	0	110	128	2.68
22	150	7958	0.12	955	3.37	115	131	2.50
23	150	7958	0.12	955	3.37	114	131	2.50
24	150	7958	0.12	955	3.37	112	132	2.37
Average	150	7958	0.12	955	3.37	114	131	2.45
25	150	7958	0.15	1194	0	118	137	2.60
26	150	7958	0.15	1194	0	117	136	2.33
27	150	7958	0.15	1194	0	116	136	2.51
Average	150	7958	0.15	1194	0	117	137	2.48
28	150	7958	0.15	1194	3.37	119	138	2.37
29	150	7958	0.15	1194	3.37	119	141	2.11
30	150	7958	0.15	1194	3.37	121	144	2.07
Average	150	7958	0.15	1194	3.37	120	141	2.18

Appendix C

Raw data of drilling tests for the analysis of damage in drilling carbon fibre reinforced plastics (Section 6.3)

No. of Drilled Hole	Cutting Speed		Feed Rate		Cooling Method	Thrust Force (N)	
	m/min	RPM	mm/rev	mm/min		Average	Maximum
1	100	5305	0.06	318	Dry	124	177
2	100	5305	0.06	318	Dry	132	180
3	100	5305	0.06	318	Dry	136	181
Average	100	5305	0.06	318	Dry	131	179
4	100	5305	0.12	637	Dry	146	238
5	100	5305	0.12	637	Dry	140	239
6	100	5305	0.12	637	Dry	141	247
Average	100	5305	0.12	637	Dry	142	241
7	100	5305	0.06	318	CO_2 (3.37 l/min)	145	200
8	100	5305	0.06	318	CO_2 (3.37 l/min)	149	200
9	100	5305	0.06	318	CO_2 (3.37 l/min)	159	215
Average	100	5305	0.06	318	CO_2 (3.37 l/min)	151	205
10	100	5305	0.12	637	CO_2 (3.37 l/min)	171	275
11	100	5305	0.12	637	CO_2 (3.37 l/min)	158	275
12	100	5305	0.12	637	CO_2 (3.37 l/min)	163	277
Average	100	5305	0.12	637	CO_2 (3.37 l/min)	164	275
13	100	5305	0.06	318	LN_2 30 s	154	211

14	100	5305	0.06	318	LN_2 30 s	159	213
15	100	5305	0.06	318	LN_2 30 s	150	210
Average	100	5305	0.06	318	LN_2 30 s	154	211
16	100	5305	0.12	637	LN_2 30 s	157	281
17	100	5305	0.12	637	LN_2 30 s	163	283
18	100	5305	0.12	637	LN_2 30 s	166	286
Average	100	5305	0.12	637	LN_2 30 s	162	283
19	100	5305	0.06	318	LN_2 120 s	168	228
20	100	5305	0.06	318	LN_2 120 s	159	220
21	100	5305	0.06	318	LN_2 120 s	163	224
Average	100	5305	0.06	318	LN_2 120 s	163	224
22	100	5305	0.12	637	LN_2 120 s	172	298
23	100	5305	0.12	637	LN_2 120 s	159	295
24	100	5305	0.12	637	LN_2 120 s	177	297
Average	100	5305	0.12	637	LN_2 120 s	169	297